DEVELOPMENT OF AN AEROSOL MASS SPECTROMETRY SYSTEM FOR THE ANALYSIS OF THE COMPOSITION OF AEROSOL PARTICLES IN REAL TIME

Sandra Elizabeth Spencer

A dissertation submitted to the faculty at the University of North Carolina at Chapel Hill in partial fulfillment of the requirements for the degree of Doctor of Philosophy in the Department of Chemistry (Analytical) in the School of Arts and Sciences

Chapel Hill
2015

Approved by:

Gary L. Glish

Mark H. Schoenfisch

Leslie M. Hicks

Jeffrey S. Johnson

Jason D. Surratt

ABSTRACT

Sandra Elizabeth Spencer: Development of an Aerosol Mass Spectrometry System for the Analysis of the Composition of Aerosol Particles in Real Time
(Under the direction of Gary L. Glish)

Commercially available aerosol mass spectrometers are capable of sampling compounds from size selected aerosol particles without the requirement for collection of aerosol particles onto a surface. However, one primary disadvantage of the systems available commercially is the inability to gain structural information from analytes in complex samples. Fragmentation of analytes during ionization results in convolution of the observed mass spectrum and prevents identification of analytes. Separation of compounds by gas chromatography prior to ionization allows analytes to be identified but limits the utility of the mass spectrometer for analysis of the composition of aerosol particles in real time. Though one commercial design employs an ion source that does not induce significant fragmentation during ionization, the mass analyzer cannot be used to perform tandem mass spectrometry and thus the instrument is not useful for structural analysis of compounds from aerosol particles.

The goal of the research presented in this dissertation is to develop an aerosol mass spectrometer for the evaluation of the structure of compounds in size-selected aerosol particles from components that are either commercially available or inexpensive and simple to custom build. Aerosol particle separations and analyte ionization are performed at atmospheric pressure to prevent preferential evaporation of the more volatile compounds from the particles in the high vacuum region of the mass spectrometer. To separate isomeric and isobaric analytes prior to mass analysis, ion mobility separations are used. Though the front end of this mass spectrometer can be retrofitted to couple with any mass analyzer, ion trap mass analyzers are used for these experiments to allow for a variety of unique capabilities including selective ion-molecule reactions and tandem mass spectrometry.

ACKNOWLEDGEMENTS

First and foremost, I would like to thank my advisor, Gary Glish. Gary, thank you for always pushing me to improve, especially when it was the most difficult. Thank you for your advice, your guidance, and all the opportunities you have made available to me in graduate school and beyond. Really and truly, no matter how unlikely this seems, thank you for every comment you have made on abstracts, papers, posters, talks, and this document. Your guidance has had a profound impact on my ability as a scientist and I count myself very lucky to have had the opportunity to learn from you.

I also would like to thank the entire Glish group, past and present members, for their friendship and support. Thank you all for having the time to brainstorm and work through problems, to help each other with experiments, and to have a laugh when it's needed. The group has been a safe place to have ideas, be they good or bad. I will remember and cherish all of our failures and triumphs, all the intellectual corners we have backed ourselves into, and all the times it felt like we were arguing when we weren't. I don't think anyone could ask for a better community in which to learn and grow.

I am so appreciative to my parents: for everything they have done for me, for all the support and encouragement they have given me, and for teaching me to work hard and reach for the stars. To my siblings, thank you for teaching me that no matter how big the problem seems you can always get past it if you work hard. To the NC Waters family: Phil, Colleen, Sean, and Matthew, thank you for welcoming me with open arms, for all the holiday dinners and weekend visits, and for making NC feel more like home. Finally, I would like to thank the friends I have made in this phase of my life. Specifically I would like to thank Kady, Michelle, Vivien, and Casey. I would not be where I am without you. Thank you to each and every one of you for being who you are and for being here for me when I have needed you most.

TABLE OF CONTENTS

LIST OF TABLES

LIST OF FIGURES

LIST OF ABBREVIATIONS

A	area
ac	alternating current
AMS	aerosol mass spectrometer
amu	atomic mass unit
APCI	atmospheric pressure chemical ionization
AU	arbitrary units
BSRI	blank subtracted relative intensity
°C	degrees Celsius
C	capacitor
c_c	slip correction coefficient
CID	collision induced dissociation
cm	centimeter
CPC	condensation particle counter
CV	compensation voltage
dc	direct current
Da	Dalton
DESI	desorption electrospray ionization
DIMS	differential ion mobility spectrometry
$\frac{dN}{dlogD_p}$	particle number density
$\frac{d[X]^+}{dt}$	rate of formation of $[X]^+$
$\frac{dW}{dlogD_p}$	particle mass density
DMA	differential mobility analyzer
D_p	particle diameter
DV	dispersion voltage
e	elementary charge on an electron
E	electric field strength

E_c	compensation field
E_D	dispersion field
EI	electron ionization
EESI	extractive electrospray ionization
ESI	electrospray ionization
f	frequency
ft	foot
FTICR	Fourier transform ion cyclotron resonance
FWHM	full width at half maximum
GC	gas chromatography
HV	high voltage
i	current
i.d.	inner diameter
IMS	ion mobility spectrometry
$I_{m/z\,\#}$	intensity of the ion of *m/z* #
$k_{\#}$	rate constant for the ion of *m/z* #
$k_{-\#}$	rate constant for the back reaction of the ion of *m/z* #
k_B	Boltzmann constant
K_H	high field ion mobility
kHz	kilohertz
K_L	low field ion mobility
kV	kilovolt
$kV_{0\text{-}p}$	kilovolt measured from zero to peak
kΩ	kiloOhm
L	liter
LC	liquid chromatography
LIT	linear ion trap
LTP	low temperature plasma

LTPI	low temperature plasma ionization
LV	low voltage
M	neutral molecule
m	meter
m/z	mass-to-charge ratio
MALDI	matrix assisted laser desorption ionization
MS	mass spectrometry
MS^n	n stages of mass spectrometry
MS/MS	tandem mass spectrometry
MeOH	methanol
MHz	megahertz
MSDS	Material Safety Data Sheet
μ	sheath gas viscosity
μF	microFarad
μg	microgram
μL	microliter
μm	micrometer
mg	milligram
min	minute
mL	milliliter
mm	millimeter
ms	millisecond
M	neutral molecule
n	number of charges
$\bar{n}$	average number of charges
nF	nanoFarad
nm	nanometer
o.d.	outer diameter

π	pi
p-	para-
PCA	principle component analysis
ppm	parts per million
psi	pounds per square inch
ρ_p	particle density
R	resolution
R#	resistor number #
rf	radio frequency
s	second
SESI	secondary electrospray ionization
t	time
T	temperature
TD	thermal desorption
TFE	tetrafluoroethylene
TOF	time of flight
V	volt
v_{te}	terminal electric velocity
v_y	velocity of a sheath gas
QIT	quadrupole ion trap
Ω	Ohm
ω	radial frequency ($2\pi f$)
XIC	extracted ion current
Z	electrical mobility
%	percent
°	degrees
[X]	concentration of chemical X
$[X]^+$	ion of the formula X

CHAPTER 1: INTRODUCTION TO AEROSOL ANALYSIS BY MASS SPECTROMETRY

1.1 Importance of compositional analysis of aerosol particles

Analysis of aerosol particles is critical due to pivotal the role of aerosols in a diverse range of applications. For example, the influence of aerosol particles on the global climate by radiative forcing due to absorption or scattering of incoming solar radiation is dependent upon both the diameter and composition of the aerosol particles.[1,2] Deposition of aerosol particles in airways is dependent upon particle diameter and as such both the diameter and composition of aerosol particles play an important role in disease development[3,4] and drug delivery[5,6]. Evaluation of the composition of aerosol particles is also of importance for purposes including secondary organic aerosol formation,[7,8] air quality monitoring,[9] and detection of biochemical warfare agents[10]. The chemical composition of aerosol particles is of particular interest because the chemical characteristics of aerosols impact their physical properties. The presence of hygroscopic compounds in an aerosol particle can influence the particle diameter because the amount of water present in the particle depends on the relative humidity.[11] Partitioning of analytes between the gas and particle phase depends on the vapor pressure, and therefore the identity, of the analyte.[12] Compounds in aerosol particles can also undergo secondary reactions,[13] resulting in a dynamic aerosol composition. The goal of the work presented herein is to develop tools to gain a more accurate understanding of the chemical composition of aerosol particles at any point in time after aerosol formation.

1.2 Analysis of the composition of aerosol particles

1.2.1 Challenges associated with compositional analysis of aerosols

Analysis of the composition of aerosol particles poses a significant analytical challenge because of the dynamic and complex nature of aerosol samples.[14,15] Aerosols exist as a mixture of solid and/or liquid particles suspended in a gaseous medium, resulting in a sample that is difficult to evaluate by traditional analytical methodolgy.[14] Deployment of an instrument for aerosol analysis can prove to be difficult, for example as a personal exposure monitor.[16] Low particle mass densities of aerosol particles

(approximately 1-100 μg/mL) are expected for applications requiring atmospheric monitoring,[14] requiring an increase in sample quantity for adequate analyte detection. For these reasons, aerosol particles are commonly collected onto a surface to increase sample quantity and allow for sample transport.

1.2.2 Collection of aerosol particles

A variety of methods exist to increase sample quantity by collection of aerosol particles in a form that is suitable for transport and analysis.[17,18] By far the most common particle collection techniques are impaction and filtration as each offer specific sampling advantages.[17] Impactors utilize the inertia of aerosol particles in a gas stream to collect the particles on a surface. Aerosol particles with an inertia greater than the cutoff inertia of the impactor collide with the surface and are collected. Impactors can be used to collect size-fractioned aerosol particles because the particle inertia is dependent on the particle size.[19,20] A cascade impactor employs multiple stages of aerosol collection to increase the inertia of particles such that aerosol particles of decreasing diameter are impacted on each subsequent stage.[20] However, solid particles can bounce off the impactor surface rather than deposit, leading to poor sampling efficiency and errors in particle sizing.[17,21] Though the impaction surface can be coated with an adhesive to reduce the extent of particle bounce, sampling artifacts are introduced depending on the composition of the adhesive used.[21,22]

Collection of aerosol particles on a porous filter is an alternative to impaction that is less expensive and has a higher sample capacity.[17] However, more evaporative loss of semi-volatile compounds is predicted to occur during filtration as opposed to impaction due to the pressure gradient across the filter.[17] Many materials are available for use as filters, each with their own advantages. Quartz filters are amenable to analytical techniques that require high temperatures such as thermogravimetric analysis but adsorption of gaseous molecules onto quartz filters[23] requires that a backup filter be used to collect gas phase material for background subtraction.[17] However, due to evaporative losses from semi-volatile compounds from aerosol particles during filter collection, there is debate about the efficacy of this background subtraction.[17] Teflon and Teflon coated glass fiber filters are also available commercially.[24] Less adsorption of gaseous neutrals from the sample onto Teflon filters occurs as opposed to quartz filters.[23]

1.2.3 Analysis of collected aerosol particles by mass spectrometry

Mass spectrometry (MS) is a valuable tool for aerosol analysis because of its speed, sensitivity, and selectivity. To make compounds collected from aerosol samples amenable to mass spectrometric analysis, gaseous ions must first be formed. Typically, analytes from aerosol particles collected onto surfaces are extracted into solution,[25,26] derivatized,[25-27] and volatilized for ionization by electron ionization (EI). EI is commonly used for ionization of compounds from aerosol particles because it is a nearly ubiquitous ion source for gaseous analytes. Enough excess internal energy is imparted to the compounds during ionization by EI to induce fragmentation of the analytes prior to mass analysis. Though these fragmentation patterns can be used to gain structural information from analyte molecules,[28] in complex mixtures of compounds such as organic aerosols fragmentation patterns overlap in the mass spectrum and little information as to the identity of the compounds in the initial sample can be elucidated.[29] Gas chromatography (GC) is often used prior to EI to separate analytes and preserve the structural information gained from ion fragmentation during ionization.[25,26] However, GC-EI-MS is not amenable to involatile or thermally labile analytes.

As an alternative to EI, electrospray ionization (ESI) can be used to ionize involatile or semi-volatile polar compounds extracted into solution from collected aerosol particles.[26] The amount of internal energy imparted to ions during ESI is low enough that little to no fragmentation of analytes occurs.[30] Tandem mass spectrometry (MS/MS) can be performed to gain structural information from the dissociation patterns of intact analyte ions.[31,32] Liquid chromatography (LC)-MS may also be used to separate isomeric analytes prior to ionization.[26]

Matrix assisted laser desorption ionization (MALDI)-MS may be used to ionize a small volume (< 10 μL) of the filter extract spotted onto a surface and coated in a matrix (often graphite).[7] A laser pulse is used to desorb matrix and analyte molecules from the surface and protonated ions are generated.[33,34] Aerosol particles collected on a surface could theoretically be coated with matrix and analyzed by MALDI-MS directly from the surface onto which they were collected, but no reports of the implementation of this technique were found in the literature.

1.2.4 Drawbacks associated with particle collection

Aerosol particle collection can be time consuming (hours to days)[35,36] and may also result in sampling artifacts from particle bounce, gas adsorption, and semi-volatile analyte evaporation as discussed in Section 1.2.2.[17] Secondary reactions and evaporative losses are known to occur within aerosol particles as the particles age, leading to changes in the chemical composition of the particles over time.[37,38] These types of reactions could also occur after particle collection during sample storage and transport.

Concerns about the analyte extraction step have also been raised. Extraction of compounds from surfaces typically involves sonication of the surface in an organic solvent for up to an hour.[25,39] Reactions of carboxylic acid and carbonyl containing compounds from organic aerosol particles with commonly used organic solvents such as methanol have been reported to occur over the course of minutes to hours, within typical analysis timeframes for aerosol particles collected onto a surface.[40] To reduce analysis time and decrease the likelihood of analyte reaction and evaporative sample loss, the sample collection and extraction steps should be eliminated. Instead, compounds should be ionized directly from the aerosol particles in the environment in which they were formed.

1.3 Ambient sampling aerosol mass spectrometry

1.3.1 Commercially available instrumentation

Three ion source designs have been made commercially available for the rapid analysis of aerosol particles.[41,42] The first two ion source designs that will be discussed utilize an aerodynamic lens to introduce aerosol particles into the vacuum system of the mass spectrometer. In the first ion source geometry, the aerosol particles are impacted on a heated surface to volatilize the compounds in the particles. EI is used to ionize the volatilized compounds from the aerosol particles.[41] In an alternative ion source design, laser ablation/ionization is used to volatilize and ionize compounds directly from the aerosol particles.[42] For organic aerosols with a complex chemical composition, typically only the percent carbon in the sample can be determined from the laser ablation/ionization or EI mass spectrum[43] because techniques such as EI and laser ablation/ionization impart enough excess internal energy to the compounds during ionization to induce fragmentation of the analytes in the ionization chamber prior to mass analysis. The degree of fragmentation during laser ablation/ionization can be reduced by lowering

the energy of the laser and the amount of time between ionization and mass analysis.[42,44] However, the use of a tunable laser in this experiment adds significant complexity and cost to the analysis.

A commercial aerosol mass spectrometer designed to separate compounds from aerosol particles before ionization to reduce or prevent mass spectral convolution due to ion fragmentation is currently under development.[45,46] Aerosol particles are collected on a surface by impaction. Thermal desorption (TD) is used to volatilize the compounds from the aerosol particles and the gaseous neutrals are separated by GC prior to ionization by EI. Though this instrument has been shown to allow the identification of analytes from complex aerosol samples, separation of compounds by TD-GC over the course of minutes to hours limits the utility of the instrument for rapid aerosol analysis.

Prior to EI or laser ablation/ionization, aerosol particles can be size selected in a high vacuum, field free time of flight drift region.[47] However, introduction of aerosol particles into a high vacuum chamber as is done in these two commercially available instruments causes evaporation of semi-volatile compounds from the aerosol particles. The increase in partitioning of compounds from the particle into the gas phase at low pressures leads to significant deviations of the physical and chemical characteristics of aerosols from their native state. It has previously been observed that when exposed to the high vacuum region of a transmission electron microscope, liquid ammonium sulfate aerosol particles become crystalline due to the evaporation of water and associated organic compounds, reducing the diameter of the particles by 40-50%.[11] Thus, particle sizing and ionization of compounds from the aerosol particles prior to introduction of the particles into the high vacuum region of the mass spectrometer is important to prevent inaccuracies in particle sizing and preferential sampling of involatile analytes.[48,49]

The third commercial ion source design utilizes an atmospheric pressure chemical ionization (APCI) source to generate ions from compounds in aerosol particles.[50] The drift tube based particle sizing system that is integrated into the EI and laser ablation/ionization mass spectrometers cannot be used with this instrument because ionization of compounds from aerosol particles occurs at atmospheric pressure. A variety of APCI reagents have been investigated for ionization of molecules from aerosol particles.[51,52] NO^+ and $(H_2O)_2H^+$ have been shown to result in little analyte fragmentation and to be the most universal of the APCI reagents investigated, NO^+ capable of ionizing even hexadecane.[51] Protonated water clusters result in ions of the type $[M+H]^+$, where M is the neutral molecule of interest, and NO^+ forms a variety of

ions including $[M-H]^-$ and $[M+NO]^+$.[51] Protonated methanol clusters $(MeOH)_2H^+$ were also investigated as APCI reagents and found to primarily form ions of the type $[M+MeOH+H]^+$.[51] To dissociate weakly bound clusters, the commercial APCI mass spectrometer is equipped with a collision cell between the ion source and the mass analyzer.[50] The reflectron time of flight (TOF) mass analyzer in this instrument[53] can provide molecular formulas for ions[54] but the TOF mass analyzer is not amenable to obtaining more detailed structural information from analytes of interest.

1.3.2 Importance of the mass analyzer for structural analysis

One benefit of using an ion source that induces little fragmentation during ionization is that structural information from the analytes of interest can be retained and ions can be dissociated in the mass analyzer by MS/MS to investigate the structure of ions. The commercial mass spectrometers discussed in the previous section come equipped with a choice of mass analyzers. The EI and laser ablation source designs have the option of a single quadrupole mass filter, a compact TOF, or a high resolution TOF mass analyzer[55] while the APCI source is coupled to a compact or high mass resolution TOF mass analyzer[53]. However, in the commercially available configuration these beam-type mass analyzers cannot be used to perform MS/MS experiments.

Though beam-type mass analyzers can be used for dissociation of analyte ions by MS/MS, these experiments require multiple mass analyzers in a tandem-in-space configuration.[56] In a tandem-in-space mass spectrometer, ions of the mass-to-charge ratio of interest are selected in one mass analyzer, transferred for MS/MS, and then the product ions from MS/MS are transferred to and mass analyzed in the final mass analyzer. Alternatively, trapping mass analyzers such as a quadrupole ion trap (QIT) can be used to perform MS/MS in a tandem-in-time configuration. Analyte ions are trapped, isolated, dissociated, and the product ions subsequently trapped for mass analysis without the need for ion transfer. Trapping mass analyzers such as the QIT are especially useful for MS/MS experiments because of their inherently high MS/MS efficiency relative to tandem-in-space mass spectrometers.[57] Multiple stages of MS/MS (MS^n) can be performed in a single mass analyzer when using a tandem-in-time instrument[57] and the MS/MS reaction time can be varied to control the extent of dissociation[58].

1.3.3 Motivation for the work presented in this dissertation

The goal of the research presented in this dissertation is to develop an aerosol mass spectrometer capable of structural analysis of compounds from size-selected aerosol particles. Each section of the aerosol mass spectrometer design presented herein is either commercially available or simple and inexpensive to custom build. This segmented design results in a highly flexible aerosol mass spectrometry system that can be tailored to the desired application. Atmospheric pressure particle separations and ionization are used to reduce sampling bias caused by introduction of aerosol particles into a high vacuum system. Ion mobility spectrometry is employed post-ionization to separate isomeric analytes. The front end of the aerosol mass spectrometer described herein can be retrofitted to couple with any mass analyzer. Ion trap mass analyzers were used for the experiments presented in this dissertation, resulting in a variety of capabilities including high resolution/high mass accuracy determination of molecular formulas, selective ion-molecule reactions, and MS/MS.

1.4 Summary

Chemical analysis of compounds from aerosol particles is important for a variety of applications and this introduction discusses current techniques for aerosol analysis by mass spectrometry. Commercial aerosol mass spectrometer designs were introduced and the advantages and limitations of currently available instrumentation were discussed. This introduction describes the impetus for the development of the instrumentation that is presented in this dissertation.

Chapter 2 provides information on the methodology used for the experiments discussed in this dissertation, including chemicals and reagents. Aerosol generation, sampling, and handling techniques are described in this chapter. Techniques for compound ionization, separation, and data analysis are also discussed.

Chapter 3 introduces three surface ionization techniques that combine the extraction of compounds from aerosol particles collected on filters with ionization. It is demonstrated that for the compounds produced from pyrolysis of natural products, sample evaporation occurs during filter and extract storage. The data presented in this chapter highlight the motivation for the development of the aerosol mass spectrometer in this dissertation.

Chapter 4 begins by detailing two ambient ionization techniques, extractive electrospray

ionization (EESI) and low temperature plasma ionization (LTPI), used for ionization of small molecules directly from aerosol particles without collection of the aerosol particles on filters. The influence of the electrospray solvent in EESI and the plasma gas in LTPI is discussed. A novel “flow-through” LTPI configuration is presented and shown to increase the sensitivity and reproducibility of LTPI for ionization of compounds in gases and aerosols.

Chapter 5 introduces size selection of aerosol particles by a differential mobility analyzer. The dependence of the aerosol particle size distribution on pyrolysis temperature is investigated. Compounds from size selected aerosol particles are ionized using LTPI and differences in the composition of aerosol particles produced by pyrolysis are shown to occur depending on particle diameter.

Chapter 6 shows data for the separation of ions produced by LTPI of compounds in aerosol particles by differential ion mobility spectrometry (DIMS). Enrichment of low abundance ions during a compensation field scan is discussed and the efficiency of the separation is evaluated. LTPI-DIMS-MS/MS is used to generate MS/MS spectra for isomeric/isobaric ions generated from the pyrolysis of cellulose.

Chapter 7 further investigates the use of MS/MS as a method for gaining structural information from compounds from aerosol particles. It is shown that changes in the dissociation pattern of ions as the pyrolysis temperature is increased are not due to incomplete thermalization of ions. Uncommon neutral losses are observed after collision induced dissociation and can be used to identify functional groups in the neutral molecule. The kinetics of ion-molecule reactions in the ion trap are used to differentiate between isomeric ions. Finally, in **Chapter 8** a summary of this dissertation is presented and suggested future experiments as well as the overall project outlook are discussed.

REFERENCES

1. Kinne, S.; Liou, K. The effects of the nonsphericity and size distribution of ice crystals on the radiative propertues of cirrus clouds. *Atmos. Res.* **1989***, 24*, 273-284.

2. Jung, C. H.; Lee, J. Y.; Kim, Y. P. Estimation of aerosol optical properties considering hygroscopicity and light absorption. *Atmos. Environ.* **2015***, 105*, 191-201.

3. Lach, K.; Steer, B.; Gorbunov, B.; Micka, V.; Muir, R. B. Evaluation of exposure to airborne heavy metals at gun shooting ranges. *Ann. Occup. Hyg.* **2015***, 59*, 307-323.

4. SCOTT, K. G.; AXELROD, D. Deposition and fate of plutonium, uranium and their fission products inhaled as aerosols by rats and man. *Arch. Pathol. (Chic)* **1949***, 48*, 31-54.

5. Arunthari, V. A Prospective, Comparative Trial of Standard and Breath-Actuated Nebulizer: Efficacy, Safety, and Satisfaction. *Respir. Care* **2012***, 57*, 1242-1247.

6. Smith, J. H. Nebulized live-attenuated influenza vaccine provides protection in ferrets at a reduced dose. *Vaccine* **2012***, 30*, 3026-3033.

7. Surratt, J. D.; Murphy, S. M.; Kroll, J. H.; Ng, N. L.; Hildebrandt, L.; Sorooshian, A.; Szmigielski, R.; Vermeylen, R.; Maenhaut, W.; Claeys, M.; Flagan, R. C.; Seinfeld, J. H. Chemical Composition of Secondary Organic Aerosol Formed from the Photooxiation of Isoprene. *J. Phys. Chem. A.* **2006***, 110*, 9665-9690.

8. Krechmer, J. E.; Coggon, M. M.; Massoli, P.; Nguyen, T. B.; Crounse, J. D.; Hu, W.; Day, D. A.; Tyndall, G. S.; Henze, D. K.; Rivera-Rios, J. C.; Nowak, J. B.; Kimmel, J. R.; Mauldinlll, R. L.; Stark, H.; Jayne, J. T.; Sipilä, M.; Junninen, H.; St. Clair, J. M.; Zhang, X.; Feiner, P. A.; Zhang, L.; Miller, D. O.; Brune, W. H.; Keutsch, F. N.; Wennberg, P. O.; Seinfeld, J. H.; Worsnop, D. R.; Jiminez, J. L.; Canagaratna, M. R. Formation of Low Volatility Organic Compounds and Secondary Organic Aerosol from Isoprene Hydroxyhydroperoxide Low-NO Oxidation. *Environ. Sci. Technol.* **2015***, 49*, 10330-10339.

9. Petit, J. -.; Favez, O.; Sciare, J.; Crenn, V.; Sarda-Estève, R.; Bonnaire, N.; Močnik, G.; Dupont, J. -.; Haeffelin, M.; Leoz-Garziandia, E. Two years of near real-time chemical composition of submicron aerosols in the region of Paris using an Aerosol Chemical Speciation Monitor (ACSM) and a multi-wavelength Aethalometer. *Atmos. Chem. Phys.* **2015***, 15*, 2985-3005.

10. Pazienza, M.; Britti, M. S.; Carestia, M.; Cenciarelli, O.; D'Amico, F.; Malizia, A.; Bellecci, C.; Fiorito, R.; Gucciardino, A.; Bellino, M.; Lancia, C.; Tamburrini, A.; Gaudio, P. Use of Particle Counter System for the Optimization of Sampling, Identification, and Decontamination Procedures for Biological Aerosols Dispersion in Confined Environment. *J. Microb. Biochem. Technol* **2014***, 6*, 43-48.

11. Posfai, M.; Xu, H.; Anderson, J.; Buseck, P. Wet and dry sizes of atmospheric aerosol particles: An AFM-TEM study. *Geophys. Res. Lett.* **1998***, 25*, 1907-1910.

12. Coon, J. J.; Syka, J. E.; Schwartz, J. C.; Shabanowitz, J.; Hunt, D. F. Anion dependence in the partitioning between proton and electron transfer in ion/ion reactions. *Int. J. Mass Spectrom.* **2004***, 236*, 33-42.

13. Tolocka, M. P.; Jang, M.; Ginter, J.; Cox, F. J.; Kamens, R. M.; Johnston, M. V. Formation of Oligomers in Secondary Organic Aerosol. *Environ. Sci. Technol.* **2004***, 38*, 1428-1434.

14. Pöschl, U. Aerosol particle analysis: challenges and progress. *Anal. Bioanal. Chem.* **2003***, 375*, 30-32.

15. Nozière, B.; Kalberer, M.; Claeys, M.; Allan, J.; D'Anna, B.; Decesari, S.; Finessi, E.; Glasius, M.; Grgić, I.; Hamilton, J. F.; Hoffmann, T.; Iinuma, Y.; Jaoui, M.; Kahnt, A.; Kampf, C. J.; Kourtchev, I.; Maenhaut, W.; Marsden, N.; Saarikoski, S.; Schnelle-Kreis, J.; Surratt, J. D.; Szidat, S.; Szmigielski, R.; Wisthaler, A. The Molecular Identification of Organic Compounds in the Atmosphere: State of the Art and Challenges. *Chem. Rev.* **2015***, 115*, 3919-3983.

16. Wang, C. H.; Chen, B. T.; Han, B. C.; Liu, A. C.; Hung, P. C.; Chen, C. Y.; Chao, H. J. Field evaluation of personal sampling methods for multiple bioaerosols. *PLoS One* **2015***, 10*, e0120308.

17. Turpin, B. J.; Saxena, P.; Andrews, E. Measuring and Simulating Particulate Organics in the Atmosphere: Problems and Prospects. *Atmos. Environ.* **2000***, 34*, 2983-3013.

18. Pardon, G.; Ladhani, L.; Sandström, N.; Ettori, M.; Lobov, G.; van der Wijngaart, W. Aerosol sampling using an electrostatic precipitator integrated with a microfluidic interface. *Sensors Actuators B: Chem.* **2015***, 212*, 344-352.

19. Mitchell, R. I. Improved Cascade Impactor for Measuring Aerosol Particle Sizes. *J. Ind. Eng. Chem.* **1959***, 51*, 1039-1042.

20. May, K. R. The Cascade Impactor: An Instrument for Sampling Coarse Aerosols. *J. Sci. Instrum.* **1945***, 22*, 187-195.

21. Stein, S. W.; Turpin, B. J.; Cai, X.; Huang, P. -.; McMurry, P. H. Measurements of the Relative Humidity-Dependent Bounce and Density for Atmospheric Particles Using the DMA-Impactor Technique. *Atmos. Environ.* **1994***, 28*, 1739-1749.

22. Vasiliou, J. G.; Sorensen, D.; McMurry, P. H. Sampling at controlled relative humidity with a cascade impactor. *Atmos. Environ.* **1999***, 33*, 1049-1056.

23. Parshintsev, J. Comparison of quartz and Teflon filters for simultaneous collection of size-separated ultrafine aerosol particles and gas-phase zero samples. *Anal. Bioanal. Chem.* **2011***, 400*, 3527-3535.

24. Pall Life Sciences, Pall Coorporation. Pallflex Filters: Emfab, Fiberfilm and Tissuquartz Filters. *https://www.pall.com/pdfs/Laboratory/02.0601_Pallflex_LR.pdf* **2002***, 2014*, 2.

25. Pietrogrande, M. C.; Bacco, D.; Chiereghin, S. GC/MS analysis of water-soluble organics in atmospheric aerosol: optimization of a solvent extraction procedure for simultaneous analysis of carboxylic acids and sugars. *Anal. Bioanal. Chem.* **2013***, 405*, 1095-1104.

26. Buiarelli, F.; Canepari, S.; Di Filippo, P.; Perrino, C.; Pomata, D.; Riccardi, C.; Speziale, R. Extraction and analysis of fungal spore biomarkers in atmospheric bioaerosol by HPLC-MS-MS and GC-MS. *Talanta* **2013***, 105*, 142-151.

27. Kawamura, K.; Tachibana, E.; Okuzawa, K.; Aggarwal, S. G.; Kanaya, Y.; Wang, Z. F. High abundances of water-soluble dicarboxylic acids, ketocarboxylic acids and alpha-dicarbonyls in the mountaintop aerosols over the North China Plain during wheat burning season. *Atmos. Chem. Phys.* **2013***, 13*, 8285-8302.

28. McLafferty, F. W.; Turecek, F. *Interpretation of Mass Spectra;* University Science Books: Mill Valley, CA, 1993.

29. Mühlberger, F.; Zimmermann, R.; Kettrup, A. A Mobile Mass Spectrometer for Comprehensive On-Line Analysis of Trace and Bulk Components of Complex Gas Mixtures: Parallel Application of the Laser-Based Ionization Methods VUV Single-Photon Ionization, Resonant Multiphoton Ionization, and Laser-Induced Electron Impact Ionization. *Anal. Chem.* **2001***, 73*, 3590-3604.

30. Collette, C.; Drahos, L.; De Pauw, E.; Vekey, K. Comparison of the Internal Energy Distributions of Ions Produced by Different Electrospray Sources. *Rapid Comm. Mass Spectrom.* **1998***, 12*, 1673-1678.

31. McFadden, W. H.; Lammert, S. A. Techniques for increased use of thermospray liquid chromatography—mass spectrometry. *J. Chromatogr. A.* **1987***, 385*, 201-211.

32. Hua, L.; Hou, K.; Chen, P.; Xie, Y.; Jiang, J.; Wang, Y.; Wang, W.; Li, H. Realization of In-Source Collision-Induced Dissociation in Single-Photon Ionization Time-of-Flight Mass Spectrometry and Its Application for Differentiation of Isobaric Compounds. *Anal. Chem.* **2015***, 87*, 2427-2433.

33. Lewis, J. K.; Wei, J.; Siuzdak, G. Matrix-assisted Laser Desorption/Ionization Mass Spectrometry in Peptide and Protein Analysis. In *Encyclopedia of Analytical Chemistry*; Meyers, R. A., Ed.; John Wiley & Sons Ltd.: Chichester, 2000; pp 5880.

34. Awad, H.; Khamis, M. M.; El-Aneed, A. Mass Spectrometry, Review of the Basics: Ionization. *Appl. Spectrosc. Rev.* **2015***, 50*, 158-175.

35. Shaltout, A. A.; Boman, J.; Shehadeh, Z. F.; Al-Malawi, D. R.; Hemeda, O. M. Spectroscopic investigation of PM2.5 collected at industrial, residential and traffic sites in Taif, Saudi Arabia. *J. Aerosol Sci.* **2015***, 79*, 97-108.

36. Mkoma, S. L.; da Rocha, G. O.; de Andrade, J. B. Determination of Carboxylic Acids and Water-soluble Inorganic Ions by Ion Chromatography in Atmospheric Aerosols from Tanzania. *South Afr. J. Chem. -Suid-Afr. Tydskr. Chem.* **2014***, 67*, 118-123.

37. VENKATARAMAN, C.; FRIEDLANDER, S. Size Distributions of Polycyclic Aromatic-Hydrocarbons and Elemental Carbon .2. Ambient Measurements and Effects of Atmospheric Processes. *Environ. Sci. Technol.* **1994***, 28*, 563-572.

38. Jang, M.; Lee, S.; Kamens, R. M. Organic aerosol growth by acid-catalyzed heterogeneous reactions of octanal in a flow reactor. *Atmospheric Environment* **2003***, 37*, 2125-2138.

39. Aldabe, J.; Santamaria, C.; Elustondo, D.; Parra, A.; Foan, L. Polycyclic Aromatic Hydrocarbons (PAHs) Sampled in Aerosol Phase at Different Sites of the Western Pyrenees in Navarra (Spain). *Environ. Eng. Manag. J.* **2012***, 11*, 1049-1058.

40. Bateman, A. P.; Walser, M. L.; Desyaterik, Y.; Laskin, J.; Laskin, A.; Nizkorodov, S. A. The Effect of Solvent on the Analysis of Secondary Organic Aerosol Using Electrospray Ionization Mass Spectrometry. *Environ. Sci. Technol.* **2008***, 42*, 7341-7346.

41. Jayne, J. T.; Leard, D. C.; Zhang, X.; Davidovits, P.; Smith, K. A.; Kolb, C. E.; Worsnop, D. R. Development of an aerosol mass spectrometer for size and composition analysis of submicron particles. *Aerosol Sci. Technol.* **2000***, 33*, 49-70.

42. Öktem, B.; Tolocka, M.; Johnston, M. On-Line Analysis of Organic Components in Fine and Ultrafine Particles by Photoionization Aerosol Mass Spectrometry. *Anal. Chem.* **2004***, 76*, 253-261.

43. Aiken, A. C.; Decarlo, P. F.; Kroll, J. H.; Worsnop, D. R.; Huffman, J. A. O/C and OM/OC Ratios of Primary, Secondary, and Ambient Organic Aerosols with High-Resolution Time-of-Flight Aerosol Mass Spectrometry. *Environ. Sci. Technol.* **2008***, 42*, 4478-4485.

44. Nash, D. G.; Liu, X. F.; Mysak, E. R.; Baer, T. Aerosol particle mass spectrometry with low photon energy laser ionization. *Int. J. Mass Spectrom.* **2005***, 241*, 89-97.

45. Williams, B. J.; Jayne, J. T.; Lambe, A. T.; Hohaus, T.; Kimmel, J. R.; Sueper, D.; Brooks, W.; Williams, L. R.; Trimborn, A. M.; Martinez, R. E.; Hayes, P. L.; Jimenez, J. L.; Kreisberg, N. M.; Hering, S. V.; Worton, D. R.; Goldstein, A. H.; Worsnop, D. R. The First Combined Thermal Desorption Aerosol Gas Chromatograph—Aerosol Mass Spectrometer (TAG-AMS). *Aerosol Sci. Technol.* **2014***, 48*, 358-370.

46. Aerodyne Research, I. Thermal Desorption Aerosol Gas Chromatograph AMS (TAG-AMS). *http://www.aerodyne.com/products/thermal-desorption-aerosol-gas-chromatograph-ams-tag-ams* **2015**.

47. Canagaratna, M. R.; Jayne, J. T.; Jimenez, J. L.; Allan, J. D.; Alfarra, M. R.; Zhang, Q.; Onasch, T. B.; Drewnick, F.; Coe, H.; Middlebrook, A.; Delia, A.; Williams, L. R.; Trimborn, A. M.; Northway, M. J.; DeCarlo, P. F.; Kolb, C. E.; Davidovits, P.; Worsnop, D. R. Chemical and microphysical characterization of ambient aerosols with the aerodyne aerosol mass spectrometer. *Mass Spectrom. Rev.* **2007***, 26*, 185-222.

48. Gill, P. S.; Graedel, T. E.; Weschler, C. J. Organic Films on Atmospheric Aerosol-Particles, Fog Droplets, Cloud Droplets, Raindrops, and Snowflakes. *Rev. Geophys.* **1983***, 21*, 903-920.

49. Mazurek, M.; Masonjones, M.; Masonjones, H.; Salmon, L.; Cass, G.; Hallock, K.; Leach, M. Visibility-reducing organic aerosols in the vicinity of grand canyon national park: Properties observed by high resolution gas chromatography. *J. Geophys. Res. -Atmos.* **1997***, 102*, 3779-3793.

50. Bertram, T. H.; Kimmel, J. R.; Crisp, T. A.; Ryder, O. S.; Yatavelli, R. L. N. A field-deployable, chemical ionization time-of-flight mass spectrometer. *Atmos. Meas. Tech.* **2011***, 4*, 1471-1479.

51. Hearn, J. D.; Smith, G. D. A Chemical Ionization Mass Spectrometry Method for the Online Analysis of Organic Aerosols. *Anal. Chem.* **2004***, 76*, 2820-2826.

52. Kuckelmann, U.; Warscheid, B.; Hoffmann, T. On-line Characterization of Organic Aerosols Formed from Biogenic Precursors Using Atmospheric Pressure Chemical Ionization Mass Spectrometry. *Anal. Chem.* **2000***, 72*, 1905-1912.

53. Aerodyne Research, I. ToF-CIMS: Chemical ionization Time-of-Flight Mass Spectrometer. *http://www.aerodyne.com/sites/default/files/ToF-CIMS%20Chemical%20Ionization%20Time-of-Fligh%20Mass%20Spectrometer%20product%20sheet.pdf* **2015**.

54. Chhabra, P. S.; Lambe, A. T.; Canagaratna, M. R.; Stark, H.; Jayne, J. T.; Onasch, T. B.; Davidovits, P.; Kimmel, J. R.; Worsnop, D. R. Application of high-resolution time-of-flight chemical ionization mass spectrometry measurements to estimate volatility distributions of α-pinene and naphthalene oxidation products. *Atmos. Meas. Tech.* **2015***, 8*, 1-18.

55. Aerodyne Research, I. AMS: Aerosol Mass Spectrometer Systems. *http://www.aerodyne.com/sites/default/files/Aerosol%20Mass%20Spectrometer%20Systems.pdf* **2015**.

56. Glish, G. L.; Vachet, R. W. The basics of mass spectrometry in the twenty-first century. *Nat. Rev. Drug Discov.* **2003***, 2*, 140-150.

57. Glish, G. L. Multiple Stage Mass Spectrometry: The Next Generation Tandem Mass Spectrometry Experiment. *Analyst* **1994***, 119*, 533-537.

58. McLuckey, S. A.; Goeringer, D. E. Slow heating methods in tandem mass spectrometry. *Journal of Mass Spectrometry* **1997***, 32*, 461-474.

CHAPTER 2: EXPERIMENTAL

2.1 Materials and reagents

Ethyl cellulose was purchased from Alfa Aesar (90-110 cps 5% in toluene, Ward Hill, MA) and cellulose was purchased from TCI America (Portland, OR). Tobacco extracts of cellulose, hemicellulose, and lignin were provided by R. J. Reynolds Tobacco Co. (Winston-Salem, NC). Syringaldehyde (98%), 2,6-dimethoxyphenol (99%), levoglucosan (99%), 3-hydroxy-2-methyl-4-pyrone (99%), and caffeine (99.8%) were purchased from Sigma-Aldrich (St. Louis, MO). E-liquids were purchased from The Vapor Girl, Inc. (Chapel Hill, NC) for analysis. Solvents were purchased from Fisher Scientific (Waltham, MA). HPLC grade methanol, water, and chloroform, were used. The toluene and acetic acid were certified ACS grade. Acetonitrile was optima grade.

A mixture of cellulose and lignin was prepared in a ratio of 60/40 cellulose/lignin by mass. This ratio was selected to mimic the ratio of lignin and cellulose found in biomass, omitting the contribution of hemicellulose.[1] Cellulose and lignin were combined and ground together with a spatula. Chloroform (6.00 mL) was added to the cellulose/lignin mixture dropwise and the solution was stirred until the analyte was fully dissolved. The chloroform was removed from the cellulose/lignin mixture by evaporation for 48 hours. A stream of nitrogen was passed over the solution to assist in solvent evaporation. Shown in Figure 2.1 is a photograph of the cellulose (left), lignin (middle), and the 60/40 cellulose/lignin mixture (right).

2.2 Aerosol generation and off-line characterization

2.2.1 Aerosol particle generation

Two pyrolysis units were used to volatilize or pyrolyze the samples of interest. The first is a custom built pyrolysis chamber (50 mm x 50 mm x 64 mm) composed of 7.0 mm thick graphite sheets (Figure 2.2) bolted together with 0.25 mm threaded

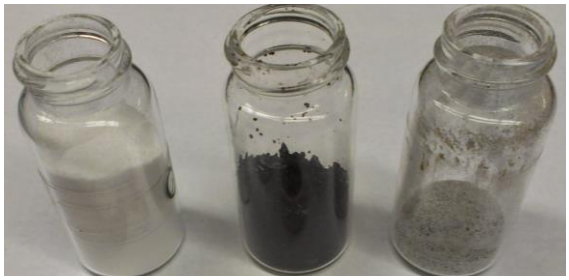

Figure 2.1. Photograph of cellulose (right), lignin (middle), and 60/40 cellulose/lignin.

rods (not shown). Nitrogen is flowed through the chamber at approximately 3 L/min for 5 minutes prior to analysis, corresponding to 250 chamber volumes. An 80/20 nickel/chromium wire (Omega, Stamford, CT) is wrapped around a quartz crucible containing between 50 and 60 mg of the sample of interest.

Heating of the sample is effected by applying a constant current i to resistively heat the nichrome wire (1.020 Ω/ft). The temperature is monitored using a thermocouple suspended in the sample. The final pyrolysis temperature was reached in roughly 2 minutes for all analyses. Electrical feedthroughs for the heating filament and thermocouple are insulated with 4.7 mm ceramic tubes that were press-fitted through ports in the graphite chamber. The aerosol exits the top of the pyrolysis chamber through a cajon fitting connected to a ½ inch steel tube. The custom chamber was used for experiments requiring a larger quantity of aerosol due to its increased sample capacity.

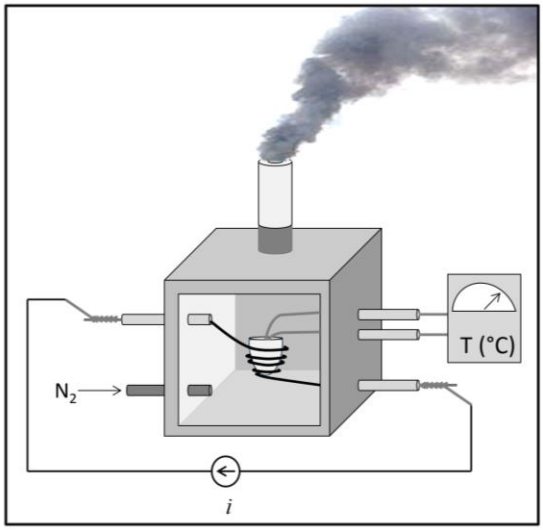

Figure 2.2. Experimental pyrolysis set-up. Sample is placed in the crucible and is heated by thermal transfer from a resistively heated wire. Temperature is monitored throughout the experiment.

As an alternative to the custom pyrolysis chamber, a PyroProbe 5250 (CDS Analytical, Oxford PA) was used to pyrolyze between 20 and 30 mg of the sample of interest at 650 °C in nitrogen pyrolysis gas with a heating rate of 10 °C/s unless otherwise noted. Nitrogen is flowed through the chamber at approximately 3 L/min. The 8-port valve of the PyroProbe was maintained at 300 °C and the aerosol transfer line to the mass spectrometer is heated to between 70 and 90 °C to prevent the condensation of the aerosols in the transfer line.

2.2.2 Determination of aerosol particle size distribution

Aerosol particles were separated based on particle diameter using a differential mobility analyzer (Model 3080, TSI Incorporated, Shoreview, MN). A detailed description of the theory of separation of particles by differential mobility is given in Chapter 5. A condensation particle counter (Model 3022A, TSI Incorporated, Shoreview, MN) was used to determine the number density of particles with each selected

diameter. Saturated t-butyl alcohol vapor was condensed onto the particles to increase the particle diameter for measurement of the number of aerosol particles in the condensation chamber by light scattering.

2.2.3 Filter collection and extraction

Aerosol particles generated by the pyrolysis of natural polymers in the custom pyrolysis chamber were collected onto tetrafluoroethylene (TFE) coated borosilicate glass filters (Pallflex Fiberfilm T60A20, Ann Arbor, MI). These filters are known to retain 96.4% of aerosol particles,[2] and minimal adsorption of gaseous compounds onto TFE coated filters has previously been reported.[3] The experimental design of the custom filter collection system is displayed in Figure 2.3. Conductive tubing was used for aerosol transport to eliminate electrostatic particle losses due to charge buildup.[4] A GE Motors 5KH36KN90GX ac motor (Raleigh, NC) was used as a vacuum pump to generate a pressure differential of 22 inches of Hg across the filter. This pressure differential was designed to assist in gas flow through the filter and thus collection of particles on the filter. Blanks were collected prior to pyrolysis of the sample. Blanks and samples were collected on filters for 5 minutes at the final pyrolysis temperature.

To extract compounds from aerosol particles from TFE coated borosilicate glass fiber filters, the portion of the filter to be extracted was submerged in 2.0 mL of extraction solvent (methanol unless otherwise noted) in a scintillation vial. The filter was sonicated in the extraction solvent for 60 minutes in an ice water bath to minimize the evaporation of semi-volatile analytes during extraction. After extraction of compounds from the filter, the filter was removed from the scintillation vial and the extract was diluted by a factor of 10 for electrospray

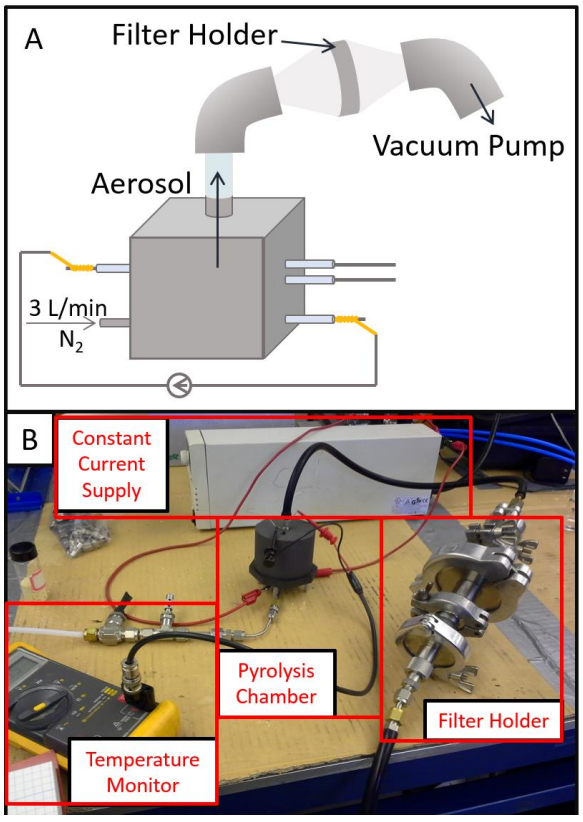

Figure 2.3 A. Schematic for and B. picture of the experimental set-up for the collection of aerosol particles on TFE coated borosilicate glass fiber filters.

ionization (ESI). The ESI solvent composition was 50/49/1 methanol/water/acetic acid unless otherwise noted.

2.3 Ionization

2.3.1 Secondary electrospray ionization

Secondary electrospray ionization (SESI) was performed to ionize compounds evaporated from the surface of the TFE coated borosilicate glass fiber filter. The filter was held at ground potential and suspended parallel to the inlet of the mass spectrometer as depicted in Figure 2.4. An Agilent ESI emitter (Agilent Technologies, Santa Clara, CA) was placed between the filter and the inlet to the mass spectrometer. The SESI solvent was pumped through the emitter at a flow rate of 2 μL/min. A nebulizing gas pressure was maintained at 10 psi above atmospheric pressure. A +4.25 kV dc voltage was applied to the ESI emitter and the capillary inlet to the mass spectrometer was held at ground potential to generate an electrospray plume. Ionization of gaseous neutrals by SESI is believed to occur by interaction of the analyte with the charged surface of the electrospray droplets and/or by chemical ionization of analytes via ion-molecule reactions between the neutral analyte molecules and the protonated solvent molecules.[5]

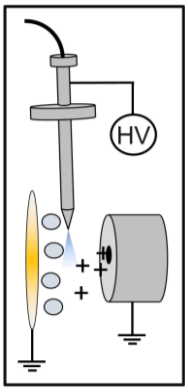

Figure 2.4. Schematic for the SESI experiment.

2.3.2 Desorption electrospray ionization

Desorption electrospray ionization (DESI) is performed by directing an electrospray plume onto a surface to generate ions from analyte collected on the surface. The experimental set-up for DESI used in the experiments detailed in this dissertation is displayed in Figure 2.5. The TFE coated borosilicate glass fiber filter is held at ground potential and positioned perpendicular to and 0.5 mm below the capillary inlet to the mass spectrometer. The capillary was held at -0.5 kV to assist in drawing positive ions to the inlet of the mass spectrometer. The Agilent ESI emitter was positioned approximately 2 mm above the filter and

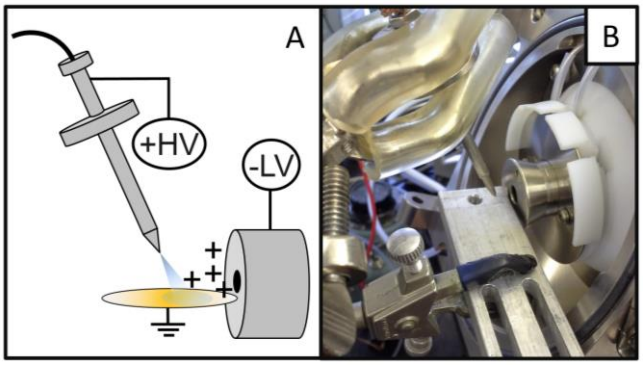

Figure 2.5. A. Schematic for and B. picture of the DESI experiment.

5 mm away from the capillary inlet to the mass spectrometer at approximately 55° from the surface of the filter. To generate an electrospray, +3.0 kV dc was applied to the ESI emitter and a DESI solvent (50/49/1 methanol/water/acetic acid unless otherwise noted) was pumped through the emitter at a flow rate of 2 μL/min. For DESI of small molecules such as the pyrolysis products of natural polymers, ions are formed by sputtering of analytes from the filter, interaction of analytes with the charged surface of the droplets, or chemical ionization of compounds via ion-molecule reactions between gaseous analytes and protonated solvent molecules.[6]

2.3.3 Paper spray ionization

The experimental configuration for paper spray ionization used for the experiments described in this dissertation is shown in Figure 2.6. The TFE coated borosilicate glass fiber filter was cut into a wedge with a pointed tip and wetted with 50 μL of paperspray solvent, 50/49/1 methanol/water/acetic acid. Solvent was flowed over the surface of the paper at a rate of 25 μL/min to extract compounds from the surface. The filter was held at +4.0 kV and -1.0 kV was applied to the inlet capillary of the mass spectrometer to generate an electrospray plume from the sharp tip of the filter. Ions are generated from analytes extracted from the surface of the filter.[7]

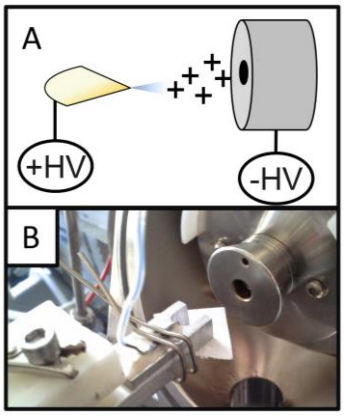

Figure 2.6. A. Schematic for and B. photo of the paper spray ionization experiment.

2.3.4 Extractive electrospray ionization

The experimental set-up for extractive electrospray ionization (EESI) is displayed schematically in Figure 2.7. The EESI solvent was 50/49/1 methanol/water/acetic acid flowed at 2 μL/min unless otherwise noted. The Agilent ESI emitter is held at ground potential and positioned approximately 3 mm away from the inlet to the mass spectrometer. The aerosol transfer line is held at ground potential. -4.25 kV dc is applied to the ESI emitter to generate the electrospray. The electrospray plume is directed through the aerosol particles to generate ions.[8]

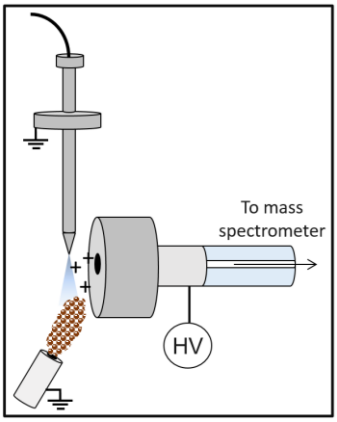

Figure 2.7. Schematic of the EESI experiment.

2.3.5 Nano-extractive electrospray ionization

The schematic for the nano-EESI experiment is displayed in Figure 2.8. A custom block is used to orient the nano-ESI emitter. The primary difference between ESI and nano-ESI is that nano-ESI uses an ESI emitter with a tip opening of only a few micrometers rather than ~100 μm for ESI.[9] The nano-ESI emitters used for the experiments discussed herein were made from 105 mm glass capillaries (i.d. 1.4 mm, o.d. 1.7 mm, Drummond Scientific, Broomball, PA) using a Narishige PC-10 puller (East Meadow, NY). The pulled glass capillary is filled with approximately 100 μL of ESI solvent. An SW-10 stylette wire (SGE Analytical Science, Austin, TX; P/N 031745, diameter = 0.10 mm) is used as the inner electrode. The electrode is held in place by screw 1 and screw 2 holds the glass capillary in place with the electrode inside. A high voltage (-2.14 kV) is applied to the inner electrode through screw 1 and the inlet capillary to the mass spectrometer is held at ground potential. The aerosol transfer line was held at ground potential. The electrospray is directed through the aerosol plume to generate ions by EESI.

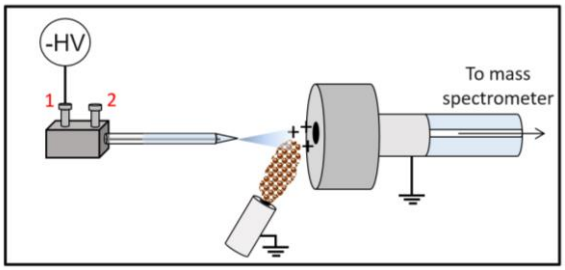

Figure 2.8. Schematic for the experimental set up of nano-EESI.

2.3.6 Low temperature plasma ionization

Two different power supplies were used to generate a high voltage sine wave for low temperature plasma ionization (LTPI). One power supply was a tunable ac voltage with a frequency of 5 kHz from a previously published design.[10] The circuit diagram for the second LTPI power supply is displayed in Figure 2.9. A LM556 dual timer (Texas Instruments, Dallas, TX) is operated in the astable mode to generate a low voltage square wave. The frequency of the waveform is determined by the value of the capacitor C1 and the resistors R1, R2, and R3. The frequency (f) of the waveform may be calculated by:

$$f = \frac{1.44}{(R1+R2+2R3)C1} \qquad \text{Equation 2.1}$$

The constant 1.44 is due to the charge/discharge time of the device. For the circuit used in these experiments, the frequency of the waveform was 5 kHz. A 10 kΩ potentiometer is used to adjust the magnitude of the square wave. A MOSFET IRF1530N (International Rectifier, Leominster, MA) is used to convert the square wave into a low voltage sine wave. An automobile ignition coil (Regitar USA,

Montgomery, AL; P/N RUC12) is used to amplify the voltage of the sine wave. The final output voltage is adjustable from 0 – 4.25 $kV_{0\text{-}p}$.

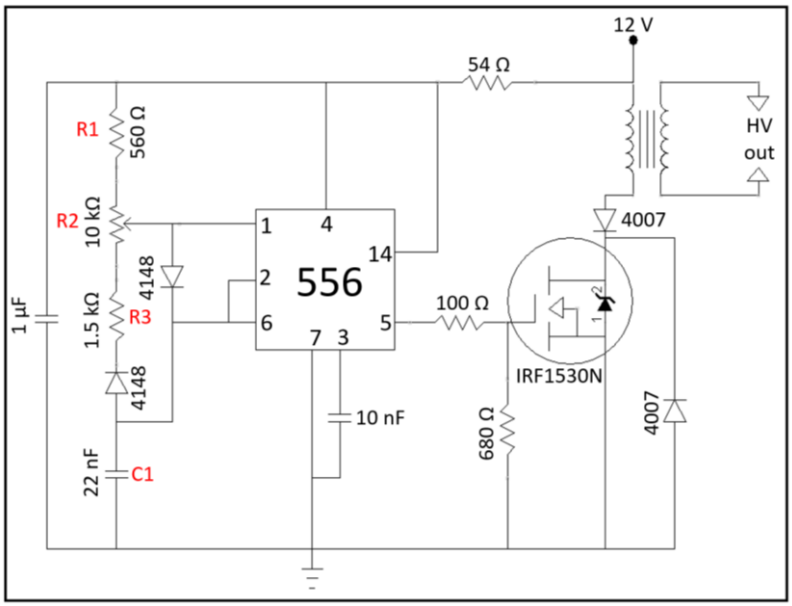

Figure 2.9. Schematic for the power supply used to generate the low temperature plasma. Variable output from 0 - 4.25 $kV_{0\text{-}p}$ with a frequency of 5 kHz.

The LTPI sources used for ionization were built based upon previously reported source designs.[11,12] Unless otherwise specified, helium is used as a plasma gas for the standard-size LTPI source (Figure 2.10A and 2.10B) and nitrogen is used as the plasma gas for the miniature LTPI source (Figure 2.10C and 2.10D). The plasma gas flow rate is approximately 3 L/min. For the standard-size LTPI source copper tape (12.7 mm width) is wrapped around the end of a glass tube (i.d. 3.9 mm, o.d. 5.9 mm, length 73 mm) and held at ground potential. A high ac voltage of approximately 4 $kV_{0\text{-}p}$ generated by either power supply was applied to the central tungsten electrode of the LTPI source (diameter = 1.0 mm). The previously reported LTPI source designs were arranged such that the high voltage sine wave was applied to the outer electrode and the central electrode was held at ground potential.[11] For the standard-size LTPI source, no significant difference was observed in the mass spectrum of ethyl cellulose or cellulose when the voltages applied to the two electrodes were switched. Thus, the high voltage lead was connected to the sturdier inner tungsten electrode as opposed to the copper tape to reduce the risk of operator contact with the high ac voltage because the high voltage lead is heavier and more insulated than the grounded lead.

The miniature LTPI source was built as shown in Figure 2.10C and 2.10D. A SW-10 stylet wire is

used as the inner electrode (SGE Analytical Science, Austin, TX; P/N 031745, diameter = 0.10 mm). The wire is threaded through a stainless steel Upchurch female-to-female fingertight zero-dead-volume union. The inner electrode is held in place by tightening the union onto the end of the gas or aerosol transfer line such that the stylet wire is secured between the threads of the union and the fitting on the end of the transfer line. Copper tape is wrapped around the zero-dead-volume union for connection of the union to a ground potential through an alligator clip. The inner electrode is also grounded because this electrode is in direct electrical contact with the stainless steel union. A glass melting point capillary (Custom Glass Tubing, Drummond Scientific Company, Broomall, PA, item number 9-000-2313-A; i.d. 1.0 mm, o.d. 1.6 mm) was cut to a length of 40 mm to be used as an insulating barrier between the inner and outer electrodes. Copper tape is wrapped around the end of the glass capillary to act as the outer electrode, leaving approximately 3 mm of the end of the glass capillary exposed. As diagramed in Figure 2.10C, the inner electrode is fed through the glass capillary, held at ground potential, and cut such that the electrode traverses ½ to ¾ of the way through the portion of the glass capillary wrapped in copper tape. The glass capillary is held in place using a fingertight PEEK nut tightened onto the other end of the zero-dead-volume union, directly opposite the plasma gas line. The high voltage sine wave from the power supply described above is applied to the copper tape using an alligator clip. The amplitude of the sine wave was set just high enough to ignite the plasma, approximately 1.5 and 2 $kV_{0\text{-}p}$ for helium and nitrogen, respectively.

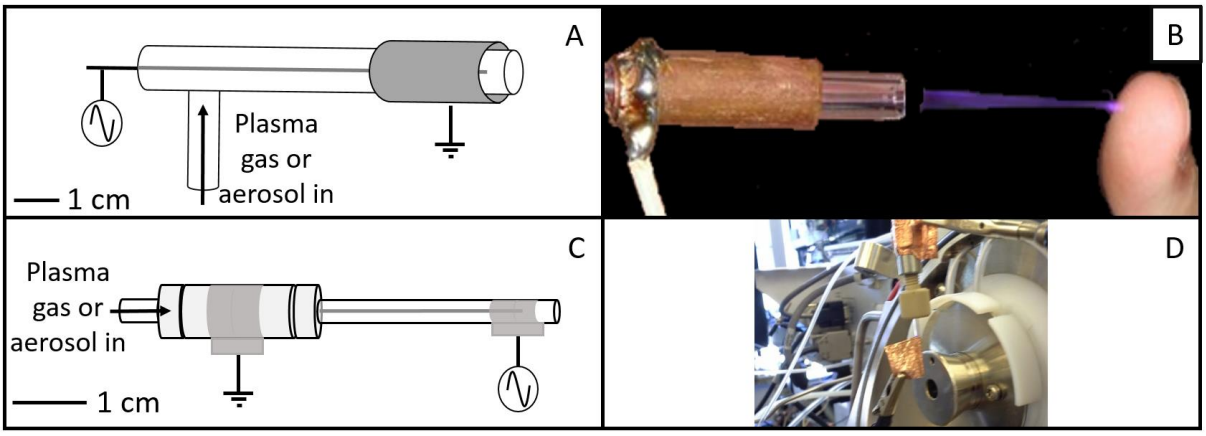

Figure 2.10. A. Schematic for and B. picture of the standard-size LTPI source and C. schematic for and D. picture of the miniature LTPI source used in these experiments.

The voltages applied to the inner and outer electrodes of the miniature LTPI source are

interchanged with respect to the standard-size LTPI source for practical reasons. To perform flow-through LTPI of an aerosol or gas, the analyte of interest is directed through the LTPI source. Though gases can be transported via non-conductive tubing, conductive tubing is required for aerosol transport to eliminate electrostatic losses due to localized charge build-up.[4] Application of the high voltage to the PEEK union when using the miniature LTPI source would cause the voltage to be applied through the tubing and to the case of the PyroProbe because the PEEK union is directly connected to the conductive aerosol transfer line. The case of the PyroProbe is directly connected to earth ground and thus if the high ac voltage was applied to the inner electrode via the PEEK union, the voltage would be directed to ground and no plasma would be generated. Consequently, the miniature LTPI source was operated with the voltage leads reversed in comparison to the standard-size LTPI source. Though this configuration presents a greater risk of electrical shock, the magnitude of the voltage as well as the area to which the voltage is applied on the miniature LTPI source is smaller and less exposed to the operator than for the standard-size LTPI source. Thus, the overall risk of operator contact with the high voltage on the miniature LTPI source is relatively low. However, precaution should still be taken when using the LTPI sources due to electrical shock hazards.

The experimental configuration for conventional LTPI-MS used in these experiments is shown in Figure 2.11. When the standard-size LTPI source is used, -4.5 kV dc was applied to the capillary inlet of the mass spectrometer as an extraction voltage to generate an electric field gradient to draw ions to the inlet of the mass spectrometer (Figure 2.11A). The extraction voltage is reduced to -1.0 kV when the miniature LTPI source was used. The miniature LTPI source can be placed closer to the inlet of the mass spectrometer without an electrical arc forming between the ion source and the mass spectrometer because a lower amplitude ac voltage is applied to the to generate the plasma (Figure 2.11B). Thus, a lower extraction voltage is used with the miniature LTPI source than for LTPI with the standard-size ion source.

2.4 Mass spectrometry

2.4.1 Gas chromatography-mass spectrometry

GC-MS was performed on a HP6890 GC system with a HP 5973 mass selective detector (Agilent Technologies, Santa Clara, CA). E-liquids were diluted by a factor of 10 or 50 in methanol and manually

injected in splitless mode onto a DB-5 column (30 m length, 0.250 mm diameter, 0.25 μm film). The helium carrier gas was at 7 psi with a total flow rate of 24.1 mL/min and the GC inlet was held at 250 °C. Table 2.1 summarizes the GC separation method used for the experiments.

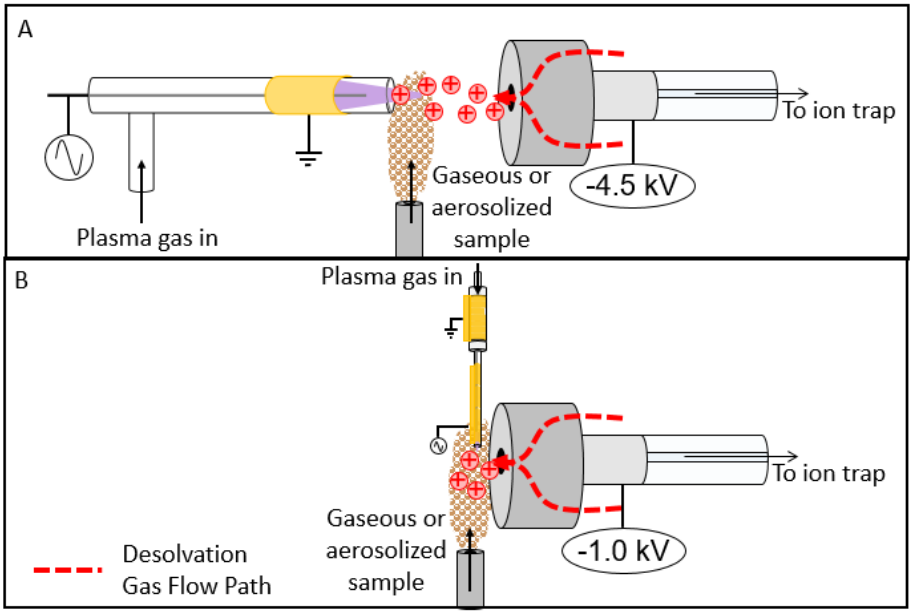

Figure 2.11. Conventional LTPI-MS experimental set up with the A. standard-size LTPI source and B. miniature LTPI source for analysis of gaseous or aerosolized samples.

The auxiliary transfer line to the electron impact (EI) source to the single quadrupole mass spectrometer was held at 320 °C. A solvent delay of 2.5 minutes was employed. The mass spectrometer was operated in Scan mode with a sampling rate of 1.87 scans/second. The mass range was scanned from 1.60 to 800 amu. The electron multiplier voltage was set to 0 with a relative voltage of 1953 V. EI mass spectra of unknowns were compared to the mass spectra in the NIST08 EI database.

Table 2.1. GC-MS heating profile for separation of compounds from e-cigarette liquids.

Oven Ramp	°C/min	Next °C	Hold (min)
Initial	---	60	2
Ramp 1	60	120	0
Ramp 2	10	200	0
Ramp 3	60	280	0

2.4.2 Ion trap mass spectrometry

Three mass spectrometers were used for mass analysis of ions generated. The first is a Bruker

Esquire 3000 (Bruker Daltonics, Billerica, MA) quadrupole ion trap mass spectrometer. The nebulizer gas pressure was 10 psi above atmospheric pressure. The desolvation gas flow rate was set to 5.0 L/min to reduce transmission of neutrals into the mass spectrometer and the inlet capillary temperature was set to 300 °C. The ion optics were set to optimally transmit ions in the range of 50 to 500 Da. The ion optics voltages were as follows: skimmer 1 = 22.1 V, skimmer 2 = 6.0 V, capillary exit offset = 68.7 V, octopole = 2.35 V, octopole rf = 75.0 $V_{0\text{-}p}$, octopole voltage difference = 2.40 V, lens 1 = -5.0 V, lens 2 = -60.0 V, trap drive = 32.1. The instrument was operated in Standard-Normal mode with a scan rate of 13,000 (*m/z*)/s. The ion current control was set to 70,000 with a maximum accumulation time of 200 ms. Mass spectra were collected over the range of 15-1,000 Da. Each mass spectrum is the average of 10 individual mass spectra and rolling averaging was off. Ions were isolated for collision induced dissociation (CID) with an isolation width of 1.0 Da. An activation voltage of 0.40 V was used and the excitation time was 40.0 ms.

The second instrument used for mass analysis is a Bruker HCT (Bruker Daltonics, Billerica, MA). The nebulizing gas pressure was 2.0 psi above atmospheric pressure and the capillary inlet to the mass spectrometer was set to 300 °C. The desolvation gas flow rate was 2.0 L/min to prevent transmission of neutrals into the mass spectrometer. The ion optics were set to optimally transmit ions in the range of 50 to 500 Da. The ion optics voltages were as follows: end plate offset = -500 V, skimmer = 40.0 V, capillary exit = 102.3 V, octopole 1 dc = 8.00 V, octopole 2 dc = 1.70 V, octopole rf = 59.15 $V_{0\text{-}p}$, lens 1 = -5.0 V, lens 2 = -60.0 V, trap drive = 35.1. The instrument was operated in Ultra Scan mode with a scan rate of 26,000 (*m/z*)/s. The ion current control was set to 100,000 with a maximum accumulation time of 200 ms. Mass spectra were collected over the range of 15-500 Da. Each mass spectrum is was the average of 10 individual mass spectra and 10 rolling averages were used. Ions were isolated for CID with an isolation width of 1.0 Da. An activation voltage of 0.80 V was used and the excitation time was 40.0 ms.

The third instrument used for mass analysis is a Thermo Scientific LTQ-FTICR (Waltham, MA). To generate an electrospray, -3.94 kV was applied to the ESI emitter and solvent flow rate was 3 μL/min. The capillary inlet to the mass spectrometer was held at 16.93 V and the capillary temperature was set to 275 °C. The sheath flow was 0.03 AU, the auxiliary flow rate was 0.33 AU and the sweep gas flow rate was 0.12 AU. The ion optics were optimized and the Fourier transform ion cyclotron resonance (FTICR)

mass analyzer was calibrated prior to each experiment to ensure optimum signal response. Mass spectra were collected over the range of 50 – 500 Da. The ion trap was operated with the mass range and scan rate in Normal mode. Each mass spectrum was the average of three microscans. The ion current control was set to 3 x 10^4 for a full MS scan and 1 x 10^4 for MS^n with a maximum accumulation time of 10 ms. Ions were isolated for CID with a width of 1.0 Da. Activation was performed using a normalized collision voltage of 35%. The activation q value was 0.25 and the ion activation time was 30.0 ms. The FTICR was operated with a resolution of 100,000 and a scan type of Full. Each mass spectrum was a single microscan and the ion current control was set to 2 x 10^5 for full MS scans and 1 x 10^5 for MS^n. The maximum ion injection time was 1,000 ms.

2.5 Differential ion mobility spectrometry

The planar DIMS device was designed to be used on the Bruker HCT and is shown in Figure 2.12. The electrodes are 10 mm long and 4 mm wide with a gap between the electrodes of 0.3 mm. The DIMS assembly is designed such that the spray shield on the mass spectrometer inlet can be removed and the DIMS assembly installed in its place. To couple the DIMS device to the inlet of the mass spectrometer, a planar flare was implemented after the electrodes. This flare allows the device to couple to a standard glass inlet capillary and maintain greater than 80% ion transmission through the assembly when both electrodes are held at the same potential. A nitrogen desolvation gas is already implemented in the source region of the mass spectrometer to assist in solvent evaporation during ESI. This desolvation gas is redirected through the housing of the assembly and serves as the carrier gas through

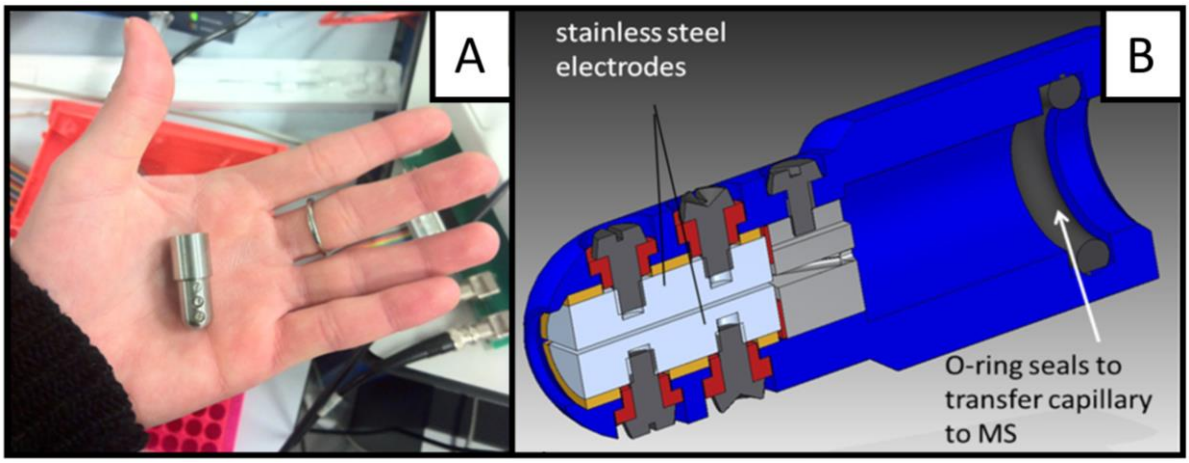

Figure 2.12. A. Picture and B. AutoCAD drawing of the DIMS assembly used for the experiments described herein.

the DIMS assembly. The DIMS electrodes are held at the same potential as the transfer capillary to which the ESI voltage is applied without DIMS.

Ideally, a rectangular waveform would be used for DIMS, alternating between low (<10 kV/cm)[13-15] and high (>10 kV) electric fields of opposing polarity. However, most DIMS waveforms are bisinusoidal, approximating a square wave because of the power requirements of high voltage, high frequency rectangle waves.[15] To approximate a rectangular waveform, a sinusoidal voltage at a set frequency and amplitude is applied to one of the electrodes, and a phase-shifted sinusoidal voltage at twice the frequency and approximately one-half the amplitude is applied to the other electrode. These waveforms are additive across the gap between the electrodes and produce an electric field equivalent to the sum of the two individual sinusoidal waveforms (Figure 2.13). The dispersion voltage (DV) is defined as the maximum $V_{0\text{-}p}$ of the bisinusoidal waveform. The dispersion field (E_D) is defined as the DV divided by the gap between the DIMS electrodes. The power supply implemented for these experiments employs a sinusoidal waveform at 2 MHz and a lower amplitude sinusoidal wave at 4 MHz added to form the bisinusoidal DIMS waveform at frequency of 2 MHz.

To adjust the trajectory of the ions to be stable through the DIMS device, a compensation voltage is applied to one electrode to generate a compensation field (E_c) between the parallel DIMS electrodes and transmit ions of a specific differential ion mobility. A static voltage can be selected to operate DIMS in "filter mode". A LabVIEW program linked to the Bruker instrument control software is used to define a static compensation voltage or to control the range of compensation voltages. In the "scanning mode", the compensation field is stepped over a range of voltages specified in the LabVIEW program to sequentially transmit ions over a corresponding range of differential mobilities. Each time point is an average of ten mass spectra and is equivalent to one compensation voltage step, where the step size is specified in the LabVIEW program.

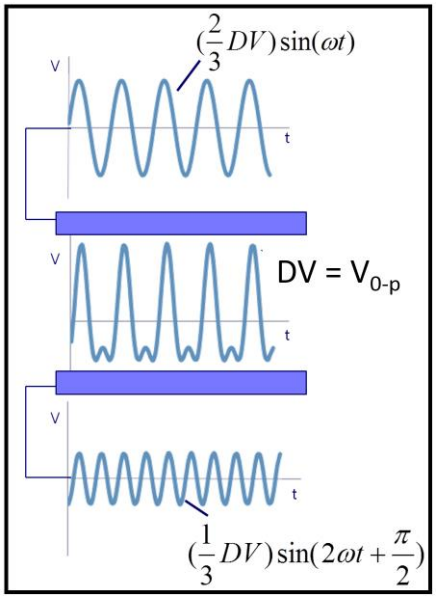

Figure 2.13. Simplified representation of the generation of a bisinusoidal waveform with two sinusoidal waveforms.

DIMS spectra were constructed by plotting the extracted ion current or total ion current from the Bruker Data Analysis 4.1 software as a function of analysis time. Several time-to-voltage points were recorded during each DIMS scan and were used to convert the time axis of the chromatogram to voltage in Microsoft Excel. The conversion is applied by using one time-to-voltage point and the compensation voltage step size to determine the voltage at each previous and subsequent time point. The other time-to-voltage points are used to confirm that there is no error in using the step size throughout the time-to-voltage conversion in the DIMS scan. The compensation voltage for each time point is then divided by the gap size (0.03 cm) of the DIMS device to convert to E_c for the x-axis of the DIMS spectra.

2.6 Data analysis

Principal component analysis was performed using SAS 9.3. The script is shown in Figure 2.14. Product ions were designated as present (1) or absent (0) in the MS/MS spectrum of each ion for

Figure 2.14. SAS 9.3 script for generation of a principal component analysis of the product ions generated by tandem mass spectrometry.

```
data losses;

     infile datalines dsd;
     input [variable 1-variable n];

datalines;

     [comma delimited data set];

run;

proc factor data=losses
            simple
            method=prin
            priors=one
            nfact=3
            mineigen=1
            scree
            rotate=varimax
            flag=.32
            out=pca;
     var v1  v2  v3  v4  v5  v6  v7  v8  v9  v10 v11 v12 ;
run;
proc gplot data=pca;
     plot Factor1*Factor2;
run;
proc g3d data=pca;
     scatter Factor1*Factor2=Factor3;
run;

proc print data=pca;
run;
```

submission of the data to the PCA. The program was designed to use the values for the 12 neutral losses or gains with the smallest mass.

REFERENCES

1. Yaman, S. Pyrolysis of biomass to produce fuels and chemical feedstocks. *Energy Conversion and Management* **2004***, 45*, 651-671.

2. Pall Life Sciences, Pall Coorporation. Pallflex Filters: Emfab, Fiberfilm and Tissuquartz Filters. *https://www.pall.com/pdfs/Laboratory/02. 0601_Pallflex_LR.pdf* **2002***, 2014*, 2.

3. Parshintsev, J. Comparison of quartz and Teflon filters for simultaneous collection of size-separated ultrafine aerosol particles and gas-phase zero samples. *Anal. Bioanal. Chem.* **2011***, 400*, 3527-3535.

4. Timko, M. T.; Yu, Z.; Kroll, J.; Jayne, J. T.; Worsnop, D. R.; Miake-Lye, R. C.; Onasch, T. B.; Liscinsky, D.; Kirchstetter, T. W.; Destaillats, H.; Holder, A. L.; Smith, J. D.; Wilson, K. R. Sampling Artifacts from Conductive Silicone Tubing. *Aerosol Sci. Technol.* **2009***, 43*, 855-865.

5. Wu, C.; Siems, W. F.; Hill Jr., H. H. Secondary Electrospray Ionization Ion Mobility Spectrometry/Mass Spectrometry of Illicit Drugs. *Anal. Chem.* **2000***, 72*, 396-403.

6. Takats, Z.; Wiseman, J. M.; Cooks, R. G. Ambient mass spectrometry using desorption electrospray ionization (DESI): instrumentation, mechanisms and applications in forensics, chemistry, and biology. *J. Mass Spectrom.* **2005***, 40*, 1261-1275.

7. Liu, J.; Wang, H.; Manicke, N. E.; Lin, J. M.; Cooks, R. G.; Ouyang, Z. Development, characterization, and application of paper spray ionization. *Anal. Chem.* **2010***, 82*, 2463-2471.

8. Law, W. S.; Wang, R.; Hu, B.; Berchtold, C.; Meier, L.; Chen, H.; Zenobi, R. On the mechanism of extractive electrospray ionization. *Anal. Chem.* **2010***, 82*, 4494-4500.

9. Konermann, L.; Ahadi, E.; Rodriguez, A. D.; Vahidi, S. Unraveling the mechanism of electrospray ionization. *Anal. Chem.* **2013***, 85*, 2-9.

10. Ridgeway, M. E.; Remes, P. M.; McKinney, C.; Glish, G. L. In *In Radio Frequency Power Supply for the Production of High Amplitude Asymmetric Waveforms;* 56th ASMS Conference on Mass Spectrometry and Allied Topics; 2008; Vol. American Society for Mass Spectrometry; Denver.

11. Harper, J. D.; Charipar, N. A.; Mulligan, C. C.; Zhang, X. R.; Cooks, R. G.; Ouyang, Z. Low-Temperature Plasma Probe for Ambient Desorption Ionization. *Anal. Chem.* **2008***, 80*, 9097-9104.

12. Wiley, J. S.; Shelley, J. T.; Cooks, R. G. Handheld Low-Temperature Plasma Probe for Portable “Point-and-Shoot” Ambient Ionization Mass Spectrometry. *Anal. Chem.* **2013***, 85*, 6545-6552.

13. Mason, E. A.; McDaniel, E. W. *Transport Properties of Ions in Gases;* Wiley: New York, 1988; .

14. Eiceman, G. A.; Karpas, Z. *Ion Mobility Spectrometry;* CRC Press: 2005; Vol. 1.

15. Purves, R. W.; Guevremont, R.; Day, S.; Pipich, C. W.; Matyjaszczyk, M. S. Mass Spectrometric Characterization of a High-Field Asymmetric Waveform Ion Mobility Spectrometer. *Rev. Sci. Instrum.* **1998***, 69*, 4094-4105.

CHAPTER 3: IONIZATION OF COMPOUNDS FROM AEROSOL PARTICLES COLLECTED ON FILTERS

3.1 Introduction

Collection of aerosol particles onto filters is a common sampling method for aerosol analysis because it exhibits unique advantages over direct atmospheric monitoring. For example, aerosol particles can be collected from ambient air onto filters over the course of hours to days to increase the quantity of sample for analysis.[1,2] Filters are also used in portable aerosol particle collection devices for monitoring personal exposure.[3] Collecting aerosol particles on filters prior to compositional analysis facilitates aerosol sample transport as compared to deploying a mass spectrometer[4] or transporting containers of aerosol samples that may deposit onto the walls of the vessel[5,6]. For the reasons described above, it is important to continue to develop methods for the analysis of compounds from aerosol particles collected on filters.

After aerosol particle collection, samples are often stored in a refrigerator or freezer prior to extraction of compounds from the filter.[7,8] However, storage of filters could potentially result in evaporative losses of semi-volatile compounds[9,10] or polymerization of reactive compounds in the aerosol particles[11]. Compounds from aerosol particles are typically extracted from filters[12,13] and derivatized[12-14] prior to analysis by mass spectrometry (MS). Typical extraction protocols call for sonication of the filter in a small volume of organic solvent for up to an hour.[12,15] Storage of compounds extracted from a filter in solution may still result in polymerization[11] or reactions of the analyte molecules with the solvent[16]. The time required for analysis and thus the potential for secondary reactions and evaporation of semi-volatile compounds from aerosol particles can be drastically reduced by eliminating sample storage and a separate compound extraction step prior to MS. In recent years, ambient ionization techniques have been developed to ionize compounds directly from surfaces.[17,18] These ionization techniques may be applied to the analysis of compounds from aerosol particles that have been collected on filters. In this chapter, the influence of the storage time on the composition of aerosol particles produced by pyrolysis of natural polymers collected on filters and extracted is evaluated. Desorption electrospray ionization (DESI) and

paper spray ionization of compounds from aerosol particles collected on filters are compared to electrospray ionization (ESI) of analytes in aerosol particles extracted from filters.

3.2 Electrospray ionization of compounds extracted from aerosol particles collected on filters

The experiments described in this chapter were performed on the Bruker Esquire ion trap mass spectrometer. Ethyl cellulose was pyrolyzed at approximately 600 °C in the custom pyrolysis chamber and the aerosol particles produced were collected on a tetrafluoroethylene (TFE) coated borosilicate glass filter following the procedure in Chapter 2.2.3. The filter was cut into thirds with clean scissors and the compounds from the aerosol particles collected on each third of the filter were extracted into either methanol, acetonitrile, or 50/49/1 methanol/water/acetic acid as described in Chapter 2.2.3. An aliquot of the filter extract was diluted by a factor of 10 in the respective extraction solvent and ESI was performed on the diluted filter extract. The ESI mass spectra shown in Figure 3.1 are from a blank filter segment collected and extracted in the same manner as the sample and electrosprayed in the extraction solvent of 50/49/1 methanol/water/acetic acid (Figure 3.1A), methanol (Figure 3.1B), or acetonitrile (Figure 3.1C).

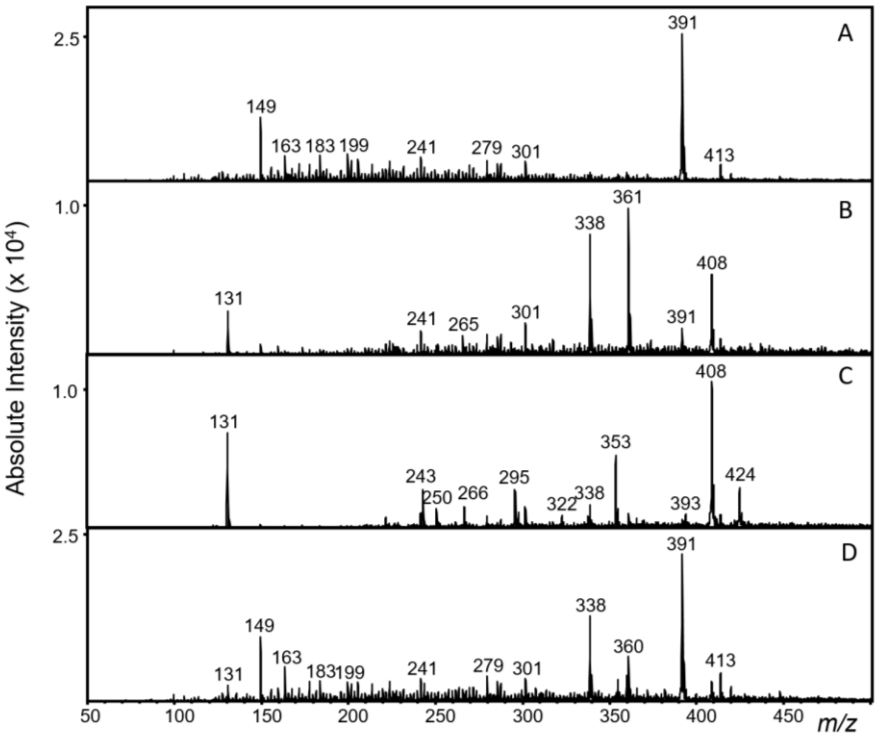

Figure 3.15. ESI-MS of a blank filter, extracted, diluted by a factor of 10 and ionized using an electrospray solvent of A. 50/49/1 methanol/water/acetic acid B. 100% methanol C. 100% acetonitrile and D. extracted in 100% methanol and diluted by a factor of 10 into 50/49/1 methanol/water/acetic acid for ESI.

As shown in Figure 3.2 for extracts diluted by a factor of 10 and ionized by ESI, the extraction and electrospray solvent influence the ions observed in the mass spectrum. The inset mass spectra in Figure 3.2B and 3.2C are the expanded low mass-to-charge ratio regions of the mass spectrum. The distribution and identity of the ions formed by ESI changes when the extraction and ESI solvent is 50/49/1 methanol/water/acetic acid (Figure 3.2A), 100% methanol (Figure 3.2B) or 100% acetonitrile (Figure 3.2C). Specifically, different ions are observed at high mass-to-charge ratios in the ESI mass spectrum of the diluted 50/49/1 methanol/water/acetic acid filter extract as opposed to the diluted methanol or acetonitrile filter extract. Though the distribution of the ions at low mass-to-charge ratios generated by ESI with each solvent is the same (Figure 3.2A and the insets of Figures 3.2B and 3.2C), the absolute intensity of the ions observed is decreased when methanol or acetonitrile is used as the extraction and ESI solvent instead of 50/49/1 methanol/water/acetic acid.

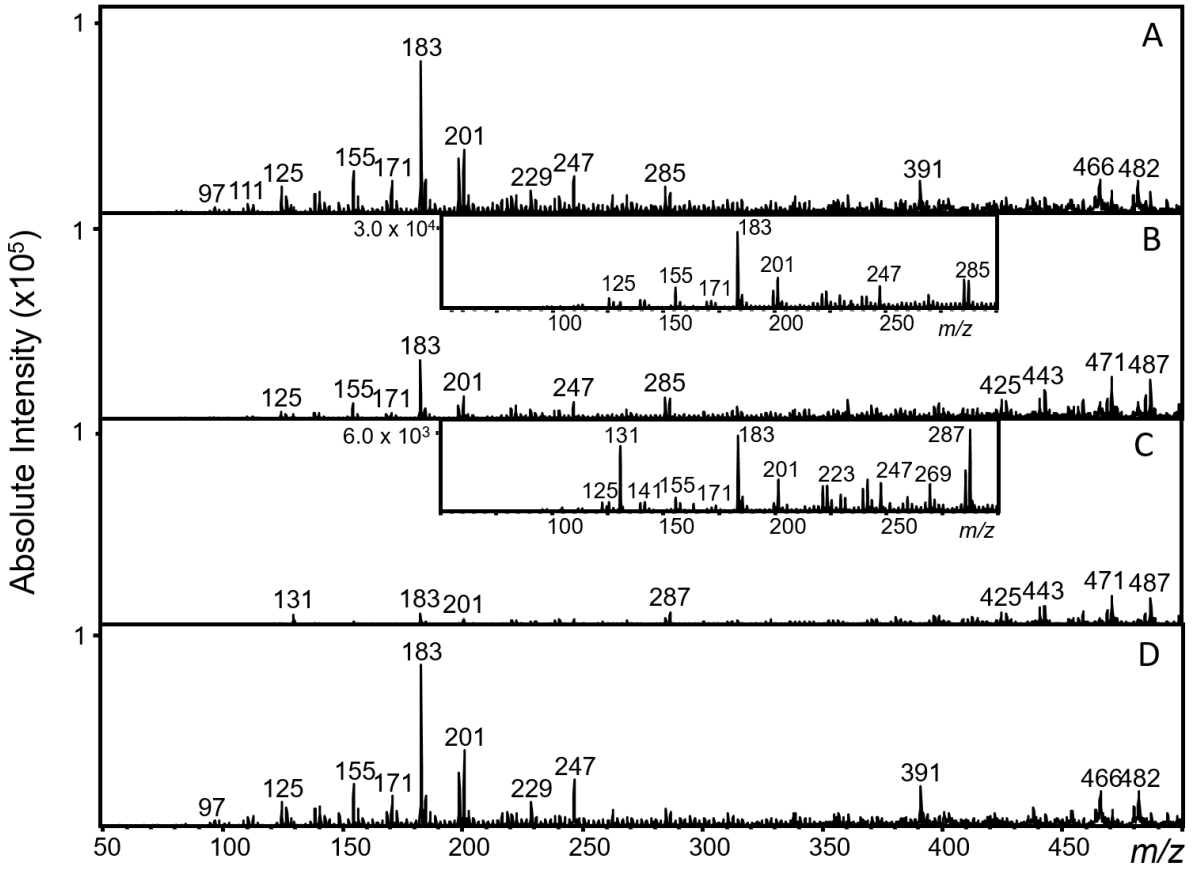

Figure 3.2. ESI-MS of the compounds from the aerosol produced by pyrolysis of ethyl cellulose collected on a filter, extracted in methanol, diluted by a factor of 10, and ionized using A. 50/49/1 methanol/water/acetic acid B. 100% methanol C. 100% acetonitrile and D. extracted in 100% methanol and diluted by a factor of 10 into 50/49/1 methanol/water/acetic acid for ESI. Prominent background ions are observed at m/z 285, 287, and 391. Acetonitrile solvent background ion at m/z 131.

The solvent dependent differences observed in the mass spectra can be attributed to the extraction and/or ionization efficiency. To determine if the differences in the ions observed in the mass spectra are due to extraction or ionization, an aliquot of the methanol filter extract was diluted by a factor of 10 into an electrospray solvent with a final composition of 50/49/1 methanol/water/acetic acid rather than diluting the filter extract by a factor of 10 into an electrospray solvent with the same composition as the extraction solvent. The ESI mass spectrum observed from the extracted blank filter is displayed in Figure 3.1D and the mass spectrum observed from pyrolyzed ethyl cellulose collected onto a filter, extracted into methanol, and electrosprayed from 50/49/1 methanol/water/acetic acid is shown in Figure 3.2D. When the methanol filter extract is electrosprayed from 50/49/1 methanol/water/acetic acid the mass spectra of the blank and sample appear nearly identical to the mass spectra observed when 50/49/1 methanol/water/acetic acid is used as both the extraction and ESI solvent. Thus, it is concluded that the differences in the mass spectra shown in Figure 3.2A-C are due to differences in ionization efficiency because of the electrospray solvent rather than solvent dependent differences in the extraction efficiency of the analytes from the filters. For subsequent experiments, methanol was selected as the extraction solvent because it is commonly used for extraction and no significant differences in the identity of the compounds extracted from the aerosols collected on filters was observed for the solvents investigated. The filter extracts were diluted into 50/49/1 methanol/water/acetic acid because the best signal response was observed for this ESI solvent system.

3.3 Effect of sample storage on the compounds observed

3.3.1 Storage of samples extracted from filters

The aerosol produced from ethyl cellulose pyrolyzed in the custom pyrolysis chamber at approximately 400 °C was collected on a TFE coated borosilicate glass fiber filter. The filter was cut into thirds with clean scissors and the compounds on one of the filter segments were extracted into methanol. The methanol filter extract was diluted by a factor of 100 into 50/49/1 methanol/water/acetic acid and stored at -18 °C for up to 7 days prior to ionization of the compounds in the methanol extract by ESI. Displayed in Figure 3.3 are the mass spectra observed when the compounds extracted from the aerosol particles on the filter are ionized by ESI immediately (Day 0, Figure 3.3A), on Day 1 (Figure 3.3B), Day 2 (Figure 3.3C), or Day 7 (Figure 3.3D). The red asterisks denote ubiquitous background ions such as

phthalates and stearic acid observed from the filter blanks (Figure 3.1) that are present in lab air or on surfaces and vary in intensity from day to day.

Changes in the relative abundance of ions occur after storage of the filter. The data in Figure 3.3 show that storage of filter extracts in methanol most likely does not result in polymerization of analyte molecules because the absolute intensity of the ions at higher mass-to-charge ratios does not increase with time. The absolute and relative ion intensity varies from day to day, and a net decrease is observed in the signal intensity of ions generated by ESI of the methanol extract within the first 24 hours of storage of methanol extracts of filters. Differences in the ions observed in the mass spectra shown in Figure 3.3 could be due to chemical transformation, adsorption of compounds onto the walls of the vessel, extraction of compounds from the container, and/or evaporation of analytes during storage at -18 °C.

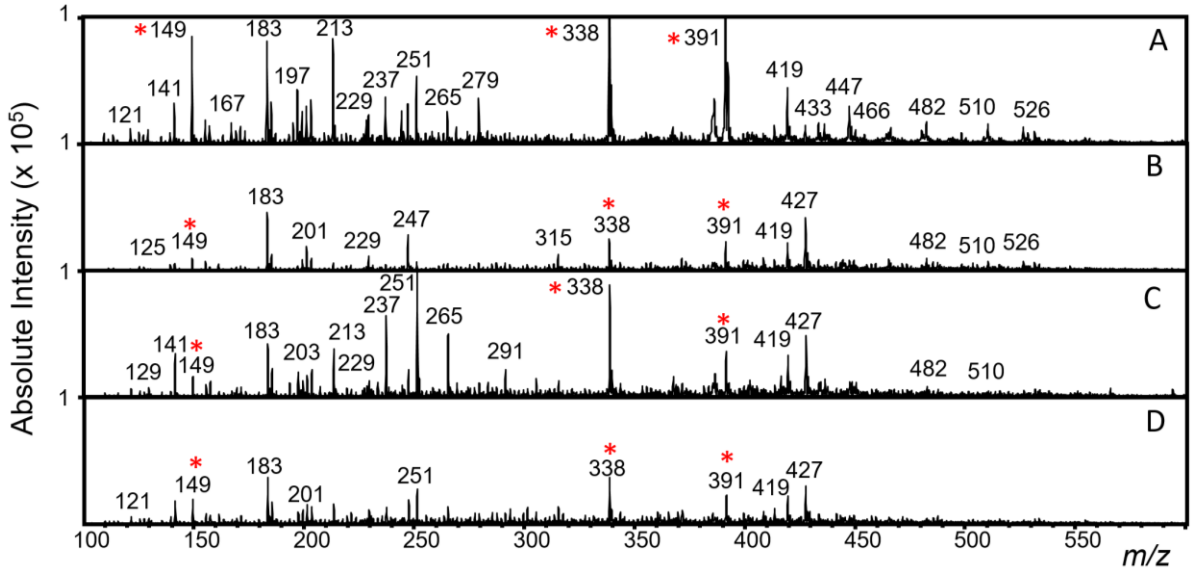

Figure 3.3. ESI-MS of the compounds from the aerosol produced by the pyrolysis of ethyl cellulose collected on filters, extracted in methanol, diluted by a factor of 100 and ionized by ESI A. immediately after extraction on Day 0 or after storage at -18 °C on B. Day 1 C. Day 2 D. Day 7.

3.3.2 Storage of unprocessed filters

To investigate the influence of storage time on the composition of aerosol particles produced by pyrolysis and collected on TFE coated borosilicate glass fiber filters, the remaining two filter segments from the experiments presented in Section 3.3.1 were stored at -18 °C for up to 14 days prior to analyte extraction. For each analysis, the compounds on one of the filter segments were extracted into methanol and the filter extract was diluted by a factor of 100 into 50/49/1 methanol/water/acetic acid prior to ESI. As

shown in Figure 3.4, differences in the ESI mass spectra are observed when the compounds on the filter were extracted into methanol immediately after sample generation or after storage of the filter. The insets in Figure 3.4 are the full mass spectra compared on the same intensity scale to visualize the decrease in absolute signal intensity. The red asterisks denote background ions. The absolute signal intensity decreased after 7 days of storage (Figure 3.4A, Intensity 1 x 10^5; Figure 3.4B, Intensity 8 x 10^4). When the filter was stored at -18 °C for 14 days and the compounds from one filter segment were extracted into methanol on Day 14, the same effect was observed, though to a greater extent (Figure 3.4C, Intensity 4 x 10^4). The methanol filter extract generated on Day 7 was stored at -18 °C and extracted for analysis on Day 14 (Figure 3.4D). Storage of the methanol filter extract for seven days results in further decrease in the absolute signal intensity (Intensity 1.5 x 10^4). The differences in the abundance and identity of analyte ions are due to chemical transformation and/or evaporation of the semi-volatile analytes from the

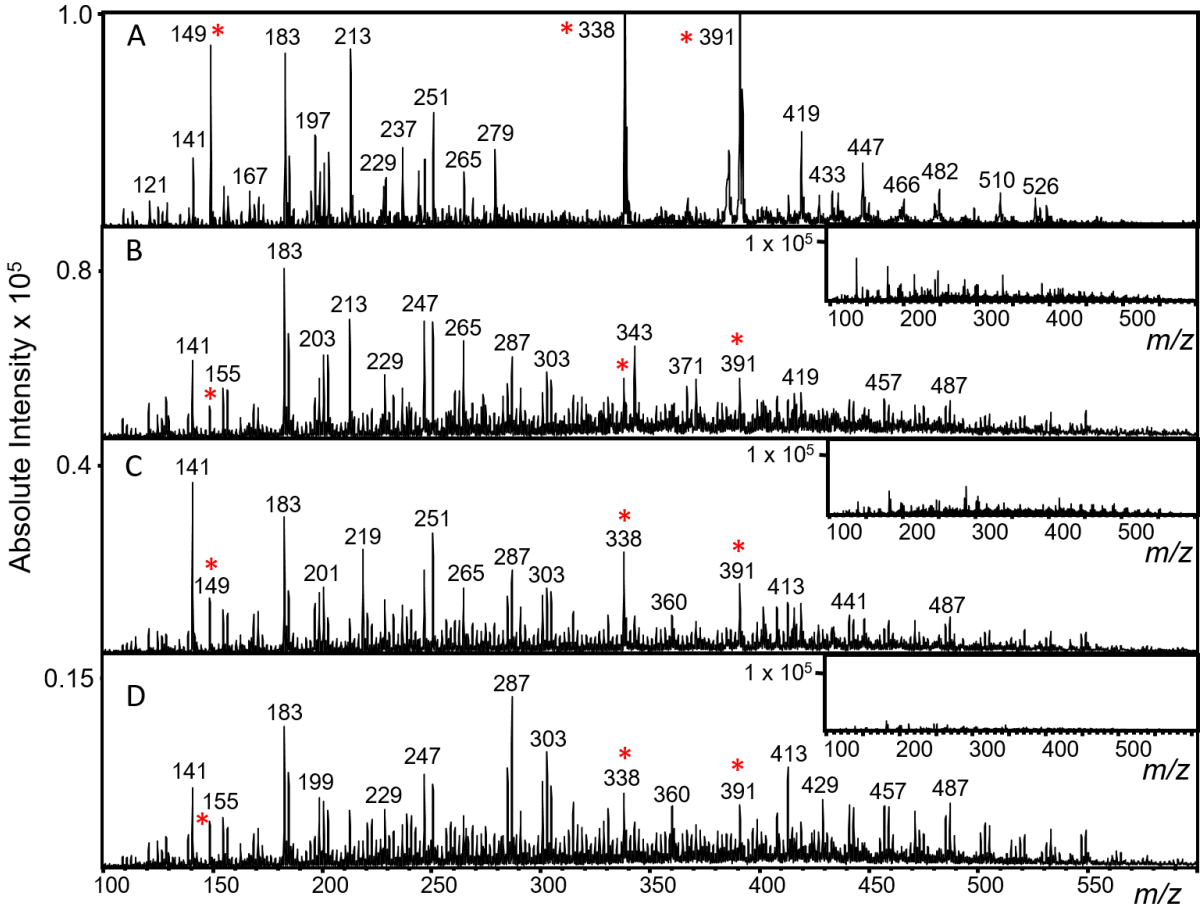

Figure 3.4. ESI-MS spectra observed when the aerosol produced from the pyrolysis of ethyl cellulose was collected on filters and stored at -18 °C prior to A. extraction Day 0, analysis Day 0, B. extraction Day 7, analysis Day 7, C. extraction Day 14, analysis Day 14 and C. extraction Day 7, analysis Day 14.

filter. Extraction of the filter on Day 7 and storage of the methanol filter extract at -18 °C until Day 14 results in a greater decrease in signal intensity than when the filter is stored at -18 °C prior to extraction on Day 14. This result indicates that if a sample must be stored, storage of the filter will result in fewer changes in chemical composition and/or evaporative losses of analyte than storage of the extract.

To confirm that the semi-volatile compounds are evaporating from the filters during storage, the gas phase compounds evaporating from the filter must be analyzed. Secondary electrospray ionization (SESI) is a derivative of ESI that generates ions from a volatilized analyte by directing an electrospray plume through the gaseous sample. Ions can be generated by SESI via two mechanisms: interaction of the gaseous neutrals with the charged electrospray droplet surface or chemical ionization by interaction of the protonated solvent molecules with the gaseous analyte molecules.[19] The description and experimental configuration of SESI used for these experiments are discussed in Chapter 2.3.1 and shown in Figure 2.4. The aerosol particles produced by the pyrolysis of ethyl cellulose in the custom pyrolysis chamber at approximately 600 °C were collected on a TFE coated borosilicate glass fiber filter and the gaseous semi-volatile compounds near the surface of the filter were ionized by SESI. The mass spectra generated are shown in Figure 3.5 for a SESI solvent of 100% methanol (Figure 3.5A) and 100% acetonitrile (Figure 3.5B). No consistent ion signal above background was observed when 50/49/1 methanol/water/acetic acid was used as the SESI solvent. As expected based on the ESI results shown

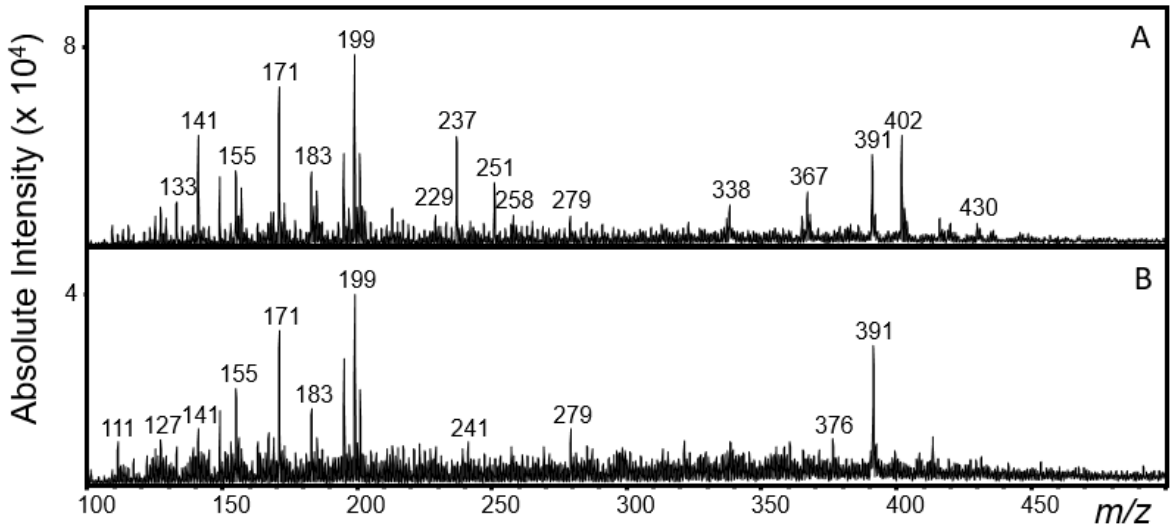

Figure 3.5. SESI-MS spectra of the volatile compounds from the aerosol particles produced from pyrolyzed ethyl cellulose collected on filters when the SESI solvent is A. methanol or B. acetonitrile.

in Figures 3.3 and 3.4 and the premise that compounds with a lower mass will typically be more volatile, ions are observed from SESI primarily at low mass-to-charge ratios. Formation of low mass-to-charge ratio ions from compounds in the gas phase over the surface of filters confirms that differential evaporation of semi-volatile compounds from the aerosol particles produced by pyrolysis of natural polymers collected on filters readily occurs. Tandem mass spectrometry experiments could be performed to determine if the compounds in the gas phase are the same as the compounds ionized from the filter.

3.4 Ionization of compounds in aerosol particles directly from filters

3.4.1 Desorption electrospray ionization

Desorption electrospray ionization (DESI) is an ambient ionization technique that can be used to generate ions from compounds on insulating surfaces.[17] The experimental DESI design used for these experiments is described in Chapter 2.3.2 and diagramed in Figure 2.5. For small molecules such as the pyrolysis products of natural polymers, DESI of compounds from surfaces occurs by one of three mechanisms: interaction of the analyte with the charged surface of the electrospray droplet, sputtering of chemicals from the surface, or ion-molecule reactions between protonated solvent molecules and volatile compounds that have evaporated from the surface.[20] DESI has previously been used to analyze the composition of secondary organic aerosols collected on filters.[21,22] DESI was used to analyze compounds from the aerosol particles produced by pyrolysis of ethyl cellulose collected on filters in positive mode for comparison to ESI. 50/49/1 methanol/water/acetic acid, methanol, or acetonitrile were used as the solvent to ionize analytes collected on the surface of the filter by DESI. The influence of the DESI solvent composition on the ions generated is shown in Figure 3.6. The greatest overall ion intensity is observed when 50/49/1 methanol/water/acetic acid is used as the DESI solvent (Figure 3.6A, Intensity 8000). The absolute intensity of the ions in the mass spectrum is decreased by an order of magnitude when methanol is used as the DESI solvent (Figure 3.6B, Intensity 800), and when acetonitrile is used as the DESI solvent, no high mass ions are observed (Figure 3.6C, Intensity 500).

Two ion distributions are observed from DESI of the compounds from pyrolyzed ethyl cellulose aerosol particles collected on TFE coated borosilicate glass fiber filters: one distribution centered around 200 Da and the other centered at approximately 400 Da. The ions observed in the low mass-to-charge ratio distribution are similar to those observed from ESI and SESI. The high mass-to-charge ratio ion

distribution is only observed when methanol is present in the DESI solvent. The decrease in abundance of high mass-to-charge ratio ions is most likely due to poor ionization efficiency of analytes by DESI with acetonitrile. Polymerization was not observed from ESI of the pyrolyzed ethyl cellulose filter extract and thus is not expected to be the cause of the high mass-to-charge ratio ions observed in DESI. Though methanol can react with carboxylic acids in acidic conditions,[23] reports of this phenomenon during DESI or ESI were not be found in the literature. Experiments to ensure that this reaction is not occurring are detailed in Chapter 8.

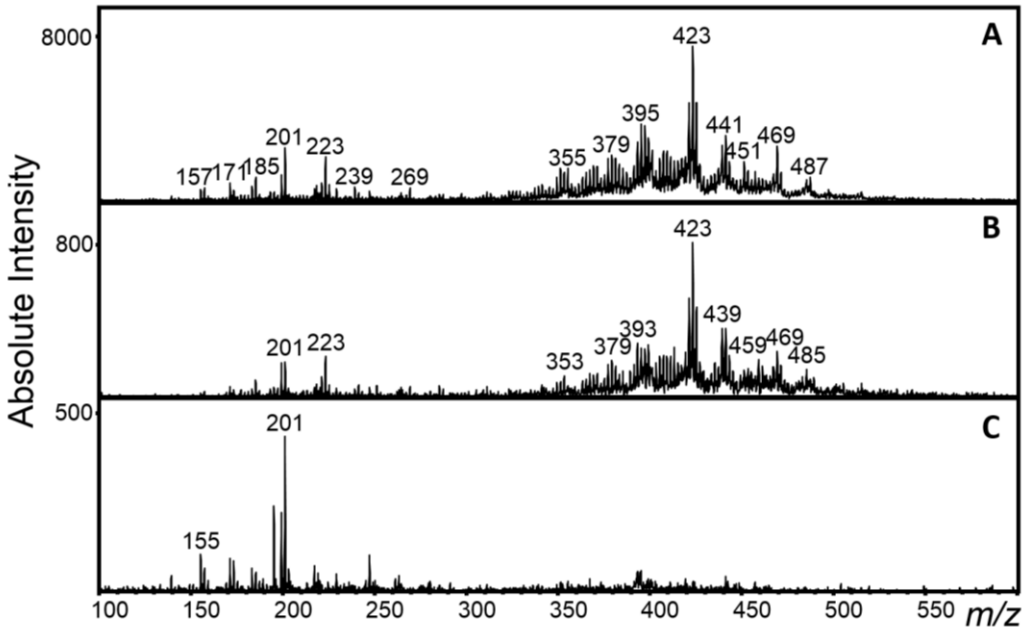

Figure 3.6. DESI-MS of the compounds produced by the pyrolysis of ethyl cellulose and collected on a filter using A. 50/49/1 methanol/water/acetic acid B. methanol and C. acetonitrile.

3.4.2 Paper spray ionization

Paper spray ionization is an alternative to DESI that is amenable to compounds on a porous, non-conductive substrate. Paper spray ionization utilizes the porous media to which the sample is applied, in this case the TFE coated borosilicate glass fiber filter, to generate an electrospray.[18,24] The porous media is cut such that it has a sharp, pointed tip and is wetted with the electrospray solvent. A high voltage is applied to the substrate and electrophoresis causes the solvent and analyte to migrate across the surface and through the channels of the porous substrate, extracting analytes from the substrate and generating an electrospray plume from the pointed tip.[18,25] The paper spray ionization source used for these experiments is described in Chapter 2.3.3 and shown in Figure 2.6. Ethyl cellulose

was pyrolyzed in the custom pyrolysis chamber at approximately 600 °C and the aerosol produced by pyrolysis was collected on a TFE coated borosilicate glass fiber filter. The filter was cut into quarters, each quarter having a sharp 90° tip, and 50 μL of 50/49/1 methanol/water/acetic acid was deposited onto the filter. The resulting paper spray ionization mass spectrum is shown in Figure 3.7.

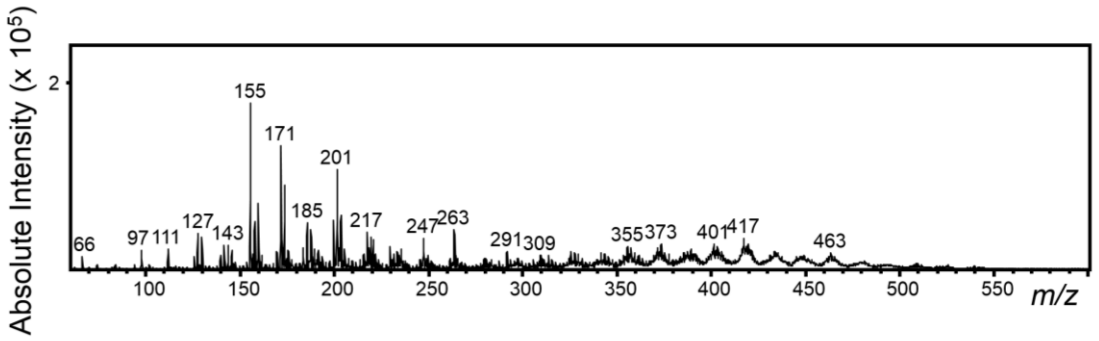

Figure 3.7. Paper spray mass spectrum observed from the aerosol produced by pyrolysis of ethyl cellulose collected on a filter and ionized using 50/49/1 methanol/water/acetic acid.

3.4.3 Comparison of ESI, DESI, and paper spray ionization

A higher intensity of low mass-to-charge ratio ions are generated from the pyrolysis products of ethyl cellulose collected on the filter by ESI or DESI as opposed to paper spray with the same spray solvent (Figure 3.2A or Figure 3.6A). ESI, DESI, and paper spray ionization were performed on aerosol particles collected onto a single filter to account for potential differences in the chemical composition of aerosol particles due to temperature dependent pyrolysis chemistry, sampling, and/or handling. A crude extract of cellulose from tobacco was pyrolyzed at approximately 600 °C in the custom pyrolysis chamber and the aerosol produced was collected on a TFE coated borosilicate glass fiber filter. The filter was cut into thirds with clean scissors and ESI, DESI, or paper spray ionization was used to ionize the compounds from the aerosol particles collected on the section of the filter. Prior to ESI, analytes from the filter section were extracted into methanol. The methanol extract was diluted by a factor of 100 into 50/49/1 methanol/water/acetic acid for ESI. The resulting mass spectra from ESI, DESI, and paper spray are displayed in Figure 3.8. The mass spectra shown in Figure 3.8 are different than in the previous sections because the data presented in Figures 3.5-3.7 is from pyrolyzed ethyl cellulose and Figure 3.8 is a pyrolyzed sample crudely extracted from tobacco.

A greater abundance of higher mass-to-charge ratio ions are observed in the ESI mass spectrum

(Figure 3.8A) as compared to either the DESI mass spectrum (Figure 3.8B) or the paper spray ionization mass spectrum (Figure 3.8C). Similar ions are observed in the DESI and paper spray ionization mass spectra of the pyrolyzed tobacco cellulose extract, though paper spray ionization results in a richer and more abundant ion distribution at low mass-to-charge ratios.

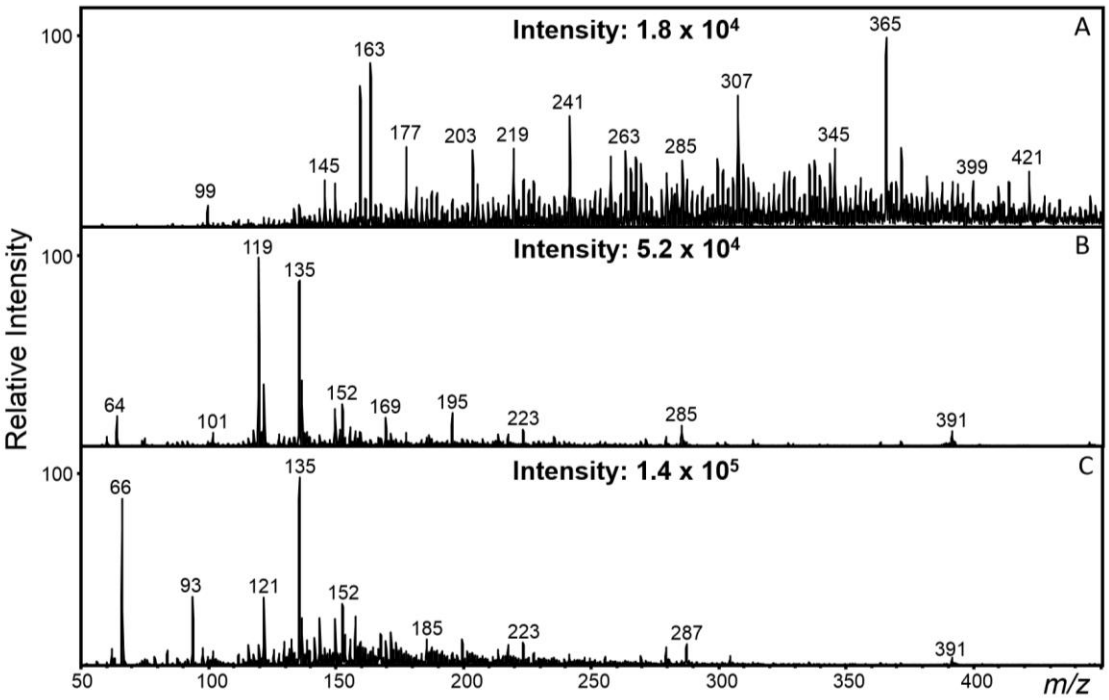

Figure 3.8. Pyrolyzed crude tobacco cellulose extract collected on filters prior to A. extraction in methanol and ESI B. DESI or C. paper spray ionization. The spray solvent used was 50/49/1 methanol/water/acetic acid for all experiments.

3.5 Summary and conclusions

Sampling of aerosol particles onto filters prior to analysis is a common aerosol sample preparation technique. However, concerns about reactions of analytes with the extraction solvent, polymerization reactions, adsorption of analytes onto the walls of the container, and evaporation of semi-volatile compounds in the sample have been raised. For the pyrolysate of ethyl cellulose collected onto TFE coated borosilicate glass fiber filters and extracted, ions were extracted with the same efficiency by methanol, acetonitrile, and 50/49/1 methanol/water/acetic acid and the ESI solvent composition has the most influence on the mass spectrum observed. Storing the pyrolysate of natural polymers as unprocessed filters or a solution of compounds extracted from filters prior to ionization results in evaporation of low volatility compounds as demonstrated using SESI-MS of the gaseous neutrals at the

surface of the filter. More analyte loss occurs from samples that are extracted and stored in solution than from samples stored on the filter, likely due to adsorption of analytes onto the walls of the container in addition to evaporation of semi-volatile compounds. No indication of time-dependent polymerization was observed, though the relative abundance of analytes changes throughout the time course of the experiment due to other chemical transformations or extraction of compounds from the walls of the container.

To expedite the analysis of compounds from aerosol particles collected on filters by MS, two ambient ion sources, DESI and paper spray ionization, are investigated as alternatives to traditional ESI experiments. Both ambient ionization techniques generate ions from compounds in aerosol particles collected on filters and eliminate the need for a separate extraction step. DESI and paper spray ionization also result in more ions at low mass-to-charge ratios than ESI. Overall, paper spray ionization results in a more abundant distribution of ions at low mass-to-charge ratios from the surface of the filter than either ESI or DESI for both the pyrolysate of ethyl cellulose and a crude tobacco cellulose extract. The results presented in this chapter exemplify the importance of filter sampling techniques such as DESI and paper spray ionization to analyze compounds from filters immediately after sample collection and highlight the benefits of the analysis of compounds from aerosol particles in real-time.

REFERENCES

1. Shaltout, A. A.; Boman, J.; Shehadeh, Z. F.; Al-Malawi, D. R.; Hemeda, O. M. Spectroscopic investigation of PM2.5 collected at industrial, residential and traffic sites in Taif, Saudi Arabia. *J. Aerosol Sci.* **2015***, 79*, 97-108.

2. Mkoma, S. L.; da Rocha, G. O.; de Andrade, J. B. Determination of Carboxylic Acids and Water-soluble Inorganic Ions by Ion Chromatography in Atmospheric Aerosols from Tanzania. *South Afr. J. Chem. -Suid-Afr. Tydskr. Chem.* **2014***, 67*, 118-123.

3. Wang, C. H.; Chen, B. T.; Han, B. C.; Liu, A. C.; Hung, P. C.; Chen, C. Y.; Chao, H. J. Field evaluation of personal sampling methods for multiple bioaerosols. *PLoS One* **2015***, 10*, e0120308.

4. DeCarlo, P. F.; Kimmel, J. R.; Trimborn, A.; Northway, M. J.; Jayne, J. T. Field-Deployable, High-Resolution, Time-of-Flight Aerosol Mass Spectrometer. *Anal. Chem.* **2006***, 78*, 8281-8289.

5. McMurry, P. H.; Grosjean, D. Gas and Aerosol Wall Losses in Teflon Film Smog Chambers. *Environ. Sci. Technol.* **1985***, 19*, 1176-1182.

6. McMurry, P. H.; Rader, D. J. Aerosol Wall Losses in Electrically Charged Chambers. *Aerosol Sci. Tech.* **1985***, 4*, 249-268.

7. Zappoli, S.; Andracchio, A.; Fuzzi, S.; Facchini, M. C.; Gelencsér, A.; Kiss, G.; Krivácsy, Z.; Molnár, Á; Mészáros, E.; Hansson, H. -.; Rosman, K.; Zebühr, Y. Inorganic, organic and macromolecular components of fine aerosol in different areas of Europe in relation to their water solubility. *Atmos. Environ.* **1999***, 33*, 2733-2743.

8. Budhavant, K.; Andersson, A.; Bosch, C.; Kruså, M.; Murthaza, A.; Zahid; Gustafsson, Ö Apportioned contributions of PM2.5 fine aerosol particles over the Maldives (northern Indian Ocean) from local sources vs long-range transport. *Sci. Total Environ.* **2015***, 536*, 72-78.

9. Shiraiwa, M.; Pfrang, C.; Koop, T.; Pöschl, U. Kinetic multi-layer model of gas-particle interactions in aerosols and clouds (KM-GAP): linking condensation, evaporation and chemical reactions of organics, oxidants and water. *Atmos. Chem. Phys.* **2012***, 12*, 2777-2794.

10. Shiraiwa, M.; Seinfeld, J. H. Equilibration timescale of atmospheric secondary organic aerosol partitioning. *Geophys. Res. Lett.* **2012***, 39*.

11. Jang, M.; Czoschke, N. M.; Northcross, A. L. Atmospheric Organic Aerosol Production by Heterogeneous Acid-Catalyzed Reactions. *Chem. Phys. Chem.* **2004***, 5*, 1646-1661.

12. Pietrogrande, M. C.; Bacco, D.; Chiereghin, S. GC/MS analysis of water-soluble organics in atmospheric aerosol: optimization of a solvent extraction procedure for simultaneous analysis of carboxylic acids and sugars. *Anal. Bioanal. Chem.* **2013***, 405*, 1095-1104.

13. Buiarelli, F.; Canepari, S.; Di Filippo, P.; Perrino, C.; Pomata, D.; Riccardi, C.; Speziale, R. Extraction and analysis of fungal spore biomarkers in atmospheric bioaerosol by HPLC-MS-MS and GC-MS. *Talanta* **2013***, 105*, 142-151.

14. Kawamura, K.; Tachibana, E.; Okuzawa, K.; Aggarwal, S. G.; Kanaya, Y.; Wang, Z. F. High abundances of water-soluble dicarboxylic acids, ketocarboxylic acids and alpha-dicarbonyls in the mountaintop aerosols over the North China Plain during wheat burning season. *Atmos. Chem. Phys.* **2013***, 13*, 8285-8302.

15. Aldabe, J.; Santamaria, C.; Elustondo, D.; Parra, A.; Foan, L. Polycyclic Aromatic Hydrocarbons (PAHs) Sampled in Aerosol Phase at Different Sites of the Western Pyrenees in Navarra (Spain). *Environ. Eng. Manag. J.* **2012***, 11*, 1049-1058.

16. Bateman, A. P.; Walser, M. L.; Desyaterik, Y.; Laskin, J.; Laskin, A.; Nizkorodov, S. A. The Effect of Solvent on the Analysis of Secondary Organic Aerosol Using Electrospray Ionization Mass Spectrometry. *Environ. Sci. Technol.* **2008***, 42*, 7341-7346.

17. Takáts, Z.; Wiseman, J. M.; Gologan, B.; Cooks, R. G. Mass Spectrometry Sampling under Ambient Conditions with Desorption Electrospray Ionization. *Science* **2004***, 306*, 471-473.

18. Liu, J.; Wang, H.; Manicke, N. E.; Lin, J. M.; Cooks, R. G.; Ouyang, Z. Development, characterization, and application of paper spray ionization. *Anal. Chem.* **2010***, 82*, 2463-2471.

19. Wu, C.; Siems, W. F.; Hill Jr., H. H. Secondary Electrospray Ionization Ion Mobility Spectrometry/Mass Spectrometry of Illicit Drugs. *Anal. Chem.* **2000***, 72*, 396-403.

20. Takats, Z.; Wiseman, J. M.; Cooks, R. G. Ambient mass spectrometry using desorption electrospray ionization (DESI): instrumentation, mechanisms and applications in forensics, chemistry, and biology. *J. Mass Spectrom.* **2005***, 40*, 1261-1275.

21. Li, M.; Chen, H.; Yang, X.; Chen, J.; Li, C. Direct quantification of organic acids in aerosols by desorption electrospray ionization mass spectrometry. *Atmos. Environ.* **2009***, 43*, 2717-2720.

22. Roach, P. J.; Laskin, J.; Laskin, A. Molecular Characterization of Organic Aerosols Using Nanospray-Desorption/Electrospray Ionization-Mass Spectrometry. *Analytical Chemistry* **2010***, 82*, 2048-2058.

23. McMurray, J. 16.3 Nucleophilic Acyl Substitution Reactions of Carboxylic Acids. In *Organic Chemistry: A Biological Approach* Thompson Brooks/Cole: Belmont, CA, 2007; p 642.

24. Manicke, N. E.; Yang, Q.; Wang, H.; Oradu, S.; Ouyang, Z.; Cooks, R. G. Assessment of paper spray ionization for quantitation of pharmaceuticals in blood spots. *Int. J. Mass Spectrom.* **2011***, 300*, 123-129.

25. Espy, R. D.; Muliadi, A. R.; Ouyang, Z.; Cooks, R. G. Spray mechanism in paper spray ionization. *Int. J. Mass Spectrom.* **2012***, 325*, 167-171.

CHAPTER 4: IONIZATION OF COMPOUNDS FROM AEROSOL PARTICLES

4.1 Introduction

As discussed in Chapter 1, there is a need for development of aerosol mass spectrometry instrumentation capable of structural analysis in real time due to the drawbacks associated with current commercial aerosol mass spectrometry instrumentation. Specifically, sampling of aerosol particles into a high vacuum chamber is biased because of evaporation of the more volatile compounds from the aerosol particles.[1] Separation of compounds prior to ionization by electron ionization (EI) is required to prevent convolution of fragmentation patterns that often occur during ionization,[2] leading to complicated workflows and increased analysis times.[3]

Isolation and dissociation of ions results in dissociation patterns that are indicative of the structure of ions. Ion sources that induce less fragmentation during ionization than EI or laser ablation can be used to generate ions from intact neutral analyte molecules. Subsequent isolation and dissociation of these intact ions results in a dissociation pattern that gives information on the structure of the ion. This structural information can be translated into information about the structure of the neutral analyte molecule. Ionization techniques that induce little to no fragmentation of analytes during ionization have become of interest as a means to generate ions from compounds in aerosol particles at atmospheric pressure. Atmospheric pressure chemical ionization (APCI) has been successfully integrated into a commercial aerosol mass spectrometer design. The goal of the experiments presented in this chapter is to investigate ambient ion sources that induce little fragmentation during ionization and provide information about the chemical composition of the sample in addition to the information gained from APCI.

Extractive electrospray ionization[4] (EESI), a derivative of electrospray ionization (ESI), is an ionization technique that induces less in-source fragmentation of compounds from aerosol particles relative to traditional ionization techniques such as EI.[5] Though no systematic studies of the solvent dependence of ionization in EESI have yet been performed, it has been demonstrated that the solubility of the analyte in the EESI solvent has a pronounced impact on ionization.[6] Low temperature plasma

ionization (LTPI) is another ambient ion source that has been shown to cause little fragmentation during ionization[7] and ionize compounds with a lower volatility than either APCI or ESI[8]. A “low temperature plasma” (LTP) is a type of self-sustaining dielectric barrier discharge that is generated by applying an ac voltage to one electrode of the device and connecting the other electrode to ground potential. As an alternative, the entire device can be floated at a selected voltage. The two electrodes between which the plasma is formed are separated by an insulating barrier, preventing charge buildup on either electrode. The plasma is composed of numerous microdischarges that cause only minor heating of the gas, resulting in a plasma temperature of approximately 30 °C.[7] Present in the plasma are reactive species such as metastable atoms or molecules, ions, radicals, and high-energy photons and electrons. Ionization of neutral analyte molecules is believed to occur via proton transfer from gaseous hydronium ions generated by the interaction of atmospheric water molecules with the reactive species in the plasma.[7] LTPI has previously been used to ionize compounds in the gas phase,[9] off of solid surfaces,[10] and from the surface of solutions.[11]

The experiments detailed in this chapter investigate the utility of EESI and LTPI for the ionization of compounds generated from pyrolysis of natural polymers. The influence of the EESI solvent composition and LTPI configuration on the ions observed in the mass spectrum are evaluated. An application using LTPI for the analysis of compounds in the aerosol produced from e-cigarette liquid is discussed.

4.2 Extractive electrospray ionization

4.2.1 Ionization of pyrolysis products from natural polymers

Four natural polymers, ethyl cellulose, cellulose, hemicellulose, and lignin were pyrolyzed in the PyroProbe at 650 °C and ionized by EESI (described in Chapter 2.3.4 and Figure 2.7) using 50/49/1 methanol/water/acetic acid as an electrospray solvent. The positive ion mode mass spectra for the pyrolyzed polymers are displayed in Figure 4.1. Unless otherwise noted, the mass spectra in this chapter were collected using the Bruker Esquire 3000 ion trap mass spectrometer. The spacing between the analyte ion peaks and the corresponding isotopes is indicative of singly charged ions. Odd mass-to-charge ratio ions are primarily observed when ethyl cellulose (Figure 4.1A), cellulose (Figure 4.1B, colloidal grade and 4.1C, binder grade), or hemicellulose (Figure 4.1D) is pyrolyzed and ionized by

EESI. Cellulose is the linear β(1→4) polymer of glucose. Ethyl cellulose has the same basic polymer structure as cellulose but with ethyl groups attached to the free hydroxyl groups. Hemicellulose is much less structured than cellulose and is a branching polymer of any of a variety of D-pentose sugars (xyloglucans).[12] All three of these natural polymers contain only carbon, hydrogen, and oxygen, and thus the presence of odd mass-to-charge ratio ions indicates the analyte molecules from the aerosol particles contain an even number of electrons and are not radicals. Though high activation energy radical reactions occur during pyrolysis, unstable radicals rapidly react to form the even electron species that are subsequently ionized by EESI.[13]

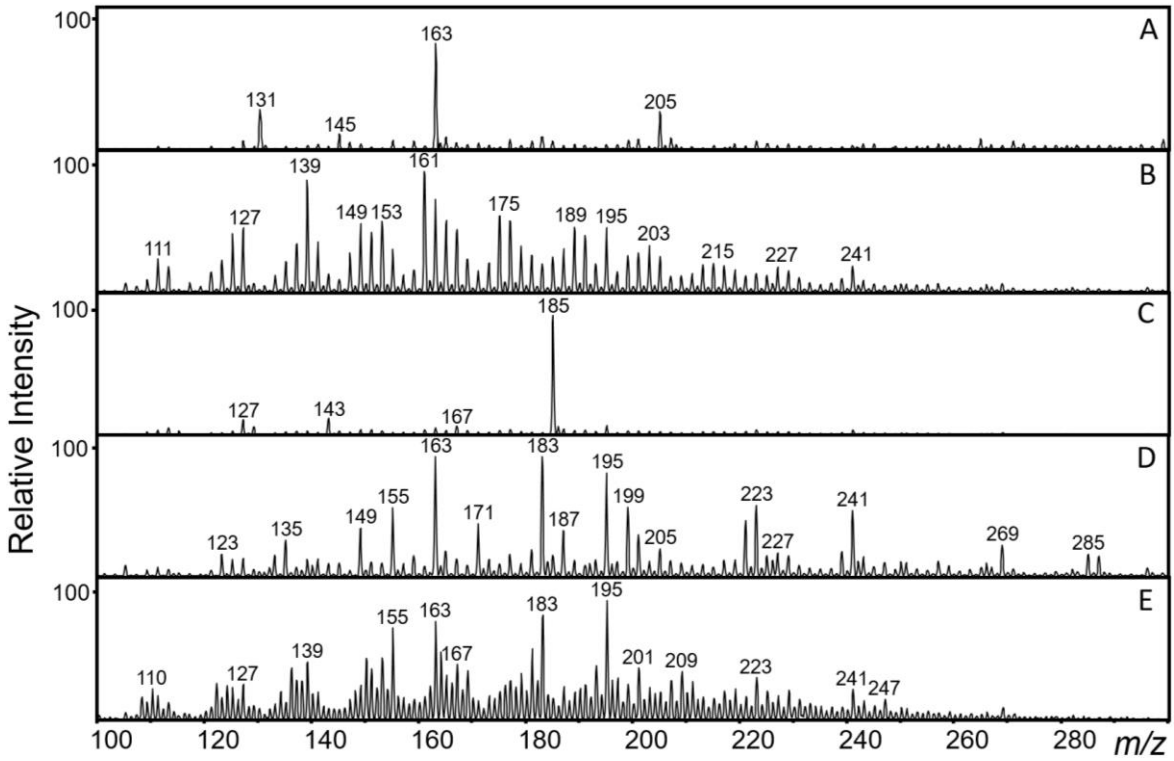

Figure 4.1. Positive ion mode EESI mass spectra produced using 50/49/1 methanol/water/acetic acid as an electrospray solvent for the pyrolysate of A. ethyl cellulose B. colloidal grade cellulose C. binder grade cellulose D. hemicellulose and E. lignin. The ion of m/z 149 is a known background contaminant.

As noted above, two types of cellulose were pyrolyzed and ionized by EESI, colloidal grade cellulose (Figure 4.1B) and binder grade cellulose (Figure 4.1C). The difference between these two types of cellulose is the diameter of the cellulose granules that undergo pyrolysis; colloidal grade cellulose has a smaller granule diameter whereas binder grade cellulose is coarser.[14] The influence of the diameter of the initial sample granules on the identity of the pyrolysis products generated is a well-established

phenomenon,[15-17] and the observation of different compounds depending on the granule size of the original sample supports the utility of EESI in investigating the composition of aerosol particles.

Lignin is a sturdy, branched chain formed by the polymerization of *p*-coumaryl alcohol, coniferyl alcohol, and sinapyl alcohol.[18] The structures of the lignin monomers are shown in Figure 4.2. Ions are observed at both odd and even mass-to-charge ratios in the EESI mass spectrum of pyrolyzed lignin (Figure 4.1E) at greater relative intensities than would be expected from the contribution of carbon or hydrogen isotopes. One potential explanation for the appearance of higher than expected intensities of even mass-to-charge ratio ions is the presence of radicals formed during pyrolysis or ionization. Though radical products from pyrolysis of model lignin compounds have been shown to be stable when formed in vacuum, these radicals are unlikely to be stable at atmospheric pressure.[19] EESI is believed to occur via selective extraction of analytes from the nebulized sample followed by ESI-type processes.[20] Though radical cations are not often observed from ESI, it has been shown that polycyclic aromatic hydrocarbons can form radical cations during ESI-MS, believed to be due to electrochemical oxidation occurring at a metal-liquid junction (e.g. the tip of the ESI emitter) or in solution.[21,22]

An alternative explanation for the presence of a higher than expected abundance of even mass-to-charge ions from EESI of pyrolyzed lignin could also be explained by the presence of nitrogen containing compounds in the original sample. It is possible that proteins or other nitrogen containing compounds are present as contamination in the lignin because, unlike the commercially purchased cellulose and ethyl cellulose samples, the lignin was produced by a crude extraction from tobacco. Contamination of the original lignin sample with nitrogen containing compounds could lead to pyrolysis products having an odd number of nitrogen atoms that would appear in positive ion mode as a protonated even electron ions with even mass-to-charge ratios after EESI.

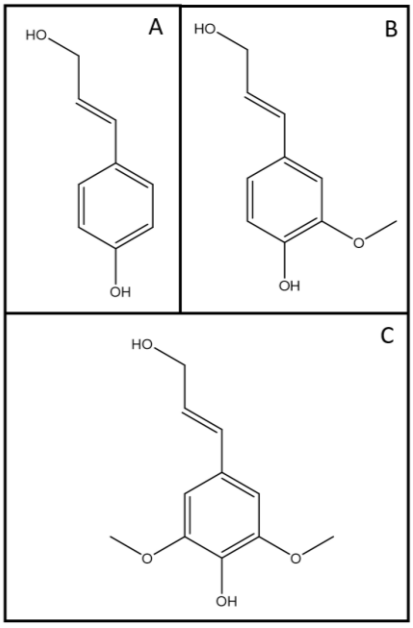

Figure 4.16. Lignin monomers A. p-coumaryl alcohol B. p-coniferyl alcohol and C. p-sinapyl alcohol.

Displayed in Figure 4.3 are the negative ion mode mass spectra for EESI of ethyl cellulose,

colloidal grade cellulose, hemicellulose, and lignin. The isotopic peak spacing indicates that singly charged ions are observed in negative ion mode. In the negative ion mode mass spectra from pyrolyzed ethyl cellulose (Figure 4.3A), pyrolyzed colloidal grade cellulose (Figure 4.3B), and pyrolyzed lignin (Figure 4.3D), a higher intensity of ions with an even mass-to-charge ratio are observed than can be attributed to the expected carbon and hydrogen isotopic peak ratios. No enrichment of even mass-to-charge ratio ions was observed in the positive ion mode EESI mass spectrum for pyrolyzed ethyl cellulose or cellulose, making it unlikely that the even mass-to-charge ratio peaks observed in negative ion mode are due to nitrogen contamination in the original ethyl cellulose or cellulose sample. Though no reports of the formation of $M^{-\bullet}$ from a neutral molecule M containing only carbon, hydrogen, and oxygen during ESI could be found in the literature, it has been shown that deprotonated phenol derivatives can undergo fragmentation to form radical anions during ion transfer into the high vacuum region of the mass spectrometer.[23]

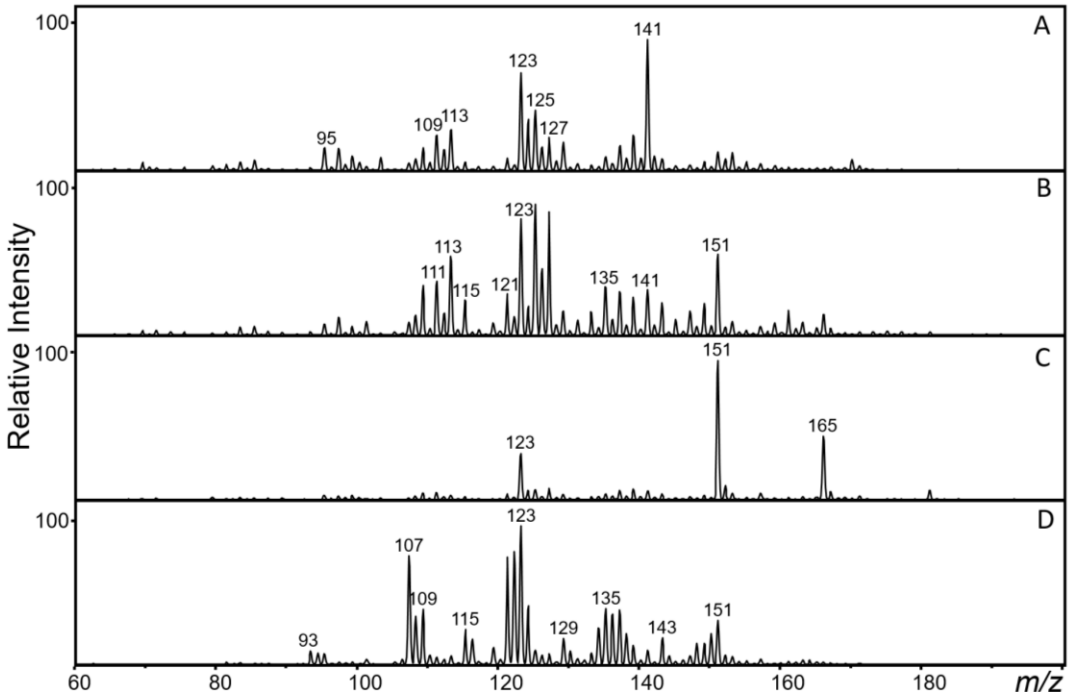

Figure 4.3. Negative ion mode EESI mass spectra produced using 50/49/1 methanol/water/acetic acid as an electrospray solvent for pyrolyzed A. ethyl cellulose B. colloidal grade cellulose C. hemicellulose and D. lignin.

4.2.2 Influence of EESI solvent on the mass spectrum

It has previously been demonstrated that the composition of the solvent used for ESI influences the ions observed in the mass spectrum due to factors including preferential ionization of compounds[24]

and the identity of adducts observed[25]. Figure 4.4 shows the mass spectra observed from EESI of ethyl cellulose pyrolyzed at 650 °C and ionized using 50/49/1 methanol/water/acetic acid (Figure 4.4A), acetonitrile (Figure 4.4B), methanol (Figure 4.4C), 50/50 methanol/chloroform (Figure 4.4D), and 50/50 methanol toluene (Figure 4.4E). Different ions are observed when the EESI solvent is changed, showing the potential for this ionization technique to be tuned to sample a diverse range of compounds from complex aerosol particles.

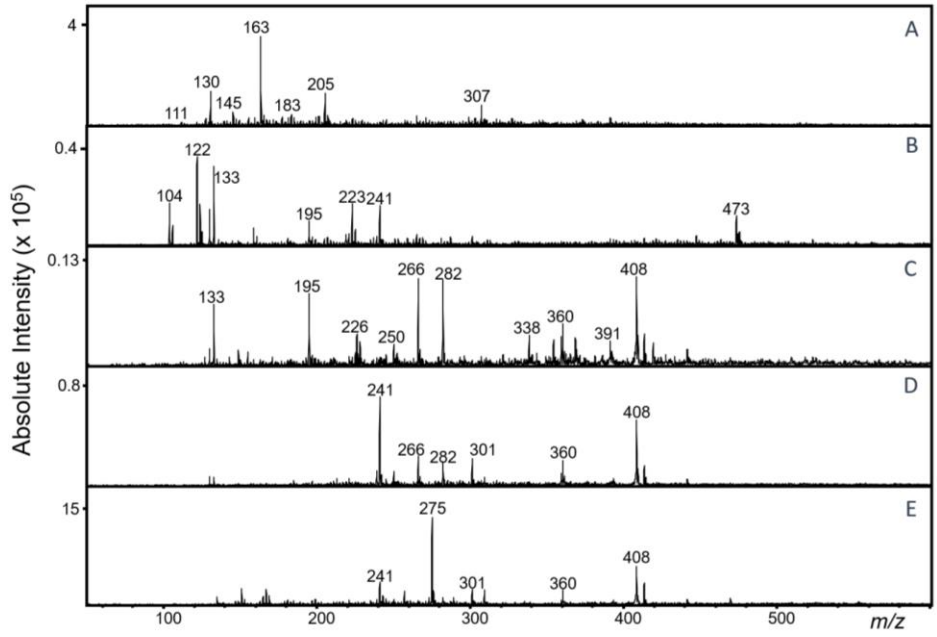

Figure 4.4. Positive ion mode EESI spectra of pyrolyzed ethyl cellulose using A. 50/49/1 methanol/water/acetic acid B. acetonitrile C. methanol D. 50/50 methanol/chloroform or E. 50/50 methanol/toluene as an electrospray solvent.

4.3 Low temperature plasma ionization

4.3.1 Influence of extraction/repelling voltage and desolvation gas flow rate

In EESI, the electric field gradient between the emitter and the capillary inlet to the mass spectrometer accelerates ions to the inlet of the mass spectrometer. To assist in sampling of ions generated by LTPI into the mass spectrometer, a small extraction voltage (between 0 and -100 V)[7,11] is typically applied to the capillary inlet of the mass spectrometer. Positive ions are accelerated to the capillary inlet of the mass spectrometer by the voltage gradient formed between the LTPI source and the mass spectrometer. However, for the standard-size LTPI source, (described in Chapter 2.3.6 and Figure 2.10A-B), no ion signal was observed when an extraction voltage between 0 and -500 V was applied to

the capillary inlet of the mass spectrometer. By increasing the magnitude of the extraction voltage to -4.0 kV, the ion transmission into the mass spectrometer was increased and the mass spectrum in Figure 4.5A was observed.

The decrease in ion sampling efficiency observed when an extraction voltage between 0 and -500 V is used as compared to previously reported results is due to the differences in the ion inlet design used by the instrument manufacturers Thermo Scientific and Bruker Daltonics, respectively. A heated nitrogen desolvation gas flows out of the front of the Bruker mass spectrometer used for these experiments, around the capillary inlet (Figure 2.11). When operated in standard electrospray mode, the desolvation gas assists in solvent evaporation but also aerodynamically repels ions from the inlet to the mass spectrometer. Though solvent evaporation is not required for LTPI, it is undesirable to reduce the countercurrent desolvation gas flow rate because the desolvation gas also prevents neutral molecules from entering the high vacuum system of the mass spectrometer during ion sampling. The extraction voltage on the capillary inlet to the mass spectrometer generates an electric field between the LTPI source and the capillary that is high enough to overcome the aerodynamic repulsion of ions from the inlet of the mass spectrometer. No desolvation gas flow is employed in the inlet design of the Thermo Scientific mass spectrometer used to generate the results previously reported in the literature. Thus, a larger voltage gradient is required to draw ions to the inlet of the Bruker Daltonics mass spectrometer than the Thermo Scientific mass spectrometer.

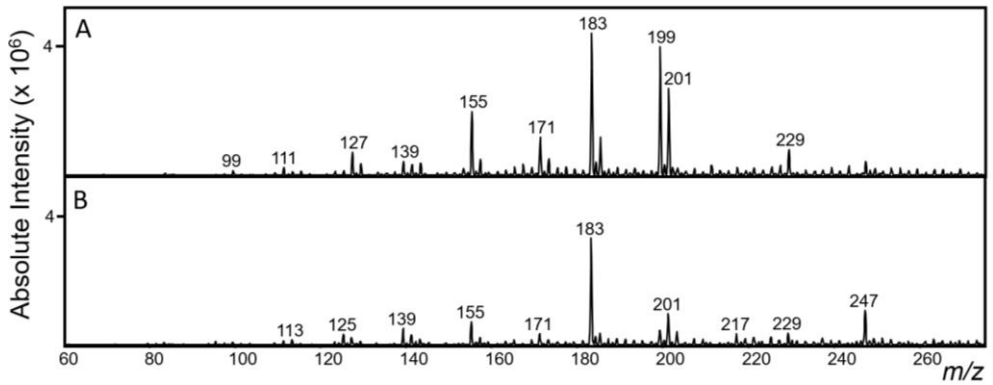

Figure 4.5. Positive mode LTPI mass spectra of pyrolyzed ethyl cellulose generated using the standard-size LTPI source with A. the LTPI source floated at 0 kV and an extraction voltage of -4.0 kV applied to the capillary inlet to the mass spectrometer and B. a repelling voltage applied by floating the LTPI source at +4.0 kV and 0 kV applied to the capillary inlet to the mass spectrometer.

As shown in Figure 4.5B, it is also possible to improve ion transmission with a repelling voltage by

floating the entire LTPI source at +4 kV relative to the grounded capillary inlet to the mass spectrometer. The absolute signal intensity as well as the intensity of the ions relative to the ion of *m/z* 183 is decreased when the LTPI source is floated at +4 kV. Additionally, the generation of a 4 $kV_{0\text{-}p}$ sine wave superimposed on +4 kV dc voltage complicates the electronics required for the experiment. For all subsequent experiments the electrical gradient used to draw ions to the inlet of the mass spectrometer was generated by applying an extraction voltage to the capillary inlet of the mass spectrometer to increase ion signal and reduce experimental complexity.

The influence of the magnitude of the desolvation gas flow rate and extraction voltage on the mass spectra generated by LTPI of pyrolyzed ethyl cellulose with the standard-size LTPI source is shown in Figure 4.6. As a general guide to this Figure, the magnitude of the extraction voltage decreases from -4.5 kV to -0.5 kV from left to right and the desolvation gas flow rate decreases from 5.0 L/min to 0.5 L/min from top to bottom. With the exception of the highest flow rate and extraction voltage setting, the absolute ion intensity stays approximately the same or decreases as the magnitude of the extraction voltage is decreased (Figure 4.6A-C; Figure 4.6D-F; Figure 4.6G-I) and increases as the flow rate is

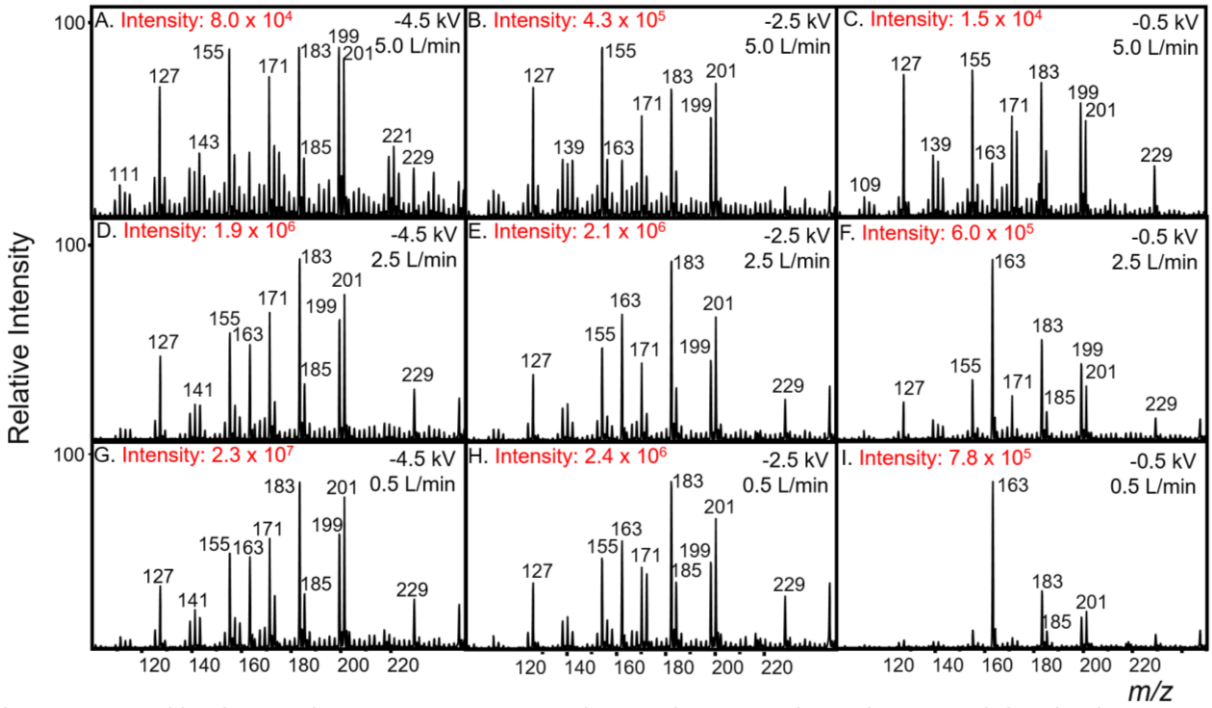

Figure 4.6. Positive ion mode LTPI mass spectra observed at extraction voltages and desolvation gas flow rates of A. -4.5 kV, 5.0 L/min B. -2.5 kV, 5.0 L/min C. -0.5 kV, 5.0 L/min D. -4.5 kV, 2.5 L/min E. -2.5 kV, 2.5 L/min F. -0.5 kV, 2.5 L/min G. -4.5 kV, 0.5 L/min H. -2.5 kV, 0.5 L/min I -0.5 kV, 0.5 L/min generated using the standard-size LTPI source.

decreased (Figure 4.6A, 4.6D, 4.6G; Figure 4.6B, 4.6E, 4.6H; Figure 4.6C, 4.6F, 4.6I). At low flow rates and extraction voltages, significant changes in the relative intensity of ions is observed. Specifically, the intensity of the ion of *m/z* 163 increases as the desolvation gas flow is decreased. However, the intensity of the other ions in the mass spectrum relative to each other remains approximately the same when the ion of *m/z* 163 is excluded. A desolvation gas flow rate of 5.0 L/min was used for subsequent experiments to prevent the potential decrease in the signal-to-noise ratio for analyte ions from transmission of background molecules into the mass spectrometer. An extraction voltage of -4.25 kV was used for subsequent experiments to maintain adequate signal intensity at this higher flow rate.

4.3.2 Ionization of pyrolysis products from natural polymers

To evaluate the potential of LTPI as an ionization technique for the pyrolysis products of natural polymers, three natural polymers were pyrolyzed at 650 °C in the PyroProbe and ionized using the standard-size LTPI source. Displayed in Figure 4.7 are the representative positive ion mode LTPI mass spectra for ethyl cellulose (Figure 4.7A), cellulose (Figure 4.7B), hemicellulose (Figure 4.7C), and lignin (Figure 4.7D). As was observed from EESI, singly charged ions are observed in the mass spectrum as

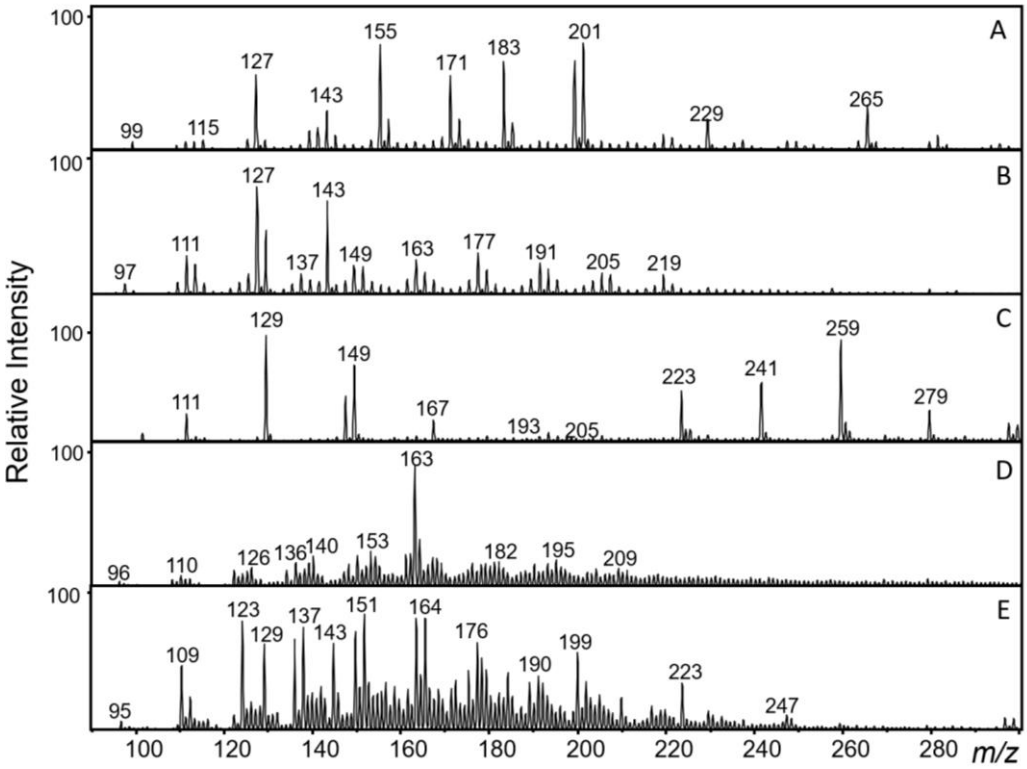

Figure 4.7. Positive ion mode LTPI mass spectrum for pyrolyzed A. ethyl cellulose B. cellulose C. hemicellulose D. lignin and E. 60/40 cellulose/lignin using the standard-size LTPI source.

indicated by the spacing of the isotopic peaks. Primarily odd mass-to-charge ratio ions are also observed in the LTPI mass spectra from pyrolyzed ethyl cellulose and cellulose, indicating that even electron compounds are generated from pyrolysis of cellulose and ethyl cellulose and ionized by LTPI.

The mass spectrum from LTPI of pyrolyzed lignin is shown in Figure 4.7D. As was discussed for EESI, LTPI of pyrolyzed lignin results in a high intensity of ions at both odd and even mass-to-charge ratios, possibly due to contamination of the sample by nitrogen-containing compounds or formation of radical cations during ionization. Many reactive species are present in the plasma such as metastable atoms or molecules, ions, radicals, and high-energy photons and electrons[7] and formation of $M^{+\bullet}$,[8,26] $[M-H]^{+\bullet}$,[27] $[M+2H]^{+\bullet}$,[27,28] as well as odd electron oxidation products[26-28] have previously been observed from LTPI. These reactions could be the reason for the presence of even mass-to-charge ratio ions in the mass spectrum. No radical ion formulas were assigned with less than 5 ppm error using high resolution/high mass accuracy data on a Fourier transform ion cyclotron resonance (FTICR)-MS. However, the presence of nitrogen-containing compounds formed by LTPI of the pyrolysis products of cellulose was confirmed.

The mass spectrum observed from LTPI of pyrolyzed 60/40 cellulose/lignin is shown in Figure 4.7E. The ions observed in this mass spectrum do not appear to be not additive between the cellulose and lignin LTPI mass spectra. Though some mass spectral characteristics are conserved, such as the presence of a larger abundance of even mass-to-charge ratio ions than can be attributed to the isotopic contribution to the sample, each sample exhibits its own unique ion profile in the mass scan. Thermogravimetric analysis experiments have shown that the mass percent loss during heating of cellulose, lignin, and hemicellulose is linear and characteristic of the identity of the natural polymer present.[29] However, this linear weight loss behavior is not necessarily indicative of the identity of pyrolysis products formed.

The negative ion mode standard-size LTPI mass spectra for these same pyrolyzed natural polymers is displayed in Figure 4.8. Though primarily odd mass-to-charge ratio ions are observed for ethyl cellulose (Figure 4.8A) and cellulose (Figure 4.8B), there is a greater intensity of even mass-to-charge ratio ions than would be expected from only the contribution of carbon and hydrogen isotopic peaks just as was observed from EESI (Figure 4.3). The presence of even mass-to-charge ratio ions in the negative ion mode mass spectra from LTPI of pyrolyzed ethyl cellulose or cellulose is unlikely

to be from nitrogen present in the sample as a contaminant because the relative abundance of even mass-to-charge ratio ions observed in the positive ion mode mass spectra is no greater than expected from the isotopic contribution. No reports of radical anions formed LTPI-MS were found in the literature. However, it could be that, as has been observed for $[M-H]^-$ ions formed by ESI, $[M-H]^-$ ions formed by LTPI fragment during ion transfer in the high vacuum region of the mass spectrometer.[23] LTPI of pyrolyzed lignin in both the positive ion mode (Figure 4.7C) and negative ion mode (Figure 4.8C) results in both odd and even mass-to-charge ratio ions, believed to be due to nitrogen containing pyrolysis products. Fewer odd mass-to-charge ratio ions are observed in negative mode when LTPI is used as the ion source as opposed to EESI.

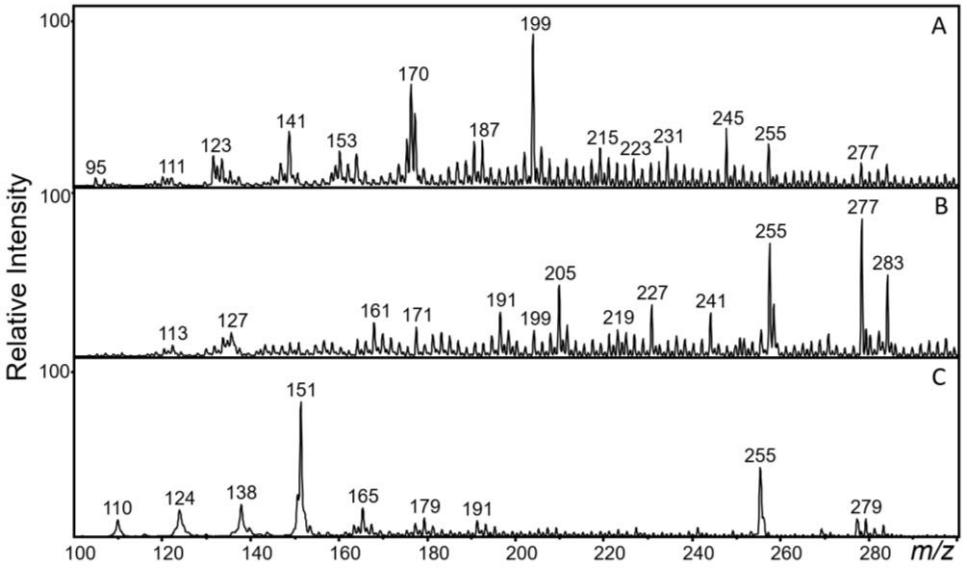

Figure 4.8. Negative ion mode LTPI mass spectrum for pyrolyzed A. ethyl cellulose B. cellulose and C. lignin generated using the standard-size LTPI source.

4.3.3 Particle phase sampling

To ensure that the ions observed from LTPI are generated from compounds in the aerosol particles, the particles were removed by filtration of the aerosol produced from the pyrolysis of ethyl cellulose in the PyroProbe at 650 °C. The positive ion mode standard-size LTPI mass spectrum of pyrolyzed ethyl cellulose observed prior to filtration is shown in Figure 4.9A. The LTPI mass spectrum observed when the pyrolysate of ethyl cellulose was filtered through a tetrafluoroethylene (TFE) coated borosilicate glass filter (Pallflex Fiberfilm T60A20, Ann Arbor MI) prior to ionization is shown in Figure 4.9B. These filters are known to retain 96.4% of aerosol particles[30] and only minimal adsorption of

gaseous compounds onto TFE coated filters has previously been reported.[31] A low intensity of analyte ions are observed after the particles are removed from the sample. The ions observed in the mass spectrum with the most significant intensity after particle filtration are also detected as background ions when ambient laboratory air is ionized by LTPI, shown in Figure 4.9C. To confirm that LTPI is a particle phase sampling technique, a XAD-4 coated[32] four-channel annular denuder (URG-2000-30B4-242, URG Corp., Chapel Hill, NC) was used to remove gaseous neutrals from the aerosol produced by pyrolysis of ethyl cellulose at approximately 600 °C in the custom pyrolysis chamber. Ions were generated from compounds in the aerosol particles by LTPI after the gaseous neutrals were removed; the representative mass spectrum is shown in Figure 4.9D. When the aerosol is passed through the denuder, the relative intensity of the major ions in the mass spectrum is changed. This change in ion distribution with and without the denuder could be explained by differential removal of compounds from smaller particles prior to ionization.[33] Smaller particles diffuse to the walls of the denuder (path length of 25 cm) more rapidly

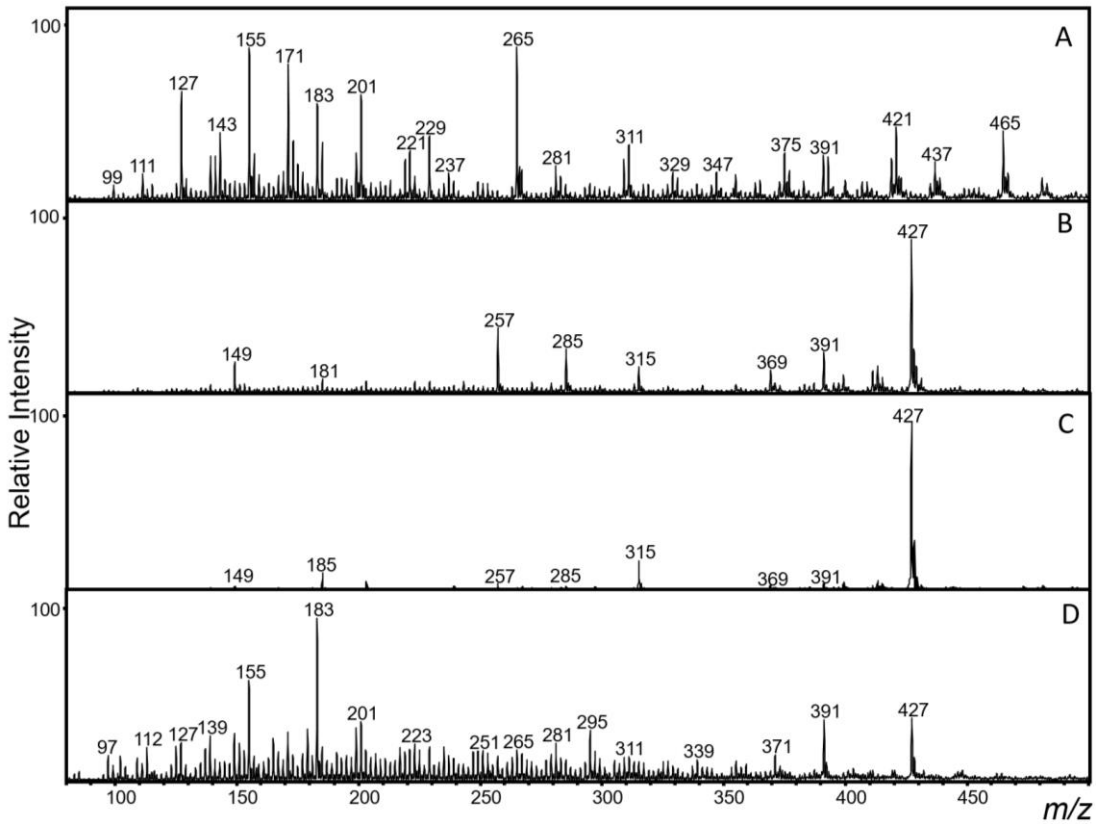

Figure 4.9. Positive ion mode LTPI mass spectrum of pyrolyzed ethyl cellulose A. through the filter holder B. after particle removal through a TFE coated borosilicate glass filter C. ambient background and D. after gaseous neutral removal through a XAD-4 coated annular denuder.

than larger particles. Thus, more adsorption of smaller particles to the walls of the denuder will occur and compounds that are primarily present in larger particles will dominate the mass spectrum. However, further experiments must be performed using size-selected aerosol particles to confirm this hypothesis. Overall, the data presented in Figure 4.9 support that LTPI generates ions from compounds in aerosol particles.

Tandem mass spectrometry (MS/MS) was performed by collision induced dissociation (CID) of three of the major ions observed from LTPI of ethyl cellulose pyrolyzed in the commercial pyrolysis chamber at approximately 600 °C with the standard-size LTPI source. The MS/MS spectra of *m/z* 155, 183, and 201 before and after the removal of gasses with the denuder are compared in Figure 4.10. MS/MS spectra for the ion of *m/z* 155 ionized directly from the aerosol pyrolysate (Figure 4.10A) and after the gaseous molecules were removed by the denuder (Figure 4.10B) are identical. Though the MS/MS spectra of the ion of *m/z* 183 without (Figure 4.10C) and with (Figure 4.10D) the denuder are similar, when gaseous compounds have been removed by the denuder the product ion at *m/z* 139 has a greater relative intensity and the product ion at *m/z* 137 has a lower relative intensity.

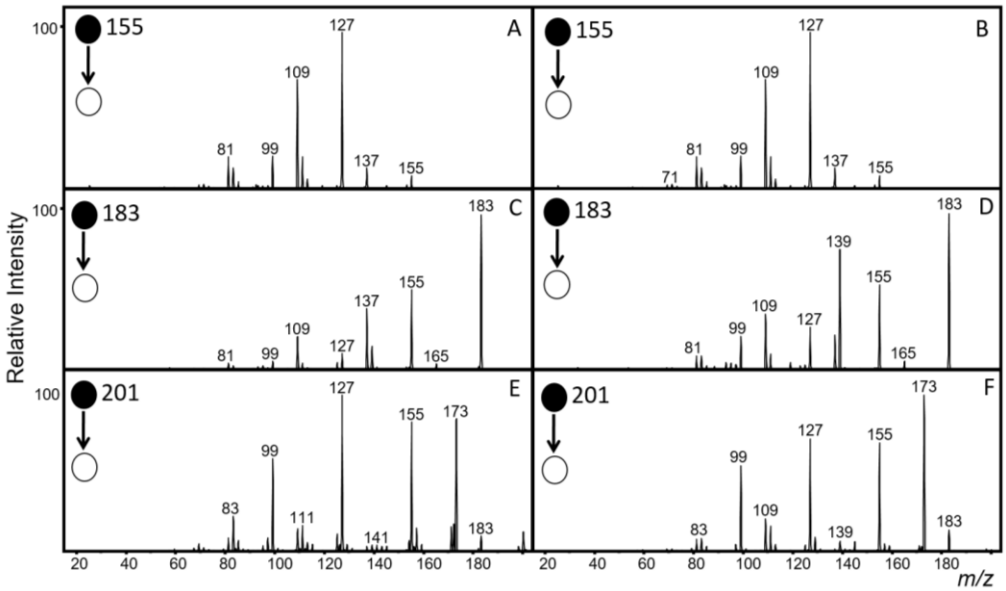

Figure 4.10. MS/MS spectra of ions generated by LTPI of A. m/z 155 without the denuder and B. m/z 155 with the denuder, C. m/z 183 without the denuder and D. m/z 183 with the denuder, E. m/z 201 without the denuder and F. m/z 201 with the denuder.

Differential ion mobility spectrometry separations as well as high resolution/high mass accuracy data on a Fourier transform ion cyclotron resonance (FTICR)-MS indicate that there are at least two ions

that contribute to the parent ion population with the unit *m/z* 183 (183.1015, $C_{10}H_{15}O_3$ -0.4 ppm; 183.1379, $C_{11}H_{19}O_2$ -0.3 ppm). One of these compounds, the one that undergoes CID to produce a larger product ion population of *m/z* 137, is differentially removed from the pyrolysate when it is passed through the denuder. As previously discussed, this may be because the parent compound is primarily present in smaller particles. Differences are also observed when comparing the spectra after CID of the ion of *m/z* 201 before (Figure 4.10E) and after (Figure 4.10F) the aerosol is passed through the denuder. The differences between the CID spectra before and after the gaseous neutrals are removed from the pyrolysate support the hypothesis that compounds are differentially removed from the pyrolysate when passed through the denuder.

4.3.4 Flow-through LTPI

A significant drawback of conventional LTPI is that external factors such as gas flow profiles and ion source orientation with respect to the sample output and the inlet of the mass spectrometer can greatly influence sensitivity.[34] Variations in gas flow profiles and electric fields impact the number of analyte ions formed and the efficiency of ion transfer into the mass spectrometer. To reduce the experimental variability of LTPI, the output of the pyrolysis chamber is directed through the standard-size LTPI source as depicted in Figure 2.10A. This configuration, termed flow-through LTPI, eliminates the variability associated with the alignment of the sample output with the LTPI source and mass spectrometer inlet.

The flow-through LTPI mass spectrum observed from ionization of the compounds in the aerosol produced by pyrolysis of ethyl cellulose at approximately 600 °C in the custom pyrolysis chamber with the standard-size LTPI source is shown in Figure 4.11A. This mass spectrum was generated using helium as both the pyrolysis and plasma gas. Though ions are observed at the same mass-to-charge ratios from both conventional LTPI-MS (Figure 4.11B) and flow-through LTPI-MS with the standard-size LTPI source, a greater relative intensity of the lower abundance peaks in the mass spectrum is observed when flow-through LTPI-MS is performed as compared to conventional LTPI-MS.

4.3.5 Development of the miniature LTPI source

To operate the LTPI source in the flow-through configuration, the plasma must be ignited in the same gas that is used for sample generation and transport. Helium was used to generate the

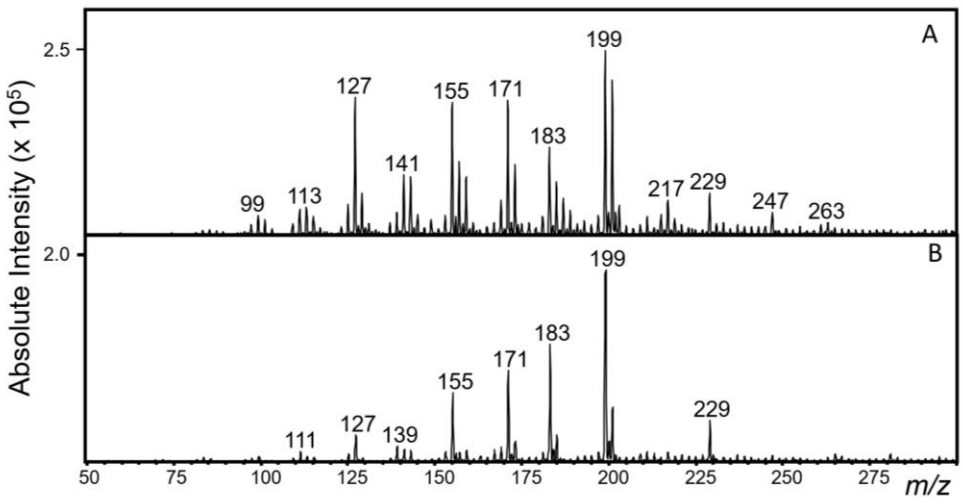

Figure 4.11. Mass spectra generated from ethyl cellulose pyrolyzed in the custom built pyrolysis chamber at approximately 600 °C and ionized by A. flow-through LTPI or B. conventional LTPI with the standard-size LTPI source and helium as the plasma gas.

flow-through LTPI mass spectrum shown in Figure 4.11, but nitrogen (or air) is often preferred for gas and aerosol sample generation because it is inexpensive and more closely simulates ambient conditions as compared to other gases. However, it is impractical to generate a discharge in nitrogen gas in the standard-size LTPI source. Though an ac voltage is used to generate the LTP, each microdischarge can be treated theoretically as a single dc discharge. The minimum voltage difference required to generate a Townsend discharge is a function of the product of the gas pressure and distance between the electrodes as described by Paschen's curve (Figure 4.12).[35,36] The standard-size LTPI source is operated at atmospheric pressure with an intra-electrode distance of 1.9 mm. Considering these pressure/distance conditions, the breakdown voltage required to generate a plasma in nitrogen is much higher than the breakdown voltage required to generate a plasma in helium (approximately 10.5 $kV_{0\text{-}p}$ and 4 $kV_{0\text{-}p}$, respectively).[36] Modifying the LTPI power supply circuit (Figure 2.9) to output a rf sine wave with an amplitude large enough to generate a discharge in nitrogen in the standard-size LTPI source would be more expensive and require more complicated electronics. Due to the risk of operator contact with the

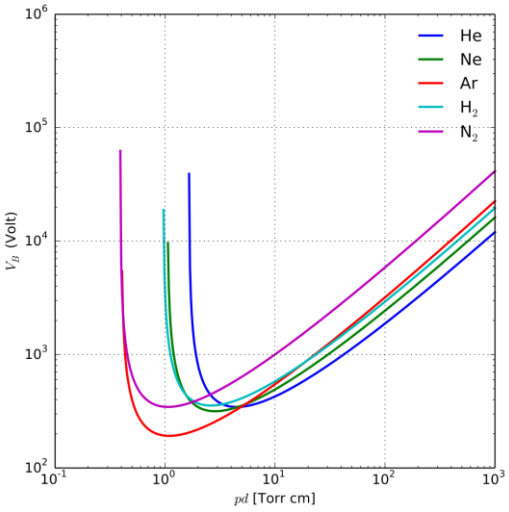

Figure 4.12. Graphical representation of Paschen's curve adapted from Lieberman, et. al. [27]

high voltage, the safety concerns associated with potential electrical shock would be greatly increased when using a voltage high enough to ignite a plasma in nitrogen gas.

To decrease the voltage requirements for LTPI using nitrogen or air as the plasma gas at atmospheric pressure, the distance between the electrodes may be reduced. A miniature LTPI source was designed as described in Chapter 2.3.6 and shown in Figure 2.10C-D to have a pressure-distance product such that ac voltages less than 4 $kV_{0\text{-}p}$ can be used to generate a Townshend discharge in nitrogen gas at atmospheric pressure (760 torr × 0.45 mm, equating to approximately 3 $kV_{0\text{-}p}$ on Paschen's curve).[11] Thus, though it is impractical to use nitrogen or air as the plasma gas for the standard-size LTPI source, the miniature LTPI source has a small enough pressure-distance product that carrier gases with higher breakdown voltages may be used. It should be noted that Paschen's curve describes a dc discharge between planar electrodes at room temperature and as such is useful to describe trends in behavior for LTPI but does not accurately predict the breakdown voltages necessary to perform LTPI. Experimentally, the voltages required to ignite the plasma are lower than the theoretical voltages.

To evaluate the performance of the miniature LTPI source compared to the standard-size LTPI source previously characterized,[37] the standard-size and miniature LTPI sources were used in the conventional configuration (Figure 2.11) to ionize compounds from the aerosol generated by pyrolysis of ethyl cellulose in nitrogen gas at 650 °C in the PyroProbe. The mass spectrum observed using the miniature LTPI source is shown in Figure 4.13A. Displayed in Figure 4.13B is the mass spectrum observed when the standard-size LTPI source was used in the conventional configuration to ionize the compounds from the aerosol produced by pyrolysis of ethyl cellulose in the custom pyrolysis chamber at approximately 600 °C. Helium was used as a plasma gas for both the standard-size and miniature LTPI source. The absolute ion intensity from the miniature LTPI source is lower than the absolute ion intensity observed from the standard-size LTPI source. It should be noted, however, that approximately twice the mass of sample is pyrolyzed in the custom pyrolysis chamber for ionization with the lower sensitivity standard-size LTPI source as opposed to in the PyroProbe with the miniature LTPI source. This difference in initial sample quantity is likely the reason for the differences in absolute ion intensity. The relative intensities of ions in the mass spectrum observed from conventional LTPI with the standard-size

LTPI source are very similar to those in the mass spectrum observed from conventional LTPI with the miniature LTPI source. Thus, the miniature LTPI source was determined to be an acceptable alternative to the standard-size LTPI source in the conventional operational configuration.

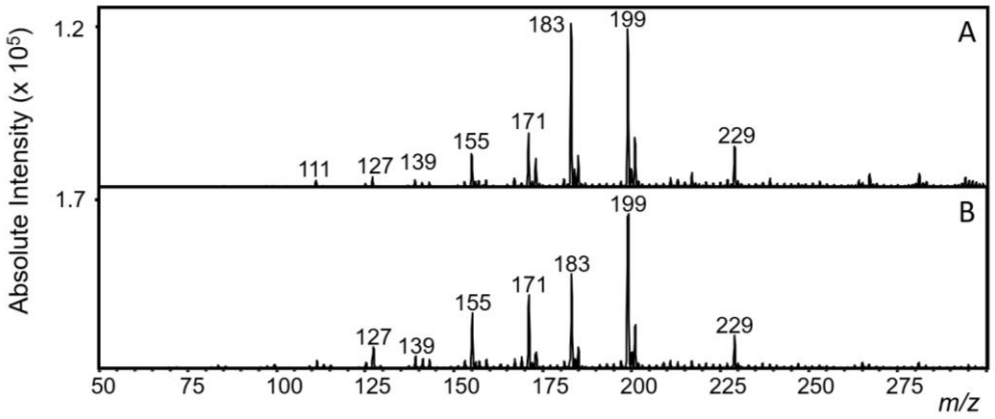

Figure 4.13. Mass spectra generated from ethyl cellulose pyrolyzed in the PyroProbe at 650 °C and ionized by conventional LTPI with the A. miniature LTPI source or B. standard LTPI source and helium as the plasma gas.

Previous studies have shown that the identity of the plasma gas influences the extent of fragmentation of analytes during ionization.[7,34] It was also demonstrated that ionization using a helium plasma increases the sensitivity of detection and induces less fragmentation during ionization compared to a nitrogen plasma.[7,28] To investigate the impact of nitrogen versus helium plasma gas on the mass spectrum, ethyl cellulose was pyrolyzed in nitrogen in the PyroProbe at 650 °C and ionized by the miniature LTPI source in the conventional configuration using nitrogen as a plasma gas. The mass spectrum produced is displayed in Figure 4.14A. The relative intensity of the ions observed in the mass spectrum is different than the relative intensity of the ions formed by LTPI of the sample generated using the same conditions but with helium as a plasma gas (Figure 4.14B). This change in relative intensity is due to the order of magnitude decrease in the absolute intensity of the ions of *m/z* 199, 183, and 171 when nitrogen is used as a plasma gas in place of helium. A lower abundance of these ions could be from fragmentation of analytes during ionization because of the use of a nitrogen plasma gas or due to a decrease in desorption/ionization efficiency of analytes.

To determine if fragmentation of ions occurs when nitrogen is used as the plasma gas in place of helium, MS/MS was performed. As discussed in Section 4.3.3 and is demonstrated in subsequent

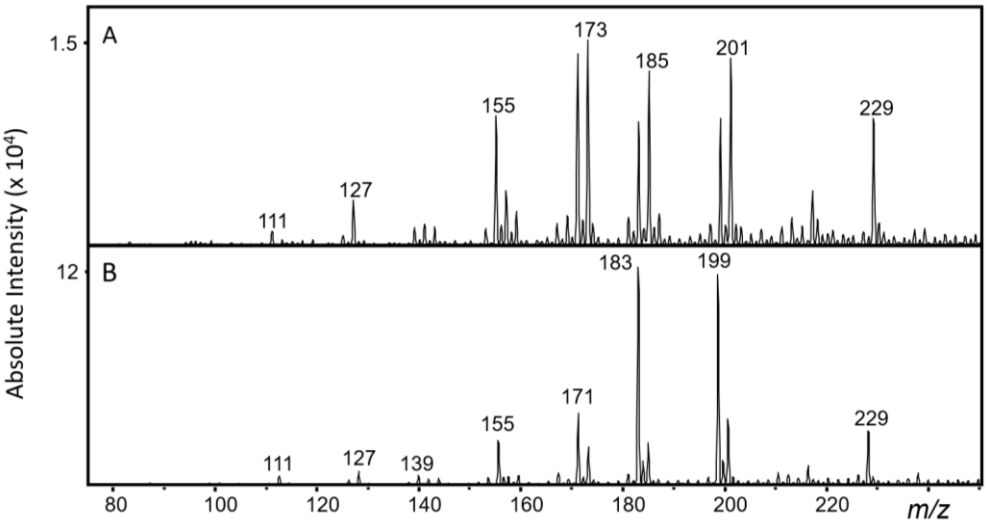

Figure 4.14. Mass spectra from ethyl cellulose pyrolyzed in the commercial pyrolysis instrument and ionized using the miniature LTPI source in the conventional configuration with A. nitrogen plasma gas and B. helium plasma gas.

chapters, a variety of isomeric and isobaric ions are expected to be present at each mass-to-charge ratio. If fragmentation is occurs during ionization, ions with the lowest activation energy barrier to fragmentation would fragment to the greatest extent, thus changing the relative ratio of isomeric or isobaric ions observed at a selected mass-to-charge ratio. MS/MS was used to determine if the population of ions generated at a selected mass-to-charge ratio changes when helium or nitrogen is used as a plasma gas. Differences in the dissociation pattern observed from MS/MS of isolated ions would indicate that the population of parent ions of that mass-to-charge ratio has changed due to less stable ions fragmenting more readily than the more stable ions. CID was performed using an isolation width of 1.0 Da and a resonant excitation voltage of 0.40 V to generate product ion spectra from the ions of *m/z* 201, 199, and 183 formed using the miniature LTPI source with helium or nitrogen as a plasma gas. This data is shown in Figure 4.15. No significant differences were observed between the product ion spectra generated from CID of ions produced by a helium plasma (Figure 4.15A-C) versus by a nitrogen plasma (Figure 4.15D-F), suggesting that the same relative distribution of parent ion isomers/isobars is present at each selected mass-to-charge ratio. Thus, it is unlikely that increased fragmentation of compounds in the pyrolysate of ethyl cellulose occurs during ionization by LTPI with nitrogen instead of helium for the pyrolysis products of ethyl cellulose. Instead, the change in relative intensity of the ions formed by LTPI with nitrogen as opposed to helium is due to changes in the desorption and/or ionization efficiency.

4.3.6 Flow-through LTPI with the miniature ion source

As discussed in Section 4.3.4, the primary motivation for operation of the LTPI source in a flow-through configuration is to reduce the impact of environmental factors on the signal response for compounds from gases and aerosol particles. In the flow-through configuration, the pyrolysis gas is used as the analyte carrier gas and subsequently the plasma gas, reducing the potential variability in the ion source orientation and gas flow profile during ionization. To evaluate the utility of the miniature LTPI source in the flow-through configuration, LTPI-MS of compounds in the aerosol produced from ethyl cellulose pyrolyzed at 650 °C in the PyroProbe was performed using nitrogen as both the pyrolysis and plasma gas. Shown in Figure 4.16 are the mass spectra produced using the miniature ion source in the conventional LTPI configuration (Figure 4.16A) and in the flow-through configuration (Figure 4.16B). The relative intensity of the low mass-to-charge ratio ions is increased for flow-through LTPI with the miniature LTPI source. This change in relative intensity is due to the increase in absolute signal intensity of up to an order of magnitude for the ions of *m/z* 111, 127, 155, 159, and 173 with flow-through LTPI.

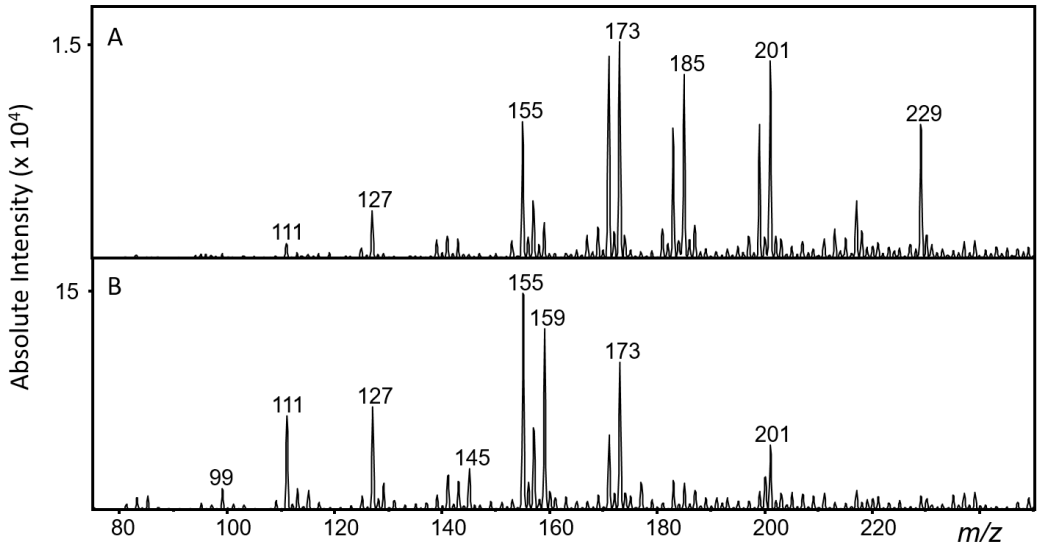

Figure 4.15. Mass spectra from ethyl cellulose pyrolyzed in the commercial pyrolysis instrument and ionized using the nitrogen plasma gas in the A. conventional configuration and B. flow-through configuration.

The increase in absolute intensity of low mass-to-charge ratio ions could be due to either an increase in fragmentation of higher mass-to-charge ratio ions or an increase in the desorption and/or ionization efficiency of analytes. To evaluate the extent of ion fragmentation during conventional and flow-through LTPI, caffeine was volatilized in nitrogen at 400 °C in the PyroProbe and ionized by the

miniature LTPI source using a nitrogen plasma gas in both the conventional and flow-through configuration. Caffeine was selected as a standard because it was observed to dissociate almost completely to a single stable product ion at resonant excitation voltages lower than those required to dissociate the majority of ions observed in the pyrolysate of ethyl cellulose. The only major fragment ion observed from CID of the protonated molecule of caffeine is the ion of *m/z* 138, which results from the neutral loss of methyl isocyanate.[38] The ratio of the fragment ion of *m/z* 138 to the protonated molecule (*m/z* 195) observed in the mass spectrum was determined to be 0.1 ± 0.1 (n = 8) for conventional LTPI and 0.07 ± 0.04 (n = 7) for flow-through LTPI. Thus, no significant difference in the extent of fragmentation is observed for protonated caffeine depending on the configuration of the LTPI source. As such, it may be concluded that no increase in fragmentation is induced by flow-through LTPI as opposed to conventional LTPI for ions with higher appearance potentials than that of the neutral loss of methyl isocyanate from protonated caffeine. Instead, the increase in absolute ion intensity observed in the flow-through configuration is likely due to more efficient desorption/ionization of compounds from the sample. The reproducibility of flow-through LTPI is greater than that of LTPI in the conventional configuration using the miniature LTPI source as demonstrated by the decrease in the standard deviation of the measurements made when flow-through LTPI-MS is performed as opposed to conventional LTPI-MS. This increase in reproducibility is likely due to the fact that the influence of factors such as flow dynamics has little impact on the interaction of the sample and plasma in flow-through LTPI, allowing for more consistent ion generation.

4.3.7 Flow-through LTPI of pyrolyzed cellulose

Shown in Figure 4.17 are the mass spectra for the compounds in the aerosol produce from cellulose pyrolyzed in the PyroProbe at 650 °C and ionized using the miniature LTPI source in the conventional (Figure 4.17A) and flow-through (Figure 4.17B) configuration. An increase in the abundance of the even mass-to-charge ratio ions relative to the odd mass-to-charge ratio ions is observed in the flow-through LTPI configuration. This phenomenon was not observed when ethyl cellulose was ionized in the conventional versus flow-through configuration (Figures 4.11 and 4.16 for the standard and miniature LTPI sources, respectively). However, because of the overall decrease in signal intensity it cannot be determined if these even mass-to-charge ions are actually formed to a greater extent during flow-through

LTPI or if the changes in the mass spectrum are due to the decrease in the relative abundance of the odd mass-to-charge ratio ions. Though the signal intensity decreases by an order of magnitude in the conventional configuration as compared to the flow-through configuration, the total ion current only decreases by a factor of 4 (approximately 6 x 10^6 to 1.5 x 10^6), suggesting that fragmentation could be occurring in the ion source. This would happen if analytes fragmented to ions with a lower appearance potential than the product ion which results from the neutral loss of methyl isocyanate from caffeine.

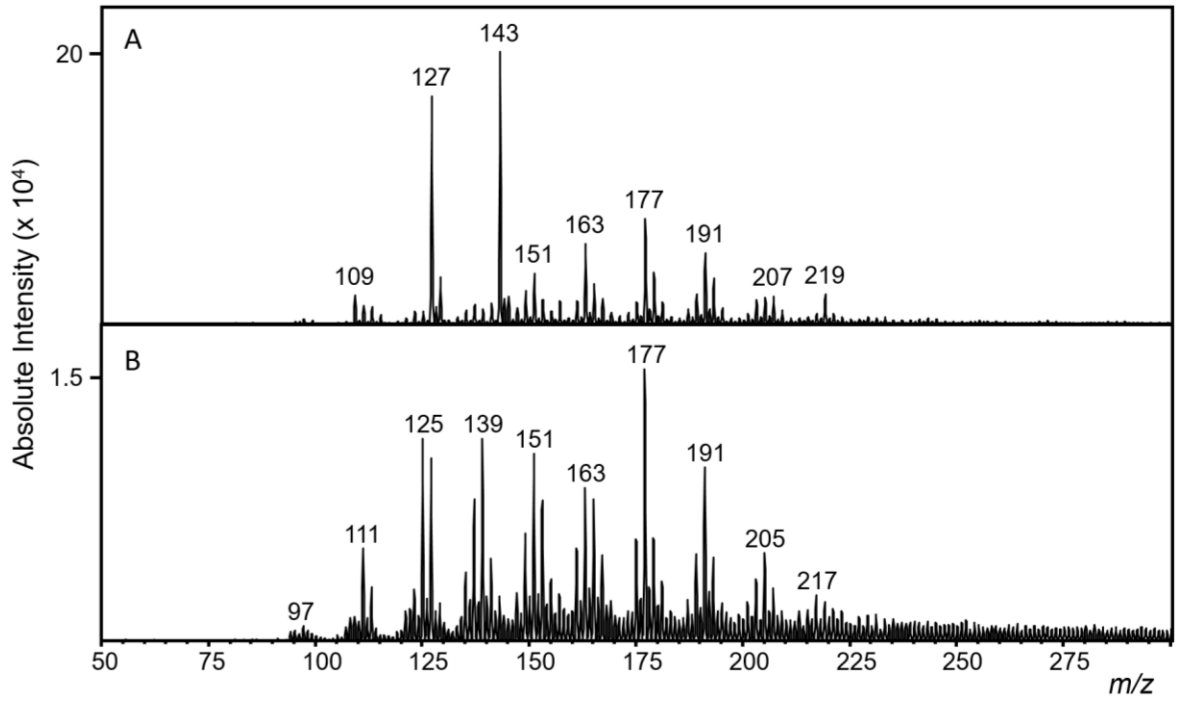

Figure 4.16. Ionization of the cellulose pyrolysis products using the miniature LTPI probe in the A. conventional or B. flow-through configuration.

High resolution/high mass accuracy FTICR data of flow-through LTPI of pyrolyzed cellulose was used to investigate the identity of the even mass-to-charge ratio ions. Ions with even mass-to-charge ratios were detected that do not correspond to an isotopic peak. Two examples of this are shown in Figure 4.17 for the ion pair of *m/z* 177 and 178 (Figure 4.17A) as well as *m/z* 195 and 196 (Figure 4.17B). Two ions are observed with unit *m/z* 177: 177.055 ($C_{10}H_9O_3$, -0.6 ppm) and 177.091 ($C_{11}H_{13}O_2$, -0.6 ppm). Isotopic peaks are observed at *m/z* 178.058 and 178.094, respectively. A third ion of *m/z* 178 is observed that does not correspond to an ion of *m/z* 177: 178.058. No radical ion formulas corresponded to the even mass-to-charge ratio ions with less than 5 ppm error and the formula of this ion was determined to be $C_{10}H_{12}O_2N$ (-0.3 ppm). The ions 195.065, 195.102 and 195.138 are $C_{10}H_{11}O_4$ (-0.4 ppm), $C_{11}H_{15}O_3$

(-0.4 ppm), and $C_{12}H_{19}O_2$, respectively. The ^{13}C isotopic peaks for the two most abundant of these ions are observed at *m/z* 196.068 and 196.105. However, three other ions are observed at significant intensity with the unit *m/z* 196. The formulas of these ions were determined to be $C_9H_{10}O_4N$ (*m/z* 196.060, -1 ppm), $C_{10}H_{14}O_3N$ (*m/z* 196.097, -0.6 ppm), and $C_{11}H_{18}O_2N$ (*m/z* 196.133, -0.5 ppm). These nitrogen containing compounds could be formed from reaction with radicals in the nitrogen plasma.[7]

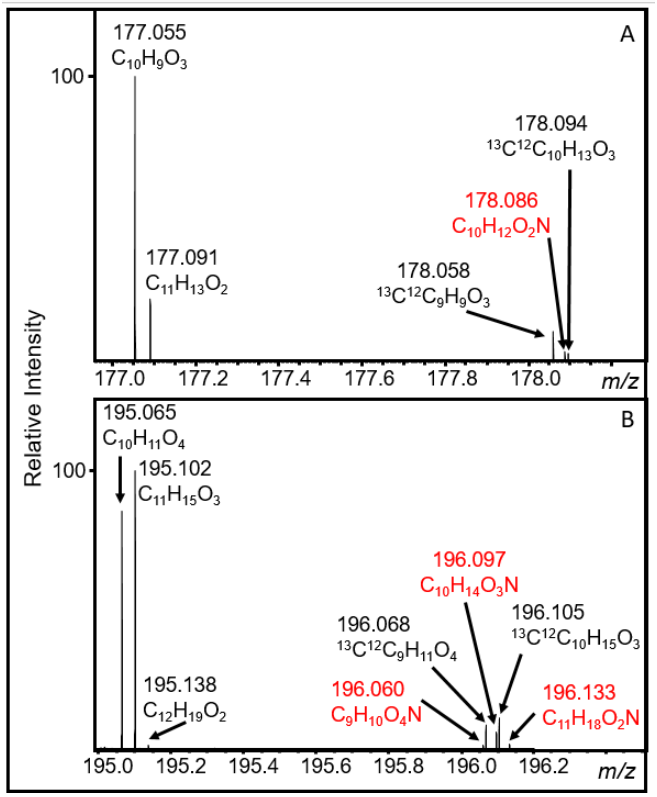

Figure 4.17. Flow-through LTPI-FTICR-MS of pyrolyzed cellulose ions of A. m/z 177 and 178 and B. m/z 195 and 196.

4.4 Comparison of EESI and LTPI

The most abundant ions observed from LTPI of pyrolyzed ethyl cellulose are at *m/z* 199, 183, and 171. Ionizing the pyrolysis products of ethyl cellulose using EESI with 50/49/1 methanol/water/acetic acid as an electrospray solvent results in primarily the ion of *m/z* 163. MS/MS has shown that the ion of *m/z* 163 is protonated levoglucosan. Though each of these ions gives insight into the neutral molecules formed by pyrolysis of ethyl cellulose, ions of nearly every odd mass-to-charge ratio between 100 and 300 Da are generated by both EESI and LTPI of the aerosol produced by the pyrolysis of ethyl cellulose at approximately 600 °C in the custom pyrolysis chamber. Differences in the relative abundance of the

ions observed from each ion source could be due to ionization of different analyte or differences in ionization efficiency of the same compounds.

MS/MS was performed on the ion of *m/z* 183 generated by EESI with 50/49/1 methanol/water/acetic acid as an electrospray solvent and LTPI to determine if different ions of *m/z* 183 are formed by each ion source. Displayed in Figure 4.18 are the MS/MS spectra of the ion of *m/z* 183 generated by EESI using 50/49/1 methanol/water/acetic acid (Figure 4.18A) and with the standard-size LTPI source (Figure 4.18B). The product ion mass spectrum observed after CID of the ion of *m/z* 183 formed by EESI using 50/49/1 methanol/water/acetic acid is vastly different than the product ion mass spectrum generated by CID of the ion of *m/z* 183 formed by LTPI with the standard-size LTPI source. This result indicates that a different population of ions of *m/z* 183 is generated by EESI versus LTPI, supporting that the differences in the mass spectra observed using the two ionization techniques are not simply due to differences in ionization efficiency of the same analytes, but that compounds with significantly different dissociation patterns may be ionized by EESI and LTPI.

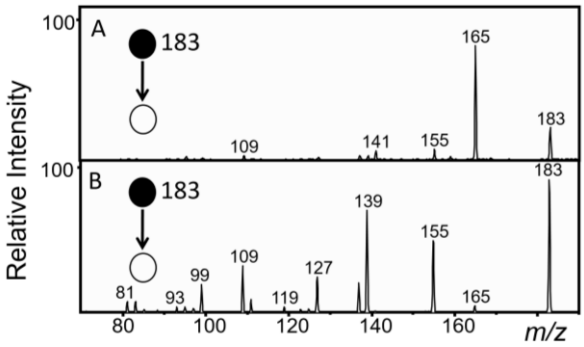

Figure 4.18. Product ion spectra generated by CID of the ion of m/z 183 formed by A. EESI with 50/49/1 methanol/water/acetic acid or B. LTPI with the standard-size source.

4.5 Influence of the distance of the EESI emitter from the capillary inlet

During the experiments presented in Section 4.2, the EESI emitter was oriented such that the cylindrical body of the emitter was approximately 3-5 mm away from the spray shield over the inlet capillary to the mass spectrometer (Chapter 2.3.4, Figure 2.7). Shown in Figure 4.19 are the EESI mass spectra for ethyl cellulose pyrolyzed in the custom pyrolysis chamber at approximately 600 °C generated with the body of the emitter 2 mm from the spray shield (Figure 4.19A), 1 mm from the spray shield (Figure 4.19B), and 0.5 mm from the spray shield (Figure 4.19C). The body of the EESI emitter could not be brought closer than 0.5 mm from the inlet of the mass spectrometer at the voltage used for these experiments (+4.25 kV) without an electrical arc forming between the emitter and the mass spectrometer. As the body of the EESI emitter is moved closer to the spray shield, the mass spectrum becomes more

indicative of LTPI. For clarity in Figure 4.19, EESI-type ions are denoted with blue asterisks and LTPI-type ions are denoted with red asterisks. When the EESI emitter is 0.5 mm from the inlet to the mass spectrometer (Figure 4.19C), the mass spectrum observed is nearly identical to that from LTPI-MS of pyrolyzed ethyl cellulose.

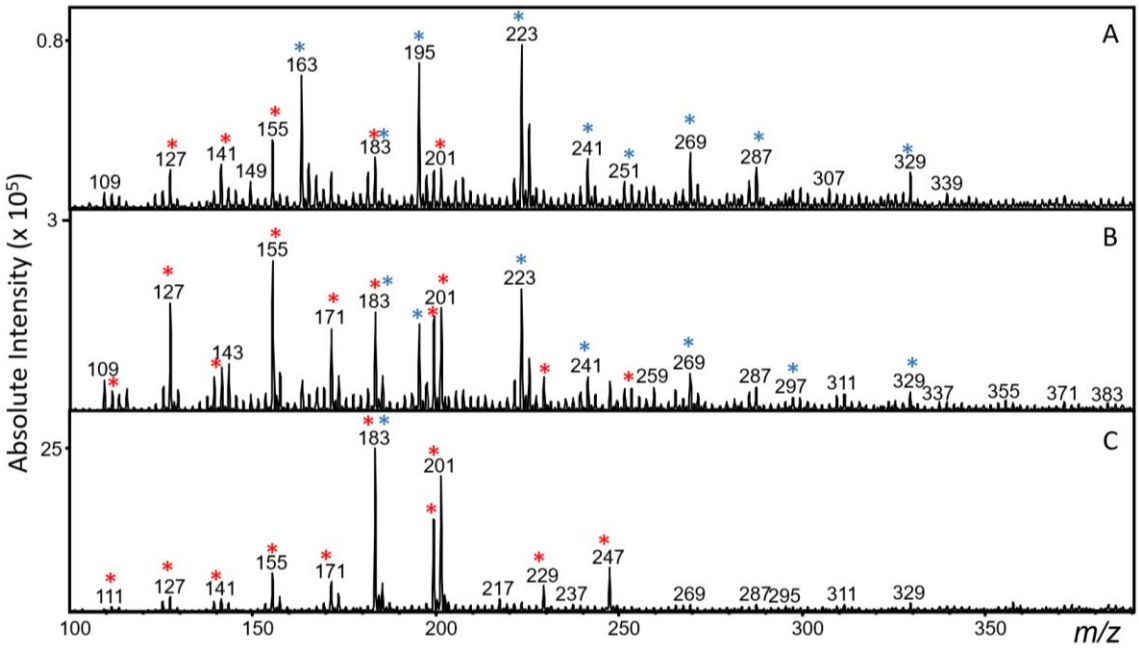

Figure 4.19. EESI-MS spectra generated using 50/49/1 methanol/water/acetic acid as an ESI solvent and the emitter placed A. 2 mm B. 1 mm or C. 0.5 mm from the inlet to the mass spectrometer. Blue asterisks denote EESI-type ions and red asterisks indicate LTPI-type ions.

LTPI is believed to occur primarily by chemical ionization of compounds via ion-molecule reactions between neutral analyte molecules and protonated water vapor (and protonated water vapor clusters) from the atmosphere formed through a cascade of reactions occurring in the plasma.[7] As the proximity of the EESI emitter to the inlet of the mass spectrometer increases, the electric field increases and a corona discharge is formed at the tip of the EESI emitter. Thus, ions can be formed by APCI, a process similar to LTPI, in addition to typical EESI mechanisms.[39]

4.6 Application of LTPI-MS to the analysis of e-cigarette vapors

4.6.1 Motivation for the analysis of e-cigarette aerosols

For a full explanation of the importance of e-cigarette research and a description of e-cigarette design and e-liquid composition as determined by gas chromatography (GC)-MS and direct infusion ESI-MS, refer to Appendix I. The popularity of e-cigarettes has risen in recent years leading to an

increased interest in research related to the composition of e-cigarette liquids. E-cigarette manufacturers advertise e-cigarettes as a safer alternative to combustible tobacco because the e-cigarette liquid is "tobacco free".[40] Though there are fewer compounds in the e-cigarette liquid than tobacco smoke,[41,42] the identity of these ingredients, not just the concentration or number of constituents, is one of the primary factors in determining the potential toxicity of the e-cigarette. Just as heating tobacco generates a wide variety of secondary reaction products, heating the fluid in e-cigarette liquids could cause reaction and degradation of the constituents of e-cigarette liquids, generating unknown compounds in the e-cigarette vapor/aerosol. Though parts of the wick of the e-cigarette may be exposed to lower temperatures,[43,44] compounds in the liquid and vapor are exposed to temperatures as extreme as that of the surface of the heating filament, causing different reactions than predicted to occur. Due to the physical action of nebulizing the e-liquid by puffing air through the e-cigarette, involatile compounds are expected to be present in the e-cigarette aerosol in addition to the compounds from the vaporized e-liquid and thermal degradation products. Thus, even if the manufacturers were to disclose the composition of e-cigarette liquids, an understanding of the chemistry occurring during heating of the e-cigarette liquid is required to predict the composition of the e-cigarette vapor/aerosol.

The physical properties of aerosol particles are directly influenced by the chemical composition. For example, when an e-cigarette liquid is vaporized, the diameter of the particles formed by condensation of the vapor is inversely proportional to the vapor pressure of the gas phase compounds.[45] Thus, smaller aerosol particles are formed by e-liquids that, when heated, generate more volatile compounds. Particle penetration and deposition in the lung are known to be highly influenced by particle diameter.[46] For example, particles with a diameter less than 1 nm are delivered into the lung with a high efficiency, but are also readily exhaled rather than absorbed.[47] An understanding of the composition of the aerosol particles is required to inform research into the human health effects of e-cigarettes.

4.6.2 Analysis of aerosols produced by vaporization of e-liquids

To evaluate the composition of the e-cigarette aerosol, the Pyroprobe 5250 was used to flash heat (500 °C/s) 30 μL of e-liquid to 120 °C and the compounds in the aerosol produced were ionized by flow-through LTPI. Two independent studies have reported e-cigarette operating temperatures to be between 180-220 °C[43] or between 65-120 °C[44]. 120 °C was chosen as a reasonable final heating

temperature. It should be noted that this is not a true simulation of e-cigarette “vaping”; the e-liquid is not “puffed” as it would be in an actual e-cigarette.

Shown in Figure 4.20A is the background subtracted mass spectrum for vaporized Peanut Butter Cookie, Figure 4.20B is from Hot Cinnamon Candies, Figure 4.20C is from Menthol Tobacco and in Figure 4.20D is the background subtracted mass spectrum from Atomic Cinnacide. A different mass spectrometric profile is observed for each of the four e-liquids investigated. The e-liquids shown in Figure 4.20A-C were all advertised to contain the same amount of nicotine: 12 mg/mL. However, the absolute intensity of the ion of *m/z* 163 varies between the three samples. This variation could be explained by differing aerosol formation mechanisms depending on the composition of the e-liquid,[45] differences in the proton affinity of other analyte ions, or could be due to variations in the true concentration of nicotine in

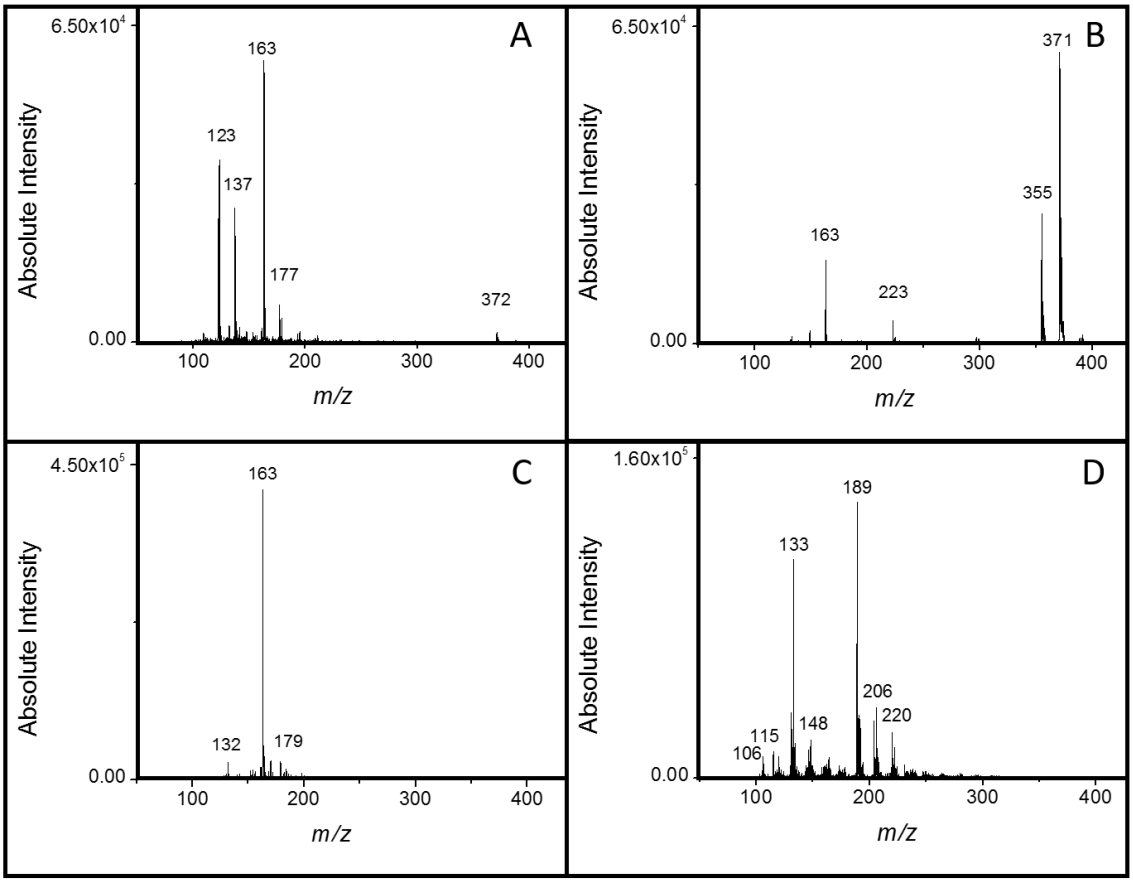

Figure 4.20. Background subtracted LTPI-MS spectra for A. Peanut Butter Cookie (12 mg/mL nicotine) B. Hot Cinnamon Candies (12 mg/mL nicotine) C. Menthol Tobacco (12 mg/mL nicotine) and D. Atomic Cinnacide (0 mg/mL nicotine). Peaks with negative absolute intensities were not plotted as they are an artifact of the background subtraction; background ions with a lower proton affinity than the analyte ions will be less abundant when the sample is present and subtraction results in a negative ion intensity.

the e-liquid. Experiments to determine the source of the variation in the nicotine intensity between the e-liquids are discussed in Chapter 8.

4.6.3 Comparison of the compounds observed in GC-EI-MS, ESI-MS, and LTPI-MS

GC-MS and ESI-MS analysis of the e-liquids was performed. This data is presented and discussed in Appendix 1. The ions generated from flow-through LTPI of Atomic Cinnacide (Figure 4.20D) are shown in Table 4.1. Many of the peaks observed are at even mass-to-charge ratios. Though the ion of *m/z* 134 could be due to the isotopic peak from cinnamaldehyde, the other even mass-to-charge ratio ions are either at too high of a relative intensity to be solely due to an isotopic peak (e.g. *m/z* 192) or do not correspond to a more intense odd mass-to-charge ratio ion.

Correlations between the ions observed by GC-MS and ESI-MS and LTPI-MS are also shown in Table 4.1 and the potential corresponding LTPI ion type is displayed. The three most commonly reported positive ion mode ion types were listed: $[M+H]^+$ $[M-H]^{+\bullet}$ and M^+ as well as potential oxidation products of compounds observed by GC-MS or ESI-MS that could be formed in the LTPI source. No ions were observed that could correspond to $[M+2H]^{+\bullet}$ or nitrogen adducts were observed. Analytes that were observed from LTPI that were not detected by GC-MS and/or ESI-MS are designated “ND”. The only

Table 4.1. Ions observed from the LTPI-MS spectrum of Atomic Cinnacide compared to GC-EI-MS and ESI-MS.

LTPI m/z	BSRI	Potential LTPI Ion Type	GC-MS ID	ESI-MS Molecular Formula
131	23	$[M-H]^{+\bullet}$	Cinnamaldehyde	ND
133	78	$[M+H]^+$	Cinnamaldehyde	C_9H_8O
134	12	Isotopic peak and/or $M^{+\bullet}$	Hydrocinnamaldehyde Dipropylene glycol	ND
146	10		ND	ND
148	12	$M^{+\bullet}$ $[M+O]^{+\bullet}$	ND Cinnamaldehyde	$C_6H_{12}O_4$ -----
189	100		ND	ND
191	23		ND	ND
192	18		ND	ND
204	19		ND	ND
206	26	$M^{+\bullet}$	ND	ND
207	11	$[M+H]^+$	ND	$C_{12}H_{14}O_3$
220	16		ND	ND
222	11	$[M+O]^{+\bullet}$	ND	$C_{12}H_{14}O_3$

compound that is detected by all three techniques is cinnamaldehyde. The ion of *m/z* 207, $C_{12}H_{14}O_3$, was observed in both ESI of the Atomic Cinnacide e-liquid and LTPI of the Atomic Cinnacide aerosol, confirming that low volatility compounds not detected by GC-MS are present in LTPI-MS. The ion of *m/z* 148 could be the molecular ion of the ion of $C_6H_{12}O_4$ observed in ESI-MS and it is possible that hydrocinnamaldehyde or dipropylene glycol, identified by GC-MS, could form a molecular ion of $M^{+\bullet}$ that contributes to the intensity of the ion of *m/z* 134. The fact that only two or three of the compounds observed from GC- or ESI-MS of the e-liquid correspond to ions formed by LTPI of the aerosol produced by vaporization of the e-liquid indicates that there are differences between the composition of the e-liquid and the aerosol produced after vaping. As will be discussed in Chapter 8, MS/MS experiments must be performed and the unknown ions should be compared to standards to ensure the same ion type is formed and the ions have similar dissociation patterns to determine the structure of the compounds observed from each method.

4.7 Summary and conclusions

Previous literature and the data presented in Chapter 3 of this dissertation highlight the importance of the development of analytical techniques for analysis of compounds in aerosol particles without the requirement of filter collection. Commonly used ion sources require collection of the particles on filters or induce fragmentation of analytes during ionization, making the ion source design the limiting factor for the analysis of compounds in aerosol particles by mass spectrometry in real time. In this chapter, EESI and LTPI are investigated for the generation of ions from compounds in aerosol particles.

EESI has previously been shown to ionize compounds from aerosol particles[6] and this ionization technique is applied to analysis of the pyrolysate of multiple natural polymers in both positive and negative mode. It is also shown that EESI can be used to detect differences in the pyrolysis products generated depending on the surface area-to-volume ratio of the initial sample. The EESI solvent has a significant impact on the identity of ions formed and can potentially be used to selectively ionize compounds from aerosol particles.

LTPI is shown to ionize different compounds than EESI from the same aerosol sample. A miniature LTPI source was developed to be used in the flow-through configuration with nitrogen as the sample carrier gas as well as the plasma gas. Ions containing nitrogen were observed from flow-through

LTPI of even electron analytes, potentially from the reaction of analytes with nitrogen containing radicals in the nitrogen plasma. The ionization efficiency for compounds from pyrolyzed ethyl cellulose was observed to increase when the flow-through configuration was used. No significant fragmentation was observed from flow-through LTPI of pyrolyzed ethyl cellulose, but cellulose pyrolysis products may be fragile enough to fragment in the LTPI source.

Decreasing the distance between the EESI emitter and the inlet capillary results in ions that are indicative of LTPI. By increasing the electric field in EESI, a corona discharge may be formed and ions are generated by APCI, a similar ionization process to LTPI, as well as EESI. The data presented in this chapter illustrates the utility and importance of the use of multiple ion sources to analyze a wider range of compounds from complex samples.

Flow-through LTPI was applied to the analysis of the composition of the aerosol produced from vaporized e-liquid. It was shown that the ions observed from LTPI of the aerosol produced from vaporization of an e-liquid are different than those observed from GC-EI-MS or ESI-MS, indicating that there is a difference between the composition of the e-cigarette liquid and the aerosol produced after heating. In the future, MS/MS experiments of the ions formed by LTPI of the aerosol produced from e-cigarette liquids will be used to confidently identify compounds in the e-cigarette aerosol.

REFERENCES

1. Posfai, M.; Xu, H.; Anderson, J.; Buseck, P. Wet and dry sizes of atmospheric aerosol particles: An AFM-TEM study. *Geophys. Res. Lett.* **1998***, 25*, 1907-1910.

2. Aiken, A. C.; Decarlo, P. F.; Kroll, J. H.; Worsnop, D. R.; Huffman, J. A. O/C and OM/OC Ratios of Primary, Secondary, and Ambient Organic Aerosols with High-Resolution Time-of-Flight Aerosol Mass Spectrometry. *Environ. Sci. Technol.* **2008***, 42*, 4478-4485.

3. Buiarelli, F.; Canepari, S.; Di Filippo, P.; Perrino, C.; Pomata, D.; Riccardi, C.; Speziale, R. Extraction and analysis of fungal spore biomarkers in atmospheric bioaerosol by HPLC-MS-MS and GC-MS. *Talanta* **2013***, 105*, 142-151.

4. Chen, H. W.; Venter, A.; Cooks, R. G. Extractive electrospray ionization for direct analysis of undiluted urine, milk and other complex mixtures without sample preparation. *Chem. Comm.* **2006***, 19*, 2044.

5. Gallimore, P. J.; Kalberer, M. Characterizing an extractive electrospray ionization (EESI) source for the online mass spectrometry analysis of organic aerosols. *Environ. Sci. Technol.* **2013***, 47*, 7324-7331.

6. Law, W. S.; Wang, R.; Hu, B.; Berchtold, C.; Meier, L.; Chen, H.; Zenobi, R. On the mechanism of extractive electrospray ionization. *Anal. Chem.* **2010***, 82*, 4494-4500.

7. Harper, J. D.; Charipar, N. A.; Mulligan, C. C.; Zhang, X. R.; Cooks, R. G.; Ouyang, Z. Low-Temperature Plasma Probe for Ambient Desorption Ionization. *Anal. Chem.* **2008***, 80*, 9097-9104.

8. Albert, A.; Engelhard, C. Characteristics of Low-Temperature Plasma Ionization for Ambient Mass Spectrometry Compared to Electrospray Ionization and Atmospheric Pressure Chemical Ionization. *Anal. Chem.* **2012***, 84*, 10657-10664.

9. Campbell, D. I.; Dalgleish, J. K.; Cotte-Rodriguez, I.; Maeno, S.; Graham Cooks, R. Chemical analysis and chemical imaging of fragrances and volatile compounds by low-temperature plasma ionization mass spectrometry. *Rapid Commun. Mass Spectrom.* **2013***, 27*, 1828-1836.

10. Dalgleish, J. K.; Hou, K.; Ouyang, Z.; Cooks, R. G. In Situ Explosive Detection Using a Miniature Plasma Ion Source and a Portable Mass Spectrometer. *Anal. Lett.* **2012***, 45*, 1440-1446.

11. Garcia-Reyes, J. F.; Mazzoti, F.; Harper, J. D.; Charipar, N. A.; Oradu, S.; Ouyang, Z.; Sindona, G.; Cooks, R. G. Direct olive oil analysis by low-temperature plasma (LTP) ambient ionization mass spectrometry. *Rapid Commun. Mass Spectrom.* **2009***, 23*, 3057-3062.

12. Cosgrove, D. J.; Jarvis, M. C. Comparative structure and biomechanics of plant primary and secondary cell walls. *Front. Plant Sci.* **2012***, 3*, 204.

13. Shen, D. K.; Gu, S. The mechanism for thermal decomposition of cellulose and its main products. *Bioresour. Technol.* **2009***, 100*, 6496-6504.

14. Prusov, A. N.; Zheleznov, K.; Alekseeva, O.; Padokhin, V.; Rozhkova, V. The effect of mechanical treatment on colloidal and chemical properties and reactivity of powdered cellulose. *Colloid J. Russ. Acad.*+ **2002***, 64*, 601-604.

15. Wang, Z.; Wan, K.; Xia, J.; Je, Y.; Liu, Y.; Liu, J. Pyrolysis Characteristics of Coal, Biomass, and Coal–Biomass Blends under High Heating Rate Conditions: Effects of Particle Diameter, Fuel Type, and Mixing Conditions. *Energ. Fuel.* **2015**.

16. Encinar, J. M.; Beltrán, F. J.; Bernalte, A.; Ramiro, A.; González, J. F. Pyrolysis of two agricultural residues: Olive and grape bagasse. Influence of particle size and temperature. *Biomass Bioenerg.* **1996***, 11*, 397-409.

17. Ahmad, N.; Williams, P. T. Influence of particle grain size on the yield and composition of products from the pyrolysis of oil shales. *J. Anal. Appl. Pyrolysis* **1998***, 46*, 31-49.

18. Vanholme, R.; Demedts, B.; Morreel, K.; Ralph, J.; Boerjan, W. Lignin Biosysnthesis and Structure. *Plant Physiol.* **2010***, 153*, 895-905.

19. Custodis, V. B. F.; Hemberger, P.; Ma, Z.; van Bokhoven, J. A. Mechanism of Fast Pyrolysis of Lignin: Studying Model Compounds. *J. Phys. Chem. B* **2014***, 118*, 8524-8531.

20. Wang, R.; Gröhn, A. J.; Zhu, L.; Dietiker, R.; Wegner, K.; Günther, D.; Zenobi, R. On the mechanism of extractive electrospray ionization (EESI) in the dual-spray configuration. *Anal. Bioanal. Chem.* **2012***, 402*, 2633-2643.

21. Van Berkel, G. J. Insights Into Analyte Electrolysis in an Electrospray Emitter from Chronopotentiometry Experiments and Mass Transport Calculations. *JASMS* **2000***, 11*, 951-960.

22. Van Berkel, G. J.; McLuckey, S. A.; Glish, G. L. Electrochemical origin of radical cations observed in electrospray ionization mass spectra. *Anal. Chem.* **1992***, 64*, 1586-1593.

23. Morishetti, K. K.; Sripadi, P.; Mariappanadar, V.; Ren, J. Generation and characterization of distonic dehydrophenoxide radical anions under electrospray and atmospheric pressure chemical ionizations. *Int. J. Mass Spectrom.* **2011***, 299*, 169-177.

24. Amad, M. H.; Cech, N. B.; Jackson, G. S.; Enke, C. G. Importance of gas-phase proton affinities in determining the electrospray ionization response for analytes and solvents. *J. Mass Spectrom.* **2000***, 35*, 784-789.

25. Zhou, S.; Hamburger, M. Effects of solvent composition on molecular ion response in electrospray mass spectrometry: Investigation of the ionization processes. *Rapid Commun. Mass Spectrom.* **1995***, 9*, 1516-1521.

26. Nørgaard, A. W.; Kofoed-Sørensen, V.; Svensmark, B.; Wolkoff, P.; Clausen, P. A. Gas Chromatography Interfaced with Atmospheric Pressure Ionization-Quadrupole Time-of-Flight-Mass Spectrometry by Low Temperature Plasma Ionization. *Anal. Chem.* **2013***, 85*, 28-32.

27. Na, N.; Xia, Y.; Zhu, Z.; Zhang, X.; Cooks, R. Birch Reduction of Benzene in a Low-Temperature Plasma. *Agnew. Chem. Int. Ed.* **2009***, 48*, 2017-2019.

28. Gong, X.; Xiong, X.; Peng, Y.; Yang, C.; Zhang, S.; Fang, X.; Zhang, X. Low-temperature plasma ionization source for the online detection of indoor volatile organic compounds. *Talanta* **2011***, 85*, 2458-2462.

29. Yang, H.; Yan, R.; Chen, H.; Lee, D. H.; Zheng, C. Characteristics of hemicellulose, cellulose and lignin pyrolysis. *Fuel* **2007***, 86*, 1781-1788.

30. Pall Life Sciences, Pall Coorporation. Pallflex Filters: Emfab, Fiberfilm and Tissuquartz Filters. *https://www.pall.com/pdfs/Laboratory/02.0601_Pallflex_LR.pdf* **2002***, 2014*, 2.

31. Parshintsev, J. Comparison of quartz and Teflon filters for simultaneous collection of size-separated ultrafine aerosol particles and gas-phase zero samples. *Anal. Bioanal. Chem.* **2011***, 400*, 3527-3535.

32. Eaton, W. C. Standard Operating Procedure for Coating Annular Denuders with XAD-4 Resin. **2008**.

33. Zhang, X.; Lin, Y. H.; Surratt, J. D.; Zotter, P.; Prevot, A. S. H.; Weber, R. J. Light-absorbing soluble organic aerosol in Los Angeles and Atlanta: A contrast in secondary organic aerosol. *Geophys. Res. Lett.* **2011***, 38*, 1-4.

34. Wiley, J. S.; Shelley, J. T.; Cooks, R. G. Handheld Low-Temperature Plasma Probe for Portable "Point-and-Shoot" Ambient Ionization Mass Spectrometry. *Anal. Chem.* **2013***, 85*, 6545-6552.

35. Friedrich, P. Ueber die zum Funkenübergang in Luft, Wasserstoff und Kohlensäure bei verschiedenen Drucken erforderliche Potentialdifferenz. *Annalen der Physik* **1889***, 273*, 69-96.

36. Lieberman, M. A.; Lichtenberg, A. J. *Principles of Plasma Discharges and Materials Processing;* John Wiley & Sons, Inc: Hoboken, NJ, 2005.

37. Spencer, S. E.; Tyler, C. A.; Tolocka, M. P.; Glish, G. L. Low-Temperature Plasma Ionization-Mass Spectrometry for the Analysis of Compounds in Organic Aerosol Particles. *Anal. Chem.* **2015***, 87*, 2249-2254.

38. Bier, D.; Hartmann, R.; Holschbach, M. Collision-induced dissociation studies of caffeine in positive electrospray ionisation mass spectrometry using six deuterated isotopomers and one N1-ethylated homologue. *Rapid Commun. Mass Spectrom.* **2013***, 27*, 885-895.

39. Huang, M.; Yuan, C.; Cheng, S.; Cho, Y.; Shiea, J. Ambient ionization mass spectrometry. *Annu. Rev. Anal. Chem.* **2010***, 3*, 43-65.

40. Trtchounian, A.; Williams, M.; Talbot, P. Conventional and electronic cigarettes (e-cigarettes) have different smoking characteristics. *Nicotine & Tobacco Research* **2010***, 12*, 905-912.

41. Talhout, R.; Schulz, T.; Floreck, E.; van Benthem, J.; Wester, P.; Opperhuizen, A. Hazardous Compounds in Tobacco Smoke. *Int. J. Environ. Res. Public Health* **2011***, 8*, 613-628.

42. Hahn, J.; Monakhova, Y. B.; Hengen, J.; Kol-Himmelseher, M.; Schüssler, J.; Hahn, H.; Kuballa, T.; Lachenmeier, D. W. Electronic cigarettes: overview of chemical composition and exposure estimation. *Tob. Induc. Dis.* **2014***, 12*, 23-35.

43. Garner, C.; Stevens, R. A Brief Discription of History, Operation, and Regulation. *E-Cigarette Task Force: Reference Report* **2014**, 1-12.

44. Schaller, K.; Ruppert, L.; Kahnert, S.; Bethke, C.; Nair, U.; Pötschke-Langer, M. Electronic Cigarettes - An Overview. In *Red Series Tobacco Prevention and Tobacco Control*German Cancer Research Center: Heidelberg, 2013; Chapter 19.

45. Polli, G. P.; Grim, W. M.; Bacher, F. A.; Yunker, M. H. Influence of formulation on aerosol particle size. *J. Pharm. Sci.* **2006***, 58*, 484-486.

46. Heyder, J.; Gehbart, J.; Rudolf, G.; Schiller, C. F.; Stahlhofen, W. Deposition of particles in the human respiratory tract in the size range 0.005-15 um. *J. Aerosol Sci.* **1986***, 17*, 811-825.

47. Westenberger, B. J. Evaluation of e-cigarettes. *St. Louis: Food and Drug Administration* **2009**, 1-8.

CHAPTER 5: LOW TEMPERATURE PLASMA IONIZATION-MASS SPECTROMETRY OF COMPOUNDS FROM SIZE SELECTED OF AEROSOL PARTICLES

5.1 Introduction

Many characteristics of aerosol particles are dependent on particle diameter including particle diffusion,[1] deposition,[2] light scattering,[3,4] coagulation,[5] and chemical composition[6,7]. Commercial aerosol mass spectrometers are designed with a time of flight drift region within the high vacuum system to size select aerosol particles prior to compositional analysis.[8-10] The particle drift time, measured by light scattering or beam chopping, is used to determine the diameter of the aerosol particles.[10,11] As discussed in Chapter 1, introducing aerosols containing semi-volatile compounds into a high vacuum system leads to preferential sampling of low volatility analytes.[12] The commercially available aerosol mass spectrometry system advertises a particle size range as low as 40 nm[14] and other studies have reported measurement of aerosol particle diameters as small as 80 nm by aerosol time of flight and laser light scattering in a mass spectrometer[13]. However, a significant increase in experimental cost and complexity is incurred if lasers are used for drift time determination by light scattering. For these reasons, it is desirable to size select aerosol particles at atmospheric pressure rather than within the vacuum system of the mass spectrometer.

A common method for size selection of aerosol particles at atmospheric pressure is impaction onto a surface.[15-17] Cascade impactors separate particles based on inertia, which is dependent on particle size.[18,19] Impactors suffer from potential overloading,[20] analyte loss from bounce of larger particles,[21,22] and result in particle fractions with ill-defined particle diameters[23] in addition to the sample evaporation associated with storage of aerosol particles containing semi-volatile compounds on a surface (Chapter 3). For these reasons, a particle sizing device that does not depend upon analyte collection is preferred for particle size selection prior to mass analysis. A differential mobility analyzer (DMA) is an alternative to impaction of aerosol particles for size selection at atmospheric pressure. The DMA uses the diameter dependence of aerosol particle movement in an electric field to size select aerosol particles.[24,25] The output of the DMA is a constant beam of aerosol particles with a narrow particle diameter range that can

be easily coupled with the ambient ion sources introduced in Chapter 4. The experiments presented in this chapter exemplify the utility of a DMA for particle size selection prior to ionization of compounds from aerosol particles by low temperature plasma ionization (LTPI).

5.2 Differential Mobility Analysis Theory

The information presented in this section is designed to be overview of differential mobility analysis and may be found in more detail in Reist, 1993.[26] A DMA separates aerosol particles based on the ratio of the particle diameter and charge. The DMA used for these experiments is shown schematically in Figure 5.1. Triboelectric charging of particles during aerosol generation results in an unpredictable particle charge distribution.[27] To give the aerosol particles a predictable charge state distribution prior to size separation, the polydisperse aerosol is passed through a ^{85}Kr radioactive source. The beta particle decay of ^{85}Kr generates bipolar ions from air that result in bipolar diffusion charging of aerosol particles.[28] The fraction of aerosol particles with n charges may be approximated by the empirical relationship

$$f(n) = 10^{\left[\sum_{i=0}^{5} a_i(n)(logD_p)^i\right]} \qquad \text{Equation 1}$$

where $a_i(n)$ is an empirically derived approximation coefficient and D_p is the particle diameter in meters.[29] It has been determined that particles smaller than approximately 20 nm carry a maximum of one positive or negative charge. If 20 nm < D_p < 70 nm, n is at most ±2, while particles larger than 70 nm may carry 3 or more charges.[29] For aerosol particles with diameters greater than 100 nm, the number of charges on a particle from bipolar charging with a radioactive source in the continuum regime may be approximated by a Boltzmann equilibrium distribution of charges.[30,31] Thus, the fraction of aerosol particles with a charge n is described by:[32]

$$f(n, D_p) = \frac{2e}{\sqrt{\pi D_p k_B T}} e^{\left(-\frac{n^2 e^2}{D_p k_B T}\right)} \qquad \text{Equation 2}$$

in which k_B is the Boltzmann constant, T is the temperature in Kelvin, and e is the elementary charge of an electron in Coulombs. The average number of charges on an aerosol particle ($\bar{n}$) may be approximated by the relationship[26]

$$\bar{n} = \sqrt{\frac{D_p k_B T}{\pi e^2}} \qquad \text{Equation 3}$$

After charge redistribution from bipolar diffusion charging in the radioactive ion source, the polydisperse aerosol enters the top of the cylindrical DMA as depicted in Figure 5.1. A sheath gas is used to direct the aerosols through the DMA toward the output at the bottom of the device with the velocity of the sheath gas, v_y. Positive aerosol particles are drawn toward the central DMA electrode by application of a voltage (-20 to -10,000 V, particle trajectory illustrated by lines a-c in Figure 5.1) and negatively charged particles are repelled towards the walls of the DMA (line d in Figure 5.1). Thus, one of the primary disadvantages of particle sizing using a DMA is that only one aerosol particle polarity is sampled. The terminal electric velocity (v_{te}, cm/s) at which a spherical particle is drawn toward the central electrode is defined as

$$v_{te} = ZE \qquad \text{Equation 4}$$

where Z is the electrical mobility of the aerosol particle in cm^2/Vs and E is the electric field strength in the device in V/cm. The electrical mobility of an aerosol particle is dependent on the number of charges on the aerosol particle and the particle diameter and is described by

$$Z = \frac{c_c ne}{3\pi\mu D_p} \qquad \text{Equation 5}$$

In Equation 5, c_c is the slip correction coefficient, a dimensionless constant related to the inverse of the Knudsen number (the ratio of the sheath gas mean free path to the aerosol particle radius), and μ is the viscosity of the sheath gas in m^2s^{-1}. Equation 5 shows that the electrical mobility of an aerosol particle is inversely proportional to the diameter-to-charge ratio of the particle. Thus, as depicted by the particle trajectory shown by line a in Figure 5.1, particles with diameter-to-charge ratios smaller than the diameter-to-charge ratio of an aerosol particle with the selected electrical mobility that is stably passed through the DMA (line c in Figure 5.1) will have a v_{te} that is large in comparison to v_y so the particles impact on the central electrode and are neutralized. Line b in Figure 5.1 shows the trajectory of particles through the DMA with a diameter-to-charge ratio that is larger than selected. Aerosol particles will be neutralized via impaction onto the DMA housing because v_{te} is low in comparison to v_y. Aerosol particles with the selected electrical mobility have a v_{te} and v_y such that the particles will follow the trajectory depicted by line c in Figure 5.1 and exit through the DMA output. The average particle diameter of the selected aerosol beam transmitted through the DMA can be changed by varying the voltage applied to the

central electrode and thus the electric field in the device. Incrementally increasing the magnitude of the voltage applied to the central DMA electrode results in a scan of the electrical mobility, and thus the diameter, of the particles selected by the DMA. A condensation particle counter (CPC) was used for measurement of the concentration of aerosol particles in the monodisperse beam. The aerosol particles were directed into a chamber saturated with isobutyl alcohol vapor, which condenses onto the monodisperse particles to increase their diameter prior to particle counting. Light scattering is used to determine the number of particles in a given volume, allowing the particle concentration to be determined and correlated to the diameter of the aerosol particles selected by the DMA.

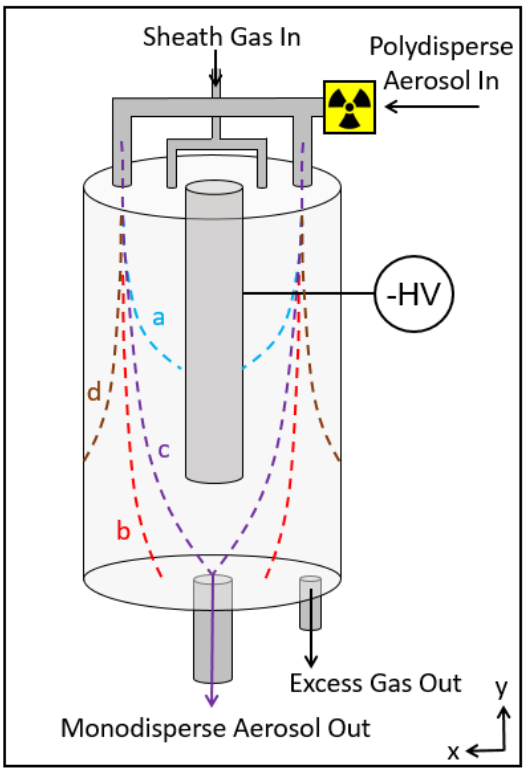

Figure 5.1. Schematic of the differential mobility analyzer used to generate monodisperse aerosol.

5.3 DMA-LTPI-MS of pyrolysis products

Ethyl cellulose was pyrolyzed in the custom pyrolysis chamber at approximately 400 ºC. The lognormal particle count distribution of ethyl cellulose produced at approximately 400 ºC as determined by the DMA-CPC is shown in Figure 5.2A. The lognormal count distribution was converted to the lognormal mass distributions using the following equation:

$$\frac{dW}{dlog(D_p)} = \rho_p \frac{\pi}{6} D_p^3 \frac{dN}{dlog(D_p)} \qquad \text{Equation 6}$$

In Equation 6, the mass concentration ($\frac{dW}{dlog(D_p)}$) is in μg/mL, ρ_p is the particle density in μg/mL, and D_p is the particle diameter in cm. For simplicity, it was assumed that the aerosol particles were spherical with densities of 1.50 x 10^6 μg/mL, equal to that of cellulose.[33] The assumption of spherical particles along with variations in particle density based on particle composition, which depends on particle diameter,[6,7] are expected and are the most significant sources of error in this conversion. The mass distribution for ethyl

cellulose pyrolyzed at approximately 600 °C is displayed in Figure 5.2B.

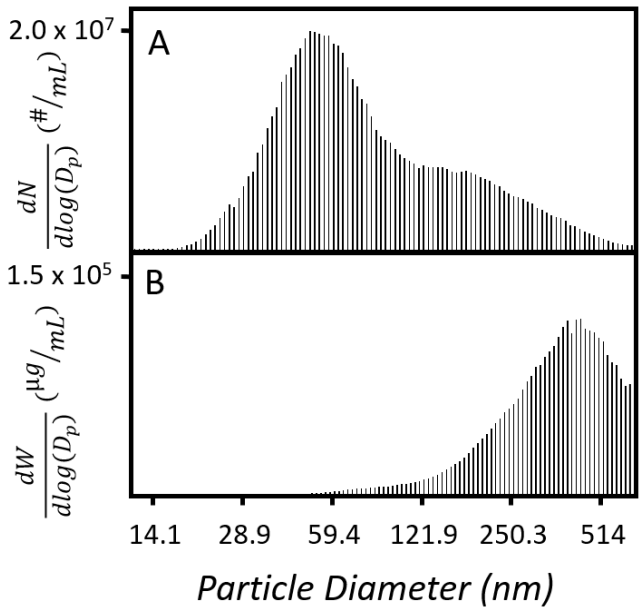

Figure 5.2. A. Lognormal count distribution and B. lognormal mass distribution for ethyl cellulose pyrolyzed at approximately 400 ℃.

To investigate the composition of size selected aerosol particles, LTPI-MS was performed on size selected aerosol particles from the output of the DMA. The Bruker Esquire 3000 was used for the experiments in this chapter. The standard size LTPI source was used in the conventional configuration to ionize compounds in the aerosol particles. The DMA was used to select two particle diameters, 50 nm and 120 nm. The background subtracted mass spectra are displayed in Figure 5.3. When particles of 50 nm are selected and ionized, as shown in Figure 5.3A, essentially no ion signal is observed. A low mass concentration of aerosol particles with a diameter of 50 nm is generated by pyrolysis of ethyl cellulose at 400 ºC (approximately 2 x 10^3 μg/mL). The mass concentration of the particles with a diameter of 120 nm is approximately 1 x 10^4 μg/mL and the mass spectrum generated by LTPI of the 120 nm aerosol particles is shown in Figure 5.3B. Ions characteristic of LTPI of pyrolyzed ethyl cellulose are generated from size selected particles of 120 nm (*m/z* 201, 199, 171, 155). The decrease in the signal of the ion of *m/z* 149, a background phthalate, relative to background occurs. The reduction in the absolute intensity of background ions such as the phthalate of *m/z* 149 when sample is present is a common phenomenon observed during ambient ionization experiments performed in this laboratory. The decrease in intensity of background ions may be because of operation of the mass analyzer in ion current control mode. To ensure adequate signal response, the time over which ions are collected in the ion trap is allowed to vary from 0.1 up to 200 ms until a specified number of ions is collected. The ion trap is filled with background ions when there is no sample present. When sample is introduced, the same total number of ions is collected but the time over which ions are collected is decreased due to the higher initial

concentration of ions. Thus, a smaller fraction of ions in the ion trap are background resulting in a decrease in absolute signal intensity of the background ions.

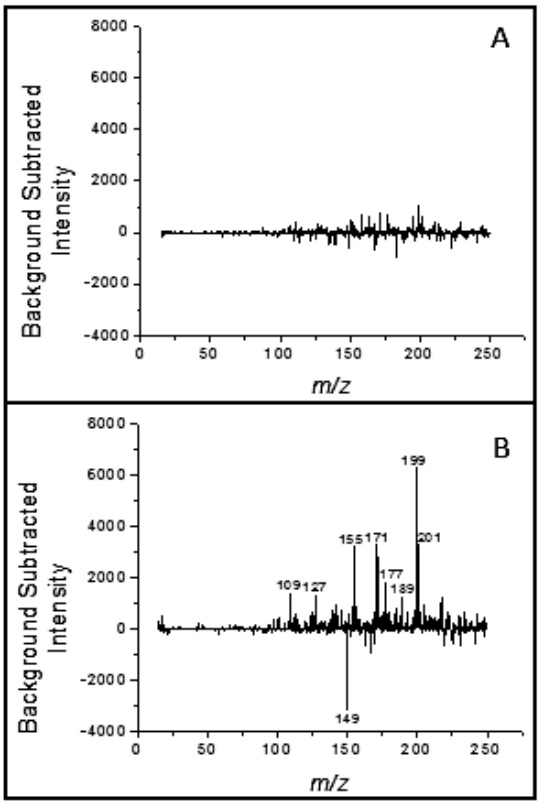

Figure 5.3. DMA-LTPI-MS of aerosol particles of A. 50 nm and B. 120 nm produced by pyrolysis of ethyl cellulose at approximately 400 ºC in the custom pyrolysis chamber.

An alternative explanation for the decrease in abundance of background ions is based on the gas phase reactions that occur during ionization. If the gas phase basicity of analyte ions is higher than that of the background phthalate of *m/z* 149, proton transfer will occur between the analyte neutrals and protonated phthalate molecules. Thus, background amount of *m/z* 149 present prior to mass analysis will be reduced. Overall, the data presented in this section shows the viability of DMA-LTPI-MS for analysis of size selected aerosol particles and it is confirmed that the signal response is dependent on the mass concentration of aerosol particles as opposed to the number concentration.

5.4 Influence of Pyrolysis Temperature on Aerosol Particle Distributions

The DMA-CPC system was used to measure the particle count distribution of aerosols produced by pyrolysis in the custom pyrolysis chamber at three different temperatures. A plot of the background subtracted lognormal count distribution of aerosol particles produced by pyrolysis at three temperatures is

shown for ethyl cellulose (Figure 5.4), pure microcrystalline cellulose (Figure 5.5), cellulose crudely extracted from tobacco (Figure 5.6), and tobacco from a Marlboro cigarette (Figure 5.7). In Figures 5.4-5.7, panel A is the distribution of aerosol particles produced at approximately 200 °C, the count distribution in panel B was produced at approximately 400 °C, and panel C is the count distribution that was produced at approximately 600 °C. A summary of the mode, median, and mean particle diameter and particle concentration for the count distributions of the four samples pyrolyzed at each temperature is shown in Table 5.1. The lognormal count distributions for the four natural polymers shown in Figures 5.4-5.7 were converted to lognormal mass distributions assuming spherical aerosol particles with a density of 1.50×10^6 μg/mL. A summary of the mode, median, and mean particle diameter and particle mass concentration for the mass distributions of the four samples pyrolyzed at each temperature is shown in Table 5.2. The background subtracted lognormal mass distributions are shown in Figure 5.8 (pyrolyzed ethyl cellulose), Figure 5.9 (pyrolyzed pure microcrystalline cellulose), Figure 5.10 (pyrolyzed cellulose crudely extracted from tobacco), and Figure 5.11 (pyrolyzed tobacco from a Marlboro cigarette). For Figures 5.8-5.11, panel A is the distribution of aerosol particles produced at approximately 200 °C, panel B was produced at approximately 400 °C, and panel C was produced at approximately 600 °C.

There is a general trend of increasing overall particle concentration with temperature. An exception to this trend is observed for purified cellulose; the particle number and mass concentration decreases between pyrolysis at 200 ºC or 400 ºC (Figure 5.5A-B count distribution, Figure 5.9A-B mass distribution). However, because of the poor temperature control in the custom chamber and thus the lack of reproducibility of these pyrolysis experiments, no significance can be attributed to this deviation from the general trend.

Though the shape of the particle size distribution changes with temperature, no obvious correlation is observed between particle count distribution and temperature. The poorly predictable variation of the dependence of the count and mass distribution of aerosol particles on pyrolysis temperature illustrates the importance of reproducible pyrolysis conditions. The pyrolysis conditions must be tightly controlled to prevent excessive variation in the particle size distribution and composition of the sample generated. For this reason, the PyroProbe should be used for sample generation because aspects of the heating profile including temperature ramp rate and maximum pyrolysis temperature are

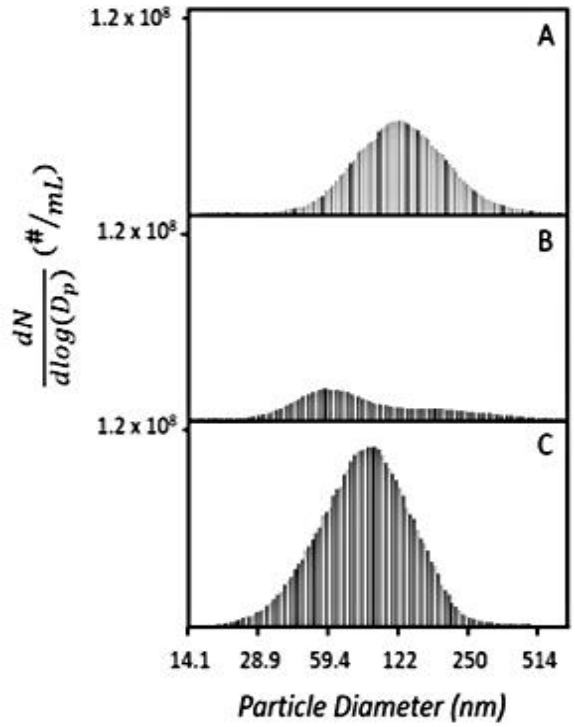

Figure 5.4. Particle count distribution for ethyl cellulose pyrolyzed in the custom pyrolysis chamber at approximately A. 200 °C B. 400 °C and C. 600 °C.

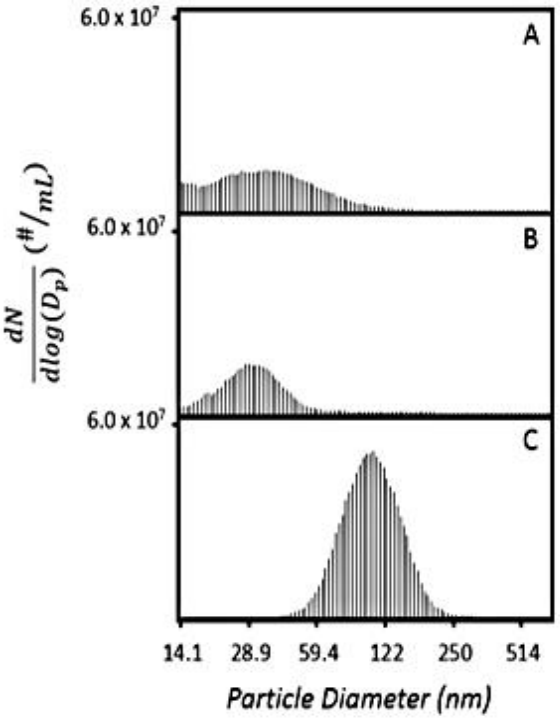

Figure 5.5. Particle count distribution for cellulose pyrolyzed in the custom pyrolysis chamber at approximately A. 200 °C B. 400 °C and C. 600 °C.

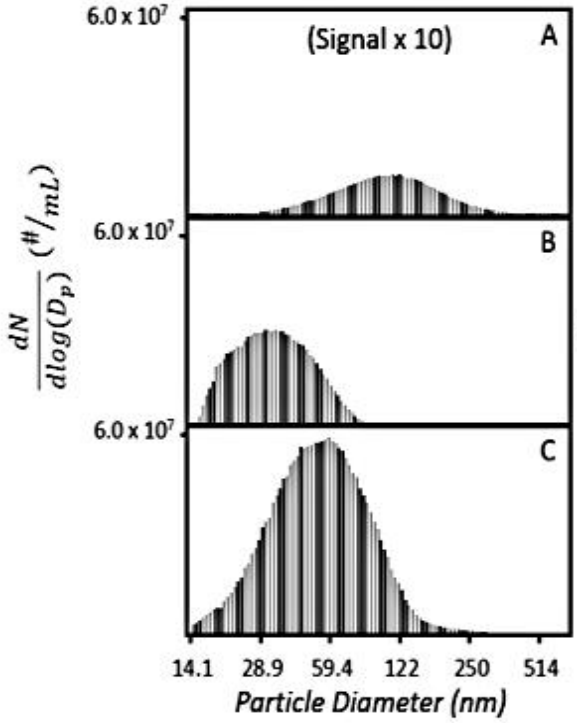

Figure 5.6. Particle count distribution for crudely extracted cellulose pyrolyzed in the custom pyrolysis chamber at approximately A. 200 °C B. 400 °C and C. 600 °C.

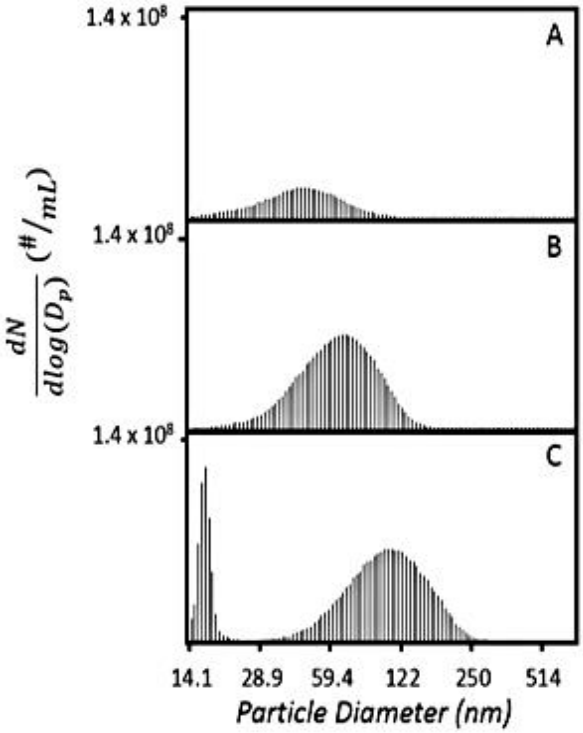

Figure 5.7. Particle count distribution for Marlboro tobacco pyrolyzed in the custom pyrolysis chamber at approximately A. 200 °C B. 400 °C and C. 600 °C.

Table 5.1. Particle size statistics for the distributions shown in Figures 5.4-5.7.

Sample	Approx. Pyrolysis Temperature (°C)	Mode Diameter (nm)	Median Diameter (nm)	Mean Diameter (nm)	Particle Concentration (µg/m³)
Ethyl Cellulose	200	162	202	271	6.2×10^4
Ethyl Cellulose	400	429	362	363	3.4×10^4
Ethyl Cellulose	600	241	265	300	8.5×10^4
Purified Cellulose	200	685	309	336	1.9×10^3
Purified Cellulose	400	685	428	417	4.4×10^3
Purified Cellulose	600	685	189	292	2.5×10^4
Crude Cellulose	200	250	270	313	1.7×10^3
Crude Cellulose	400	59.3	63.8	152	8.3×10^2
Crude Cellulose	600	685	192	260	1.2×10^4
Tobacco	200	71.0	114	207	1.6×10^3
Tobacco	400	98.2	113	218	9.5×10^3
Tobacco	600	181	202	283	4.9×10^4

Table 5.2. Particle mass statistics for the distributions shown in Figures 5.8-5.11.

Sample	Approx. Pyrolysis Temperature (°C)	Mode Diameter (nm)	Median Diameter (nm)	Mean Diameter (nm)	Particle Concentration (#/cm³)
Ethyl Cellulose	200	122	122	139	2.8×10^7
Ethyl Cellulose	400	55.2	73.0	110	1.1×10^7
Ethyl Cellulose	600	94.7	86.4	97.0	5.2×10^7
Purified Cellulose	200	34.6	33.9	42.1	8.0×10^6
Purified Cellulose	400	28.9	30.9	44.5	6.3×10^6
Purified Cellulose	600	106	103	111	1.7×10^7
Crude Cellulose	200	113	107	123	7.2×10^5
Crude Cellulose	400	31.0	33.5	36.9	1.5×10^7
Crude Cellulose	600	57.2	52.0	60.0	3.1×10^7
Tobacco	200	46.1	43.3	48.0	1.0×10^7
Tobacco	400	63.8	61.5	65.7	3.0×10^7
Tobacco	600	16.2	89.5	92.9	3.7×10^7

controllable.

Shown in Figure 5.12A is the particle mass distribution of cellulose pyrolyzed in the PyroProbe at 650 °C. The mode of the observed particle mass distribution is also larger than was observed from the custom pyrolysis unit (615 nm). The larger particle diameters are likely due to the lower concentration of analyte, resulting in less nucleation of aerosol particles and more condensation of compounds onto pre-existing particles and a larger average particle diameter.

Also shown in Figure 5.12 are the mass spectra produced from LTPI of size selected aerosol

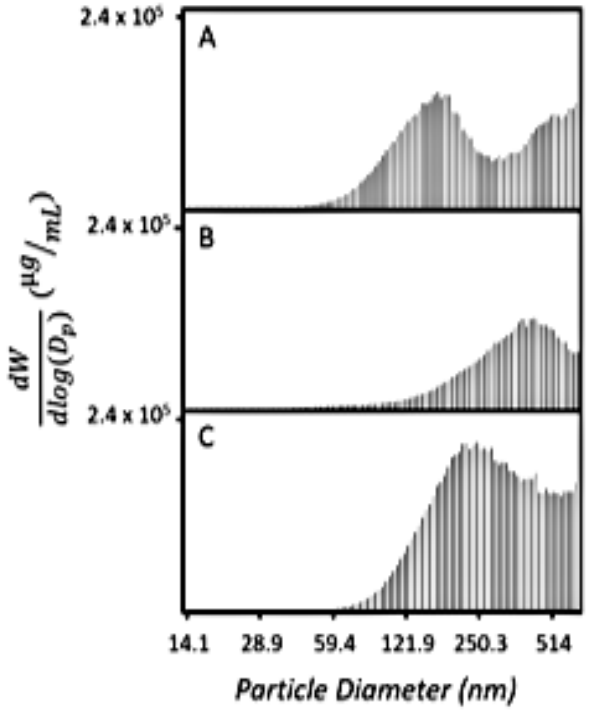

Figure 5.8. Particle mass distribution for ethyl cellulose pyrolyzed in the custom pyrolysis chamber at approximately A. 200 °C B. 400 °C and C. 600 °C.

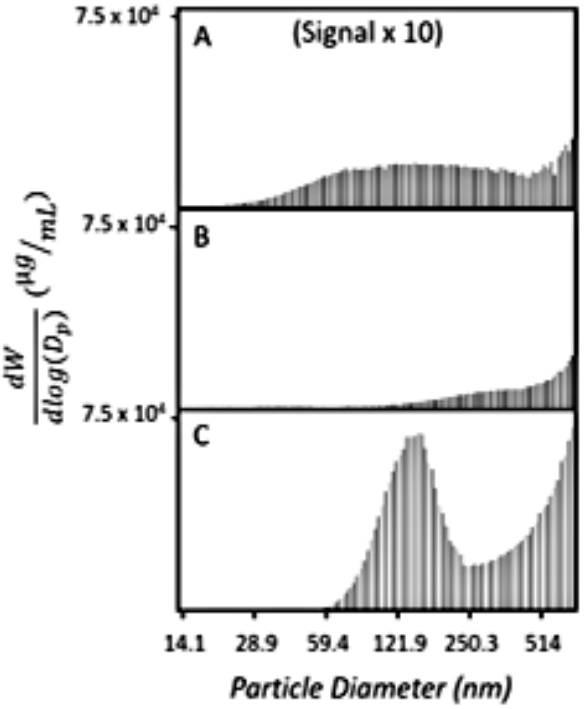

Figure 5.9. Particle mass distribution for cellulose pyrolyzed in the custom pyrolysis chamber at approximately A. 200 °C B. 400 °C and C. 600 °C.

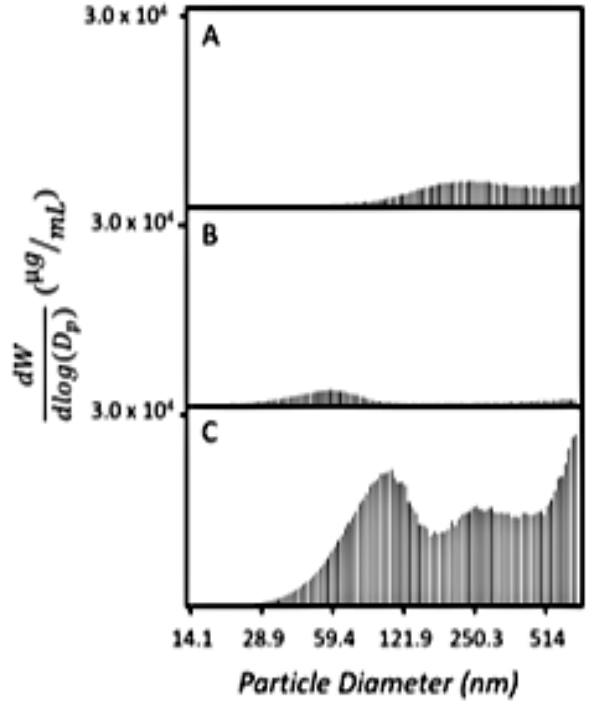

Figure 5.10. Particle mass distribution for a crude cellulose extract pyrolyzed in the custom pyrolysis chamber at approximately A. 200 °C B. 400 °C and C. 600 °C.

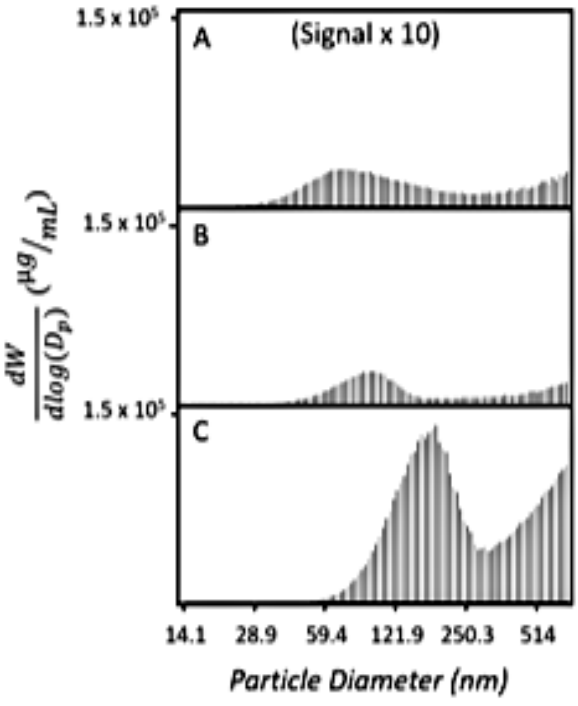

Figure 5.11. Particle mass distribution for Marlboro tobacco pyrolyzed in the custom pyrolysis chamber at approximately A. 200 °C B. 400 °C and C. 600 °C.

particles produced by pyrolysis of cellulose in the PyroProbe at 650 °C. No ion signal is observed when the DMA is set to pass particles of approximately 20 nm because almost no aerosol is present (Figure 5.12B, 0.73 μg/mL). Differences in the ions generated by LTPI are observed when the DMA is set to pass particles of approximately 100 nm (Figure 5.12C, 1 x 10^3 μg/mL) as compared to approximately 150 nm (Figure 5.12D, 4 x 10^3 μg/mL). However, the low mass concentration of aerosol particles and thus the reproducibility of this method severely limit the application. Improvements to the DMA-LTPI system to improve signal intensity and increase reproducibility will be discussed in Chapter 8.

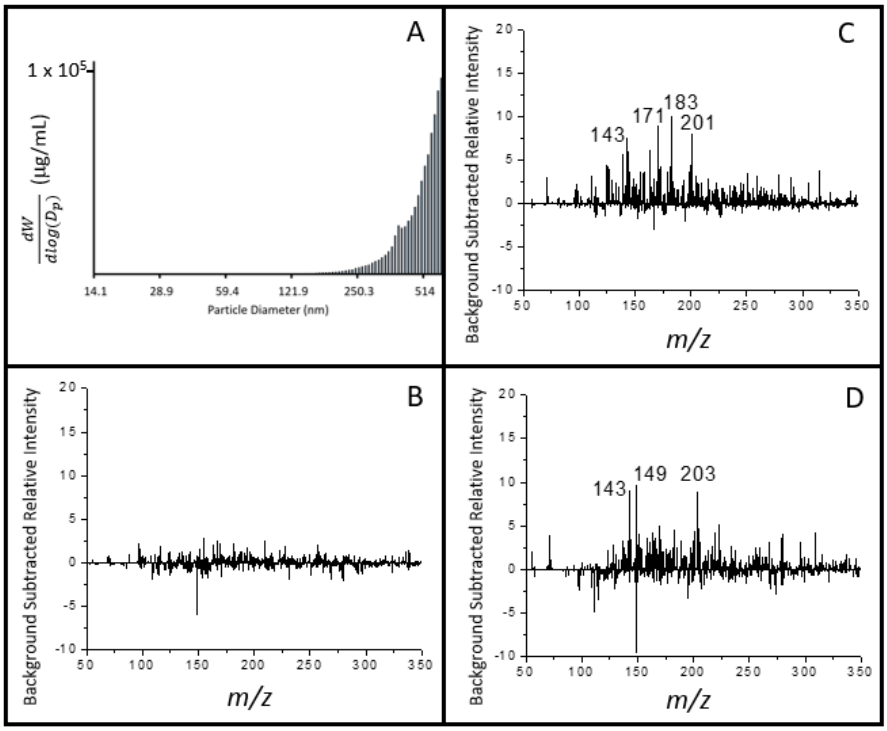

Figure 5.12. A. Particle mass distribution of cellulose generated at 650 °C in the PyroProbe and mass spectra produced from selected particle diameters of B. 20 nm C. 100 nm and D. 150 nm.

5.4 Summary and conclusions

Aerosol particle composition is known to vary depending on particle diameter.[6,7] Commonly used particle sizing methods are associated with a number of drawbacks and are not compatible with analysis of aerosol particles in real time. In this chapter, a DMA was investigated for use as an aerosol size selection technique prior to ambient ionization of compounds from aerosol particles.

LTPI was used to ionize compounds from size selected aerosol particles generated by pyrolysis of ethyl cellulose. It was confirmed that the signal response from DMA-LTPI-MS is more influenced by the

mass concentration of aerosol particles than the number concentration of aerosol particles. When a particle diameter corresponding to a low particle mass concentration is selected, only background signal is observed from LTPI. Size selection of aerosol particles with a higher particle mass concentration prior to ionization resulted in the generation of typical LTPI-type analyte ions from the sample. These results show that the DMA-LTPI system is viable for size selection and ionization of compounds from aerosol particles prior to mass spectrometric analysis.

The influence of the final pyrolysis temperature on the count and mass distributions of aerosol particles was investigated for four samples of interest, ethyl cellulose, cellulose, a crude cellulose extract, and Marlboro tobacco. Variation of the particle size distribution with the pyrolysis temperature was observed, emphasizing the importance of reproducible pyrolysis conditions for studies involving size selected aerosol particles. DMA-LTPI-MS was performed from aerosols produced from pyrolysis using the PyroProbe and it is shown that DMA-LTPI-MS could be used for investigation of differences in the composition of aerosol particles with different diameters. Improvements to the methods presented in this chapter to increase the reproducibility of DMA-LTPI-MS will be discussed in Chapter 8.

REFERENCES

1. Kasper, G. Dynamics and Measurement of Smokes. I Size Characterization of Nonspherical Particles. *Aerosol Sci. Tech.* **1982***, 1*, 187-199.

2. Yu, C. P.; Diu, C. K. Total and regional deposition of inhaled aerosols in humans. *J. Aerosol Sci.* **1983***, 14*, 599-609.

3. Salt, K.; Noble, C. A.; Prather, K. A. Aerodynamic Particle Sizing versus Light Scattering Intensity Measurement as Methods for Real-Time Particle Sizing Coupled with Time-of-Flight Mass Spectrometry. *Anal. Chem.* **1996***, 68*, 230-234.

4. Li, Y.; Xue, R.; Ezell, M. J.; Finlayson-Pitts, B. J. Experimental and Theoretical Investigation of Aerosol Optical Properties. *Procedia Eng.* **2015***, 102*, 1204-1211.

5. Eggersdorfer, M. L.; Gröhn, A. J.; Sorensen, C. M.; McMurry, P. H.; Pratsinis, S. E. Mass-mobility characterization of flame-made ZrO2 aerosols: Primary particle diameter and extent of aggregation. *J. Colloid Interface Sci.* **2012***, 387*, 12-23.

6. Jang, M.; Czoschke, N. M.; Northcross, A. L. Atmospheric Organic Aerosol Production by Heterogeneous Acid-Catalyzed Reactions. *Chem. Phys. Chem.* **2004***, 5*, 1646-1661.

7. Zhang, X.; Lin, Y. H.; Surratt, J. D.; Zotter, P.; Prevot, A. S. H.; Weber, R. J. Light-absorbing soluble organic aerosol in Los Angeles and Atlanta: A contrast in secondary organic aerosol. *Geophys. Res. Lett.* **2011***, 38*, 1-4.

8. Noble, C. A.; Nordmeyer, T.; Salt, K.; Morrical, B.; Prather, K. A. Aerosol Characterization Using Mass-Spectrometry. *Trends Anal. Chem.* **1994***, 13*, 218-222.

9. Middlebrook, A. M.; Murphy, D. M.; Lee, S.; Thompson, D. S.; Prather, K. A.; Wenzel, R. J.; Liu, D.; Phares, D. J.; Rhoads, K. P.; Wexler, A. S.; Johnston, M. V.; Jimenez, J. L.; Jayne, J. T.; Worsnop, D. R.; Yourshaw, I.; Seinfeld, J. H.; Flagan, R. C. A Comparison of Particle Mass Spectrometers During the 1999 Atlanta Supersite Project. *J. Geophys. Res.* **2003***, 108*, 8424-8442.

10. Gard, E.; Mayer, J. E.; Morrical, B. D.; Dienes, T.; Fergenson, D. P.; Prather, K. A. Real-Time Analysis of Individual Atmospheric Aerosol Particles: Design and Performance of a Portable ATOFMS. *Anal. Chem.* **1997***, 69*, 4083-4091.

11. Canagaratna, M. R.; Jayne, J. T.; Jimenez, J. L.; Allan, J. D.; Alfarra, M. R.; Zhang, Q.; Onasch, T. B.; Drewnick, F.; Coe, H.; Middlebrook, A.; Delia, A.; Williams, L. R.; Trimborn, A. M.; Northway, M. J.; DeCarlo, P. F.; Kolb, C. E.; Davidovits, P.; Worsnop, D. R. Chemical and microphysical characterization of ambient aerosols with the aerodyne aerosol mass spectrometer. *Mass Spectrom. Rev.* **2007***, 26*, 185-222.

12. Posfai, M.; Xu, H.; Anderson, J.; Buseck, P. Wet and dry sizes of atmospheric aerosol particles: An AFM-TEM study. *Geophys. Res. Lett.* **1998***, 25*, 1907-1910.

13. Gälli, M.; Guazzotti, S. A.; Prather, K. A. Improved Lower Particle Size Limit for Aerosol Time-of-Flight Mass Spectrometry. *Aerosol Sci. Tech.* **2001***, 34*, 381-385.

14. Aerodyne Research, I. AMS: Aerosol Mass Spectrometer Systems. *http://www.aerodyne.com/sites/default/files/Aerosol%20Mass%20Spectrometer%20Systems.pdf* **2015**.

15. Udisti, R.; Dayan, U.; Becagli, S.; Busetto, M.; Frosini, D.; Legrand, M.; Lucarelli, F.; Preunkert, S.; Severi, M.; Traversi, R.; Vitale, V. Sea spray aerosol in central Antarctica. Present atmospheric behaviour and implications for paleoclimatic reconstructions. *Atmos. Environ.* **2012***, 52*, 109-120.

16. Mitchell, R. I. Improved Cascade Impactor for Measuring Aerosol Particle Sizes. *J. Ind. Eng. Chem.* **1959***, 51*, 1039-1042.

17. Aceves, M.; Grimalt, J. O. Seasonally dependent size distributions of aliphatic and polycyclic aromatic hydrocarbons in urban aerosols from densely populated areas. *Environ. Sci. Technol.* **1993***, 27*, 2896-2908.

18. May, K. R. The Cascade Impactor: An Instrument for Sampling Coarse Aerosols. *J. Sci. Instrum.* **1945***, 22*, 187-195.

19. Flynn, S. J.; Tong, Z. B.; Yang, R. Y.; Kamiya, H.; Yu, A. B.; Chan, H. K. Computational fluid dynamics (CFD) investigation of the gas–solid flow and performance of Andersen cascade impactor. *Powder Technol.* **2015***, doi: 10.1016/j.powtec.2015.03.039*.

20. van Gulijk, C.; Marijnissen, J. C. M.; Makkee, M.; Moulijn, J. A. Oil-soaked sintered impactors for the ELPI in diesel particulate measurements. *J. Aerosol Sci.* **2003***, 34*, 635-640.

21. Kang, M.; Cho, H.; Kwak, H.; Park, K. Evaluation of Particle Bounce in Various Collection Substrates to be Used as Vaporizer in Aerosol Mass Spectrometer. *Aerosol Sci. Technol.* **2015***, 49*, 332-339.

22. Jain, S.; Petrucci, G. A. A New Method to Measure Aerosol Particle Bounce Using a Cascade Electrical Low Pressure Impactor. *Aerosol Sci. Technol.* **2015***, 49*, 390-399.

23. Cavalli, F.; Facchini, M. C.; Decesari, S.; Mircea, M.; Emblico, L.; Fuzzi, S.; Ceburnis, D.; Yoon, Y. J.; O'Dowd, C. D.; Putaud, J. -.; Dell'Acqua, A. Advances in characterization of size-resolved organic matter in marine aerosol over the North Atlantic. *J. Geophys. Res.* **2004***, 109*, 2156-2202.

24. Rader, D. J.; McMurry, P. H. Application of the tandem differential mobility analyzer to studies of droplet growth or evaporation. *J. Aerosol Sci.* **1986***, 17*, 771-787.

25. Li, M.; You, R.; Mulholland, G. W.; Zachariah, M. R. Development of a Pulsed-Field Differential Mobility Analyzer: A Method for Measuring Shape Parameters for Nonspherical Particles. *Aerosol Sci. Technol.* **2014***, 48*, 22-30.

26. Reist, P. C. *Aerosol Sci. Technol.,* McGraw-Hill, Inc: New York, NY, 1993; p 379.

27. Matsusaka, S.; Maruyama, H.; Matsuyama, T.; Ghadiri, M. Triboelectric charging of powders: A review. *Chem. Eng. Sci.* **2010***, 65*, 5781-5807.

28. Kallinger, P.; Szymanski, W. W. Experimental determination of the steady-state charging probabilities and particle size conservation in non-radioactive and radioactive bipolar aerosol chargers in the size range of 5–40 nm. *J. Nanopart. Res.* **2015***, 17*, 171.

29. Wiedensohler, A. An approximation of the bipolar charge distribution for particles in the submicron size range. *J. Aerosol Sci.* **1988***, 19*, 387-389.

30. Fuchs, N. A. On the Stationary Charge Distribution on Aerosol Particles in a Bipolar Ionic Atmosphere. *Geofis. Pura Appl.* **1963***, 56*, 185-193.

31. Kousaka, Y.; Adachi, M.; Okuyama, K.; Kitada, N.; Motouchi, T. Bipolar Charging of Ultrafine Aerosol Partiles. *Aerosol Sci. Tech.* **1983***, 2*, 421-427.

32. Hinds, W. C. *Aerosol Technology: Properties, Behavior, and Measurement of Airborned Particles;* Wiley-Interscience: New York, 1982; p 442.

33. Malm, C. J.; Genung, L. B.; Fleckenstein, J. V. Densities of Cellulose Esters. *Ind. Eng. Chem.* **1947***, 39*, 1499-1504.

CHAPTER 6: DIFFERENTIAL ION MOBILITY SPECTROSCOPY OF CELLULOSE PYROLYSIS PRODUCTS

6.1 Introduction

A significant limitation of mass spectrometry for the analysis of complex mixtures, such as the aerosols produced by pyrolysis, is that it is difficult to differentiate between isomeric or isobaric compounds using a mass spectrometer.[1,2] One method to differentiate isomers is the comparison of dissociation patterns generated by tandem mass spectrometry (MS/MS).[3] To deconvolute MS/MS spectra of unresolved isomeric compounds complex algorithms are required, the dissociation patterns of the pure compounds must be known, and the ions observed in the MS/MS spectra must be a linear combination of the dissociation patterns of the pure compounds.[4] Instead of attempting to deconvolute MS/MS spectra, chromatographic separations are often performed prior to ionization to distinguish between isomeric or isobaric analytes.[5,6] However, typical separation techniques such as gas chromatography (GC) or liquid chromatography (LC) are time consuming and require that the analyte be in the gas phase or in solution. These separation techniques, though amenable to samples collected on and extracted from filters, cannot be coupled with the analysis of the composition of aerosol particles in real time.

As an alternative to pre-ionization separations, ion mobility spectrometry (IMS) can be performed to separate ions prior to mass analysis. MS/MS can subsequently be used to interrogate the structure of ions and comparison of MS/MS dissociation patterns as well as the ion mobility of the analyte to ionized standards allows for confident identification of analytes. Differential ion mobility spectrometry (DIMS) separates ions in space based on the difference between the mobility of ions in high and low electric fields. In this chapter, DIMS is coupled with low temperature plasma ionization (LTPI) to investigate mixtures of isomeric and isobaric analytes from aerosol particles produced by pyrolysis. Differences in the ions observed from LTPI with and without DIMS are discussed. The reproducibility and quality of DIMS separations for the pyrolysis experiment is evaluated and LTPI-DIMS-MS/MS is performed on cellulose pyrolysis products.

6.2 Ion mobility spectrometry theory

IMS takes advantage of the dependence of the low field ion mobility (K_L) on the shape-to-charge ratio of ions travelling through a buffer gas. A schematic for separations of ions by IMS is shown in Figure 6.1. An electric field gradient is applied across sequential ring electrodes through a resistive network. Ions with a smaller shape-to-charge ratio undergo fewer collisions with the buffer gas and have a higher mobility than ions with a larger shape-to-charge ratio. Thus, ions with a smaller shape-to-charge ratio reach the detector before larger ions.

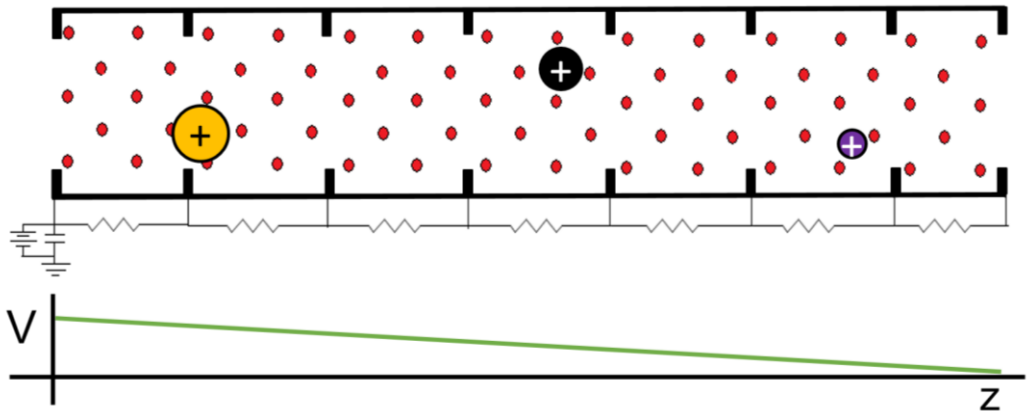

Figure 6.1. Schematic of a low field ion mobility separation. The voltage gradient is depicted below the schematic.

At low electric field strengths (less than approximately 10 kV/cm indicated in Figure 6.2 with a red dashed line) the ion mobility is independent of the magnitude of the electric field. Figure 6.2 depicts how the high field ion mobility (K_H) becomes dependent upon the electric field as the electric field strength is increased to greater than 10 kV/cm.[7-9] This change in mobility as the electric field strength is increased depends on the identity of the ion. For example, at high electric field strengths the red and blue ions have different mobilities whereas they have the same low-field ion mobility as depicted by the purple line in Figure 6.2. DIMS utilizes the differences in K_H and K_L to separate gaseous ions. The

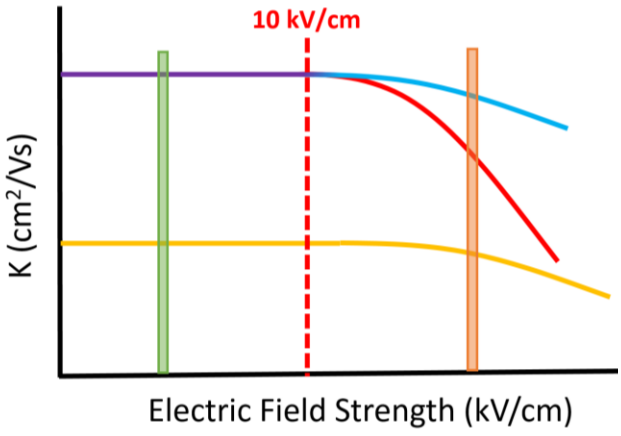

Figure 6.2.Schematic for the trend of the change in ion mobility with electric field strength.

schematic and a description of the DIMS device used for the experiments detailed in this chapter are shown in Figure 2.12. As described in detail in Chapter 2.5 a waveform is applied to the DIMS electrodes to approximate a square waveform (Figure 2.13). This DIMS waveform is depicted at the bottom of Figure 6.3. The dispersion field (E_D) between the two parallel electrodes alternates between the low field indicated with a green bar in Figure 6.2 and the high field indicated with the orange bar.

When the DIMS waveform is negative and in the low field positive ions are drawn toward the electrode to which the waveform is applied with the mobility K_L. The polarity of the DIMS waveform is then reversed and the magnitude of the voltage is increased into the high field. Positive ions are repelled from the electrode with the mobility K_H. Ions with a non-zero difference between K_H and K_L, such as the ions depicted by the red and grey lines in Figure 6.3, will exhibit a net displacement toward the DIMS electrodes. A dc compensation voltage (CV) can be applied to one of the DIMS electrodes to generate a compensation field (E_c) between the DIMS electrodes and correct the trajectory of ions with a selected differential mobility through the DIMS device. The schematic of the DIMS separation in Figure 6.3 depicts a E_c applied to correct the trajectory of the ions represented by the yellow and blue lines. These two ions follow the same trajectory because, as shown in Figure 6.2, they have the same differential ion mobility. Ions with increasing differential ion mobility can be sequentially passed through the DIMS device with a stable trajectory for mass analysis by incrementally increasing E_c to generate a E_c scan.

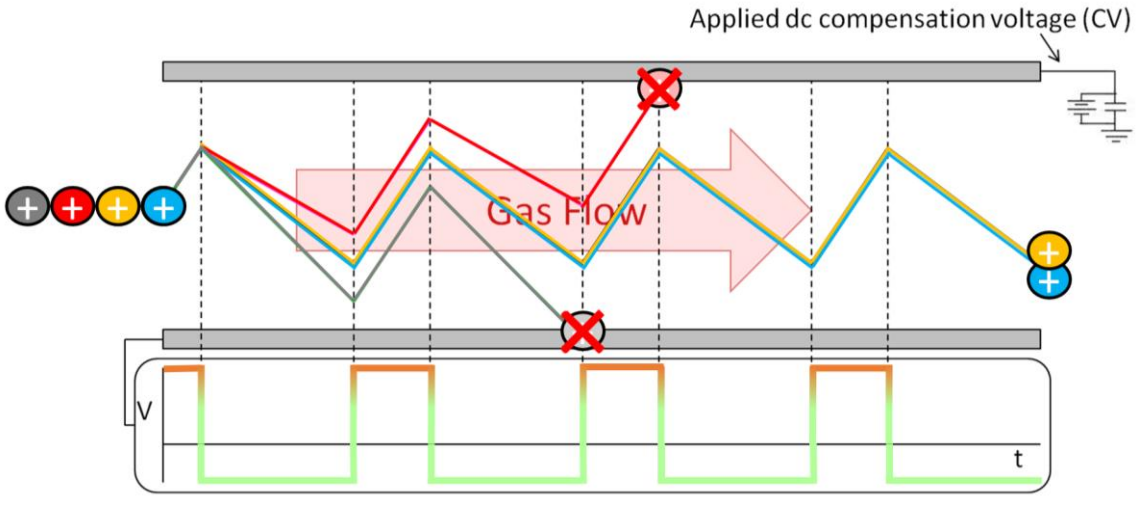

Figure 6.3. Schematic representation of the separation of ions in the DIMS device.

6.3 Application of DIMS to the separation of ionized pyrolysis products from aerosol particles

6.3.1 LTPI-DIMS-MS

Previous analyses of the gas and particle phase composition of the pyrolysis products of natural polymers have resulted in the identification of multiple isomeric and isobaric compounds.[10,11] Shown in Figure 6.4 is a comparison between the low and high resolution mass spectra generated by flow-through LTPI of cellulose pyrolyzed at 650 °C in the Pyroprobe. Figure 6.4A is of the mass spectrum generated using the low resolution Thermo Scientific linear ion trap mass spectrometer. As shown in Chapter 4, ions are observed at every mass-to-charge ratio. The odd mass-to-charge ratio ions are more abundant than even mass-to-charge ratio ions because LTPI is believed to occur by chemical ionization from protonated water clusters. A higher intensity of even mass-to-charge ratio ions in the flow-through versus the conventional LTPI configuration is proposed to be due to the reaction of analytes with radical species in the nitrogen plasma to form nitrogen-containing adducts, as discussed in detail in Chapter 4.

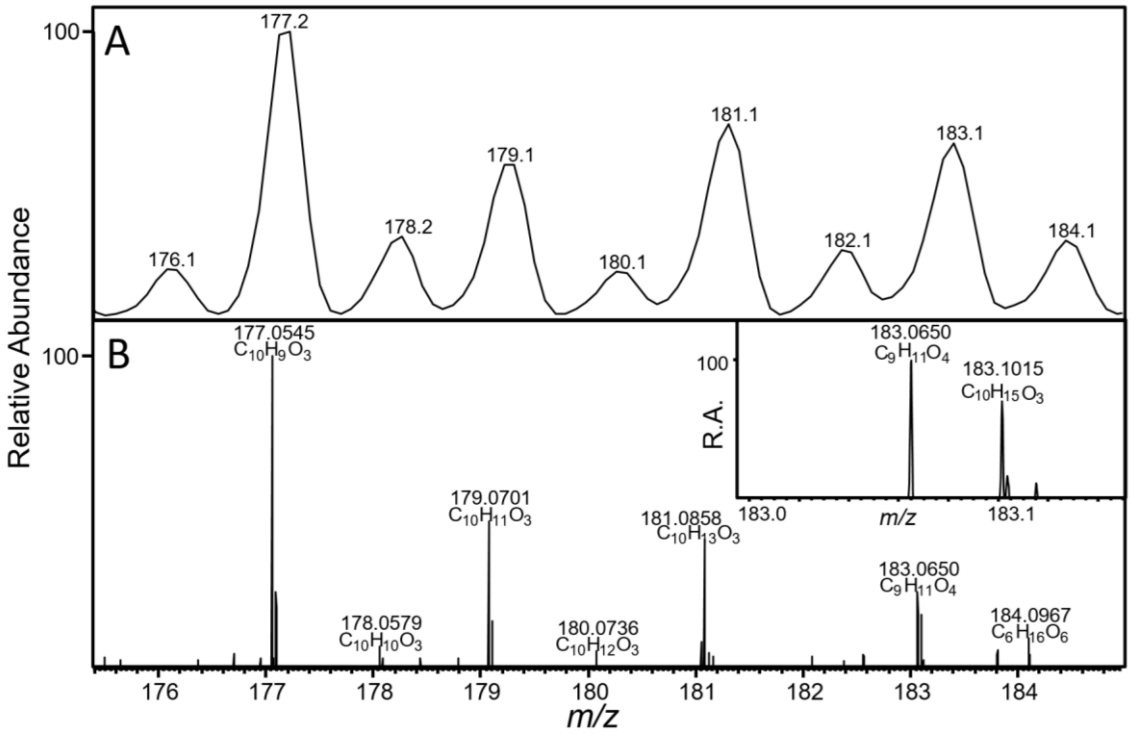

Figure 6.4. Cellulose pyrolyzed at 650 °C, ionized by LTPI, and mass analyzed using the A. linear ion trap or B. FTICR mass analyzer.

Figure 6.4B shows the high resolution/high mass accuracy mass spectrum generated using a Fourier transform ion cyclotron resonance (FTICR) mass analyzer. For each peak observed in the low

resolution mass scan shown in Figure 6.4A, multiple different protonated compounds can be distinguished in Figure 6.4B. The inset of Figure 6.4B shows the region of the high resolution mass spectrum between 183.0 and 183.2 Da. Two ions can be differentiated using the high resolution FTICR mass analyzer: *m/z* 183.0650 and 183.1015. The high mass accuracy of the FTICR mass analyzer allows the molecular formulas of these to ions to be determined as $C_9H_{11}O_4$ (1.0 ppm error) and $C_{10}H_{15}O_3$ (0.3 ppm error), respectively. Though the ability to generate molecular formulas for the analyte ions is highly useful, the FTICR mass analyzer was not the primary instrument used for the experiments in this dissertation. The poor sampling efficiency of low mass-to-charge ratio ions resulting from diffusion in the transfer tube required to conduct ions into the FTICR mass analyzer within the superconducting magnet limits the utility of this instrument.[12]

To investigate the extent of isomeric and isobaric convolution in low resolution mass spectra, DIMS was used in conjunction with the Bruker Esquire HCT. The ions generated by LTPI of cellulose pyrolyzed at 650 °C were separated by DIMS. A dispersion field of 33.3 kV/cm was used for the DIMS separations. The E_c was scanned from -10 V/cm to +300 V/cm. The DIMS separation of the ions formed by LTPI of background laboratory air is shown in Figure 6.5. A representative DIMS separation of the ions generated by LTPI of pyrolyzed cellulose is shown in Figure 6.6. Ions are binned into 1 Da wide windows centered at unit mass-to-charge ratios (e.g. 122.0, 123.0 etc.) to ensure that neighboring peaks are separated. For the purposes of visualization, the ion intensity for each mass-to-charge bin is normalized in the compensation field domain. Red indicates the highest ion abundance and purple indicates the

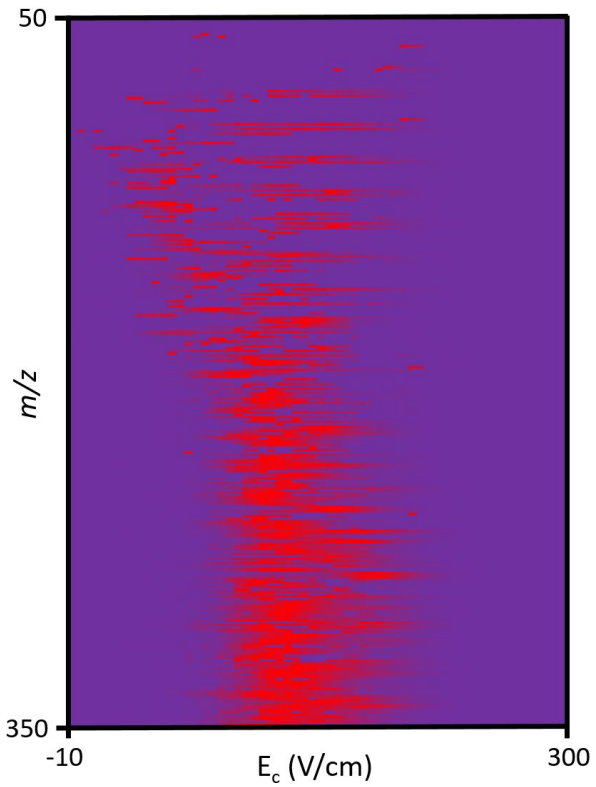

Figure 6.5. DIMS separation of background ions generated by LTPI. For the purposes of visualization, each mass-to-charge ratio is normalized in the compensation field domain to the most intense ion.

lowest ion abundance. For comparison, the mass spectrum from DIMS averaged over the course of the E_c scan (Figure 6.7A) and the mass spectrum observed without the DIMS device (Figure 6.7B) are shown in Figure 6.7.

The portion of the DIMS heat map highlighted with a yellow box in Figure 6.6 (*m/z* 95 – 135) is expanded and displayed in Figure 6.8. For clarity, each mass-to-charge ratio bin is delineated with black. To further investigate the separation of ions in the complex mixture of cellulose pyrolysis products, ion current traces were extracted from the DIMS heat map in Figure 6.8 and plotted to generate a compensation field scan as shown in Figure 6.9 for the ions of *m/z* 121 and 122 (outlined in blue in Figure 6.8).

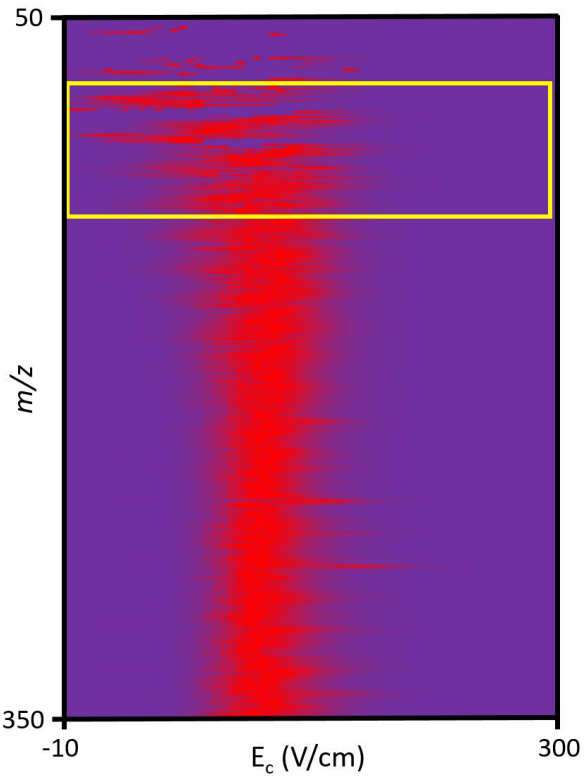

Figure 6.6. DIMS separation of ions produced by LTPI of cellulose pyrolyzed at 650 °C in the PyroProbe. For the purposes of visualization, each mass-to-charge ratio is normalized in the compensation field domain to the most intense ion.

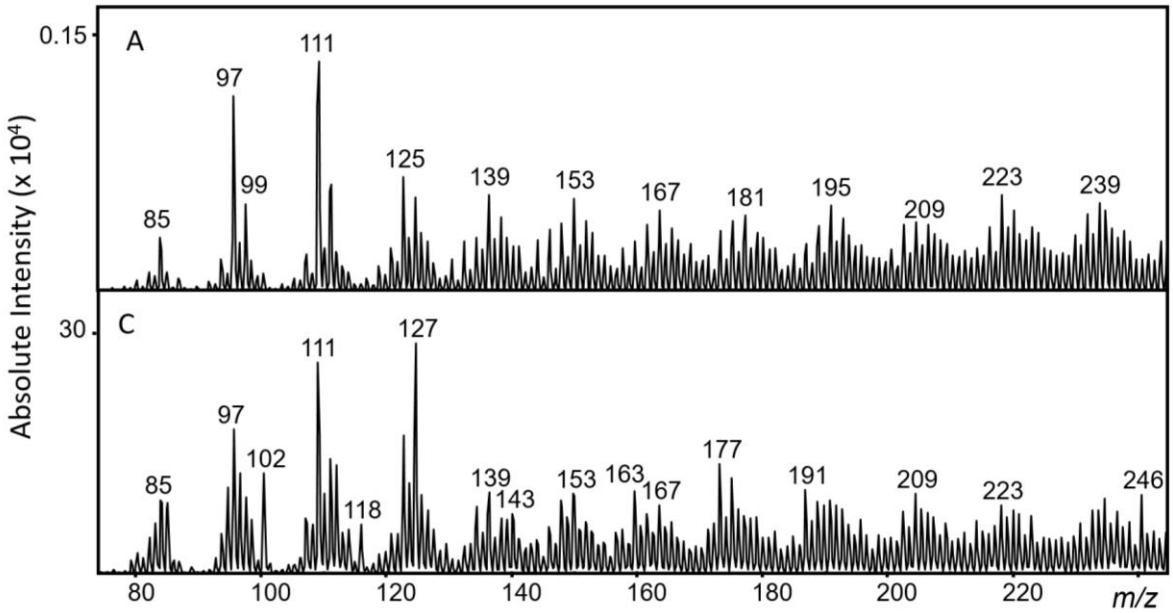

Figure 6.7. Cellulose pyrolyzed at 650 °C and ionized by flow-through LTPI A. averaged over the course of a compensation field scan B. with the DIMS electrode set at the same potential as the capillary and C. with no DIMS.

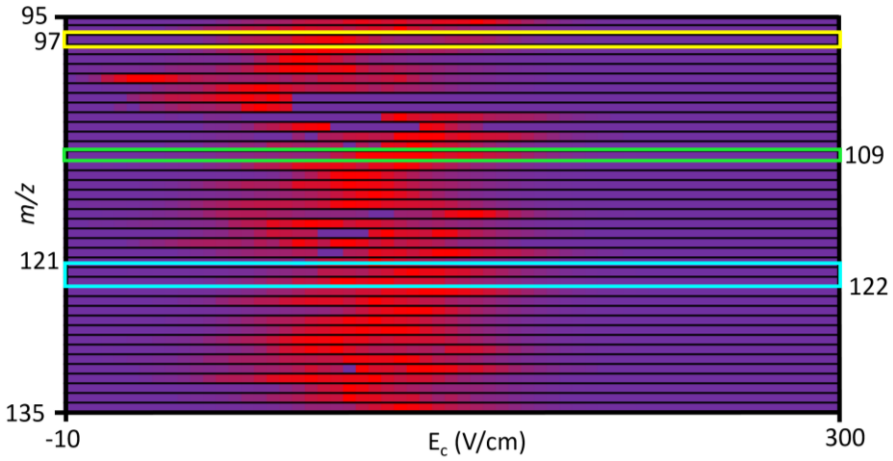

Figure 6.8. Expanded region of the heat map produced by LTPI-DIMS-MS of the pyrolysis products of cellulose produced at 650 °C in the PyroProbe.

The extracted ion current (XIC) traces displayed in Figure 6.9 demonstrate that there are analytes present at *m/z* 122 other than ^{13}C isotope of the ion of *m/z* 121. The relative abundance of the ions of *m/z* 121 and 122 varies between approximately +75 to +200 V/cm. Ions that differ by a ^{12}C versus a ^{13}C can be separated in DIMS[13] but separation of isotopes is not expected to be attainable with the settings used in these experiments. At some points in the compensation field scan shown in Figure 6.9, the abundance of the ion of *m/z* 122 relative to *m/z* 121 is greater than expected from the predicted isotopic contribution of ^{13}C. The ion of *m/z* 122 is anticipated to be due only to the isotopic contribution from ^{13}C (1.1% of the natural population of carbon atoms) because the pyrolysate of cellulose is expected to contain carbon, hydrogen, and oxygen. If the only ions at *m/z* 122 were due to the ^{13}C isotopic contribution of *m/z* 121 the relationship between the intensity of the ions of *m/z* 121 and 122 would be predicted by:

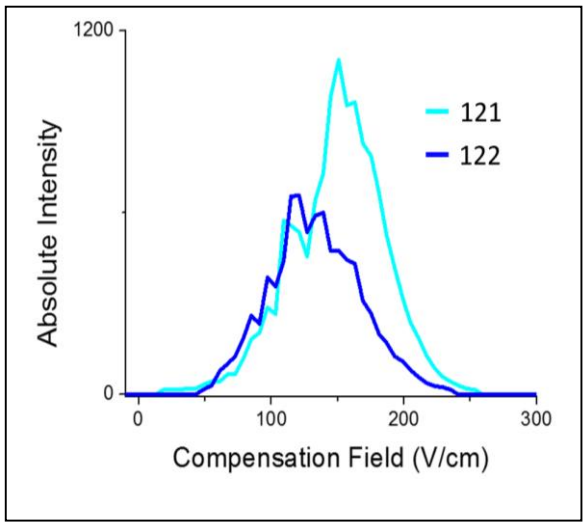

Figure 6.9. Compensation field scan for the ions of m/z 121 and 122 produced by LTPI of compounds from cellulose pyrolyzed at 650 °C.

$$\frac{Intensity\ M+1}{Intensity\ M} \times 100\% = Number\ of\ Carbons \times (1.1\%) \qquad \text{Equation 6.1}$$

If the only ions at *m/z* 122 were due to the ^{13}C isotopic contribution of *m/z* 121 the relative abundance of the ion of *m/z* 122 would be expected to be no more than 8.8% of the intensity of the ion of *m/z* 121 because a maximum of 8 carbon atoms can be logically present in a molecule of 120 amu that would be protonated in LTPI. As can be seen in Figure 6.8, differences in the shapes of the M and M+1 peaks is a common occurrence for the pyrolysis products of cellulose separated by DIMS, further confirming the presence of odd mass-to-charge ions other than isotopic peaks.

The widths and shapes of the peaks generated by DIMS separations are useful to evaluate the composition of the population of ions of each mass-to-charge ratio. For example, the XIC trace of the ion of *m/z* 109 generated by flow-through LTPI-DIMS-MS of the aerosol produced by the pyrolysis of cellulose at 650 °C in the PyroProbe (outlined in green in Figure 6.8) is shown over the course of the compensation field scan by the pink line in Figure 6.10. The typical FWHM of a single ionized small molecule in the E_c domain is between 10 and 30 V/cm for the DIMS device used in these experiments (peaks with a FWHM less than 10 V/cm are typically noise). For example, the FWHM for sodium cationized levoglucosan formed from ESI passing through the DIMS device using the same experimental conditions is 24.8 ± 0.2 V/cm. The broad, trailing peak observed from the DIMS separation of *m/z* 109 in Figure 6.10 is indicative of the presence of multiple analyte ions that are not resolved by the DIMS separation.

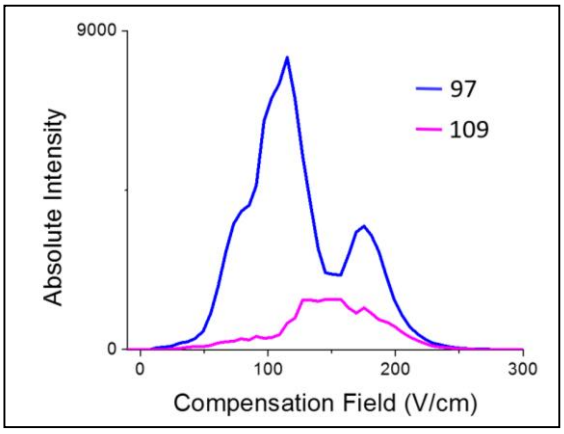

Figure 6.10. Compensation field scan for the ions of m/z 97 and 109 produced by LTPI of compounds from cellulose pyrolyzed at 650 °C.

Ions that are fairly well resolved in DIMS may also be identified in Figure 6.7. The XIC trace for the ion of *m/z* 97 (outlined in yellow in Figure 6.8) is shown in blue in Figure 6.10. As predicted from the DIMS heat map two peaks in the XIC compensation field scan of *m/z* 97 in Figure 6.10 are visually distinguishable. A shoulder with a centroid of approximately +75 V/cm is also observed which suggests a third partially resolved ion of *m/z* 97.

The typical FWHM of an ionized pure compound passed through the DIMS device is less than 30 V/cm but the majority of the XIC traces observed in the DIMS separation of the ions produced by LTPI

of pyrolyzed cellulose exhibit peak FWHMs greater than 30 V/cm and/or multiple resolved peaks (Figures 6.8 and 6.10). Origin 6.0 was used to fit one or two Gaussian curves to the XIC traces of ions with mass-to-charge ratios between 50 and 250 Da based on the following selection rules. If the FWHM of a single Gaussian curve fitted to an XIC trace was greater than 10 V/cm (an XIC trace with a FWHM less than 10 V/cm is considered to be noise) and less than 50 V/cm, one Gaussian peak was fitted to the data. The FWHM threshold of 50 V/cm as opposed to 30 V/cm was used to account for potential experimental variation; if a peak in the E_c scan was between 30 and 50 V/cm the ion intensity and resolution were typically too low to confidently select two centroid E_c values. If visual inspection of the XIC trace showed that there were in fact two resolved distributions, only one of which was fitted with the Gaussian curve, two Gaussian curves were fitted to the data. For example when the peak of *m/z* 97 shown in Figure 6.10 is fitted with a Gaussian curve only the low E_c peak is fitted automatically. If the FWHM of a peak was greater than 50 V/cm, it was assumed that the peak was a convolution of multiple unresolved analytes and two Gaussian curves were fitted to the data. No more than two Gaussian curves were fitted to each XIC trace even if the FWHM of the estimated Gaussian curves was greater 50 V/cm. Fitting more than two Gaussian curves to an XIC trace would result in a closer fit to the XIC traces and theoretically could be used to describe the convolution of unresolved ions observed from DIMS. However, for the purpose of this evaluation, little additional insight into the quality of the ion separation would be gained from fitting more than two peaks to each mass-to-charge ratio due to the poor demarcation of peak centroids in the DIMS separations and because the resolution in a separation is defined as between two peaks.

The peak center and FWHM of each Gaussian curve were determined for each XIC trace from two replicate experiments. Figure 6.11 shows graphically the correlation between the centroid E_c for the Gaussian curves that were fitted to the XIC traces for each of the two experiments. Data points on the x- and y-axes are due to ions that are observed in only one of the two experiments. These data points were omitted from the data set when performing the linear regression. The slope of the line of best fit was determined to be 0.90 with an R^2 of 0.90 (solid orange line). The red dotted line in Figure 6.11 indicates the line with a unity correlation coefficient. Preliminary experiments from this laboratory (data not shown) have shown that for replicate separations of a complex mixture of peptides from a tryptic digest of bovine serum albumin using DIMS system used in these experiments the slope of the line is 1.04 with an R^2 of

0.996. The near-unity slope and correlation coefficient between technical replicates of the DIMS separation of a complex mixture of known analytes illustrates the high reproducibility of the hardware used for DIMS of compounds generated by LTPI of the pyrolysis products of cellulose. Thus, the lower correlation of the centroid E_c value between replicate pyrolysis experiments is not due to the DIMS device but rather can be attributed to experimental variation associated with the aerosol generation and sampling or Gaussian fitting. Low abundance ions are more difficult to reproducibly fit with a Gaussian curve and can result in variation in the calculated centroid E_c. In summary, the LTPI-DIMS-MS experiment is relatively reproducible and the errors associated with the separation result primarily from low abundance ions and simplifications made for the theoretical treatment of the complex mixture of unknown ions.

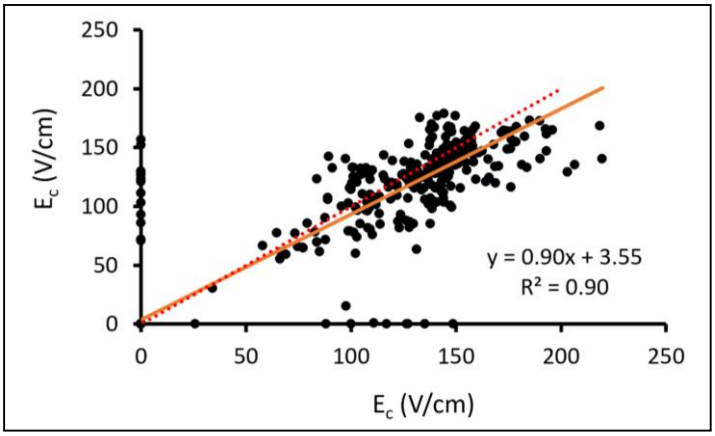

Figure 6.11. Comparison of the centroid compensation field values determined from Gaussian fitting of the XIC traces generated by DIMS separation of the ions generated by LTPI of pyrolyzed cellulose.

6.3.2 LTPI-DIMS-MS/MS

The quality of the DIMS separation of isomeric and isobaric compounds produced from the pyrolysis of cellulose may be investigated by assessing the resolution of the peaks in the XIC traces. The resolution of the ion separation was determined using the FWHM of the Gaussian curves calculated in Section 6.3.1 for the ions between *m/z* 50 and 250. The average resolution (R) and standard deviation between the two experiments was calculated. This data is shown in Appendix 1. The R values shown in Appendix 1 were clustered to sort the XICs from the LTPI-DIMS analysis of pyrolyzed cellulose based on resolution. Each mass-to-charge ratio was classified into three resolution groups. If ions of a selected mass-to-charge ratio are separated with a resolution of 1.0 or greater, they are classified as resolved. If the separation occurs with a resolution between $1.0 < R < 0.5$, the ions are classified as poorly resolved. Ions separated with a resolution of less than 0.5 were classified as unresolved. These “unresolved” analytes are believed to be multiple analytes because the FWHM of each Gaussian fit is greater than 50. Table 6.1 summarizes the number of XIC traces in each of the three categories of resolution described

above. XIC traces that were fitted with only one Gaussian curve were not included Table 6.1.

Though relatively few ions are separated with a resolution greater than 1.0, analytes may be separated enough that the structure of analyte ions of interest can be investigated by generating MS/MS spectra at each point over the course of a E_c scan. As an example MS/MS was performed on the ion of *m/z* 155 generated by flow-through LTPI of cellulose pyrolyzed at 650 °C in the PyroProbe. Small differences are observed in the averaged MS/MS spectrum generated over the course of the DIMS separation (Figure 6.12A) when compared to the MS/MS spectrum of *m/z* 155 generated when no DIMS scan is performed (Figure 6.12B). For example, a low abundance of the ions of *m/z* 173, 154, and 138 are observed in MS/MS spectrum averaged over the course of a DIMS separation.

Table 6.1. Summary of the resolution of ions separated by DIMS.

Resolution	Number
R > 1.0	5
0.5 ≤ R < 1.0	72
R < 0.5	74

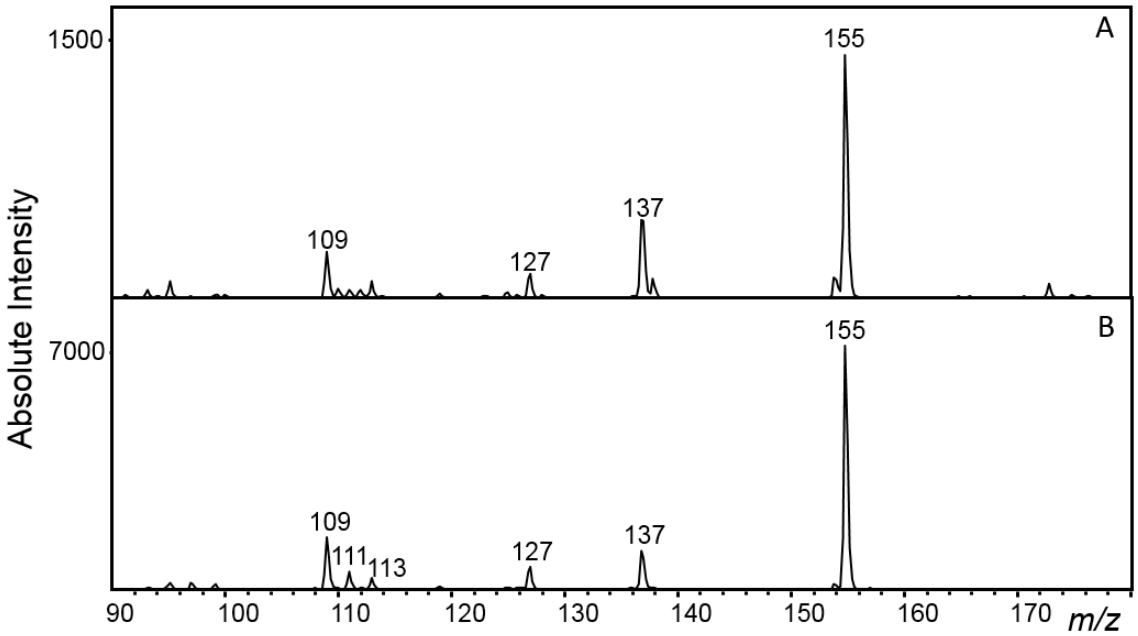

Figure 6.12. MS/MS of the ion of m/z 155 produced by LTPI of the aerosol produced by pyrolysis of cellulose at 650 °C A. averaged over the course of a DIMS separation or B. without any ion separation.

These E_c dependent differences are more notable in the extracted MS/MS spectra generated when CID is performed on the ion of *m/z* 155 over the course of the DIMS separation (Figure 6.13). The XIC trace for the product ions of *m/z* 173, 137, and 109 from MS/MS of *m/z* 155 from cellulose pyrolyzed at 650 °C, ionized by LTPI, and the ions separated by DIMS with a E_D of 5 kV/cm is shown in Figure 6.13A. The corresponding values of the E_c for the MS/MS spectra shown in Figure 6.13B-D are

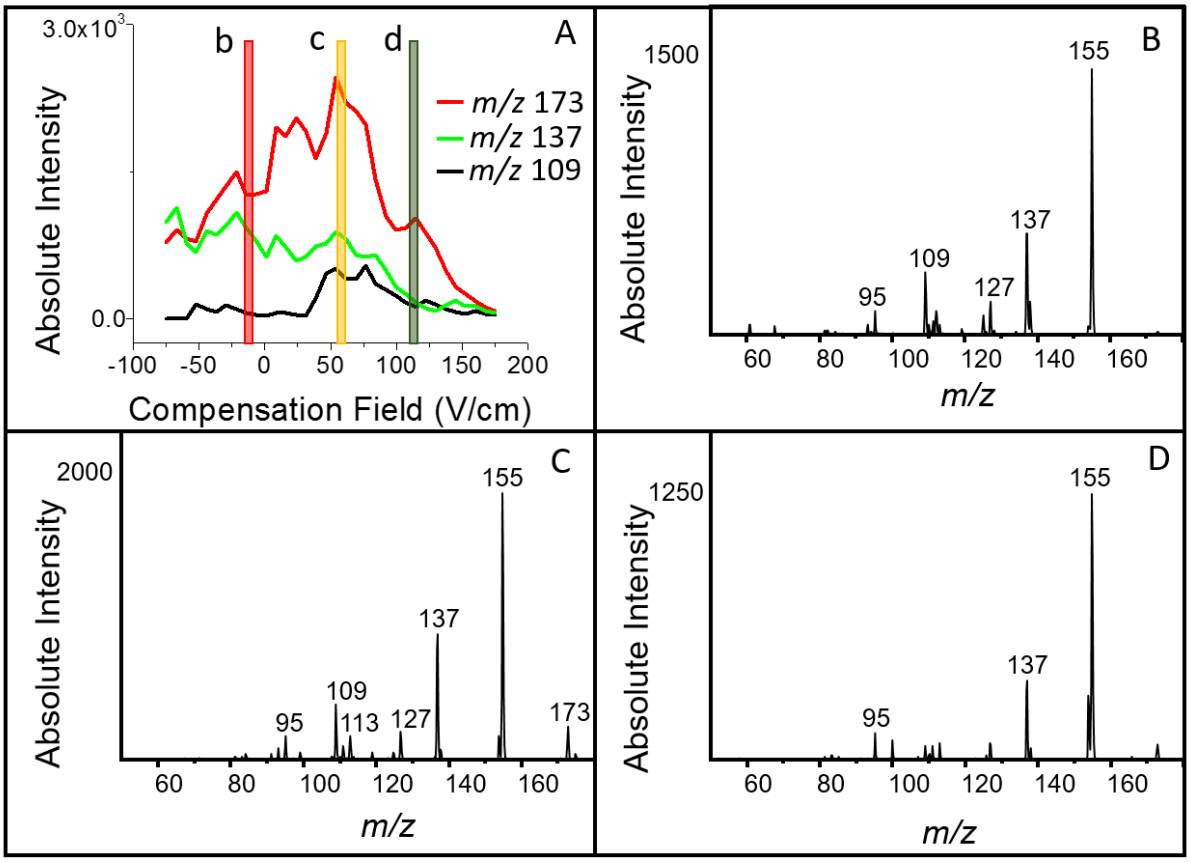

Figure 6.13. LTPI-DIMS-MS of the aerosol produced by the pyrolysis of cellulose at 650 °C in the PyroProbe A. XIC trace for the ion of m/z 155 and LTPI-DIMS-MS/MS spectra generated with a E_c of B. 5 V/cm C. +60 V/cm and D. +120 V/cm.

highlighted and labeled in lower case letters in Figure 6.13A. The ion of *m/z* 155 that has a stable trajectory through the DIMS device at E_c = -5 V/cm (Figure 6.13B) has a different MS/MS pattern than the ion passed stably through the DIMS device when E_c = +60 V/cm (Figure 6.13C) or when E_c = +120 V/cm (Figure 6.13D). The ion of *m/z* 155 that passes through the DIMS device with a stable trajectory at E_c = +60 V/cm (Figure 6.13C) adducts with neutral water in the ion trap, a diagnostic ion-molecule reaction that will be discussed in Chapter 7 in further detail. A peak at *m/z* 173 is observed in Figure 6.12D, but the low abundance of this ion may be due to incomplete separation of isobaric ions. The MS/MS spectrum shown in Figure 6.13D exhibits a much lower relative abundance of the ions of *m/z* 127 and *m/z* 109 than the MS/MS spectra shown in Figure 6.13B or 6.13C. Each of the neutral losses observed in Figure 6.13B-D give insight into the structure of the ions separated by DIMS and thereby provide information on the structure of the neutral analyte of interest in the pyrolysis. These data also

inform fitting Gaussian curves to the data shown in Section 6.3.1. Though only two ions were observed from the high resolution/high mass accuracy data and used for the calculation of resolution, three ions can be tentatively identified and the centroids approximated by DIMS-MS/MS.

The differences in the MS/MS spectra observed at each E_c value are the reason for the differences in the averaged MS/MS spectra with and without DIMS (Figure 6.12) and exemplify a benefit of using DIMS separations coupled to a quadrupole ion trap. The ions that were observed at a higher abundance in the averaged DIMS MS/MS spectrum in Figure 6.12A as opposed to MS/MS without DIMS (Figure 6.12B) were observed as unique product ions in the individual MS/MS spectra separated by DIMS. Lower abundance ions with a different E_c than the more abundant ions that dominate the MS/MS spectrum without DIMS can be selectively accumulated. The ion trap is set to accumulate until a designated number of ions are trapped, resulting in an effective enrichment of the lower abundance ions in the MS/MS spectrum.

De novo interpretation of the neutral losses observed from MS/MS will be discussed in Chapter 7. LTPI-DIMS-MS/MS of standards must be performed and the compensation field as well as the MS/MS spectra compared to confidently identify the ion(s) of interest. The current LTPI-DIMS-MS/MS experiment is poorly reproducible because of low ion intensity due to ion losses. The data shown in Figure 6.13, however, are a proof of concept for the potential of the experiment. Methods to increase the reproducibility of the LTPI-DIMS-MS/MS experiment are discussed in Chapter 8.

6.3 Summary and conclusions

Aerosols generated by the pyrolysis of natural polymers are expected to contain a mixture of isomeric and isobaric compounds, but traditional separation techniques such as LC and GC are not amenable to analysis of compounds in real time. Post-ionization separations may be utilized to separate ions when ion sources that induce minimal fragmentation during ionization and preserve structural information are used, such as those shown in Chapter 4. The data displayed in this chapter demonstrate the utility of DIMS as a post-ionization separation technique for compounds in the aerosol particles generated by pyrolysis of cellulose and ionized by LTPI.

Investigation of the DIMS separation of the M + 1 peaks generated by LTPI of pyrolyzed cellulose demonstrates that the even mass-to-charge ions observed in the averaged mass spectrum are not due

solely to the isotopic peak of the odd mass-to-charge ratio ions; nitrogen containing compounds are believed to be present in the sample as is discussed in Chapter 4. Gaussian curves were fitted to the XIC traces generated by a DIMS separation of the pyrolysis products of cellulose ionized by LTPI. It was found that the overall the pyrolysis-LTPI-DIMS-MS experiment is reproducible and the correlation coefficient between replicate experiments was determined to be 0.90 with a slope of 0.90. The resolution of the ions between *m/z* 50 and 250 was used to classify ions as resolved ($n = 5$, $R > 1$), poorly resolved ($n = 72$, $1 < R \leq 0.5$), and unresolved ($n = 74$, $R < 0.5$).

LTPI-DIMS-MS/MS was performed on the pyrolysate of cellulose. It was shown that DIMS may be used to assist in the deconvolution of the MS/MS spectra of isomeric compounds generated by LTPI even when the ions are separated with a resolution of less than 1.0. Information gained from these types of experiments can be used to evaluate ions of interest and to identify analytes by comparison to standards.

REFERENCES

1. Li, H.; Bendiak, B.; Kaplan, K.; Davis, E.; Siems, W. F.; Hill Jr., H. H. Evaluation of ion mobility-mass spectrometry for determining the isomeric heterogeneity of oligosaccharide-alditols derived from bovine submaxillary mucin. *Int. J. Mass Spectrom.* **2013***, 352*, 9-18.

2. Lalli, P. M.; Corilo, Y. E.; Rowland, S. M.; Marshall, A. G.; Rodgers, R. P. Isomeric Separation and Structural Characterization of Acids in Petroleum by Ion Mobility Mass Spectrometry. *Energy Fuels* **2015***, 29*, 3626-3633.

3. Waridel, P.; Wolfender, J.; Ndjoko, K.; Hobby, K. R.; Major, H. J.; Hostettmann, K. Evaluation of quadrupole time-of-flight tandem mass spectrometry and ion-trap multiple-stage mass spectrometry for the differentiation of C-glycosidic flavonoid isomers. *J. Chromatog. A* **2001***, 926*, 29-41.

4. Kushnir, M. M.; Rockwood, A. L.; Nelson, G. J. Simultaneous quantitative analysis of isobars by tandem mass spectrometry from unresolved chromatographic peaks. *J. Mass Spectrom.* **2004***, 39*, 532-540.

5. Kocadağlı, T.; Yılmaz, C.; Gökmen, V. Determination of melatonin and its isomer in foods by liquid chromatography tandem mass spectrometry. *Food Chem.* **2014***, 153*, 151-156.

6. Isaacman, G.; Wilson, K. R.; Chan, A. W. H.; Worton, D. R.; Kimmel, J. R.; Nah, T.; Hohaus, T.; Gonin, M.; Kroll, J. H.; Worsnop, D. R.; Goldstein, A. H. Improved Resolution of Hydrocarbon Structures and Constitutional Isomers in Complex Mixtures Using Gas Chromatography-Vacuum Ultraviolet-Mass Spectrometry. *Anal. Chem.* **2012***, 84*, 2335-2342.

7. Mason, E. A.; McDaniel, E. W. *Transport Properties of Ions in Gases;* Wiley: New York, 1988.

8. Eiceman, G. A.; Karpas, Z. *Ion Mobility Spectrometry;* CRC Press: 2005; Vol. 1.

9. Purves, R. W.; Guevremont, R.; Day, S.; Pipich, C. W.; Matyjaszczyk, M. S. Mass Spectrometric Characterization of a High-Field Asymmetric Waveform Ion Mobility Spectrometer. *Rev. Sci. Instrum.* **1998***, 69*, 4094-4105.

10. Kehrwald, N.; Zangrando, R.; Gabrielli, P.; Jaffrezo, J.; Boutron, C.; Barbante, C.; Gambaro, A. Levoglucosan as a specific marker of fire events in Greenland snow. *Tellus Ser. B.* **2012***, 64*, 18196.

11. Rathsack, P.; Reichel, D.; Krzack, S.; Otto, M. Komprehensive Gaschromatographie-Massenspektrometrie von Alkylbenzolen in Pyrolyseölen aus Biomasse und Kohle; Alkylbenzene Analysis in Pyrolysis Oils from Biomass and Coal by Comprehensive Gas Chromatography Mass Spectrometry. *Chemie Ingenieur Technik* **2014***, 86*, 1779-1789.

12. Zekavat, B.; Szulejko, J. E.; LaBrecque, D.; Olaitan, A. D.; Solouki, T. Efficient injection of low-mass ions into high magnetic field Fourier transform ion cyclotron resonance mass spectrometers. *Rapid Commun. Mass Spectrom.* **2014***, 28*, 230-238.

13. Shvartsburg, A. A.; Clemmer, D. A.; Smith, R. D. Isotopic Effect on Ion Mobility and Separation of Isotopomers by High-Field Ion Mobility Spectrometry. *Anal. Chem.* **2010***, 82*, 8047-8051.

14. Nørgaard, A. W.; Kofoed-Sørensen, V.; Svensmark, B.; Wolkoff, P.; Clausen, P. A. Gas Chromatography Interfaced with Atmospheric Pressure Ionization-Quadrupole Time-of-Flight-Mass Spectrometry by LowTemperature Plasma Ionization. *Anal. Chem.* **2013***, 85*, 28-32.

15. Gong, X.; Xiong, X.; Peng, Y.; Yang, C.; Zhang, S.; Fang, X.; Zhang, X. Low-temperature plasma ionization source for the online detection of indoor volatile organic compounds. *Talanta* **2011***, 85*, 2458-2462.

16. Na, N.; Xia, Y.; Zhu, Z.; Zhang, X.; Cooks, R. Birch Reduction of Benzene in a Low-Temperature Plasma. *Agnew. Chem. Int. Ed.* **2009***, 48*, 2017-2019.

CHAPTER 7: INTERROGATION OF ION STRUCTURE USING TANDEM MASS SPECTROMETRY

7.1 Introduction

Limitations to commercial aerosol mass spectrometers such as the costly integration of lasers[1] and the inability to identify analyte ions in a complex mixture[2] were discussed in Chapter 1 and are the motivation for the work described in this dissertation. Presented in Chapters 4-6 is instrumentation for the sampling, separation, and mass analysis of compounds from aerosol particles. The function of the aerosol mass spectrometry system as described thus far is comparable to the real-time aerosol mass spectrometry instrumentation that is currently available commercially. However, a primary advantage of the techniques presented herein over commercially available aerosol mass spectrometers is the capability to evaluate the structure of analyte ions.

The ion sources introduced in Chapter 4 impart little excess internal energy to the analyte ions during ionization and thereby result in minimal fragmentation of analytes during ionization.[3,4] The lack of fragmentation of analytes during ionization allows each neutral molecule to be associated with a single parent ion in the mass spectrum. Tandem mass spectrometry (MS/MS) can be used to partially or fully determine analyte structure because the structure of an ion is related to the structure of the neutral species.[5,6] In this chapter MS/MS is used to investigate the structure of ions generated by low temperature plasma ionization (LTPI) and extractive electrospray ionization (EESI) of the aerosol produced by pyrolysis of cellulose.

7.2 MS/MS of ions produced from pyrolysis

7.2.1 Influence of pyrolysis heating rate and maximum temperature on MS/MS spectra

The identity of the products of pyrolysis has been shown to depend on the pyrolysis temperature and heating rate.[7] To investigate the utility of MS/MS for the evaluation of changes in the composition of aerosol particles produced by pyrolysis, cellulose was used as a standard analyte and pyrolysis was performed at different maximum temperatures and heating ramp rates. Cellulose was pyrolyzed at 650 °C and the heating ramp rate was changed from 10 – 100 °C/s. The data in Section 7.2 were collected on

the Bruker HCT ion trap mass spectrometer. No difference in the mass spectrum of the ions formed by flow-through LTPI is observed when the heating rate is increased from 10 °C/s (Figure 7.1A) to 100 °C/s (Figure 7.1B).

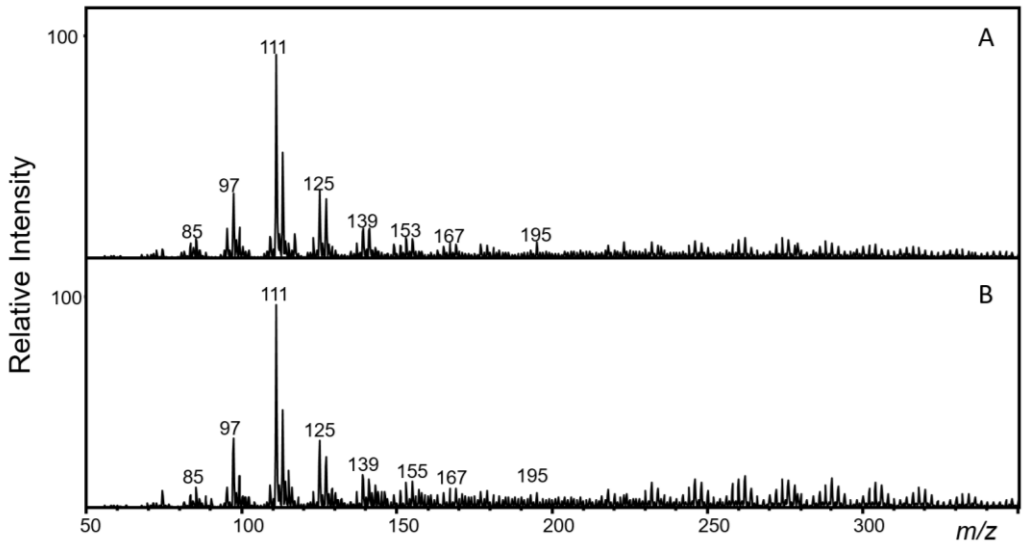

Figure 7.1. MS spectra generated by LTPI of cellulose pyrolyzed at 650 °C with a heating rate of A. 10 °C/s or B. 100 °C/s.

Though no change in the mass spectrum is observed, it is possible that different isomeric species are formed depending on the heating rate. Displayed in Figure 7.2 are the MS/MS spectra from CID of the ion of *m/z* 155 produced by pyrolysis of cellulose at 650 °C with a heating ramp rate of 10 °C/s (Figure 7.2A), 50 °C/s (Figure 7.2B), and 100 °C/s (Figure 7.2C). The relative intensities of ions in the MS/MS spectra are not significantly different (n = 3). No difference in the MS/MS spectrum is observed from CID of the ion of *m/z* 143 formed by pyrolysis of cellulose with a heating ramp rate of 10 °C/s (Figure 7.2D), 50 °C/s (Figure 7.2E), and 100 °C/s (Figure 7.2F). Though the identity of the products of pyrolysis is expected to be dependent on the pyrolysis temperature and heating rate,[7] the lack of difference in dissociation pattern is likely due to the fact that MS and MS/MS were performed when the pyrolysis temperature was held constant after heating the sample to the maximum temperature to standardize between experiments. In this case, the composition of the aerosol particles is more likely to be dependent on the final pyrolysis temperature rather than the heating rate.

To investigate the influence of the final pyrolysis temperature on the composition of the aerosol produced by pyrolysis, cellulose was pyrolyzed at 200 °C, 400 °C, 650 °C, and 900 °C and the aerosol produced was ionized by flow-through LTPI. To standardize between experiments, the heating rate was

maintained at 10 °C/s. Shown in Figure 7.3 are mass spectra from the background (Figure 7.3A) and from the cellulose pyrolysate generated at 200 °C (Figure 7.3B), 400 °C (Figure 7.3C), 650 °C (Figure 7.3D), and 900 °C (Figure 7.3E). Though the ion distribution observed from LTPI-MS of pyrolyzed cellulose is similar at all pyrolysis temperatures investigated, the ions of *m/z* 109, 127, 129, and 143 exhibit a notable change in relative intensity.

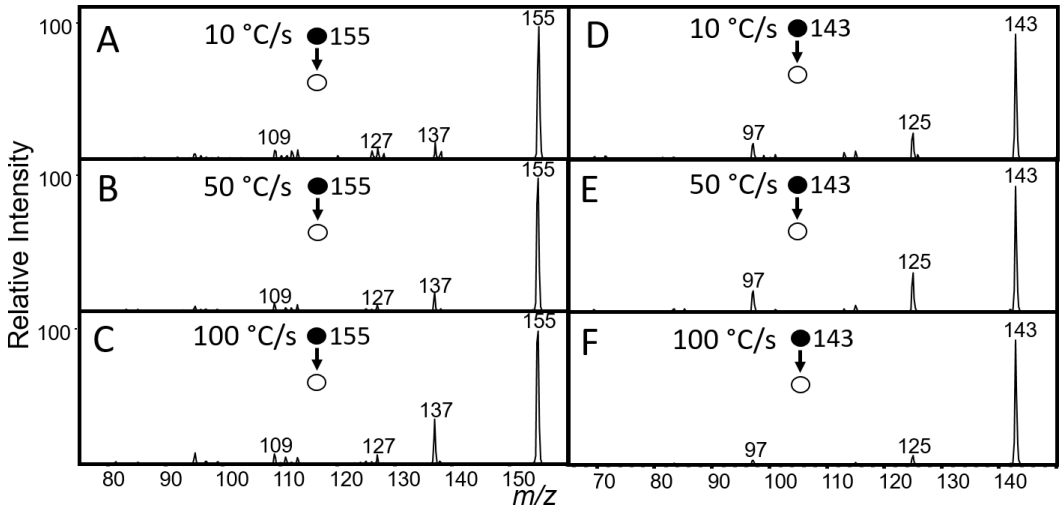

Figure 7.2. CID of ions produced by LTPI of cellulose pyrolyzed at 650 °C. MS/MS of the ion of m/z 155 produced with a heating rate of A. 10 °C/s B. 50 °C/s C. 100 °C/s and MS/MS of the ion of m/z 143 produced with a heating rate of D. 10 °C/s E. 50 °C/s F. 100 °C/s.

To investigate the dependence of the structure of the ions formed by pyrolysis on the final pyrolysis temperature, MS/MS was performed on the ions formed from LTPI-MS of cellulose pyrolyzed at the final pyrolysis temperatures shown in Figures 7.3. The ions of *m/z* 143 and 155 were selected for MS/MS experiments because the relative intensity of the ion of *m/z* 143 changes with pyrolysis temperature while the ion of *m/z* 155 has approximately the same relative intensity at all four pyrolysis temperatures.

Displayed in Figure 7.4 are the MS/MS spectra produced by CID of the ion of *m/z* 155 generated by pyrolysis of cellulose with a heating rate of 10 °C/s and a maximum pyrolysis temperature of 400 °C (Figure 7.4A), 650 °C (Figure 7.4B), and 900 °C (Figure 7.4C) and for the ion of *m/z* 143 produced by pyrolysis of cellulose at 400 °C (Figure 7.4D), 650 °C (Figure 7.4E), and 900 °C (Figure 7.4F). Boxed in red are product ions that exhibit a statistically significant change in relative intensity (no overlap between the standard deviation of the measured intensity) when the maximum pyrolysis temperature is increased (n = 3).

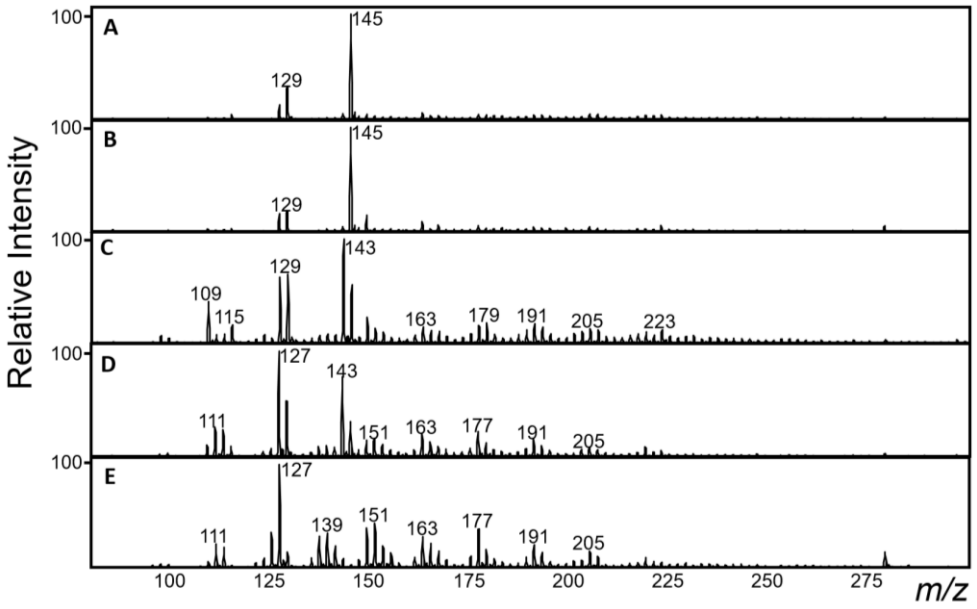

Figure 7.3. MS spectra generated by LTPI of A. background or cellulose pyrolyzed at a maximum temperature of B. 200 °C C. 400 °C D. 650 °C and E. 900 °C.

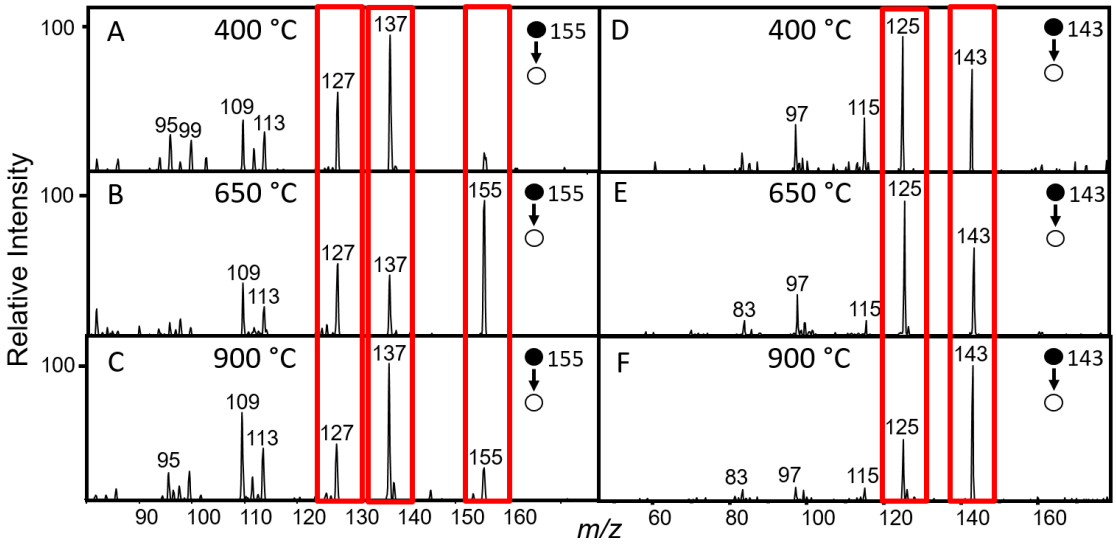

Figure 7.4. MS/MS spectra produced by CID of m/z 155 from cellulose pyrolyzed at A. 400 °C B. 650 °C C. 900 °C or CID of m/z 143 from cellulose pyrolyzed at D. 400 °C E. 650 °C F. 900 °C.

The differences in dissociation pattern at higher final pyrolysis temperatures could be due to changes in the pyrolysis product identity and/or relative abundance. Alternatively, temperature dependent differences in the MS/MS spectra of ions produced by LTPI of the cellulose pyrolysate could be due to increasing analyte internal energy with pyrolysis temperature. Though analytes are known to be thermalized at atmospheric pressure after ionization by traditional ion sources such as electrospray

ionization[8] the high pyrolysis temperature and rapid temperature ramp rates could result in an increased analyte internal energy. After CID these “hot” ions could dissociate to a greater extent and/or via higher energy pathways than thermal ions.[9] To ensure that MS/MS patterns are reproducible ions must be thermalized prior to CID.

7.2.2 Are ions thermalized prior to MS/MS?

To determine if ions generated by LTPI of pyrolyzed cellulose are thermalized prior to CID, the ions produced by flow-through LTPI of cellulose pyrolyzed at 400 °C, 650 °C, and 900 °C were trapped for 100 ms and allowed to undergo collisional cooling in the quadrupole ion trap to thermalize ions prior to MS/MS. Differences in the relative abundance or identity of product ions formed by CID before and after 100 ms cooling time would indicate that the ions are not thermalized prior to MS/MS. As shown in Figure 7.5 the relative intensity of the product ions after MS/MS does not change significantly (n = 3) when the ions of *m/z* 155 and 143 are dissociated immediately after trapping (Figure 7.5A and Figure 7.5C, respectively) or after collisional cooling for 100 ms prior to CID (Figure 7.5B and Figure 7.5D, respectively). This result indicates that the analytes are fully thermalized by collisions in the ion source and during ion trapping prior to MS/MS. Differences in the relative intensity of MS/MS product ions when the pyrolysis temperature is changed are not due to different internal energy distributions of analyte ions after heating but are indicative of differences in the composition of the aerosol particles formed at each pyrolysis temperature.

The temperature dependent differences in the composition of aerosol particles produced from pyrolysis of cellulose could be due either to changes in the relative abundance of compounds formed at each temperature or due to higher energy pyrolysis pathways that can be accessed when the pyrolysis temperature is increased. Differential ion mobility spectrometry (DIMS) was used prior to mass analysis to separate ions formed by flow-through LTPI of cellulose pyrolyzed at 400 °C, 650 °C, and 900 °C to determine if different molecules are produced at higher pyrolysis temperatures. The extracted ion current (XIC) trace is plotted versus compensation field (E_c) in Figure 7.6 for the ions of *m/z* 155 (Figure 7.6A) and *m/z* 143 (Figure 7.6B). The ion intensity for each XIC trace was normalized to the maximum ion intensity in the trace to plot the E_c scans on the same scale.

The XIC peak shape varies depending on maximum pyrolysis temperature. High resolution/high

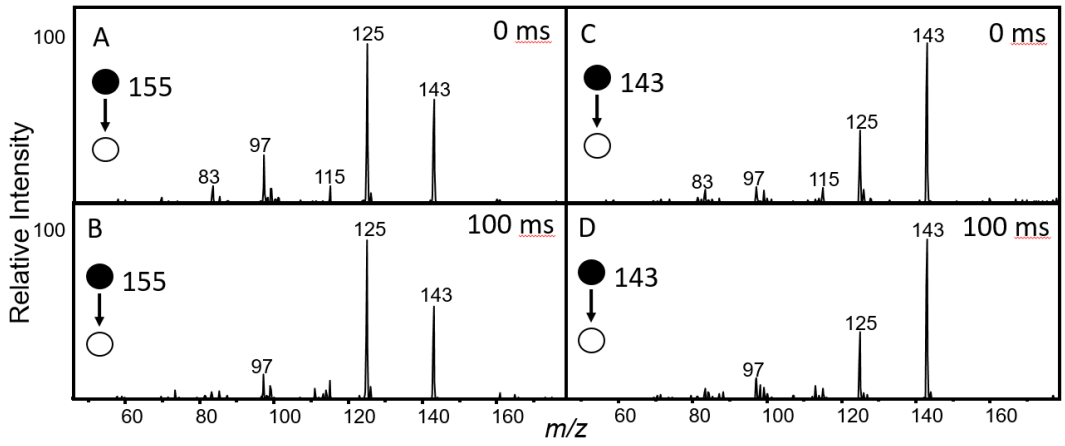

Figure 7.5. MS/MS spectra produced by CID of the ion of m/z 143 formed from LTPI of the products of pyrolysis of cellulose heated at 10 °C/s to A. 650 °C with 0 ms cooling time and B. 650 °C with 100 ms cooling time or C. 900 °C with 0 ms cooling time and D. 900 °C with 100 ms cooling time.

mass accuracy mass spectrometry was performed in a Fourier transform ion cyclotron resonance (FTICR) mass spectrometer to determine the minimum number of ions of each unit mass-to-charge ratio present in the sample. Two ions of each unit mass-to-charge ratio are observed in the FTICR mass spectrum (143 Da: 143.070 Da, $C_7H_{11}O_3$, 1.9 ppm; 143.107 Da, $C_8H_{15}O_2$, 2.4 ppm; Figure 7.7A. 155 Da: 155.070 Da, $C_8H_{11}O_3$, 1.7 ppm; 155.107 Da, $C_9H_{15}O_2$, 2.2 ppm; Figure 7.7B). Two maxima are observed in the DIMS separation of the ion of *m/z* 155, corresponding to the number of ions observed in the FTICR mass spectrum. The distinction between these maxima is most noticeable in the XIC trace of the ion of *m/z* 155 formed at 900 °C. The XIC trace of the DIMS separation of the ions of *m/z* 143 has three maxima, as observed in the trace of the ion of *m/z* 143 formed at 650 °C, though only two ion formulas are determined from the FTICR mass spectrum. This result indicates that there are at least three different

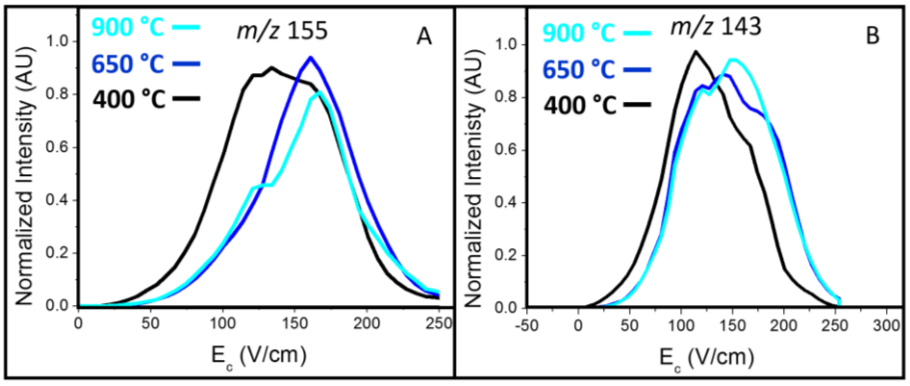

Figure 7.6. LTPI-DIMS-MS of the ion of A. m/z 155 and B. m/z 143 formed from the pyrolysis of cellulose at three temperatures.

ion structures of *m/z* 143 with the protonated molecular formula $C_7H_{11}O_3$ or $C_8H_{15}O_2$.

Origin 6.0 was used to fit two (*m/z* 155) or three (*m/z* 143) Gaussian curves to the XIC traces shown in Figure 7.6. The fitted Gaussian curves (grey lines) are shown in Figure 7.8. The dotted red lines are the traces of the sum of the Gaussian curves for comparison to the XIC traces which are plotted in shades of black and blue. The centroid E_c (V/cm), peak full width at half maximum (FWHM, V/cm) and area (A, AU x V/cm) for each of the Gaussian curves are summarized in Table 7.1. The highest E_c peak (E_c = 185 V/cm) observed from the ion of *m/z* 143 is not present at 400 °C ($A_{400\,°C}$ = 7 ± 7 AU x V/cm). At higher pyrolysis temperatures the peak at E_c = 185 V/cm becomes significant ($A_{650\,°C}$ = 39 ± 2, $A_{900\,°C}$ = 38 ± 1 AU x V/cm). This result indicates that the ion of *m/z* 143 that has a differential ion mobility that is stably transmitted through the DIMS device at E_c = 185 V/cm is only formed at pyrolysis temperatures higher than 400 °C.

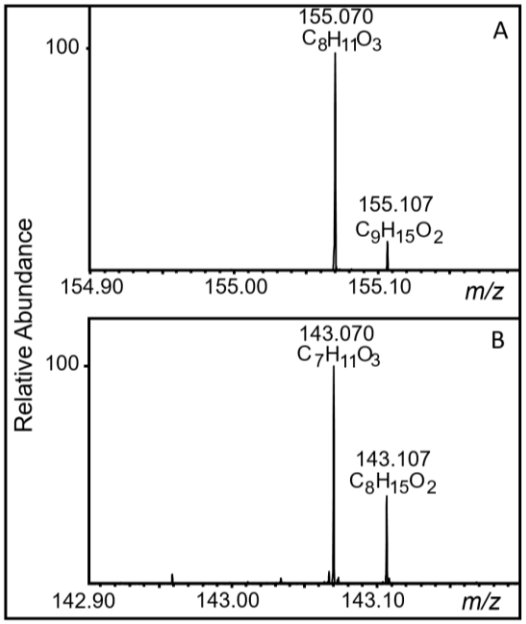

Figure 7.7. FTICR-MS of the ions of A. m/z 155 and B. m/z 143 formed by flow-through LTPI of cellulose produced at 650 °C.

The relative intensity of the fitted Gaussian curves is related to the relative abundance of each ion. Tentative peak assignments can be made by correlating the relative intensity of the Gaussian curves fitted to the XIC trace from the DIMS separation and relative abundance of the ions observed from flow-through LTPI-FTICR-MS of cellulose pyrolyzed at 650 °C (Figure 7.7). For *m/z* 155, there are two ions observed in the high resolution mass spectrum and two Gaussian curves were fitted to the data. The ratio of the peak heights in both experiments is approximately 100:15. Thus, the low abundance ion in the DIMS scan at E_c = 115 V/cm can be assigned as $C_9H_{15}O_2$ and the higher abundance ion at E_c = 165 V/cm is assigned as $C_8H_{11}O_3$. The three Gaussian curves fit to the DIMS separation of the ion of *m/z* 143 may also be correlated to the two ions resolved in the FTICR mass spectrum. The ratio of the absolute intensity of the ions of *m/z* 143 in DIMS is approximately 80:55:70 (listed from low E_c to high) and the ratio of the ions in the FTICR mass spectrum is approximately 100:40. The only way for both of these

relationships to be true for the same set of ions is if the ions of *m/z* 143 observed at E_c = 110 and 185 V/cm have the same ion formula and both contribute to the more abundant ion in the FTICR spectrum of $C_7H_{11}O_3$ and the ions observed at E_c = 150 V/cm correspond to the protonated molecule $C_8H_{15}O_2$. Thus, the ratio between the ions with different molecular formulas separated by DIMS is (80+70):55 or approximately 100:40.

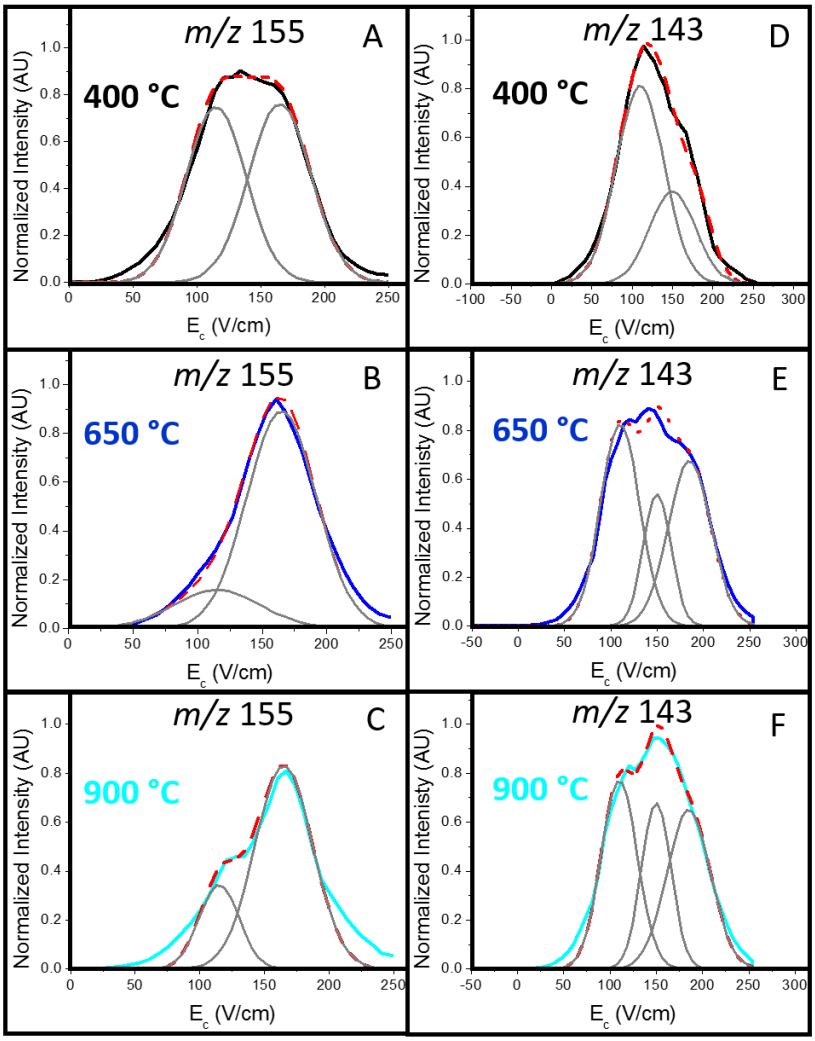

Figure 7.8. Gaussian fits to the DIMS-MS spectra produced from LTPI-DIMS-MS of m/z 155 at A. 400 °C B. 650 °C C. 900 °C and m/z 143 at D. 400 °C E. 650 °C F. 900 °C.

As the final pyrolysis temperature is changed, the relative intensity of the fitted Gaussian peaks changes. Thus, DIMS separations of isomeric and isobaric ions produced at the three temperatures investigated indicate that both the relative abundance and identity of ions varies as the maximum pyrolysis temperature is changed. This result indicates that the relative composition of the aerosol

changes as the pyrolysis temperature is changed. Overall, the results presented in this section lead to the conclusion that both the identity and relative abundance of ions in the pyrolysate change depending on the pyrolysis temperature.

Table 7.1. Summary of Gaussian fit parameters (peak centroid E_c, FWHM, and area (A)) for the curves shown in Figure 7.7.

	m/z 155								
	400 °C			650 °C			900 °C		
	Gaussian 1	Gaussian 2	Gaussian 3	Gaussian 1	Gaussian 2	Gaussian 3	Gaussian 1	Gaussian 2	Gaussian 3
E_c (V/cm)	115	165	----	115	165	----	115	165	----
FWHM (V/cm)	55 ± 2	57 ± 4	----	80 ± 10	63 ± 2	----	36 ± 7	53 ± 3	----
A (AU x V/cm)	44 ± 2	46 ± 2	----	13 ± 2	60 ± 2	----	13 ± 3	47 ± 3	----
	m/z 143								
	400 °C			650 °C			900 °C		
	Gaussian 1	Gaussian 2	Gaussian 3	Gaussian 1	Gaussian 2	Gaussian 3	Gaussian 1	Gaussian 2	Gaussian 3
E_c (V/cm)	110	150	185	110	150	185	110	150	185
FWHM (V/cm)	70 ± 4	70 ± 30	40 ± 10	50 ± 2	35 ± 3	54 ± 3	46 ± 2	37 ± 2	55 ± 2
A (AU x V/cm)	60 ± 6	27 ± 15	7 ± 7	44 ± 2	20 ± 2	39 ± 2	38 ± 1	27 ± 1	38 ± 1

It should be noted that there may be other unresolved isomeric and isobaric analytes present in the sample. The FWHM for the fitted Gaussian curves changes with the final pyrolysis temperature and is larger than expected (sodiated levoglucosan has a FWHM of 24.8 V/cm and sodiated glucose has a FWHM of 29.21 V/cm when DIMS is performed using the same experimental conditions). DIMS-MS/MS could be used to better estimate the number of analytes in the mixture, as shown in Chapter 6, but the conservative estimates herein are adequate to examine the XIC traces displayed in Figure 7.8.

7.3 Differentiation of functional groups using neutral losses

7.3.1 Tandem mass spectrometry of ionized cellulose pyrolysis products

The Bruker Esquire 3000 was used to perform CID on the 50 most abundant ions generated from LTPI of the aerosol produced by the pyrolysis of cellulose at approximately 600 °C in the custom pyrolysis chamber. The 12 smallest mass neutral losses observed from the MS/MS spectra are summarized in Table 7.2. A green check indicates that the neutral loss of that mass was observed and a red x indicates that the parent ion did not dissociate via a pathway resulting in a product ion corresponding to that neutral loss mass. Some neutral loss pathways observed from the pyrolysis products of cellulose are nearly ubiquitous. For example the neutral loss of water (18 Da) or the neutral loss of 28 Da (CO or C_2H_4) are observed from 49 of the 50 ions investigated. In these cases the lack of the neutral loss may be more structurally informative than the neutral loss itself and could indicate the absence of functional groups in an ion.

Table 7.2. Summary of MS/MS product ions observed from CID of 50 most abundant ions produced by LTPI of the pyrolysate of cellulose.

	Mass of Neutral Loss											
Parent *m/z*	-2	-10	-15	-18	-28	-30	-32	-36	-42	-44	-46	-48
99	✗	✗	✗	✓	✓	✓	✗	✗	✓	✗	✗	✗
111	✗	✗	✗	✓	✓	✗	✗	✓	✓	✗	✗	✗
113	✗	✗	✗	✓	✓	✗	✗	✗	✓	✗	✗	✗
115	✗	✗	✗	✓	✓	✗	✗	✗	✗	✗	✓	✗
121	✗	✓	✗	✓	✓	✗	✗	✗	✓	✗	✗	✗
123	✗	✗	✗	✗	✓	✗	✗	✗	✓	✗	✓	✗
127	✗	✗	✗	✓	✓	✓	✗	✗	✓	✓	✓	✗
129	✓	✗	✗	✓	✓	✓	✗	✗	✓	✓	✓	✗
133	✗	✓	✗	✓	✓	✗	✗	✗	✓	✓	✗	✗
135	✗	✗	✗	✓	✓	✗	✗	✗	✓	✗	✗	✗
137	✗	✗	✗	✓	✓	✗	✗	✗	✓	✓	✓	✗
139	✗	✗	✗	✓	✓	✗	✗	✗	✓	✓	✓	✗
141	✗	✗	✗	✓	✓	✗	✗	✗	✓	✓	✓	✗
143	✗	✗	✓	✓	✓	✗	✗	✓	✗	✗	✓	✗
145	✗	✗	✗	✓	✓	✗	✗	✓	✗	✗	✓	✓
147	✗	✗	✗	✓	✓	✓	✗	✗	✓	✗	✓	✗
149	✗	✗	✗	✓	✓	✗	✗	✗	✓	✗	✗	✗
151	✗	✗	✗	✓	✓	✗	✗	✗	✓	✗	✗	✗
153	✗	✗	✗	✓	✓	✗	✗	✗	✓	✓	✓	✗
155	✗	✗	✓	✓	✓	✗	✓	✗	✗	✓	✓	✗
157	✗	✓	✗	✓	✓	✗	✗	✗	✗	✗	✓	✗
159	✗	✗	✗	✓	✓	✗	✗	✓	✗	✗	✓	✗
161	✗	✗	✗	✓	✓	✗	✗	✗	✓	✓	✓	✗
163	✗	✗	✗	✓	✓	✗	✗	✓	✓	✗	✓	✗
167	✗	✗	✗	✓	✓	✗	✗	✗	✗	✓	✗	✗
169	✗	✗	✗	✓	✓	✗	✗	✗	✗	✗	✓	✗
171	✗	✗	✗	✓	✓	✗	✗	✗	✗	✓	✓	✗
173	✗	✗	✗	✓	✓	✗	✗	✗	✓	✗	✓	✗
177	✓	✗	✗	✓	✓	✗	✗	✗	✓	✓	✓	✗
181	✗	✓	✓	✓	✓	✗	✗	✗	✓	✓	✓	✗
183	✗	✗	✗	✓	✓	✗	✗	✗	✗	✓	✓	✗
185	✗	✗	✗	✓	✓	✗	✗	✗	✗	✗	✓	✗
191	✗	✗	✗	✓	✓	✗	✗	✗	✓	✓	✓	✗
199	✗	✗	✗	✓	✓	✗	✗	✗	✗	✗	✓	✗
201	✗	✗	✗	✓	✓	✗	✗	✓	✓	✓	✓	✗
203	✗	✗	✗	✓	✓	✗	✗	✗	✓	✓	✓	✗
207	✗	✗	✗	✓	✓	✗	✗	✓	✓	✗	✓	✗
217	✗	✗	✗	✓	✓	✗	✗	✗	✓	✗	✓	✗
219	✗	✗	✗	✓	✓	✗	✗	✓	✓	✗	✓	✗
223	✗	✗	✓	✓	✓	✗	✗	✓	✓	✗	✓	✗
225	✗	✗	✗	✓	✓	✗	✗	✓	✓	✗	✓	✗
229	✗	✗	✗	✓	✓	✗	✗	✗	✓	✗	✓	✗
235	✗	✗	✗	✓	✓	✗	✗	✗	✗	✗	✓	✗
241	✗	✗	✗	✓	✓	✗	✗	✓	✓	✗	✓	✗
243	✗	✗	✗	✓	✓	✗	✗	✓	✓	✗	✓	✗
247	✗	✗	✗	✓	✓	✗	✗	✗	✓	✗	✓	✗
257	✗	✗	✗	✓	✓	✗	✗	✗	✓	✗	✓	✗
271	✗	✗	✗	✓	✓	✗	✗	✓	✓	✗	✓	✗
279	✗	✗	✗	✓	✓	✗	✗	✗	✓	✗	✓	✗
285	✗	✗	✗	✓	✗	✗	✗	✗	✓	✗	✗	✗

7.3.2 Principal component analysis of neutral losses

As indicated by FTICR data as well as the DIMS separations shown in Chapter 6 and the previous section, multiple isomeric and isobaric analytes are present in the sample. Thus, the MS/MS spectra are the result of the convolution of the dissociation patterns of all the ions present at the selected mass-to-charge ratio. To exemplify the use of the neutral loss pathways shown in Table 7.2 to differentiate between analyte ions, a principal component analysis (PCA) was performed using SAS 9.3 as described in Chapter 2.6. Product ions were designated as present (1) or absent (0) in the MS/MS spectrum of each ion for submission of the data to the PCA. A plot of the first two principal components (Factor 1 and Factor 2) of the data displayed in Table 7.2 is shown in Figure 7.9 with the smallest one, two, or three neutral losses labeled. Figure 7.9 shows visually that even though some neutral loss pathways are nearly ubiquitous, many ions can be differentiated by evaluating subsequent dissociation pathways. Generation of a database of MS/MS spectra from standards, as discussed in detail in Chapter 8, would allow the MS/MS patterns and the associated structural motifs to be used as a training set for PCA identification of functional groups in the pyrolysis products of cellulose.

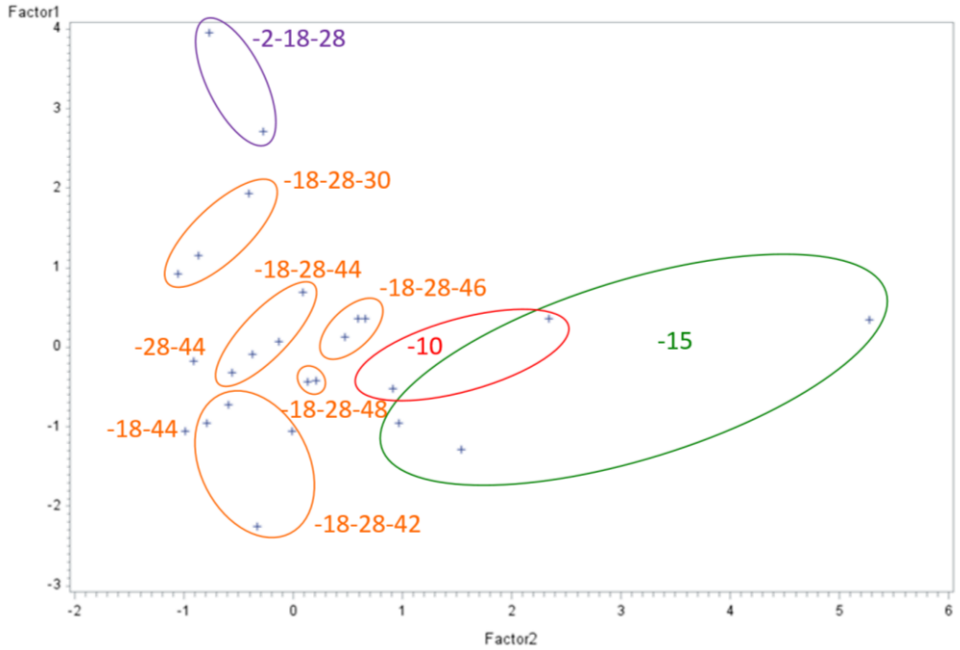

Figure 7.9. PCA of the first 12 neutral losses from 50 ions most abundant ions formed by LTPI of cellulose aerosol product.

7.3.3 Insights from high mass accuracy tandem mass spectrometry

High resolution/high mass accuracy FTICR data may be used to further distinguish between

common dissociation patterns by determining the molecular formula of nearly isobaric neutral losses. As previously discussed, the neutral loss of 28 Da could be attributed to the molecular formula CO or C_2H_4. The ion of *m/z* 201 generated from flow-through LTPI of the aerosol produced from ethyl cellulose pyrolyzed at 650 °C in the PyroProbe was dissociated by CID in a linear ion trap (LIT) and the product ions were mass analyzed in a FTICR. The MS/MS spectrum is shown in Figure 7.10A. The formula of the parent ion (*m/z* 201.112) was determined to be $C_{10}H_{17}O_4$ (0.7 ppm error) based on the measured mass. The product ion formed after the neutral loss of 28 Da (*m/z* 173.081) was determined to have a molecular formula of $C_8H_{13}O_4$ (1 ppm error). The molecular formula of the neutral loss observed from MS/MS is determined to be C_2H_4 from the difference between the parent and product ion molecular formulas. The neutral loss of 28 Da has been typically observed to be C_2H_4 for the pyrolysis products of ethyl cellulose, possibly due to the ethyl functionalized hydroxyl groups on the rings. MS/MS of cellulose could result in the neutral loss of CO because no ethyl functionalization is performed on the ring hydroxyl groups. The high resolution/high mass accuracy data for the pyrolysis products of cellulose could be used to inform the PCA by differentiating between CO and C_2H_4.

Limitations of the FTICR prevent it from being a feasible option for anything more than a supplement to the quadrupole ion trap (QIT) MS/MS data. MS/MS is performed in the higher pressure LIT and the ion isolation window is limited by the mass resolution of the LIT, approximately a 1 Da width. Product ions formed by MS/MS in the LIT must then be transferred into in the FTICR cell in the magnet. Comparison of the MS/MS spectrum observed from the LIT (Figure 7.10B) to that generated in the FTICR (Figure 7.10A) reveals that lower

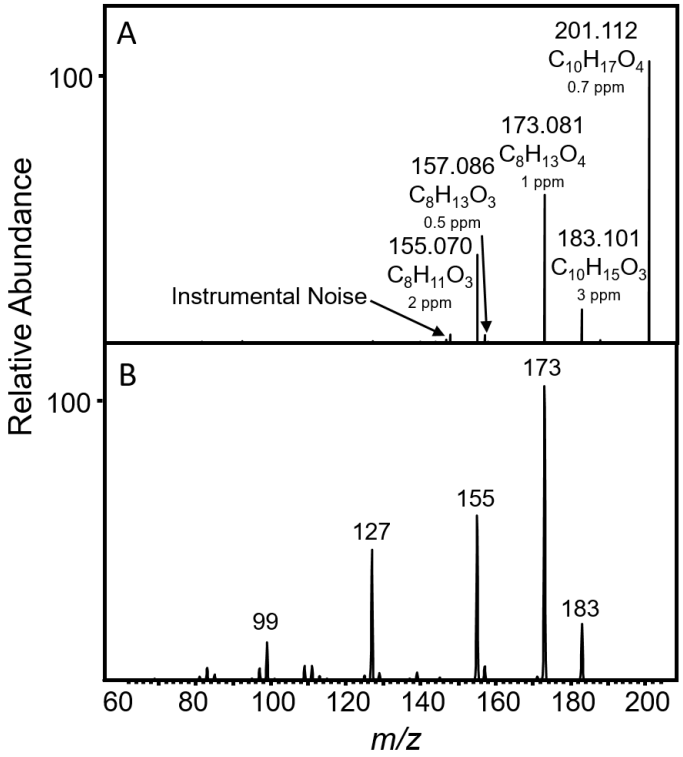

Figure 7.10. LTPI-MS/MS of the ion of m/z 201 mass analyzed in the A. FTICR and B. LIT.

mass-to-charge ratio ions are less efficiently transferred through the 1 m drift tube to the FTICR.[10] Thus, fewer product ions are observed from MS/MS when the FTICR is used as a mass analyzer and the structural information gained is decreased. A larger relative intensity of higher mass-to-charge ratio ions (e.g. *m/z* 201) is also observed because of this mass discrimination.

7.3.4 Structural information gained from unexpected neutral losses

Though some neutral losses are nearly ubiquitous from CID of small organic molecules such as the pyrolysis products of cellulose, other neutral loss pathways are much less common. For example, the neutral loss of H_2 (2 Da) is observed from the ions of *m/z* 129 and 177 produced by LTPI-MS of the pyrolysis products of cellulose and the neutral loss of 48 Da (CH_4O_2) is observed from only *m/z* 145. A 15 Da neutral loss is observed from the ions of *m/z* 143, 155, and 181. The only molecular formula that can account for this neutral loss is $CH_3^{\bullet}$ because the analyte ions contain only carbon, hydrogen, and oxygen. Only small amounts of internal energy are imparted to the ion with each collision during CID which results in ion dissociation via the lowest energy reaction pathways. However, the homolytic cleavage required to produce $CH_3^{\bullet}$ is typically a much higher energy process than a heterolytic rearrangement process. Thus, the cleaved bond must be weaker than typical carbon bonds. Previously published CID data suggests that dissociation of methoxy-containing compounds can result in the neutral loss of $CH_3^{\bullet}$.[11] To confirm the plausibility of a neutral loss of $CH_3^{\bullet}$ from a methoxy-containing cellulose aerosol product during CID, 2,6-dimethoxyphenol was volatilized, ionized by LTPI, and the protonated molecule (*m/z* 155) was isolated and dissociated by CID in the Bruker Esquire 3000 with a resonant excitation voltage of 0.40 V. The MS/MS spectrum is displayed in Figure 7.11A. The ion of *m/z* 140 is generated by the neutral loss of $CH_3^{\bullet}$ and the product ion of *m/z* 123 from the neutral loss of methanol. The neutral loss of 60 Da (*m/z* 95) has two potential net ion formulas for analytes containing only carbon, hydrogen, and oxygen: $C_2H_4O_2$ and C_3H_8O.

Neutral losses may be due to dissociation of a single molecule or multiple smaller dissociation steps. For example, the formula C_3H_8O could be a single neutral loss or it could be due to either a neutral loss of C_3H_6 and H_2O or the neutral loss of two CH_4 molecules and one CO. The net neutral loss of $C_2H_4O_2$ may be accounted for by the single neutral loss of $C_2H_4O_2$ or it could be due to the separate neutral losses of H_2O and C_2H_2O or CO and CH_4O. In the case of 2,6-dimethoxyphenol the most likely

neutral loss pattern can be determined based on the known structure of the molecule. The only dissociation products that can form without a benzene ring opening are CO and CH_4O and thus are the most likely neutral losses from CID of 2,6-dimethoxyphenol to form an ion of *m/z* 95.

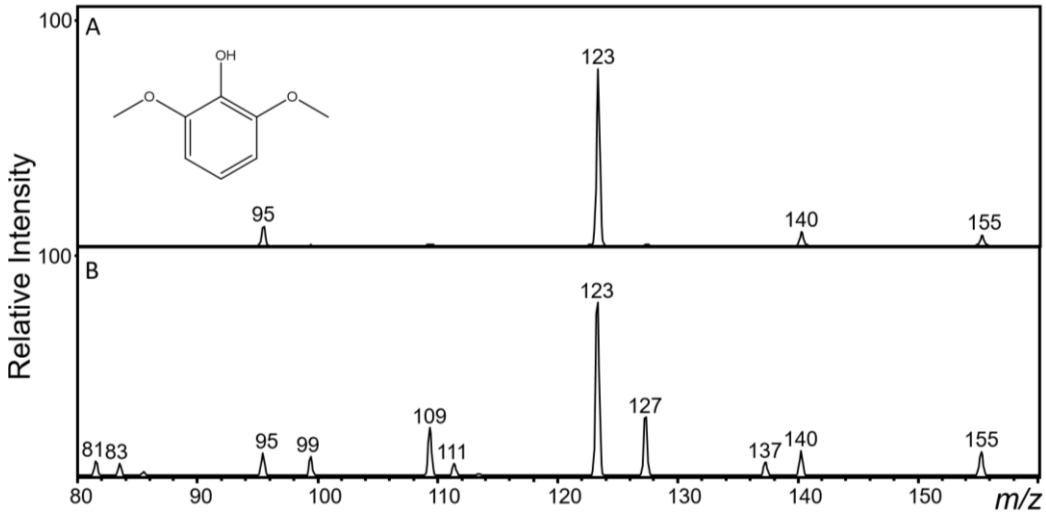

Figure 7.11. MS/MS of m/z 155 formed from LTPI of A. volatilized 2,6-dimethoxyphenol or B. cellulose aerosol product formed at 650 °C.

The MS/MS spectrum from 2,6-dimethoxyphenol is compared to the MS/MS spectrum of the ion of *m/z* 155 from pyrolyzed cellulose generated under the same MS/MS conditions (Figure 7.11B). All three 2,6-dimethoxyphenol product ions (*m/z* 140, 123, and 95) are present in the MS/MS product ion spectrum generated from the ion of *m/z* 155 from pyrolyzed cellulose with the same relative intensity ratios. Thus a component of the population of ions of *m/z* 155 can be identified as 2,6-dimethoxyphenol. The variety of other product ions formed by MS/MS of *m/z* 155 generated by pyrolysis of cellulose indicates that other isobaric compounds are present in the pyrolyzed cellulose sample.

Another unexpected reaction observed from CID of protonated cellulose pyrolysis product is that of 10 Da. For an ion containing only carbon, hydrogen, and oxygen atoms, no logical molecular formula accounts for the neutral loss of 10 Da. This neutral loss can be explained by considering ion-molecule reactions that can occur in the QIT. Multiple ions produced by LTPI or EESI of the pyrolysis products of cellulose undergo a neutral gain of 18 Da in the QIT. As an example, the MS spectrum generated by EESI of volatilized levoglucosan, a major pyrolysis product, using 50/49/1 methanol/water/acetic acid is shown in Figure 7.12. The ion of *m/z* 163 is the protonated levoglucosan molecule, the ion of *m/z* 149 is a ubiquitous background phthalate and the ion of *m/z* 145 is the dehydration product formed by heating

during sample volatilization or ionization. The MS/MS spectrum resulting from CID of the ion of *m/z* 163 formed by EESI is shown in the inset of Figure 7.12. The dehydration product ion is observed at *m/z* 145. This dissociation pathway is nearly ubiquitous, as shown in Table 7.2, and could be due to the neutral loss of water from an alcohol, aldehyde, ketone, or carboxylic acid. Little information is gained from the neutral loss of water. An ion of *m/z* 181 is also observed after CID of protonated levoglucosan from the adduction of the ion of *m/z* 163 with water in the QIT. If a product ion formed by the neutral loss of 28 undergoes an adduction with water in the ion trap a net neutral loss of 10 Da would be observed.

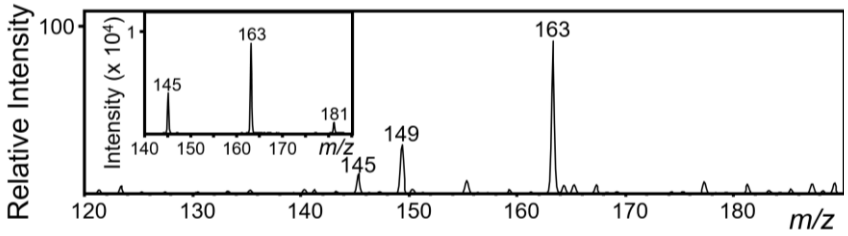

Figure 7.12. MS scan produced by volatilized levoglucosan ionized by EESI with 50/49/1/ methanol/water/acetic acid. The inset is the MS/MS spectrum of m/z 163.

7.4 In-trap ion-molecule reactions

7.4.1 Phenomenological rate constant for protonated levoglucosan

It has been demonstrated in this dissertation using DIMS separations and high resolution/high mass accuracy FTICR-MS data that the pyrolysis products of natural polymers are a complex mixture of isomeric and isobaric compounds. This result has also been shown in the literature. For example, levoglucosan (an indicator of biomass burning) has been exists in three isomeric forms.[12] Volatilized levoglucosan undergoes an ion-molecule reaction with water in the Bruker Esquire 3000 ion trap as shown in Figure 7.12. The kinetics of an ion-molecule reaction are expected to change depending on the ion structure and ion molecule reaction kinetics can be used to identify compounds.[13,14] The kinetics of the adduction of water with protonated levoglucosan in the Bruker Esquire 3000 ion trap were investigated by varying the trapping time of the ion of *m/z* 163 from 0 to 1000 ms. Shown in Figure 7.13 are the mass spectra observed after the protonated levoglucosan ions were isolated and subsequently trapped for 0 ms (Figure 7.13A), 300 ms (Figure 7.13B), 600 ms (Figure 7.13C), or 900 ms (Figure 7.13D). Increasing the ion trapping time results in a decrease in the intensity of the protonated levoglucosan ion ($I_{m/z\ 163}$) and an increase in the intensity of the protonated levoglucosan-water adduct

($I_{m/z\,181}$). The water adduct is observed at the 0 ms time point because a finite amount of time in the QIT is required for collisional cooling, trapping, and isolation of the ions. An ion is observed at *m/z* 195 formed via adduction of protonated levoglucosan with gaseous in-trap methanol from the EESI solvent at reaction times greater than 500 ms. An ion corresponding to the product resulting from the adduction of methanol and the neutral loss of water from protonated levoglucosan is also observed at *m/z* 177.

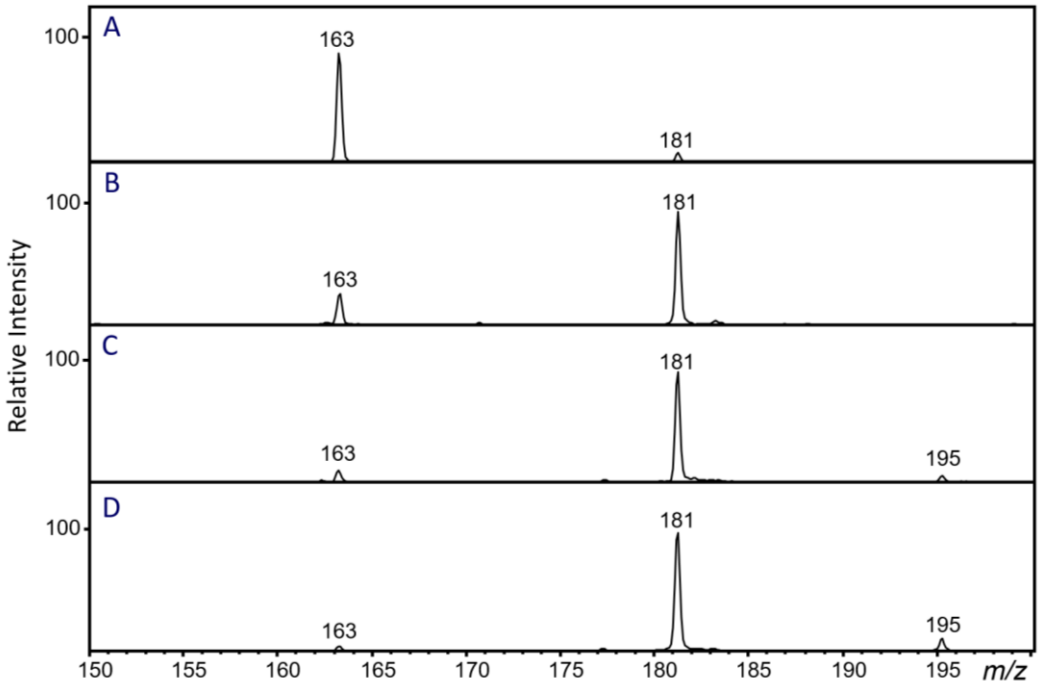

Figure 7.13. Mass spectra of protonated levoglucosan ionized by EESI, isolated, and trapped for A. 0 ms, B. 300 ms, C. 600 ms, D. 900 ms.

The fraction of protonated levoglucosan present in the non-adducted form $\left(\frac{I_{m/z\,163}}{I_{m/z\,163}+I_{m/z\,177}+I_{m/z\,181}+I_{m/z\,195}}\right)$ with respect to time is plotted in Figure 7.14A. The term $(I_{m/z\,163} + I_{m/z\,177} + I_{m/z\,181} + I_{m/z\,195})$ can be used as a surrogate for the initial abundance of levoglucosan in the denominator of the fraction because these are all of the forms of protonated levoglucosan observed in the mass spectrum. Substituting for the initial abundance of levoglucosan this manner allows the data to be collected in a single experiment, which reduces experimental variability, accounts for ion losses due to increased trapping time, and streamlines the experiment. A plot of the increase in the fraction of the products of the ion-molecule reaction of protonated levoglucosan with gaseous neutrals in the ion trap is shown in Figure 7.14B. For clarity, the curves for the fraction of $[M+H+MeOH]^+$ (purple) and

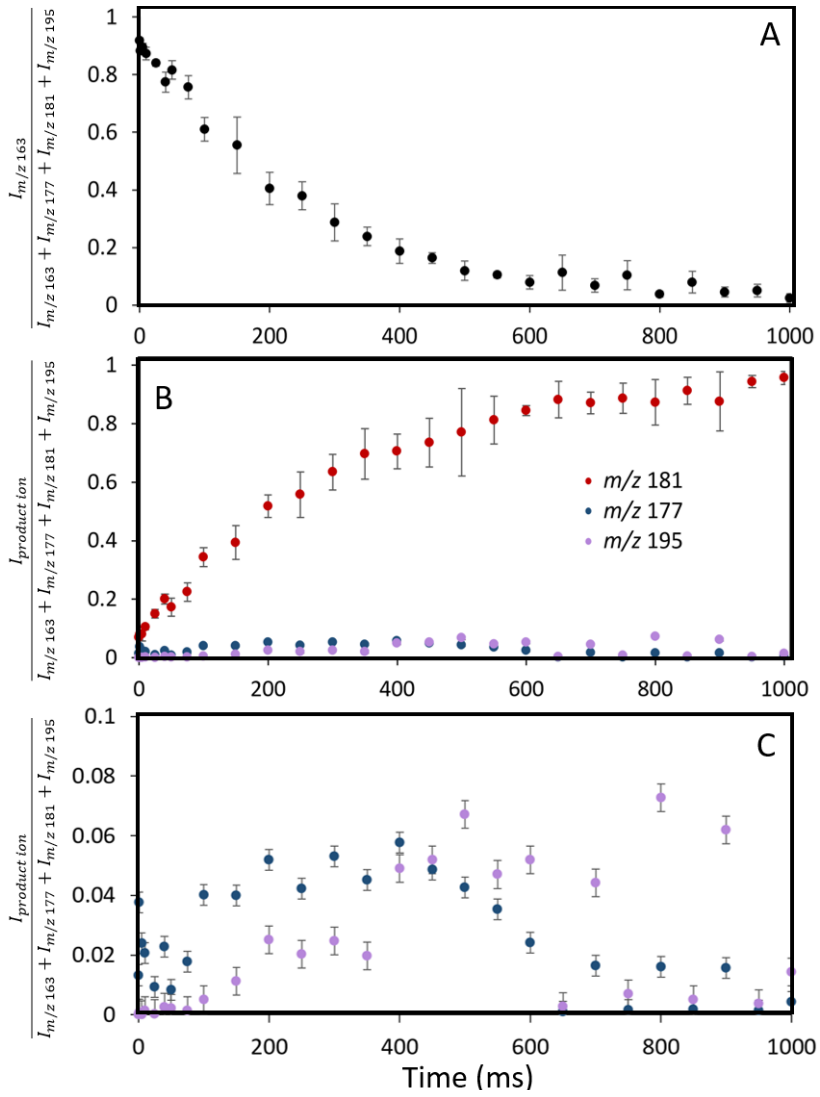

Figure 7.14. Fraction of A. levoglucosan in the adducted form with respect to time B. Fraction of adducted levoglucosan present with respect to time and C. plot of the integrated first order rate law for the reaction of levoglucosan when 50/49/1 methanol/water/acetic acid is used as the EESI solvent.

$[M+H+MeOH-H_2O]^+$ (blue) present in the QIT with increasing trapping time are expanded and shown in Figure 7.14C. The rate of the formation of each of the ion-molecule reaction products is described by

$$\frac{d[M+H+H_2O]^+}{dt} = k_{181}[H_2O][M+H]^+ \quad \text{Equation 7.1}$$

$$\frac{d[M+H+MeOH]^+}{dt} = k_{195}[MeOH][M+H]^+ - \frac{d[M+H+MeOH-H_2O]^+}{dt} \quad \text{Equation 7.2}$$

$$\frac{d[M+H+MeOH-H_2O]^+}{dt} = k_{177}[M+H+MeOH]^+ - k_{-177}[M+H+MeOH-H_2O]^+ \quad \text{Equation 7.3}$$

where $\frac{d[M+H+H_2O]^+}{dt}$, $\frac{d[M+H+MeOH]^+}{dt}$, and $\frac{d[M+H+MeOH-H_2O]^+}{dt}$ are the rates of the formation of the ions of *m/z* 181, 195, and 177, respectively. k_{181} is the rate constant for the formation of *m/z* 181, k_{195} is the rate

constant for the formation of *m/z* 195, k_{177} and k_{-177} are the rate constants for the forward and back reaction of the neutral gain/loss of water from the ion of *m/z* 195, respectively. [H_2O] is the concentration of water vapor in the QIT, [MeOH] is the concentration of gaseous methanol in the QIT from the 50/49/1 methanol/water/acetic acid solvent, and the concentration of protonated levoglucosan, the protonated levoglucosan and methanol adduct, and the concentration of the water loss product from the levoglucosan and methanol adduct are $[M+H]^+$, $[M+H+MeOH]^+$, and $[M+H+MeOH-H_2O]^+$, respectively. The deviation in the shape of the curves shown in Figure 7.14C from an exponential increase is due to incomplete trapping of the low abundance ions of *m/z* 195 and 177 at longer trapping times. It could also be that the ion of *m/z* 177 back-reacts with gaseous water in the ion trap to form *m/z* 195 at longer reaction times as described in Equation 7.3. The change in abundance of the ion of *m/z* 163 with respect to time $\left(\frac{d[M+H]^+}{dt}\right)$ can be described by the following equation:

$$\frac{d[M+H]^+}{dt} = -\left(\frac{d[M+H+H_2O]^+}{dt} + \frac{d[M+H+MeOH]^+}{dt}\right) \quad \text{Equation 7.4}$$

and can be re-written as:

$$\frac{d[M+H]^+}{dt} = -(k_{181}[H_2O] + k_{195}[MeOH])[M+H]^+ + k_{177}[M+H+MeOH]^+ - k_{-177}[M+H+MeOH-H_2O]^+ \quad \text{Equation 7.5}$$

Though the concentration of water and methanol present in the QIT are unknown, $[M+H]^+$ is expected to be small in comparison to [H_2O] and [MeOH] and it may be assumed that the decrease in the concentration of water and methanol as the reaction progresses are negligible with respect to the initial water and methanol concentration.

A phenomenological rate constant for the pseudo first-order reaction of *m/z* 163 with methanol or water can be defined as

$$k_{163} = k_{181}[H_2O] + k_{195}[MeOH] \quad \text{Equation 7.6}$$

As may be seen in Figure 7.14C, the ion of *m/z* 177 contributes to 6% or less of the total ion population in the QIT. Neglecting the contribution of $\frac{d[M+H+MeOH-H_2O]^+}{dt}$ to $\frac{d[M+H]^+}{dt}$ simplifies the equation and the pseudo first order reaction of *m/z* 163 may be plotted as shown in Figure 7.15. A linear response (R^2 = 0.968) is observed for the first order integrated rate law for the reaction of protonated levoglucosan (Figure 7.14C) with gaseous neutrals in the QIT. This result supports the acceptability of neglecting the contribution of

the ion of *m/z* 177 from the rate of reaction of *m/z* 163. From the equation for the line of best fit shown in Figure 7.15 ($y = -0.0035t - 0.1477$), k_{163} of protonated levoglucosan formed by EESI using 50/49/1 methanol/water/acetic acid is determined to be 3.5 (± 0.1) x 10^{-3} ms^{-1}. This phenomenological rate constant is expected to be characteristic of the structure of levoglucosan formed by ionization of volatilized levoglucosan with EESI using 50/49/1 methanol/water/acetic acid.

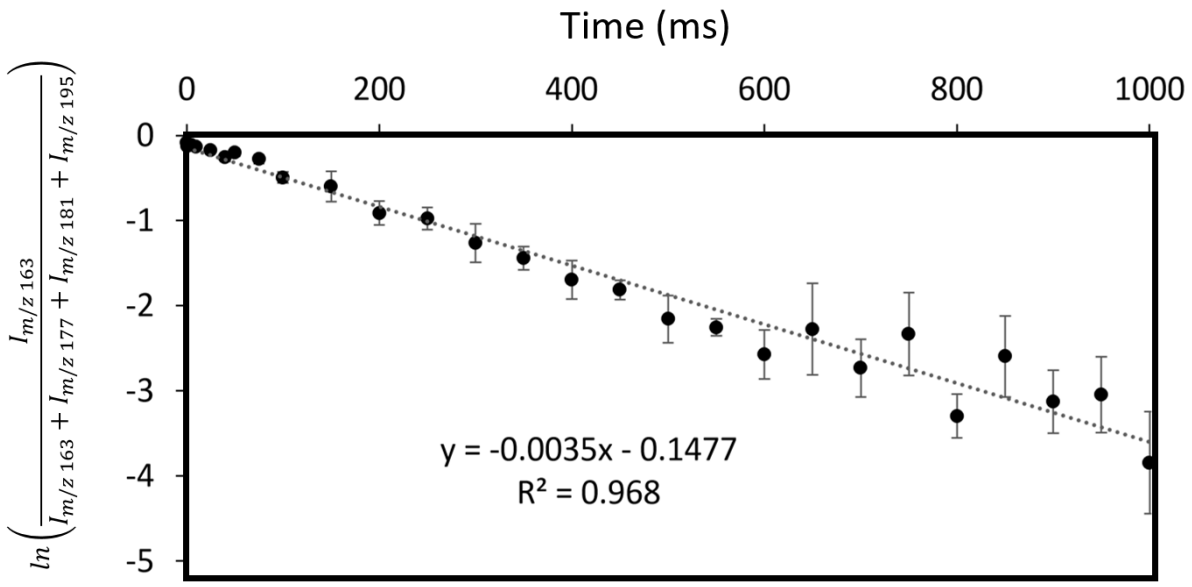

Figure 7.15. Plot of the pseudo first order integrated rate law for the reaction of m/z 163 with water and methanol in the ion trap.

7.4.2 Source of the gaseous neutrals in the QIT

The formation of methanol adducts of *m/z* 177 and 195 from protonated levoglucosan at longer reaction times indicates that the EESI solvent may be the source of the gaseous neutrals present in the QIT. To assist in electrospray solvent evaporation and to prevent gaseous neutrals from entering the capillary inlet to the mass spectrometer, the Bruker Esquire 3000 QIT used for these experiments employs a desolvation gas that flows away from the instrument around the inlet capillary of the mass spectrometer. The desolvation gas flow rate was changed from 5 L/min to 0.5 L/min or 8 L/min and the extent of the reaction between protonated levoglucosan and methanol was monitored to evaluate the effectiveness of the desolvation gas to prevent EESI solvent molecules from entering the high vacuum chamber of the mass spectrometer. The change in the fraction of protonated levoglucosan adducted with methanol $\left(\frac{I_{m/z\,177}+I_{m/z\,195}}{I_{m/z\,163}+I_{m/z\,177}+I_{m/z\,181}+I_{m/z\,195}}\right)$ with respect to reaction time for three different desolvation gas

flow rates is displayed in Figure 7.16A. Decreasing the desolvation gas flow rate from 5 L/min (black circles) to 0.5 L/min (green triangles) results in an increase in the fraction of protonated levoglucosan in the methanol adduct form. The decrease in the fraction of methanol adducted levoglucosan detected at longer reaction times for desolvation gas flow rates of 0.5 L/min and 5 L/min may be due to inefficient trapping of these relatively low intensity ions. No protonated levoglucosan-methanol adducts are observed when the desolvation gas flow rate is increased to 8 L/min (blue squares). The results displayed in Figure 7.16A suggest that at desolvation gas flow rates of less than 8 L/min, EESI solvent molecules are not completely excluded from the high vacuum region of the mass spectrometer. Increasing the desolvation gas flow rate to 8 L/min prevents EESI solvent molecules from entering the mass

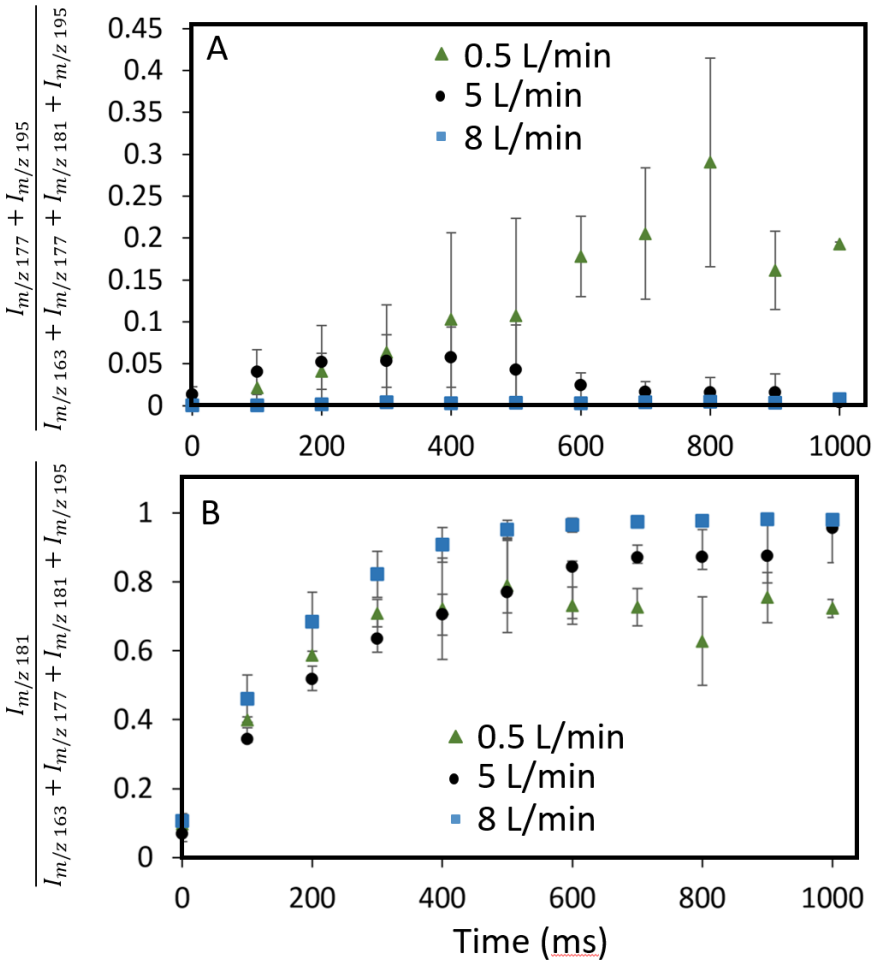

Figure 7.16. A. Fraction of protonated levoglucosan formed by EESI present as a methanol adduct with respect to time and B. fraction of protonated levoglucosan present as a water adduct with respect to time.

spectrometer. The fraction of the levoglucosan-water adduct $\left(\frac{I_{181}}{I_{m/z\,163}+I_{m/z\,177}+I_{m/z\,181}+I_{m/z\,195}}\right)$ present with respect to time at 0.5, 5, and 8 L/min is shown in Figure 7.16B. The adduct from the reaction of protonated levoglucosan and water is still observed to a significant extent at a desolvation gas flow rate of 8 L/min when the EESI solvent is excluded from the mass spectrometer. In fact, the reaction of protonated levoglucosan occurs to a greater extent when the desolvation gas flow rate was 8 L/min because the competitive reactions of protonated levoglucosan with methanol are eliminated. This result indicates that the EESI solvent is not the only source of the water vapor available for reaction with protonated levoglucosan. The residual water vapor available in the ion trap is most likely introduced into the high vacuum system through the helium collision gas line or small leaks in the system. Nitrogen desolvation gas was flowed even when the system was not in use to prevent gaseous water from entering the vacuum system over the time course of these experiments. Residual water adsorbed to surfaces inside the mass spectrometer after exposure to atmospheric pressure is expected to be degassed because the phenomenological rate constant for the reaction of *m/z* 163 did not change when the analysis was performed on different days.

7.4.3 Influence of EESI solvent on ion structure

Though there are methods available to remove the water vapor from the mass spectrometry system, these ion-molecule reactions are not necessarily deleterious to the analysis of protonated levoglucosan by EESI-MS/MS. For example, the rate and extent of the adduction of water with protonated levoglucosan may be used to probe the structures of protonated levoglucosan ions. As opposed to the ion formed by protonation of levoglucosan with an EESI solvent of 50/49/1 methanol/H_2O/acetic acid, the protonated levoglucosan ion generated by EESI using 99/1 acetonitrile/acetic acid does not react with the adventitious water in the ion trap at reaction times of up to 1000 ms (Figure 7.17). This behavior is shown graphically in Figure 7.17, a plot of the fraction of levoglucosan in the protonated form with respect to time when 99/1 acetonitrile/acetic acid is used as an EESI solvent. The lack of reactivity indicates that the structure of the protonated levoglucosan ions formed from EESI with 50/49/1 methanol/H_2O/acetic acid is different than the structure of the protonated levoglucosan ions generated using 99/1 acetonitrile/acetic acid as an EESI solvent.

Differences in the behavior of protonated gaseous levoglucosan are also observed when 50/49/1 methanol/D_2O/acetic acid is used as the EESI solvent in place of 50/49/1 methanol/H_2O/acetic acid. The mass spectra observed when 50/49/1 methanol/H_2O/acetic acid is used as opposed to 50/49/1 methanol/D_2O/acetic acid are shown in Figure 7.18A and 7.18B, respectively. Though little increase in intensity of the ion of *m/z* 164 is observed when D_2O is used in the EESI solvent, the deuteration pattern corresponds to the exchange of up to 5 hydrogen atoms with deuterium atoms. It is expected that only the hydroxyl hydrogens of levoglucosan will be easily exchangeable for deuterium. Thus, this data suggests that ring opening of both of the rings in levoglucosan occurs on the timescale of ionization. After isolation of the ion of *m/z* 163 formed by EESI, no enrichment of the protonated levoglucosan and deuterated water adduct (*m/z* 183) is observed when H_2O is used in the EESI solvent as opposed to D_2O (Figure 7.19) and only a small increase in the $[M+H+HDO]^+$ adduct (*m/z* 182) is observed.

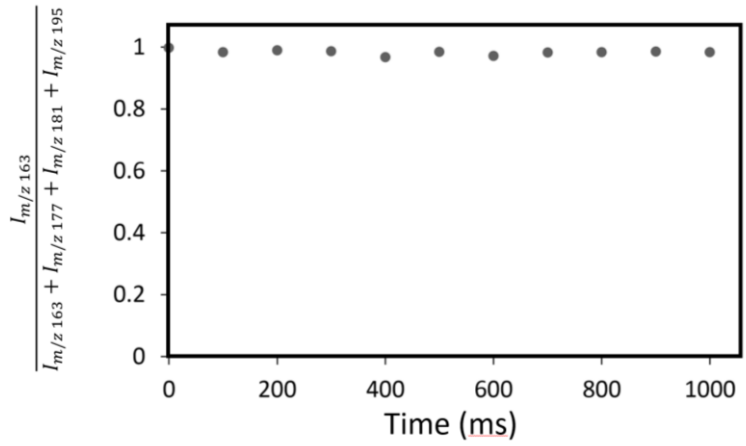

Figure 7.17. Fraction of levoglucosan in the protonated form with respect to time when 99/1 acetonitrile/acetic acid is used as the EESI solvent.

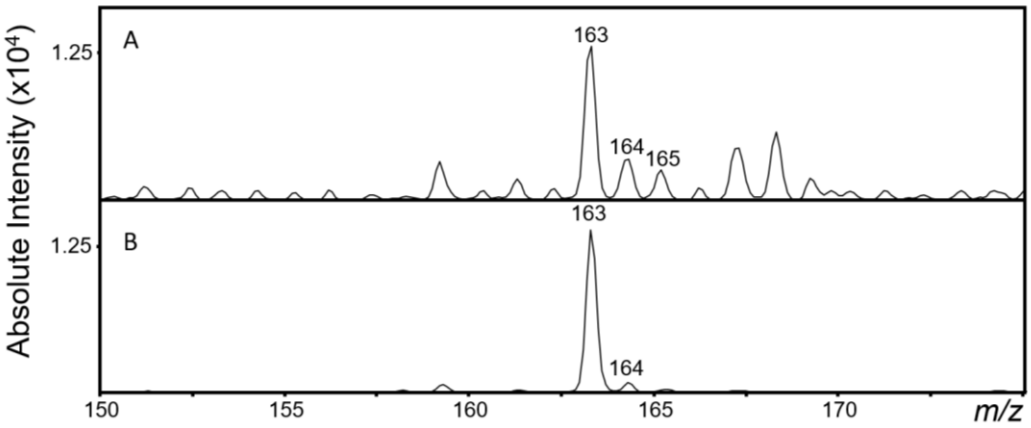

Figure 7.18. EESI-MS of volatilized levoglucosan ionized using A. 50/49/1 methanol/D_2O/acetic acid and B. 50/49/1 methanol/H_2O/acetic acid.

It is expected that the majority of the neutral water and water ions/clusters at the inlet to the mass

spectrometer are in the H_2O or HDO (or H_3O^+/DH_2O^+) form because of the relative abundance of hydrogen as opposed to deuterium in the ion source. It has previously been determined that the interaction of D_3O^+ with H_2O (or H_3O^+ with D_2O) results in the redistribution of the hydrogen and deuterium atoms at a rate nearly equal to the rate of collision.[15,16] Thus, at atmospheric pressure, hydrogen and deuterium are expected to statistically distribute between the ionized protonated or deuterated water molecules from the EESI solvent and undeuterated water in the atmosphere.

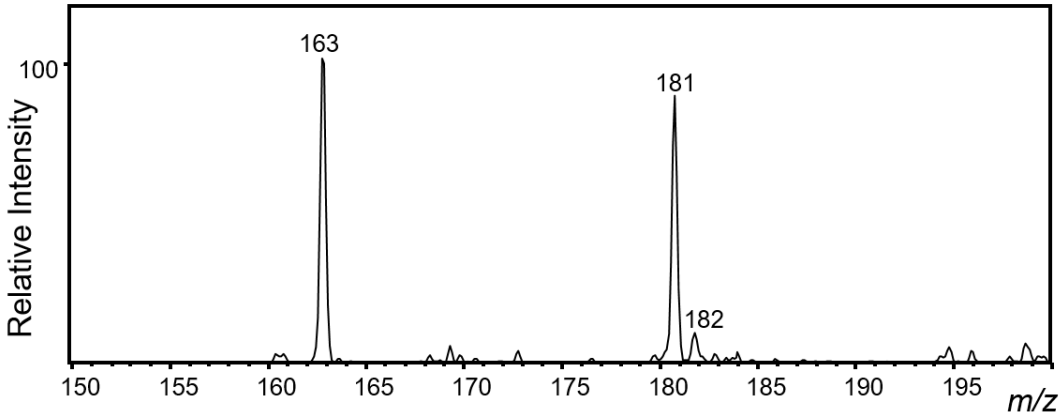

Figure 7.19. EESI-MS with 50/49/1 methanol/D_2O/acetic acid of volatilized levoglucosan after isolation and trapping of the ion of m/z 163.

A plot of the fraction of non-adducted levoglucosan present when 50/49/1 methanol/D_2O/acetic acid is used as the EESI solvent $\left(\frac{I_{m/z\,163}+I_{m/z\,164}+I_{m/z\,165}}{I_{m/z\,163}+I_{m/z\,164}+I_{m/z\,165}+I_{m/z\,177}+I_{m/z\,181}+I_{m/z\,182}+I_{m/z\,195}}\right)$ with respect to time (Figure 7.20A) reveals that there are two populations of protonated levoglucosan ions formed: one water reactive structure and one unreactive structure. The plot of the first order integrated rate law for this reaction (Figure 7.20B) further illustrates this phenomenon. The equation of the line of best fit for linear portion of the trend, corresponding to the reactive structure, is $y = -0.0022t - 0.1341$. Thus, the phenomenological rate constant, k_{163}, for the reaction is 2.2 (± 0.1) x10^{-3} ms^{-1}. The total concentration of solvent available for adduction in the ion trap is expected to be the same when 50/49/1 methanol/H_2O/acetic acid or when 50/49/1 methanol/D_2O/acetic acid is used as the EESI solvent because the desolvation gas flow rate was 5 L/min for both experiments. The isotope effect on the rate of reaction of D_2O is assumed to be negligible because the water present for reaction is in the form of H_2O or HDO[15,16] and as such no bonds to deuterium are believed to be broken in the adduction of protonated levoglucosan with water.[17] It can then be concluded that the rate constant for the adduction of H_2O and/or

D_2O with protonated levoglucosan is different for the protonated levoglucosan ions generated by the respective EESI solvents. Thus, the structures of the reactive protonated levoglucosan ion generated using 50/49/1 methanol/H_2O/acetic acid or 50/49/1 methanol/D_2O/acetic acid as the EESI solvent are different.

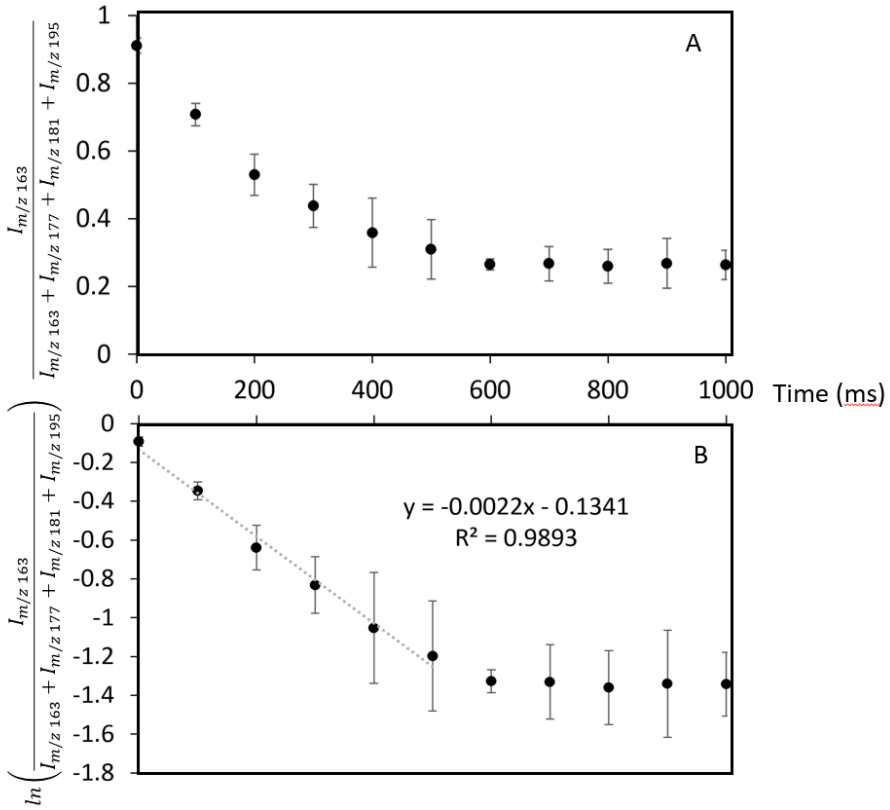

Figure 7.20. A. Fraction of protonated levoglucosan generated by EESI using 50/49/1 methanol/water/acetic acid remaining with respect to time and B. first order integrated rate law for the reaction of levoglucosan with solvent in the ion trap.

7.4.4 MS/MS to investigate protonated levoglucosan ion structures

To confirm that the ions produced by EESI of volatilized levoglucosan have different gas-phase structures, MS/MS was performed on the protonated levoglucosan ion (*m/z* 163) generated by EESI with each solvent (Figure 7.21). Drastic differences in the MS/MS spectrum for the ion of *m/z* 163 formed by EESI of volatilized levoglucosan using 50/49/1 methanol/H_2O/acetic acid (Figure 7.21A) and 99/1 acetonitrile/acetic acid (Figure 7.21B) are observed. CID of the protonated levoglucosan ion formed using 50/49/1 methanol/H_2O/acetic acid as an EESI solvent results only in product ions from the neutral loss or gain of water while product ions of *m/z* 121, 105, and 81 are observed after CID of protonated levoglucosan formed by EESI with 99/1 acetonitrile/acetic acid. Though the dissociation pattern shown in

Figure 7.21C for levoglucosan protonated by EESI with 50/49/1 methanol/D_2O/acetic acid is similar to that shown in Figure 7.21A for 50/49/1 methanol/D_2O/acetic acid, the presence of the ion of *m/z* 103 indicates that the two ion populations are not identical. The ion of *m/z* 163 formed from EESI with 50/49/1 methanol/D_2O/acetic acid is in fact a mixture of two ions as determined from Figure 7.20. The reactive structure formed from EESI with 50/49/1 methanol/D_2O/acetic acid can be distinguished from the reactive protonated levoglucosan structure formed from EESI with 50/49/1 methanol/H_2O/acetic acid using the phenomenological rate constant (k_{163} = 3.5 (± 0.1) x 10^{-3} ms^{-1} using 50/49/1 methanol/H_2O/acetic acid, k_{163} = 2.2 (± 0.1) x10^{-3} ms^{-1} using 50/49/1 methanol/D_2O/acetic acid). It would be expected that if the non-reactive structure formed by 99/1 acetonitrile/acetic acid was formed by EESI using 50/49/1 methanol/H_2O/acetic acid, the ions of *m/z* 121, 105, and 81 would be observed in Figure 7.21C because the non-reactive structure comprises 25% of the ion population of *m/z* 163. Thus, it can be tentatively concluded that the protonated levoglucosan ions formed by EESI with 99/1 acetonitrile/acetic acid or 50/49/1 methanol/H_2O/acetic acid have different structures. Further MS/MS experiments (discussed in Chapter 8) are required to determine if the structure of the non-reactive structure formed by EESI with 50/49/1 methanol/D_2O/acetic acid is the same as that formed by 99/1 acetonitrile/acetic acid.

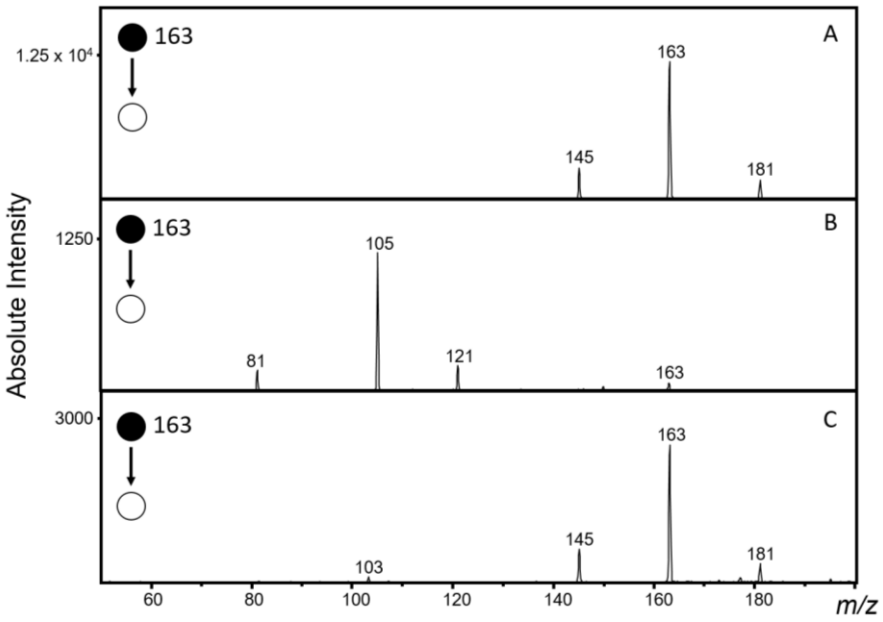

Figure 7.21. MS/MS spectra generated by CID of protonated levoglucosan formed by EESI using A. 50/49/1 methanol/H_2O /acetic acid B. 99/1 acetonitrile/acetic acid and C. 50/49/1 methanol/D_2O/acetic acid.

7.5 Limitations of CID for identification of ions

Though de novo identification of analyte ions from MS/MS spectra is possible, common isobaric neutral losses occur from small protonated molecules containing only carbon, hydrogen, and oxygen (shown in Section 7.3) making it difficult to identify small organic molecules. To illustrate this limitation, consider the MS/MS spectra shown in Figure 7.22. The MS/MS spectrum in Figure 7.22A is generated by CID of the ion of *m/z* 127 produced by LTPI of volatilized 5-(hydroxymethyl)furfural and the MS/MS spectrum in Figure 7.22B is from CID of the ion of *m/z* 127 produced by LTPI of volatilized 3-hydroxy-2-methyl-4-pyrone. Both compounds have been previously been identified in the gas phase of pyrolyzed cellulose.[18,19] The ion of *m/z* 127 produced by LTPI of volatilized 5-(hydroxymethyl)furfural undergoes only the neutral loss of water upon CID. Little structural information is gleaned from this collisionally induced neutral loss; water could dissociate from the hydroxyl group or the aldehyde. Though the product ion observed in the MS/MS spectrum matches a peak observed from MS/MS of the cellulose pyrolysis product of *m/z* 127 (Figure 7.22C) the neutral loss of water from these small organic molecules is nearly ubiquitous and therefore not diagnostic. It also cannot be determined whether or not 3-hydroxy-2-methyl-4-pyrone is present in the cellulose pyrolysate. Protonated 3-hydroxy-2-methyl-4-pyrone fragments with a very low efficiency using typical conditions (Figure 7.22B). Without a significant intensity of product ions from CID the MS/MS spectra of standards and unknowns cannot be compared to identify

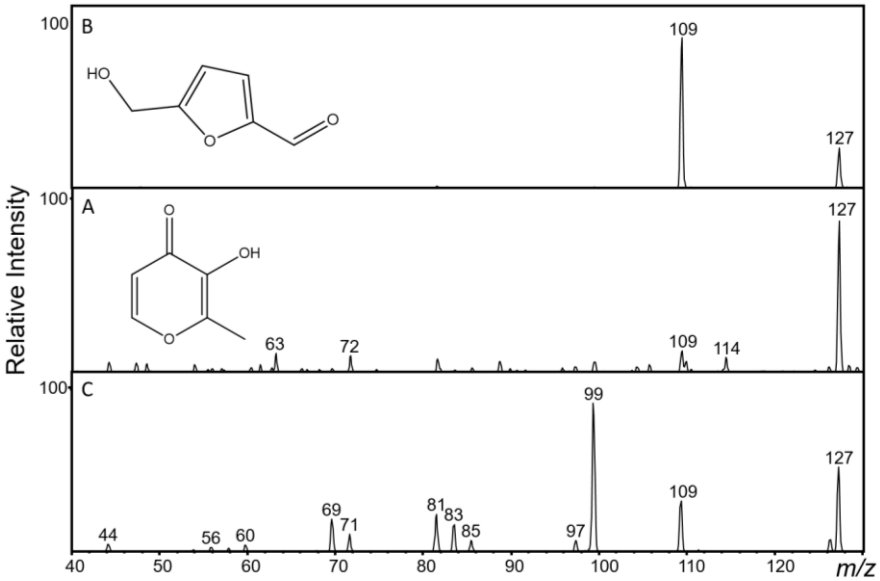

Figure 7.22. MS/MS spectra from the ion of m/z 127 produced by LTPI of A. volatilized 5-(hydroxymethyl)furfural B. volatilized 3-hydroxy-2-methyl-4-pyrone and C. cellulose aerosol product.

the analyte and further optimization of MS/MS parameters must be performed to compare the MS/MS spectrum of the standard to the unknown.

7.6 Summary and conclusions

MS/MS is a useful tool for the partial or complete structural interpretation of ions. The low extent of fragmentation of analytes during ionization in the ion sources presented in Chapter 4 allows each neutral molecule to be associated with a single parent ion observed in the mass spectrum. MS/MS is used in conjunction with the aerosol mass spectrometry system presented in Chapters 4-6 to investigate the structure of cellulose pyrolysis products.

The influence of the pyrolysis temperature and heating rate on the chemical composition of the aerosol produced by pyrolysis was evaluated. Collisional cooling experiments were used to determine that ions produced by LTPI of the pyrolysis products of cellulose are thermalized prior to CID. It was found that though the heating rate does not influence the composition of the aerosol in these experiments, the final pyrolysis temperature has a significant influence on the aerosol composition: both the ratio and identity of ions produced by LTPI of pyrolyzed cellulose changes as the final pyrolysis temperature is increased. MS/MS data used in conjunction with DIMS is shown to be useful for investigation of changes in the composition of aerosol particles.

A survey of the MS/MS spectra of ions generated by LTPI of pyrolyzed cellulose was performed. PCA was used to exemplify the ability to discriminate between analyte structures based on neutral loss patterns. High mass accuracy data was used to determine the molecular formula of neutral losses from CID but the transmission efficiency of low mass ions limits the utility of an FTICR for MS or MS/MS analysis of small molecules. Unexpected neutral losses from ions containing only carbon, hydrogen and nitrogen were identified and discussed. The neutral loss of 15 Da was shown to be due to the loss of a methyl radical from a methoxy group and the neutral loss of 10 Da was proposed to be due to a neutral loss of 28 Da followed by an ion-molecule reaction with water. The observed neutral loss patterns can be used to identify structural features in an unknown ion.

The kinetics of an ion-molecule reaction were used to differentiate between isomeric ions. Three protonated levoglucosan structures were differentiated based on the kinetics of the adduction with water. Two non-reactive protonated levoglucosan structures formed by different EESI solvents were

differentiated by MS/MS. Further MS/MS experiments are described in Chapter 8 to confirm that the non-reactive protonated levoglucosan ion generated by EESI with 50/49/1 methanol/D_2O/acetic acid and 99/1 acetonitrile/acetic acid have the different structures.

REFERENCES

1. Öktem, B.; Tolocka, M.; Johnston, M. On-Line Analysis of Organic Components in Fine and Ultrafine Particles by Photoionization Aerosol Mass Spectrometry. *Anal. Chem.* **2004***, 76*, 253-261.

2. Jimenez, J. L.; Jayne, J. T.; Shi, Q.; Kolb, C. E.; Worsnop, D. R.; Yourshaw, I.; Seinfeld, J. H.; Flagan, R. C.; Zhang, X.; Smith, K. A.; Morris, J. W.; Davidovits, P. Ambient aerosol sampling using the Aerodyne Aerosol Mass Spectrometer. *J. Geophys. Res. Atmos.* **2003***, 108*.

3. Harper, J. D.; Charipar, N. A.; Mulligan, C. C.; Zhang, X. R.; Cooks, R. G.; Ouyang, Z. Low-Temperature Plasma Probe for Ambient Desorption Ionization. *Anal. Chem.* **2008***, 80*, 9097-9104.

4. Gallimore, P. J.; Kalberer, M. Characterizing an extractive electrospray ionization (EESI) source for the online mass spectrometry analysis of organic aerosols. *Environ. Sci. Technol.* **2013***, 47*, 7324-7331.

5. McFadden, W. H.; Lammert, S. A. Techniques for increased use of thermospray liquid chromatography—mass spectrometry. *J. Chromatogr. A.* **1987***, 385*, 201-211.

6. Hua, L.; Hou, K.; Chen, P.; Xie, Y.; Jiang, J.; Wang, Y.; Wang, W.; Li, H. Realization of In-Source Collision-Induced Dissociation in Single-Photon Ionization Time-of-Flight Mass Spectrometry and Its Application for Differentiation of Isobaric Compounds. *Anal. Chem.* **2015***, 87*, 2427-2433.

7. Onay, O. Influence of pyrolysis temperature and heating rate on the production of bio-oil and char from safflower seed by pyrolysis, using a well-swept fixed-bed reactor. *Fuel Process. Technol.* **2007***, 88*, 523-531.

8. Carl, D. R.; Moision, R. M.; Armentrout, P. B. In-Source Fragmentation Technique for the Production of Thermalized Ions. *J. Am. Soc. Mass Spectrom.* **2009***, 20*, 2312-2317.

9. Racine, A. H. Thermally Assisted Collision Induced Dissociation in a Quadrupole Ion Trap Mass Spectrometer, UNC-Chapel Hill, Chapel Hill, 2005.

10. Zekavat, B.; Szulejko, J. E.; LaBrecque, D.; Olaitan, A. D.; Solouki, T. Efficient injection of low-mass ions into high magnetic field Fourier transform ion cyclotron resonance mass spectrometers. *Rapid Commun. Mass Spectrom.* **2014***, 28*, 230-238.

11. Menezes, J. C. J. M. D. S.; Cavaleiro, J. A. S.; Domingues, M. R. M. Structural analysis of 2-arylidene-1-indanone derivatives by electrospray ionization tandem mass spectrometry. *Rapid Commun. Mass Spectrom.* **2013***, 27*, 2461-2471.

12. Piot, C.; Jaffrezo, J. -.; Cozic, J.; Pissot, N.; El Haddad, I.; Marchand, N.; Besombes, J. -. Quantification of levoglucosan and its isomers by High Performance Liquid Chromatography - Electrospray Ionization tandem Mass Spectrometry and its applications to atmospheric and soil samples. *Atmos. Meas. Tech.* **2012***, 5*, 141-148.

13. Tao, W. A.; Gozzo, F. C.; Cooks, R. G. Mass spectrometric quantitation of chiral drugs by the kinetic method. *Anal. Chem.* **2001***, 73*, 1692-1698.

14. Blagojevic, V.; Bohme, D. K. Differential mobility spectrometer as an ion/molecule reactor: Peptide H–D exchange in mobility separation. *Int. J. Mass Spectrom.* **2015***, 378*, 180-185.

15. Adams, N. G.; Smith, D.; Henchman, M. J. Isotope exchange in the reactions $H_3O^+ + D_2O$, $NH_4^+ + ND_3$, CH_5^+ CD_4 and their mirror reactions at thermal energies. *Int. J. Mass Spec. Ion Phys.* **1982***, 42*, 11-23.

16. Smith, D.; Adams, N. J.; Henchman, M. J. Studies of the binary reactions of $H_3O^+ \cdot (H_2O)_{0,1,2}$ ions and their deuterated analogues with D_2O, H_2O, and NH_3. *J. Chem. Phys* **1980***, 72*, 4951-4957.

17. Wiberg, K. A. The Deuterium Isotope Effect. *Chem. Rev.* **1955***, 55*, 713-743.

18. Sanders, E. B.; Goldsmith, A. I.; Seeman, J. I. A model that distinguishes the pyrolysis of d-glucose, d-fructose, and sucrose from that of cellulose. Application to the understanding of cigarette smoke formation. *J. Anal. Appl. Pyrolysis* **2003***, 66*, 29-50.

19. Evans, R. J.; Milne, T. A. Molecular Characterization of the Pyrolysis of Biomass. 1. Fundamentals. *Energy Fuels* **1987***, 1*, 123-137.

CHAPTER 8: SUMMARY AND FUTURE DIRECTIONS

8.1 Summary

In this dissertation a mass spectrometry system designed for the analysis of compounds from aerosol particles in real-time is presented. In Chapter 3 the utility of surface-sampling techniques for the analysis of compounds from aerosol particles is investigated. The motivation for the development of aerosol mass spectrometers is also highlighted in Chapter 3. Not only can aerosol collection and extraction of compounds from filters be time consuming, but storage of semi-volatile compounds on filters or as filter extracts results in a decrease in the overall signal response and changes in the chemical composition of the sample.

In Chapter 4, the atmospheric pressure ion sources extractive electrospray ionization (EESI) and low temperature plasma ionization (LTPI) are used to generate ions from compounds in aerosol particles. These ionization techniques are shown to form ions from small molecules in a variety of complex mixtures including pyrolyzed natural polymers and e-cigarette liquids. The dependence of the aerosol particle size distribution on the heating parameters is investigated in Chapter 5, and the importance of reproducible pyrolysis conditions prior to analysis is emphasized. Ionization of compounds from size selected aerosol particles was performed by coupling LTPI to a differential mobility analyzer (DMA).

The goal of Chapters 6 and 7 is to highlight the advantages of the aerosol mass spectrometry system presented in this dissertation over current commercial aerosol mass spectrometry instrumentation. As discussed in Chapter 6, separation of ions prior to mass analysis by differential ion mobility spectrometry (DIMS) can be used to partially or fully resolve ions in complex mixtures such as the pyrolysate of cellulose in real time. It is shown that DIMS separations of ions from complex mixtures are highly reproducible and the observed experimental variation is likely due to the variability of the pyrolysis experiment rather than the DIMS hardware. In Chapter 7 the kinetics of ion-molecule reactions that occur in the ion trap are used to differentiate between isomeric ions. The dissociation patterns observed after tandem mass spectrometry (MS/MS) of ions are shown give insight into the functional groups present in

an ion. The structural information gained from MS/MS can be related back to the structure of the neutral molecule because the ion sources used for sampling of compounds from aerosol particles induce little to no fragmentation during ionization. Comparison of the dissociation pattern of analytes to the dissociation pattern of standards allows confirmation of the presence or absence of a compound in the sample. Even for compounds separated with a resolution of less than 1.0, DIMS-MS/MS can provide deconvoluted MS/MS spectra that may be used to compare to standards and to identify compounds in aerosol particles.

The primary advantage of the system presented herein over commercially available aerosol mass spectrometers is the ability to obtain structural information from compounds in complex mixtures. However, further development and optimization of the mass spectrometer presented in this dissertation is required. The remainder of this chapter is dedicated to the description of suggested experiments and directions for progression of this project.

8.2 Suggested future experiments

8.2.1 On-Filter Derivatization (Chapter 3)

Desorption electrospray ionization (DESI) and paperspray ionization were used in Chapter 3 to ionize compounds from aerosol particles collected on filters. Selective chemical reactions have been performed previously by both reactive DESI[1] and reactive paper spray ionization[2] prior to mass spectrometry to increase the selectivity of an analysis. For example, hydroxylamine has been used in the DESI solvent to react with the carbonyl group of steroids from urine on a polytetrafluoroethylene surface.[1] It is proposed that selective derivatization be performed after collection of the aerosol particles on filters to identify functional groups present in the analytes by DESI or paper spray ionization. 1-bromobutane could be added to the DESI or paper spray solvent to identify carboxylic acids and phenol hydroxyl groups in aerosol samples containing no nitrogen or sulfur.[3] Heating of the acidic spray solvent or the sample during ionization could allow identification of esters by hydrolysis to carboxylic acids,[4] though evaporative losses of semi-volatile analytes from the filter would be expected to occur.

Derivatization of analytes could also be used to confirm that analyte molecules do not react with the spray solvent during ionization. By changing the methanol in an acidified DESI or paper spray solvent to ethanol and/or n-propanol, the occurrence of Fischer esterification[5] of carboxylic acids would be identified by the mass-to-charge ratio shift of the ions. This esterification experiment could also be

performed by EESI to confirm that analyte molecules do not react with the electrospray solvent during ionization.

8.2.2 Nano-EESI (Chapter 4)

Nano-ESI is a common alternative to ESI that has been shown to increase sensitivity and enhance ionization efficiency as compared to conventional ESI.[6] Smaller solvent droplets are formed by nano-ESI as opposed to conventional ESI, resulting in more efficient ionization of compounds in the sample.[7] Preliminary results are shown in Figure 8.1 for the ionization of compounds in the pyrolysate of ethyl cellulose generated at approximately 600 °C in the custom pyrolysis chamber by nano-EESI with 50/49/1 methanol/water/acetic acid. To perform nano-EESI, a nano-ESI emitter was used in place of the ESI emitter for EESI as described in Chapter 2.3.5 and shown in Figure 2.8. When nano-EESI with 50/49/1 methanol/water/acetic acid (Figure 8.1A) or acetonitrile (Figure 8.1C) is used to ionize the pyrolysis products of ethyl cellulose instead of EESI (Figure 8.1B: 50/49/1 methanol/water/acetic acid, Figure 8.1D: acetonitrile), an increase in the signal intensity is observed. The abundant ions at low mass-to-charge ratios are due to contaminants in the acetonitrile and were observed in the background mass spectra. A mixture of EESI (blue asterisks) and LTPI-type (red asterisks) ions are formed when 50/49/1 methanol/water/acetic acid is used as a nano-EESI solvent. If a discharge was occurring at the tip of the nano-EESI emitter as in Section 4.5.2, LTPI-type ions would be observed regardless of the solvent

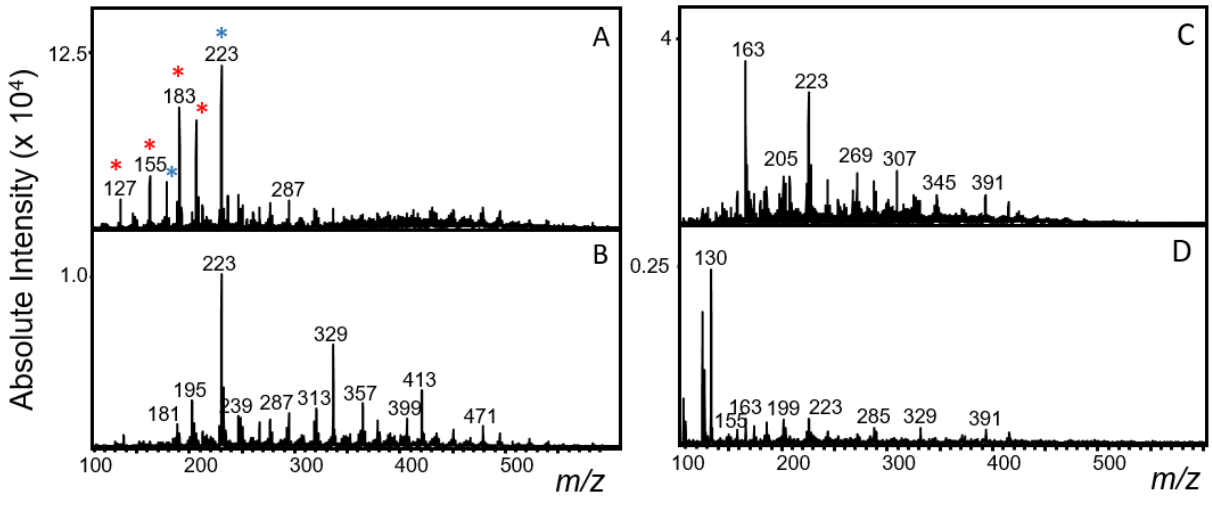

Figure 8.1. Mass spectra observed from pyrolyzed ethyl cellulose ionized using nano-EESI and a solvent of A. 50/49/1 methanol/water/acetic acid B. acetonitrile and EESI with a solvent of C. 50/49/1 methanol/water/acetic acid and D. acetonitrile.

used for nano-EESI. However, LTPI-type ions were not observed when acetonitrile was used for nano-EESI, indicating that no discharge is occurring at the tip of the nano-EESI emitter.

Nano-EESI should be further investigated as a potential ambient ion source for the aerosol mass spectrometer. Ionization of an aerosolized analyte with a low vapor pressure, such as oleic acid (1.9×10^{-6} Pa)[8], could be used to determine if gas or particle phase compounds are sampled by nano-EESI. Systematic investigation of the solvent dependence of nano-EESI could also give insight into the mechanism of EESI.

8.2.3 Evaluation of the vaporized e-liquid nicotine content (Chapter 4)

Though the advertised nicotine concentration was 12 mg/mL for each of the three nicotine containing e-liquids investigated in Chapter 4, the absolute intensity of the protonated nicotine ion of *m/z* 163 formed by LTPI-MS of the vaporized e-liquid was different. MS/MS of the ion at *m/z* 163 formed by LTPI-MS of the vaporized e-liquid indicates that no analyte ions other than nicotine are present in a significant quantity in the vapor that would result in the observed change in intensity. LC-ESI-MS should be performed to quantify the nicotine concentration in each sample because the actual concentration of nicotine in e-cigarette liquids has previously been shown to deviate from the concentration reported on the label by up to 105%.[9] To evaluate potential matrix effects due to the flavorings in the e-liquid, standard e-cigarette liquid solutions containing known concentrations of nicotine and flavoring compounds identified by GC-MS and LC-MS/MS could be volatilized and ionized by LTPI. Differences in the ionization efficiency of nicotine in the presence of flavorings would indicate that the composition of the e-liquid directly influences the aerosol formation characteristics or that vaporization of the flavorings results in compounds with a higher proton affinity than nicotine.

8.2.4 Improving the reproducibility of LTPI-MS of size-selected aerosol particles (Chapter 5)

The PyroProbe is preferred over the custom pyrolysis chamber for aerosol generation because the PyroProbe heating profile is highly controllable and reproducible. However, the smaller sample capacity of the PyroProbe in comparison to the custom chamber results in a decrease in the quantity of aerosol present for ionization by LTPI. After particle size selection by the DMA an even smaller fraction of the initial aerosol sample is available for analysis. As shown in Chapter 5, DMA-LTPI-MS of the output of the PyroProbe results in low signal intensity, poor signal-to-noise ratios, and overall irreproducibility in the

blank subtracted mass spectra. The flow-through miniature LTPI source was shown to increase the sensitivity for detection of analytes as well as the reproducibility of the signal response. Using the DMA in conjunction with the miniature LTPI source in the flow-through configuration could result in more reproducible and sensitive analyses of low mass concentration aerosol samples.

8.2.5 Tandem mass spectrometry with differential ion mobility spectrometry (Chapter 6)

Though flow-through LTPI was used to increase the sensitivity and reproducibility of ionization for DIMS-MS/MS, poor signal intensity of product ions was still observed because of the lowered transmission efficiency of ions into the mass spectrometer when the high voltage sinusoidal waveform is applied to the DIMS electrodes (approximately 50%). To improve the signal response from a DIMS separation, an instrument with a more sensitive mass analyzer could be used. The mass spectrometer with the highest sensitivity currently available in the laboratory is a Thermo Scientific LTQ-FT. However, the DIMS device used in the experiments presented in this dissertation is designed to fit onto the capillary inlet of a Bruker instrument. A DIMS device has recently been designed by researchers in this laboratory to fit onto the front end of the Thermo LTQ-FT to allow more sensitive ion detection for DIMS-MS/MS experiments. Coupling DIMS to the high resolution/high mass accuracy MS will also allow better differentiation between ions in complex samples. For higher abundance ions it may also be possible to determine the high mass accuracy formulas of product ions after MS/MS.

8.2.6 Tandem mass spectrometry of unreactive levoglucosan structures (Chapter 7)

The kinetics of the reaction of protonated levoglucosan (*m/z* 163) with adventitious water vapor in the ion trap were used to differentiate at least three different protonated levoglucosan structures: two structures that react with water and at least one that does not. A protonated levoglucosan ion that was non-reactive with water was observed when 99/1 acetonitrile/acetic acid was used as an EESI solvent as well as when 50/49/1 methanol/D_2O/acetic acid was used as an EESI solvent. The product ions formed by MS/MS of the ions of *m/z* 163 formed from 50/49/1 methanol/D_2O/acetic acid and 99/1 acetonitrile/acetic acid indicate that the structure of these two non-water reactive protonated levoglucosan ions are different. To generate a MS/MS spectrum showing the dissociation pattern of only the non-reactive protonated levoglucosan ion the ion of *m/z* 163 formed by 50/49/1 methanol/D_2O/acetic acid can be trapped for 700 ms so that all of the reactive structure is converted to a water adduct of *m/z* 181.

CID may then be performed to obtain a MS/MS spectrum from the non-reactive ion of *m/z* 163. The dissociation pattern of the non-reactive protonated levoglucosan ion formed from 50/49/1 methanol/D_2O/acetic acid may then be compared to that of the non-water-reactive ion formed by EESI of volatilized levoglucosan using 99/1 acetonitrile/acetic acid.

8.2.7 Confirmation of analyte identification

DIMS may be used to increase the confidence in the identification of compounds from the pyrolysis products of cellulose by MS/MS. Comparing both the compensation field at which ions are stably transmitted through the DIMS device and the MS/MS spectra, a more accurate identification of an unknown can be made. Another method for increasing the confidence in the identification of analytes by comparison to standards is to perform multiple stages of MS/MS on the ions of interest. For example, though the neutral loss of water is a common and uninformative product ion for the pyrolysis products of natural polymers, performing MS/MS on the water loss product ion (MS^3) may result in unique and structurally informative product ions. Comparison of the spectra generated by MS^3 or MS^n of unknown ions to those of standards will result in more accurate identification of compounds. The primary limiting factor for confirmation of the identity of cellulose aerosol products is the fact that analytical standards for the molecules of interest are typically expensive and often are not available commercially. Methods for limiting the number of potential analytes are discussed in Section 8.3. once potential analyte compounds have been obtained commercially or synthetically, DIMS-MS, DIMS-MS/MS, and MS^n experiments can be performed to more confidently identify analytes.

8.3 Overall project outlook

For identification of analytes using the aerosol mass spectrometer presented in this dissertation, the characteristics of analyte ions such as the dissociation pattern and differential ion mobility must be compared to standards. However, standards of many of the compounds potentially present in the aerosol sample[10] are either expensive or unavailable commercially and synthesis of standards is a time consuming and often expensive process. To narrow down the number of potential analytes prior to purchase or synthesis of standards, experimental and theoretical data may be used to eliminate unlikely candidates. Molecular formulas determined by FTICR-MS are searched in the ChemSpider database to populate a list of potential analytes. The collisional cross section of analyte ions can be determined from

low field ion mobility experiments.[11] The experimental data for the unknown analytes can then be compared to theoretical calculations for the heat of formation, proton affinity, and collisional cross section to determine the most likely candidates. The theoretical data will be compiled in a freely available, searchable database for rapid comparison of data from the unknowns to candidate compounds. After elimination of unlikely matches, the most likely analytes will be purchased or synthesized for comparison of the dissociation patterns. A searchable repository of these MS/MS spectra will also be compiled for rapid identification of analytes.

REFERENCES

1. Huang, G.; Chen, H.; Zhang, X.; Cooks, R. G.; Ouyang, Z. Rapid screening of anabolic steroids in urine by reactive desorption electrospray ionization. *Anal. Chem.* **2007***, 79*, 8327-8332.

2. Yan, X.; Augusti, R.; Li, X.; Cooks, R. G. Chemical Reactivity Assessment Using Reactive Paper Spray Ionization Mass Spectrometry: The Katritzky Reaction. *Chem. Plus Chem.* **2013***, 78*, 1142-1148.

3. Sakaguchi, Y.; Kinumi, T.; Yamazaki, T.; Takatsu, A. A novel amino acid analysis method using derivatization of multiple functional groups followed by liquid chromatography/tandem mass spectrometry. *Analyst* **2015***, 140*, 1965-1973.

4. McMurray, J. 16.6 Chemistry of Esters. In *Organic Chemistry: A Biological Approach.* Thompson Brooks/Cole: Belmont, CA, 2007; p 653-658.

5. McMurray, J. 16.3 Nucleophilic Acyl Substitution Reactions of Carboxylic Acids. In *Organic Chemistry: A Biological Approach.* Thompson Brooks/Cole: Belmont, CA, 2007; p 642.

6. Wilm, M.; Mann, M. Analytical Properties of the Nanoelectrospray Ion Source. *Anal. Chem.* **1996***, 68*, 1-8.

7. Kebarle, P. P.; Verkerk, U. H. Electrospray: from ions in solution to ions in the gas phase, what we know now. *Mass Spec. Rev.* **2009***, 28*, 898-917.

8. Cappa, C. D.; Lovejoy, E. R.; Ravishankara, A. R. Evaporation Rates and Vapor Pressures of the Even-Numbered C_8-C_{18} Monocarboxylic Acids. *J. Phys. Chem. A.* **2008***, 112*, 3959-3964.

9. Cheng, T. Chemical evaluation of electronic cigarettes. *Tobacco Control* **2014***, 23*, ii11-ii17.

10. Rodgman, A.; Perfetti, T. A. *The Chemical Components of Tobacco and Tobacco Smoke;* CRC Press: Boca Raton, FL, 2009; p 1784.

11. Isenberg, S. L. Improvements in mass Spectrometric Analyses with Differential Ion Mobility Spectrometry. *Ph. D. Dissertation, University of North Carolina* **2014**.

APPENDIX I: ANALYSIS OF E-CIGARETTE LIQUIDS

As of the time of this writing, the FDA has regulatory power only over electronic cigarettes (e-cigarettes) marketed for therapeutic purposes (e.g. smoking cessation devices or e-cigarettes containing pharmaceuticals such as e-Cialis).[1] As shown in Figure AI.1 there are many designs for e-cigarettes,[2] but in general the e-cigarette consists of three parts: a battery (yellow asterisks), an atomizer (red asterisks), and a cartridge (Figure AI.1A) or tank (Figure AI.1B) containing the "e-liquid" to be aerosolized (blue asterisks).[3,4] The cartridge style e-cigarettes shown in Figure AI.1A are either fully disposable or have a disposable cartridge/atomizer (or "cartomizer") and the tank-style e-cigarettes usually are refillable. Typically, a wick made of glass fibers is used to draw the e-cigarette liquid to the atomizer via capillary action or electrophoretic movement.[3] A resistively heated wire is wrapped around the wick as shown in Figure AI.2, heating the e-cigarette liquid to form a vapor. As the vapor is drawn to the mouthpiece by air flow, the e-liquid is nebulized and the vapor condenses into an aerosol that is inhaled by the user.[5,6]

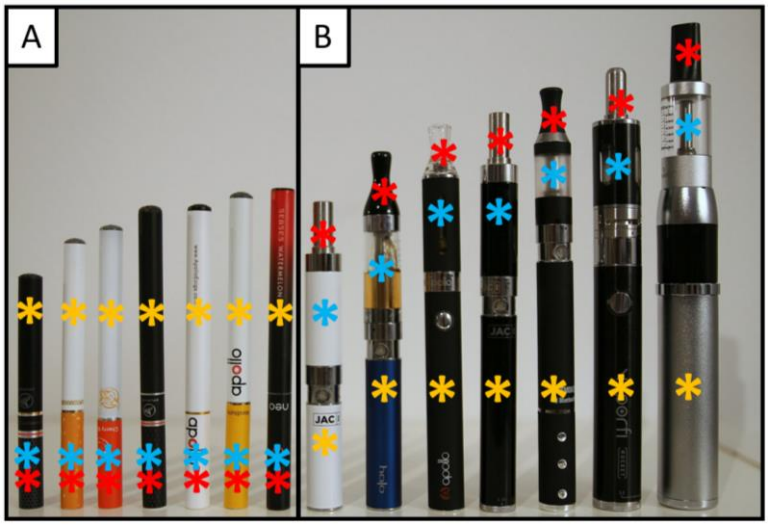

Figure AI.1. Representative e-cigarette devices. Picture modified from https://www.flickr.com/photos/127173209@N05/15249922438.

The actual composition of most of the 7000+ commercial e-liquids is undisclosed, advertised as consisting of a humectant (propylene glycol and/or glycerin), nicotine, and "flavorings".[5] Though the concentration of nicotine is often advertised on the e-cigarette packaging, the actual concentration of nicotine in the e-cigarette liquid has been shown to deviate from the concentration reported on the label by up to 105%.[10] The body of knowledge surrounding the composition of the "flavorings" in e-cigarette

liquids is disjointed and at times contradictory. For example, a 2008 study by Health New Zealand Ltd. reported low concentrations of targeted carcinogens and concluded that the brand of e-cigarette liquid in question was safe.[11] In contrast, a 2009 study performed by the FDA reported the presence of tobacco specific nitrosamines and impurities in numerous e-cigarette liquids as well as the presence of diethylene glycol, a compound that is known to be toxic and, in high concentrations, fatal.[3] These two studies highlight the variability in the composition of e-cigarette liquids between brands and flavors of e-cigarettes. Coupling this inconsistency in composition with the abundance of "mom-and-pop" e-cigarette shops and the many online tutorials for "vapers" to mix their own liquids,[12] the potential variability in the identity and concentration of compounds used as flavorings in the e-liquids becomes evident.

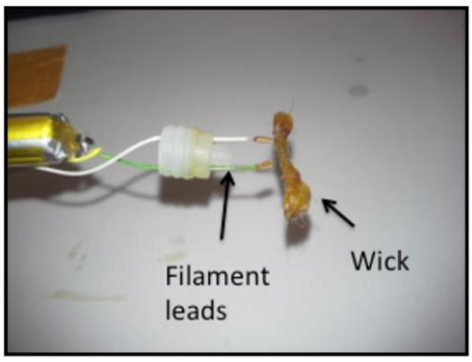

Figure AI.2 - Picture of the wick/filament from a cartomizer-style e-cigarette.

GC-MS is often used to analyze the semi-volatile and volatile compounds in e-liquids.[13] For the experiments described in this Appendix, GC-MS of e-liquids was performed as described in Chapter 2.4.1. The chromatogram for the separation of the compounds from Atomic Cinnacide e-liquid is shown in Figure AI.3. The dissociation pattern observed in the EI spectra of the ten top scored compounds from the database were compared by visual inspection to the dissociation pattern of the unknown. The compound from the database with the closest match for each unknown along with pertinent safety hazards from the Material Safety Data Sheet (MSDS) are listed in Table AI.1. After preliminary identification of compounds from the NIST database, the EI spectra were visually inspected to confirm the identifications. The italicized compound in Table AI.1 indicates a tentative identification based on visual inspection of the EI-MS data. Propylene glycol and glycerin were excluded from the list as they are known components of the e-cigarette liquids.

GC-MS reveals a number of flavoring compounds common to many of the e-liquids analyzed in this laboratory thus far, including vanilla and cinnamon related flavorings. Additives (e.g. vanillin and cinnamaldehyde) that have been approved for use in ingested foods are often used in e-cigarette liquids. However, as shown in Table AI.2, these compounds may have different health effects when inhaled

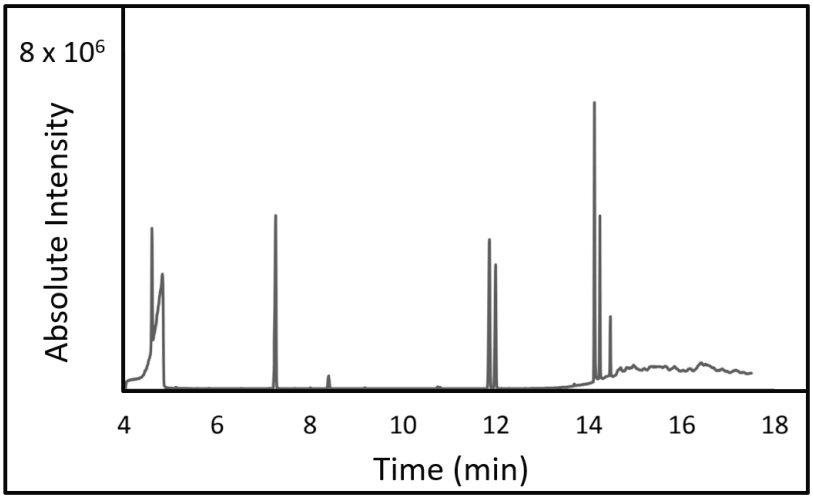

Figure AI.17. Chromatogram from GC-MS of nicotine-free Atomic Cinnacide diluted 50x in methanol.

rather than ingested. For example, cinnamaldehyde is an additive that is approved by the FDA for use in cinnamon flavored candies but has been shown to be highly toxic to human cells when introduced to the cells as a vapor.[14,15] This data explains the frequent reports of cinnamon flavored e-cigarette liquids causing lung irritation to e-cigarette users.[15] Numerous chemicals known to be hazardous were also identified in the Atomic Cinnacide e-liquid by GC-MS. Specifically, eugenol and benzyl alcohol, chemicals that can be toxic if inhaled, were identified in the e-liquid by GC-MS. Two compounds that extract small molecules from plastics, benzyl alcohol and triacetin, were also identified in the Atomic Cinnacide e-liquid. These chemicals can potentially extract hazardous compounds from the plastics in the e-cigarette tank and mouthpiece into the e-liquid and vapor.

Involatile compounds are also expected to be present in the vaped e-liquid because of the physical action of nebulization of the e-liquid when the user inhales. To analyze the involatile components of the e-liquid, ESI-MS was performed. Electrospray ionization (ESI) was coupled to a Fourier transform ion cyclotron resonance (FTICR)-MS for high resolution/high mass accuracy measurements. The Atomic Cinnacide e-liquid was diluted 50x in 50/49/1 methanol/water/acetic acid for ESI. The ESI mass spectra for Atomic Cinnacide is shown in Figure AI.4. The ionic formulas for 16 compounds were determined with less than 5 ppm mass error from the high mass accuracy mass spectrum of Atomic Cinnacide. These formulas are shown in Table AI.3 along with the blank subtracted relative intensity (BSRI). Though Atomic Cinnacide is advertised as a nicotine-free e-liquid, nicotine ($C_{10}H_{15}N_2$, *m/z* 163.124) was detected as a

Table AI.1. Compounds identified in Atomic Cinnacide e-liquid by GC-MS with pertinent MSDS information.

Name	Molar Mass	Known MSDS Health Hazards
Benzyl Alcohol	108.1	**Skin:** Irritant, Sensitizer **Eye:** Irritant **Inhalation:** Hazardous **Ingestion:** Slightly Hazardous **Target Organs:** Central Nervous System, Liver **Heating:** Flash Point 100 °C, when heated to decomposition it emits acrid smoke and irritating fumes.
Cinnamaldehyde	132.0	**Inhalation:** Irritant **Target Organs:** Reproductive System The toxicological properties of this substance have not been fully investigated.
Dipropylene glycol	134.2	**Inhalation:** Irritant **Heating:** Flash Point 138 °C, Decomposes to CO, CO_2
Hydrocinnamaldehyde	134.2	**Skin:** Serious Irritant **Eye:** Irritant
4-Methyl-2-phenyl-1,3-dioxolane	*164.2*	***Skin:*** *Irritant* ***Eye:*** *Serious Irritant* ***Inhalation:*** *Irritant* ***Heating:*** *Flash Point 98 °C*
Eugenol	164.2	**Skin:** Irritant, Permeator **Eye:** Irritant **Inhalation:** Hazardous **Ingestion:** Hazardous **Target Organs:** Lungs, Nervous System, Mucous Membranes **Heating:** Flash Point 104 °C
Triacetin	218.2	**Skin:** Irritant, Permeator **Eye:** Irritant **Inhalation:** Irritant **Ingestion:** Slightly Hazardous **Heating:** Flash point 153 °C

contaminant in the Atomic Cinnacide e-liquid by ESI-MS. Tandem mass spectrometry (MS/MS) of the ion of *m/z* 163 in the linear ion trap confirms the identification of nicotine.

Most ions that are observed from ESI-MS of the e-liquids are not observed from GC-EI-MS and vice versa. The majority of the ions detected by ESI-MS are sodium adducts as opposed to protonated. Only two compounds from Atomic Cinnacide (Cinnamaldehyde, C_9H_8O and dipropylene glycol $C_3H_8O_3$) are ionized and detected in positive ion mode by both ionization techniques. The discrepancy between

the compounds observed from ESI and EI could be because GC-EI-MS is designed for the analysis of volatile and semi-volatile compounds and ESI-MS for semi-volatile and involatile compounds. However, it is also possible that because the e-liquid is rapidly heated to 250 °C upon injection into the inlet of the GC, thermally labile analytes may degrade prior to separation and detection.

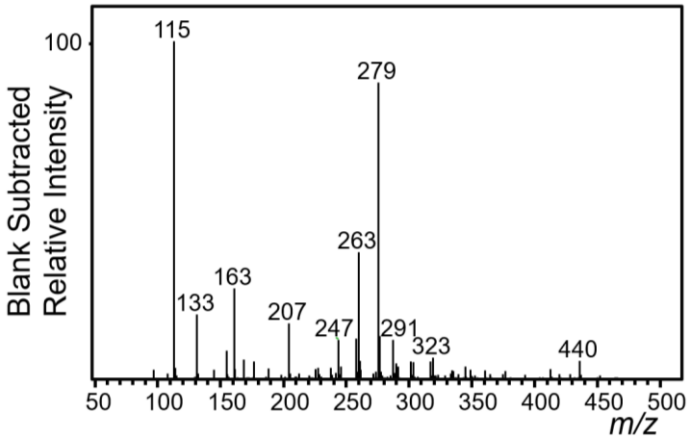

Figure AI.4. ESI-FTICR-MS of nicotine-free Atomic Cinnacide.

Table AI.2. Ionic formulas for ions detected by ESI-MS from Atomic Cinnacide.

m/z	BSRI	Formula
115	100	$C_3H_8O_3Na$
133	19	C_9H_9O
157	9	$C_6H_{14}O_3Na$
163	27	$C_{10}H_{15}N_2$
171	6	$C_6H_{12}O_4Na$
179	6	$C_{10}H_{15}ON_2$
207	17	$C_{12}H_{15}O_3$
247	12	$C_{12}H_{16}O_4Na$
261	12	$C_{13}H_{18}O_4Na$
263	38	$C_{13}H_{20}O_4Na$
279	88	$C_{13}H_{20}O_5Na$
291	12	$C_{15}H_{24}O_4Na$
305	5	$C_{15}H_{22}O_5Na$
307	5	$C_{15}H_{24}O_5Na$
321	6	$C_{15}H_{22}O_6Na$
323	7	$C_{15}H_{24}O_6Na$

REFERENCES

1. U.S. Food and Drug Administration Electronic Cigarettes (e-Cigarettes). 2015.

2. United States Patent and Trademark Office *http://www.uspto.gov/* (accessed 6/10, 2014).

3. Westenberger, B. J. Evaluation of e-cigarettes. *St. Louis: Food and Drug Administration* **2009**, 1-8.

4. Williams, M.; Talbot, P. Variability Among Electronic Cigarettes in the Pressure Drop, Airflow Rate, and Aerosol Production. *Nicotine & Tobacco Research* **2011***, 13*, 1276-1283.

5. Njoy Njoy: What's an E-Cigarette? *https://www.njoy.com/whats-an-e-cigarette* (accessed 6/10, 2014).

6. Lorillard Technologies, I. How To Blu. *http://www.blucigs.com/how-blu-works/how-to-blu/* (accessed 6/10, 2014).

7. Trtchounian, A.; Williams, M.; Talbot, P. Conventional and electronic cigarettes (e-cigarettes) have different smoking characteristics. *Nicotine & Tobacco Research* **2010***, 12*, 905-912.

8. Talhout, R.; Schulz, T.; Floreck, E.; van Benthem, J.; Wester, P.; Opperhuizen, A. Hazardous Compounds in Tobacco Smoke. *Int. J. Environ. Res. Public Health* **2011***, 8*, 613-628.

9. Hahn, J.; Monakhova, Y. B.; Hengen, J.; Kol-Himmelseher, M.; Schüssler, J.; Hahn, H.; Kuballa, T.; Lachenmeier, D. W. Electronic cigarettes: overview of chemical composition and exposure estimation. *Tob. Induc. Dis.* **2014***, 12*, 23-35.

10. Cheng, T. Chemical evaluation of electronic cigarettes. *Tobacco Control* **2014***, 23*, ii11-ii17.

11. Laugesen, M. Safety Report on the Ruyan® e-cigarette Cartridge and Inhaled Aerosol. *Health New Zealand, Ltd.* **2008**.

12. VaporSearchUSA United States E-Cigarette Vendors Map. *http://vaporsearchusa.com/* (2015).

13. Oh, J. -.; Shin, H. -. Identification and Quantification of Several Contaminated Compounds in Replacement Liquids of Electronic Cigarettes by Gas Chromatograpy-Mass Spectrometry. *J. Chromatogr. Sci.* **2015***, 53*, 841-848.

14. Bahl, V.; Lin, S.; Xu, N.; Davis, B.; Wang, Y. -.; Talbot, P. Comparison of electronic cigarette refill fluid cytotoxicity using embryonic and adult models. *Reproductive Toxicology* **2012***, 34*, 529-537.

15. Behar, R. Z.; Davis, B.; Wang, Y.; Bahl, V.; Lin, S.; Talbot, P. Identification of toxicants in cinnamon-flavored electronic cigarette refill fluids. *Toxicology in Vitro* **2014***, 28*, 198-208.

16. Garner, C.; Stevens, R. A Brief Discription of History, Operation, and Regulation. *E-Cigarette Task Force: Reference Report* **2014**, 1-12.

17. Schaller, K.; Ruppert, L.; Kahnert, S.; Bethke, C.; Nair, U.; Pötschke-Langer, M. Electronic Cigarettes - An Overview. In *Red Series Tobacco Prevention and Tobacco Control.* German Cancer Research Center: Heidelberg, 2013; pp Chapter 19.

18. Polli, G. P.; Grim, W. M.; Bacher, F. A.; Yunker, M. H. Influence of formulation on aerosol particle size. *Journal of Pharmaceutical Sciences* **2006***, 58*, 484-486.

19. Heyder, J.; Gehbart, J.; Rudolf, G.; Schiller, C. F.; Stahlhofen, W. Deposition of particles in the human respiratory tract in the size range 0.005-15 um. *Journal of Aerosol Sci.* **1986***, 17*, 811-825.

APPENDIX II: RESOLUTION OF FLOW-THROUGH-LTPI-DIMS SEPARATIONS OF PYROLYZED CELLULOSE

m/z	Resolution Experiment 1	Resolution Experiment 2	Average Resolution	Standard Deviation
50	---	---	---	---
51	---	---	---	---
52	---	---	---	---
53	---	---	---	---
54	---	---	---	---
55	---	---	---	---
56	---	---	---	---
57	---	---	---	---
58	---	---	---	---
59	---	---	---	---
60	---	---	---	---
61	---	---	---	---
62	---	---	---	---
63	---	---	---	---
64	---	---	---	---
65	---	---	---	---
66	---	---	---	---
67	---	---	---	---
68	---	---	---	---
69	---	---	---	---
70	---	---	---	---
71	---	---	---	---
72	---	---	---	---
73	---	---	---	---
74	---	---	---	---
75	---	---	---	---
76	---	---	---	---
77	---	---	---	---
78	---	---	---	---
79	---	---	---	---
80	---	---	---	---
81	0.7	0.6	0.7	0.09
82	---	---	---	---
83	1.1	0.5	0.8	0.36
84	---	0.7	0.7	---
85	0.5	0.8	0.7	0.15
86	0.6	0.5	0.6	0.07
87	---	---	---	---
88	---	1.2	1.2	---

89	---	---	---	---
90	---	---	---	---
91	---	---	---	---
92	---	---	---	---
93	---	---	---	---
94	---	3.5	3.5	---
95	0.5	0.4	0.4	0.10
96	0.6	0.6	0.6	0.01
97	0.9	0.9	0.9	0.01
98	0.7	0.1	0.4	0.40
99	---	---	---	---
100	0.1	1.0	0.6	0.65
101	---	---	---	---
102	0.6	0.5	0.6	0.05
103	---	---	---	---
104	---	---	---	---
105	---	---	---	---
106	---	---	---	---
107	---	---	---	---
108	0.9	0.7	0.8	0.14
109	1.0	0.9	0.9	0.06
110	---	---	---	---
111	---	---	---	---
112	---	---	---	---
113	0.6	0.7	0.7	0.13
114	0.6	0.6	0.6	0.00
115	1.2	0.8	1.0	0.24
116	0.7	0.8	0.7	0.05
117	---	---	---	---
118	---	---	---	---
119	---	1.0	1.0	---
120	---	0.2	0.2	---
121	0.6	0.6	0.6	0.06
122	0.4	0.8	0.6	0.27
123	0.6	0.6	0.6	0.03
124	0.4	0.8	0.6	0.28
125	0.8	1.0	0.9	0.10
126	0.8	0.8	0.8	0.01
127	0.4	0.7	0.5	0.17
128	0.6	0.4	0.5	0.11
129	0.8	0.8	0.8	0.06
130	0.6	0.8	0.7	0.11
131	---	0.6	0.6	---

132	0.5	0.6	0.6	0.14
133	0.6	0.6	0.6	0.02
134	0.1	0.8	0.4	0.50
135	0.5	0.5	0.5	0.06
136	0.6	0.6	0.6	0.01
137	0.6	0.4	0.5	0.12
138	0.5	0.7	0.6	0.11
139	0.7	0.6	0.7	0.01
140	0.4	0.0	0.2	0.27
141	0.5	0.8	0.7	0.24
142	0.5	0.5	0.5	0.00
143	0.6	0.7	0.7	0.08
144	0.5	0.7	0.6	0.16
145	0.6	0.6	0.6	0.02
146	0.6	0.0	0.3	0.39
147	0.0	0.1	0.1	0.06
148	0.0	0.8	0.4	0.55
149	0.5	0.5	0.5	0.02
150	0.5	0.4	0.5	0.04
151	0.6	0.3	0.4	0.24
152	0.2	0.4	0.3	0.15
153	0.4	0.2	0.3	0.12
154	0.4	0.8	0.6	0.28
155	0.8	0.5	0.6	0.25
156	0.2	0.1	0.1	0.03
157	0.5	0.4	0.5	0.10
158	0.6	0.4	0.5	0.17
159	0.5	0.5	0.5	0.00
160	0.7	0.7	0.7	0.04
161	0.1	0.6	0.3	0.41
162	0.5	0.5	0.5	0.02
163	0.4	0.5	0.4	0.03
164	0.6	0.7	0.7	0.12
165	0.7	0.1	0.4	0.40
166	0.2	0.7	0.4	0.29
167	0.7	0.5	0.6	0.11
168	0.4	0.7	0.6	0.20
169	0.5	0.5	0.5	0.03
170	0.5	0.5	0.5	0.01
171	0.1	0.6	0.4	0.34
172	0.0	0.5	0.3	0.36
173	0.0	0.4	0.2	0.30
174	0.6	0.1	0.3	0.34

175	0.3	0.3	0.3	0.06
176	0.8	0.0	0.4	0.54
177	0.1	0.6	0.4	0.35
178	0.4	0.4	0.4	0.01
179	0.1	0.6	0.4	0.35
180	0.5	0.2	0.3	0.17
181	0.3	0.1	0.2	0.11
182	0.0	0.6	0.3	0.39
183	0.3	0.1	0.2	0.11
184	0.5	0.7	0.6	0.16
185	0.6	0.5	0.5	0.10
186	0.1	0.4	0.2	0.24
187	0.4	0.7	0.6	0.18
188	0.1	0.7	0.4	0.44
189	0.7	0.8	0.7	0.08
190	0.3	0.6	0.4	0.23
191	0.9	0.0	0.5	0.60
192	0.6	0.7	0.6	0.09
193	0.0	0.2	0.1	0.13
194	0.4	0.7	0.5	0.18
195	0.3	0.5	0.4	0.08
196	0.2	0.4	0.3	0.18
197	0.0	0.2	0.1	0.11
198	0.3	0.2	0.2	0.07
199	0.5	0.1	0.3	0.29
200	0.6	0.4	0.5	0.10
201	0.0	0.4	0.2	0.25
202	0.4	0.4	0.4	0.00
203	0.0	0.5	0.2	0.31
204	0.6	0.1	0.3	0.36
205	0.8	0.5	0.7	0.23
206	0.4	43.9	22.1	30.73
207	0.6	0.4	0.5	0.12
208	0.4	0.2	0.3	0.13
209	0.4	0.5	0.4	0.06
210	0.4	0.1	0.3	0.21
211	0.5	0.5	0.5	0.02
212	0.5	0.2	0.3	0.24
213	0.0	0.3	0.2	0.19
214	0.1	0.2	0.2	0.09
215	0.0	0.2	0.1	0.13
216	0.2	0.7	0.4	0.33
217	0.0	0.5	0.3	0.34

218	0.2	0.0	0.1	0.13
219	0.0	0.2	0.1	0.15
220	0.7	0.5	0.6	0.17
221	0.3	0.1	0.2	0.12
222	0.1	0.5	0.3	0.26
223	0.4	0.5	0.5	0.07
224	0.4	0.3	0.3	0.06
225	0.6	0.5	0.5	0.06
226	0.5	0.2	0.3	0.25
227	0.1	0.5	0.3	0.31
228	0.5	0.3	0.4	0.15
229	0.1	0.5	0.3	0.30
230	0.9	0.3	0.6	0.43
231	0.2	0.1	0.2	0.06
232	0.2	0.3	0.3	0.07
233	0.1	0.5	0.3	0.28
234	0.2	0.3	0.3	0.08
235	0.0	0.5	0.2	0.31
236	0.1	0.4	0.2	0.22
237	0.8	0.4	0.6	0.26
238	0.2	0.6	0.4	0.30
239	0.1	0.4	0.2	0.22
240	0.1	0.5	0.3	0.31
241	0.1	0.2	0.2	0.06
242	0.7	0.5	0.6	0.13
243	0.0	0.0	0.0	0.01
244	0.3	0.5	0.4	0.18
245	1.0	0.6	0.8	0.28
246	0.1	0.9	0.5	0.57
247	1.0	0.4	0.7	0.48
248	0.5	0.6	0.6	0.08
249	0.3	0.3	0.3	0.01
250	0.0	0.4	0.2	0.24